

**Improving our understanding of
the role of biogenic emissions on
urban air quality**

Daniel Bryant

Doctor of Philosophy

University of York

Chemistry

January 2022

“All we have to decide is what to do with the time that is given us.”

J. R. R. Tolkien

Abstract

Secondary organic aerosol (SOA), formed from the atmospheric oxidation of volatile organic compounds has known adverse effects on air quality and human health. However, the contributions of biogenic SOA to organic aerosol in urban areas, with high levels of anthropogenic pollutants, is poorly understood. In this study, biogenic SOA markers are identified and quantified using liquid chromatography coupled to mass spectrometry. Time resolved samples were collected across several Asian mega cities and represent good case studies for anthropogenic-biogenic interactions to be investigated. Difficulties surrounding accurate quantification of these markers is addressed, and new methods proposed to start to overcome these challenges. Significant concentrations of biogenic organosulfates and nitrooxy-organosulfates were identified across the megacities of Beijing, Guangzhou and Delhi. Local isoprene emissions and high levels of anthropogenic pollutants, in particular NO_x and particulate SO_4^{2-} , led to significant formation of isoprene organosulfates and nitrooxy-organosulfates under both high- and low-NO oxidation conditions, with significant heterogeneous transformations of isoprene-derived oxidation products to particulate species. Local isoprene emissions were found to be highly influenced by local temperatures, with higher temperatures promoting higher concentrations, an important observation for a warming climate. Monoterpene derived organosulfates and nitrooxy-organosulfaes were observed to have strong diurnal variations using high time resolution filter sampling, but were observed in much lower concentrations than those formed from isoprene. Due to a significant lack of authentic standards, accurate quantification of markers is a challenge. A new method for the prediction of ionisation efficiencies was developed, and for the first time applied to biogenic SOA markers. This prediction allowed for the differences in ionisation efficiencies to be considered, leading to more reliable quantification. This method was then applied to the quantification of biogenic organic acids across Beijing, Delhi and Guangzhou and are some of the first observations of their kind for these species.

Contents

| | |
|--|-----------|
| Abstract | iii |
| List of Figures | ix |
| List of Tables | xx |
| List of Abbreviations | xxv |
| Acknowledgements | xxviii |
| Author's declaration | xxix |
| 1 Introduction | 1 |
| 1.1 Motivation | 2 |
| 1.2 Tropospheric Aerosol – composition and sources | 4 |
| 1.3 Emission of Biogenic Volatile Organic Compounds | 6 |
| 1.4 Secondary Organic Aerosol | 9 |
| 1.5 Tropospheric VOC oxidants | 10 |
| 1.6 SOA Formation Pathways | 13 |
| 1.6.1 Isoprene Derived SOA | 16 |
| 1.7 Effect of Anthropogenic Emissions on biogenic SOA formation | 22 |
| 1.7.1 Sulfate concentrations and aerosol acidity | 23 |
| 1.7.2 NO _x | 24 |
| 1.8 BSOA characterisation and quantification | 25 |
| 1.9 Thesis Outline | 31 |
| 2 Isoprene secondary organic aerosol in Beijing: Formation of Organosulfates and Nitrooxy organosulfate | 34 |
| 2.1 Introduction | 35 |

| | | |
|---------|--|----|
| 2.2 | Experimental | 38 |
| 2.2.1 | PM _{2.5} filter sampling and extraction | 38 |
| 2.2.2 | Ultra-high performance liquid chromatography tandem mass spectrometry (UHPLC-MS ²) | 39 |
| 2.2.3 | Construction of accurate mass library | 40 |
| 2.2.4 | Automated method for SOA tracer analysis | 41 |
| 2.2.5 | Hydrophilic Liquid Interaction Chromatography | 41 |
| 2.2.6 | Gas Chromatography – Mass Spectrometer | 42 |
| 2.2.7 | High-Resolution Aerosol Mass Spectrometry measurements | 43 |
| 2.2.8 | Iodide CIMS | 43 |
| 2.2.9 | Gas-phase measurements | 44 |
| 2.3 | Results and discussion | 45 |
| 2.3.1 | Isoprene gas phase concentrations and loss processes | 45 |
| 2.3.2 | Anthropogenic tracers | 47 |
| 2.3.3 | Isoprene SOA in Beijing | 50 |
| 2.3.4 | Quantification of isoprene OS tracers | 51 |
| 2.3.5 | Organosulfates | 56 |
| 2.3.5.1 | 2-methyltetrol OS (2-MT-OS) | 56 |
| 2.3.5.2 | 2-methyl glyceric acid OS (2-MG-OS) | 61 |
| 2.3.5.3 | Other isoprene-related OSs | 64 |
| 2.3.6 | Isoprene nitrooxy organosulfates | 65 |
| 2.3.6.1 | Mono-nitrate NOS | 66 |
| 2.3.6.2 | Di- and Tri-Nitrated NOS | 71 |
| 2.3.7 | Contribution of Isoprene SOA in Beijing | 75 |

3 Importance of Oxidants and Temperature in the Formation of Biogenic Organosulfates and Nitrooxy Organosulfates 77

| | | |
|-------|-----------------------------|----|
| 3.1 | Introduction | 78 |
| 3.2 | Experimental | 80 |
| 3.2.1 | Filter collection | 80 |

| | | |
|----------|--|------------|
| 3.2.2 | Extraction | 81 |
| 3.2.3 | Ultrahigh-Performance Liquid Chromatography Tandem Mass Spectrometry (UHPLC–MS ²) | 82 |
| 3.2.4 | Data Processing and Compound Library | 82 |
| 3.2.5 | Calibration and Matrix Effects | 83 |
| 3.2.6 | Gas-Phase Measurements | 86 |
| 3.2.7 | Ion Chromatography | 86 |
| 3.3 | Results and Discussion | 87 |
| 3.3.1 | Biogenic Organosulfates and Nitrooxyorganosulfates | 89 |
| 3.3.1.1 | Monoterpene Nitrooxy Organosulfates (NOS _{MT}). | 89 |
| 3.3.1.2 | Monoterpene Organosulfates (OS _{MT}) | 100 |
| 3.3.1.3 | Isoprene Nitrooxy Organosulfates (NOSi) | 101 |
| 3.3.1.4 | Isoprene Organosulfates (OSi) | 108 |
| 3.3.2 | Conclusion | 113 |
| 4 | Biogenic and anthropogenic sources of isoprene and monoterpenes and their secondary organic aerosol in Delhi, India | 115 |
| 4.1 | Introduction | 116 |
| 4.2 | Experimental | 117 |
| 4.2.1 | Filter collection and site information | 117 |
| 4.2.2 | Filter extraction | 118 |
| 4.2.2.1 | Ultra-high performance liquid chromatography tandem mass spectrometry (UHPLC-MS ²) | 119 |
| 4.2.3 | Quantification and uncertainties | 119 |
| 4.2.4 | Supplementary measurements | 121 |
| 4.2.5 | Radical Modelling | 122 |
| 4.3 | Results | 123 |
| 4.3.1 | Meteorology | 123 |
| 4.3.2 | Particle phase observations | 123 |
| 4.3.3 | Gas phase observations | 125 |

| | | |
|----------|--|------------|
| 4.3.4 | Isoprene and monoterpene measurements | 129 |
| 4.4 | Secondary organic aerosol formation | 134 |
| 4.4.1 | Isoprene SOA | 134 |
| 4.4.2 | Monoterpene secondary organic aerosol | 141 |
| 4.4.3 | Contributions of total quantified SOA (qSOA) to particulate mass | 144 |
| 4.5 | Conclusion | 145 |
| 5 | Overcoming the lack of authentic standards for the quantification of biogenic secondary organic aerosol markers | 147 |
| 5.1 | Introduction | 148 |
| 5.2 | Experimental | 151 |
| 5.2.1 | Instrument and data analysis | 151 |
| 5.2.2 | Commercially available standards | 152 |
| 5.2.3 | Chamber samples | 155 |
| 5.2.4 | Ambient Samples: collection and extraction | 156 |
| 5.3 | Results and Discussion | 156 |
| 5.3.1 | Development of a RIE predictive model | 156 |
| 5.3.2 | Predicted BSOA RIE factors | 161 |
| 5.3.3 | Quantification of BSOA in summertime Beijing | 165 |
| 5.4 | Conclusion | 168 |
| 6 | Formation of organic acids across three Asian Megacities | 170 |
| 6.1 | Introduction | 171 |
| 6.2 | Experimental | 173 |
| 6.2.1 | Biogenic secondary organic aerosol generation | 173 |
| 6.2.2 | Filter Sampling | 173 |
| 6.2.2.1 | Beijing | 173 |
| 6.2.2.2 | Delhi | 174 |
| 6.2.2.3 | Guangzhou | 174 |
| 6.2.3 | Extractions | 175 |

| | | |
|----------|--|------------|
| 6.2.4 | Ultra-high performance liquid chromatography tandem mass spectrometry (UHPLC-MS ²) | 175 |
| 6.2.5 | Matrix Effects | 176 |
| 6.2.6 | Data processing and compound library | 179 |
| 6.2.7 | Supplementary measurements | 179 |
| 6.3 | Results | 180 |
| 6.3.1 | Aerosol Composition | 180 |
| 6.3.2 | α -pinene markers | 189 |
| 6.3.3 | Limonene markers | 194 |
| 6.3.4 | β -caryophyllene | 198 |
| 6.3.5 | Impact of Ozone and Temperature | 200 |
| | 6.3.5.1 Ozone | 200 |
| | 6.3.5.2 Temperature | 206 |
| 6.4 | Conclusion | 207 |
| 7 | Summary and future work | 209 |
| 7.1 | Summary | 210 |
| 7.2 | Future work | 215 |

List of Figures

| | | |
|-----|---|----|
| 1.1 | Particle size distributions and general sources. Taken from https://www.dwd.de/EN/research/observing_atmosphere/composition_atmosphere/aerosol/cont_nav/particle_size_distribution_node.html%7D | 3 |
| 1.2 | PM _{2.5} composition across selected sites across the world, taken from Jimenez et al., 2009. [47] | 5 |
| 1.3 | Global flux estimates of VOC and OA, taken from Hallquist et al., 2009. [1] | 7 |
| 1.4 | January and July 2000 global emissions of isoprene, α -pinene and β -caryophyllene simulated with MEGAN 2.1, taken from Guenther et al., 2012. | 9 |
| 1.5 | HO _x cycle taken from Lu et al.,2012. Primary radical production is shown via the blue arrows, while radical chain reactions are shown via the red arrows. | 13 |
| 1.6 | Simplified VOC degradation mechanism, taken from Kroll and Seinfeld., 2008. | 14 |
| 1.7 | Simplified ozonolysis schematic of an alkene, taken from Kroll and Seinfeld., 2008. | 16 |
| 1.8 | Auto-oxidation of the O ₃ initiated degradation of α -pinene, taken from Iyer et al., 2021.[113] | 16 |
| 1.9 | Low NO Isoprene OH degradation pathway, taken from Surratt et al., 2010. | 17 |

| | | |
|------|---|----|
| 1.10 | High NO Isoprene OH degradation pathway, taken from Lin et al., 2013. | 19 |
| 1.11 | Schematic highlighting the effect of core-shell morphology on IEPOX uptake, taken from Zhang et al., 2019. | 21 |
| 1.12 | Diagram of the Main Products Formed from NO ₃ Oxidation of Isoprene, taken from Schwantes et al., 2015. | 22 |
| 1.13 | Potential formation mechanisms of organosulfates, taken from Brüggemann et al., 2020. | 24 |
| 1.14 | Filter sample collected in Delhi. | 27 |
| 1.15 | van Krevelen plots for molecular formulas assigned to FT- ICR mass spectra peaks in aerosol WSOC samples from a) New York and b) Virginia. Blue diamonds represent compounds containing only C, H, and O, yellow squares represent S-containing compounds, and red triangles are N-containing compounds. Black ovals represent traditional potential source molecular classes. Taken from Wozniak et al., 2008. [183] | 28 |
| 1.16 | Kendrick mass defect plot of CHOS-containing formulae from samples collected in central Amazonia. Periods with low and very high incidents of fires are marked as blue and red markers respectively. Taken from Kourtchev et al., 2016.[180] | 29 |
| 2.1 | Time series of isoprene, nitric oxide (NO), nitrogen dioxide (NO ₂), ozone (O ₃) and particulate sulfate (SO ₄). The black lines are at midnight every 72 hours. | 46 |
| 2.2 | (A) Average diurnal profile of isoprene mixing ratio measured using DC-GC-FID. (B) Diurnal profile of 2-methyltetrol sulfate (2-MT-OS) in PM _{2.5} collected on filters hourly over the 11 th to 12 th June 2017. Black lines indicate length of filter sampling period. | 47 |
| 2.3 | Campaign average diurnal profiles of OH measured by FAGE, O ₃ measured by UV spectroscopy and NO ₃ measured by BBCEAS. | 48 |

| | | |
|------|---|----|
| 2.4 | (A) Diurnal loss rate of isoprene calculated using measured average diurnal profiles of isoprene, OH, NO ₃ and O ₃ . (B) Average diurnal of the percentage loss of isoprene from reactions with OH, O ₃ and NO ₃ radicals. The IUPAC rate constants used for the calculations are as follows, NO ₃ : 7x10 ⁻¹³ , O ₃ :1.27x10 ¹⁷ , OH: 1x10 ¹⁰ cm ³ molecule ⁻¹ s ⁻¹ . [102] | 49 |
| 2.5 | PollutionRose plot (Openair) of particulate sulfate measured by AMS, for the sampling period. Highlighting under what wind conditions the highest concentrations of sulfate occur. | 50 |
| 2.6 | Correlation plot (R, Openair, CorPlot) highlighting the correlations between known iSOA tracers and anthropogenic pollutants. The number represents the R correlation between the two species. With redder more elongated circles highlighting a higher correlation. | 52 |
| 2.7 | Comparison of 2-MT-OS calibration (R ² =0.9804) (Blue) and 2-MG-OS calibration (R ² =0.9978) (Red). Highlighting the difference in gradients between the two species. The error bars highlight the standard error for each concentration. | 53 |
| 2.8 | (A) 2-MG-OS standard addition calibration of filter extract 205 in Table 2.4. The error bars highlight the standard error for each concentration. (B) 2-MT-OS standard addition calibration of filter extract 204 in Table 2.3. The error bars highlight the standard error for each concentration. | 54 |
| 2.9 | Time series of observed concentrations of iSOA tracers in Beijing during APHH. (A) 2-MT-OS (C ₅ H ₁₂ O ₇ S) (B) 2-MG-OS (C ₄ H ₈ O ₇ S) (C) C ₅ H ₁₀ SO ₆ . The red bars indicate the length of the sampling time. | 58 |
| 2.10 | Campaign average diurnal variation with 95% confidence interval of C ₅ H ₁₀ O ₃ measured in the gas phase using I-CIMS. | 59 |
| 2.11 | Campaign average diurnal variation with 95% confidence interval of C ₅ H ₉ NO ₄ measured in the gas phase using I-CIMS. | 60 |

| | | |
|------|--|----|
| 2.12 | Plot of 2-MT-OS ($C_5H_{12}O_7S$, blue) and 2-MG-OS ($C_4H_8O_7S$, red) concentrations versus $[O_3][SO_4]$. The high time resolution data (O_3 and AMS SO_4) has been averaged to the filter sampling time. | 61 |
| 2.13 | Extracted ion chromatograms (m/z 215.0) using hydrophobic interaction liquid chromatography (HILIC) of 2-methyltetrol OS (2-MT-OS) isomers, highlighting improved separation of isomers using this technique. Upper: Extract of filter collected on the 28/05/2017 between 11:33 and 14:23. Lower: 10 ppm 2-MT-OS standard.[187] | 62 |
| 2.14 | Campaign average diurnal of relative humidity (%). | 63 |
| 2.15 | Diurnal profile of 2-methylglyceric acid sulfate (2-MG-OS) in particulate matter collected on filters hourly over the 11 th to 12 th June 2017. Black lines indicate length of sampling. | 64 |
| 2.16 | A) Time series of $PM_{2.5}$ over the sampling period. B) Time series of the total known isoprene SOA signal (2-MT-OS, 2-MG-OS, $C_5H_{10}SO_7$ (MW 214), $C_5H_8SO_7$ (MW 212), $C_5H_{11}NSO_9$ (MW 261), $C_5H_9NSO_{10}$ (MW 275), $C_5H_{10}O_{11}N_2S$ (MW 306), $C_5H_9O_{13}N_3S$ (MW 351) and the total signal from the other iSOA tracers quantified in this study. | 66 |
| 2.17 | Time series of the measured concentrations of NOS in Beijing aerosol. The vertical lines are at midnight of each day of sampling. A) $C_5H_{11}NO_9S$ (MW 261). B) $C_5H_9NO_{10}S$ (MW 275). C) Sum of $C_5H_{10}N_2O_{11}S$ species (MW 306). D) Sum of $C_5H_9N_3O_{13}S$ (MW 351) species. The blue and red bars on each point show the full filter sampling time. The mid-sample points are connected with a line to show the temporal trend. | 67 |

| | | |
|------|--|----|
| 2.18 | Box and whisker plots of observed NOS concentrations separated by the time of day the filter was collected. A) C ₅ H ₁₁ O ₉ NS, B) C ₅ H ₉ O ₁₀ NS, C) C ₅ H ₁₀ O ₁₁ N ₂ S, D) C ₅ H ₉ O ₁₃ N ₃ S. The filter mid-points were split into different times of day, 00:00-07:00, 07:00-11:00, 11:00-13:00 and 13:00 -17:00 based on the general sampling times of the filters and labeled as night, morning, midday and afternoon respectively. The thick black line represents the median value, the upper and lower hinges represent the 75 th and 25 th percentiles respectively, with the upper and lower whiskers representing the largest value in the set. Outliers were removed so the diurnal profiles could be seen more clearly. | 68 |
| 2.19 | Proposed Formation Pathways of Mono-Nitrated OS and Di-Nitrated OS Species Observed in the Aerosol from the NO ₃ Initiated Oxidation of Isoprene. Note that only one of six possible INP isomers is shown, for simplicity, with δ -[1,4]-INP and β -[1,2]-INHE the dominant isomers observed in Schwantes et al.,2015. | 69 |
| 2.20 | Proposed Formation Pathway of the Mono-Nitrated OS C ₅ H ₉ NO ₁₀ S species. | 70 |
| 2.21 | Boundary layer height (m) diurnal across the Beijing summer campaign. | 74 |
| 3.1 | Time series of pollutants across the summer (left) and winter (right) campaigns. The highlighted section in the summer campaign indicates typhoon Wipha. The blue dotted lines indicate midnight of each day. | 88 |
| 3.2 | Diurnal variations of temperature (°C), relative humidity (RH,%), NO (ppbv), NO ₂ (ppbv), O ₃ (ppbv) and PM _{2.5} (µg m ⁻³) across summer (left) and winter (right) campaigns. The shaded area surrounding the black line is the 95% confidence interval. | 89 |

| | | |
|-----|---|-----|
| 3.3 | A- Time series of SO ₂ during winter, B – Diurnal variation of SO ₂ during winter with the shaded area around the black representing the 95% confidence interval. | 90 |
| 3.4 | Diurnal variations of (A) NOS _{MT} during summer, (B) NOS _{MT} during winter, (C) OS _{MT} during summer, and (D) OS _{MT} during winter. The lower and upper parts of the box represent the 25 th and 75 th percentiles, with the upper and lower lines extending no further than 1.5× the interquartile range of the highest and lowest values within the line, respectively. Any data points outside of this range are shown as red circles. | 92 |
| 3.5 | Correlation between NOS _{MT} and binned SO ₄ ²⁻ concentrations during summer (A) and winter (B). Correlation between OS _{MT} and binned SO ₄ ²⁻ concentrations during summer (C), and winter (D). The dots represent the mean tracer concentrations for the binned sulfate concentrations, with the lines representing ± standard deviation. | 93 |
| 3.6 | Binned correlation plots between markers and temperature: (A) NOS _{MT} during summer, (B) NOS _{MT} during winter, (C) OS _{MT} during summer, and (D) OS _{MT} during winter. The points represent the mean concentration ± SD within each temperature range bin. | 95 |
| 3.7 | Diurnal variations of three mononitrated NOSi species across (A, C, and E) the summer (left) and (B, D, and F) the winter (right). Data points were then colored by the average temperature over the filter sampling time period. Where temperature measurements were not available, the data points are in gray. | 96 |
| 3.8 | Diurnal variations of the steady state approximations of NO ₃ concentrations during summer (A) and winter (B). | 97 |
| 3.9 | Correlation between OS _{MT} and NOS _{MT} concentrations coloured by season. | 102 |

| | | |
|------|---|-----|
| 3.10 | C ₅ H ₁₁ O ₈ NS vs binned NO _x concentrations across both campaigns: (A) NO ₂ and (B) NO. NO ₂ concentrations were filtered to below 70 ppbv due to a limited number of data points. Data points were then colored by the average temperature over the filter sampling time period. Where temperature measurements were not available, the data points are in gray. | 105 |
| 3.11 | Diurnal variations of di-nitrated NOSi species across summer (left) and winter (right), coloured by temperature. | 106 |
| 3.12 | C ₅ H ₁₀ O ₁₁ N ₂ S isomers A-1.92 min, B – 2.95 min concentrations correlated to NO ₂ during across both campaigns. | 107 |
| 3.13 | Correlation plot (CorPlot, Openair R package) between isoprene OS species during the summer campaign. | 109 |
| 3.14 | Correlation plot (CorPlot, Openair R package) between OSi species during the winter campaign. | 110 |
| 3.15 | A – Correlation between OSi concentrations and particulate sulfate, coloured by season. B – Correlation between OSi and the product of [O3][SO ₄ ²⁻], coloured by season. C- Correlation between OSi concentration and NO, coloured by season. D- Correlation between OSi and temperature across both campaigns, coloured by SO ₄ ²⁻ concentrations, with the shape indicating the campaign. | 112 |
| 4.1 | Time series variations of measured temperature, planetary boundary layer height (PBLH) and relative humidity (RH) across pre- (left) and post- (right) monsoon. | 124 |
| 4.2 | Diurnal variations of measured monoterpene VOC's, temperature, planetary boundary layer height (PBLH) and relative humidity (RH) across pre- (left) and post- (right) monsoon. | 125 |

| | | |
|------|--|-----|
| 4.3 | Time series of pollutants across the pre- (A,C,E,G,I) and post – monsoon (B,D,F,H,J) campaigns. NO concentrations were filters to below 60 ppbv, due to a large enhancement in concentrations at the start of the campaign. The full time series is shown in figure 4.5. NO, NO ₂ , O ₃ and HR-AMS – SO ₄ ²⁻ were averaged to 15 minutes. PM _{2.5} was measured hourly. | 126 |
| 4.4 | Diurnal variations of pollutants during pre- (left) and post- (right) monsoon. | 127 |
| 4.5 | Full time series of NO concentrations during the pre-monsoon campaign. | 128 |
| 4.6 | Diurnal variations (A-D) and time series (E-H) of modelled OH and NO ₃ concentrations across the pre- (A,C,E,G) and post-monsoon (B,D,F,H). The band represents the 95 % confidence interval. The red line represents midnight (00:00) at each day. | 129 |
| 4.7 | Time series across the pre- (left) and post-monsoon (right) campaigns of Isoprene (A,B), total quantified potential OSi marker concentrations (C, D), total quantified potential NOSi marker concentrations (E, F) and inorganic sulfate concentrations (G,H). The horizontal lines represent the length of time the filter sample was collected for. | 130 |
| 4.8 | Correlations between isoprene and butadiene and diurnal variations of isoprene across pre– (A, B) and post-monsoon (C, D) campaigns. The plots are coloured by the time of day to highlight the dual biogenic/anthropogenic sources of isoprene. | 131 |
| 4.9 | Time series across the pre- (left) and post-monsoon (right) campaigns of α-pinene (A,B),limonene (C,D), total quantified potential OSMT marker concentrations (E, F), andtotal quantified potential NOSMT marker concentrations (G, H). | 133 |
| 4.10 | Correlation between measured monoterpenes and CO across the pre-monsoon (A,B) and post-monsoon (bottom). | 135 |

| | | |
|------|---|-----|
| 4.11 | Diurnal variations of quantified BSOA classes (OSi, NOSi, OS _{MT} , NOS _{MT}) across the pre- (left) and post-monsoon (right) campaigns. The lower and upper part of the box representing the 25 th and 75 th percentiles, with the upper and lower lines extending no further than 1.5 times the interquartile range of the highest and lowest values within the hinge respectively. All data points used for the boxplots are also plotted, coloured by the average PBLH for the filter collection period. | 139 |
| 5.1 | Comparison between measured logRIE and predicted logRIE produced by a linear model. The solid black line is 1:1 i.e would represent perfect predictions of the measured values. The blue dotted lines represent 2 x RMSE from the 1:1 line. The grey vertical lines represent predicted logRIE ± RMSE. | 160 |
| 5.2 | Concentration comparison for the 9 BSOA species identified in the ambient samples, quantified by <i>cis</i> -pinonic acid, and then “corrected” using the predicted RIE factors. The concentration of <i>cis</i> -pinonic acid stayed the same due to having an RIE factor of 1 (logRIE = 0). | 166 |
| 6.1 | Map of filter sampling sites with pie charts highlighting the targeted BSOA acid mass composition. | 185 |
| 6.2 | corPlot of BSOA acid markers identified in 30 % of the total samples across the 6 campaigns, alongside temperature (TEMP), ozone (O ₃), NO ₂ , NO and relative humidity (RH). | 187 |

| | | |
|-----|---|-----|
| 6.6 | Time series and diurnal variations of the sum of the β -caryophyllene derived acid markers: Bcary_197 (3,3-dimethyl-2-(3-oxobutyl)cyclobutanecarboxylic acid, $C_{11}H_{18}O_3$), β -caryophyllinic acid (Bcary_253b, $C_{14}H_{22}O_4$) and Bcary_255a (4-(2-(2-carboxyethyl)-3,3-dimethylcyclobutyl)-4-oxobutanoic acid, $C_{13}H_{20}O_5$) across the Beijing, Guangzhou and Delhi campaigns. The lower and upper part of the box represents the 25 th and 75 th percentiles, with the upper and lower lines extending no further than 1.5 * the interquartile range of the highest and lowest values within the line respectively. | 201 |
| 6.7 | Diurnal variations of measured ozone concentrations across the Beijing, Delhi and Guangzhou campaigns. | 203 |
| 6.8 | Measured ozone concentrations versus temperature for the six campaigns. Ozone concentrations and temperature were averaged to 1 hour. A- Beijing Summer, B- Beijing winter, C- Pre-monsoon Delhi, D- Post-monsoon Delhi, E - Guangzhou Summer, F- Guangzhou Winter. | 204 |
| 6.9 | A,B,C – Correlation between total BSOA acid concentrations and binned ozone concentrations (bin size = 20 ppbv). D,E,F – Correlations between total BSOA acid concentrations and binned temperature (bin size = 10 °C). The boxplots represent the mean (horizontal middle line) with the lower and upper hinges corresponding to the 25 th and 75 th percentiles respectively. The upper and lower whiskers extend to the larger or smallest value no further than 1.5 * IQR from the respective hinge. G, H, I - Correlation between BSOA acid concentrations and temperature, coloured by campaign. | 205 |

List of Tables

| | | |
|-----|--|----|
| 2.1 | Anthropogenic pollutants measured during the sampling period analysed in this study. | 49 |
| 2.2 | Molecular formulas, negative ion masses, retention times (RT), time weighted means (ng m^{-3}) for the entire sampling period and original reference to where the tracer was found of each proposed iSOA tracer. BD = Below detection. The estimated uncertainties calculated as 60 %, accounting for the use of the matrix correction factors. | 51 |
| 2.3 | 2-MT-OS concentrations (ppm) for three samples (144, 204, 208) calculated from standard addition, 2-MG-OS and 2-MT-OS external calibrations. | 54 |
| 2.4 | 2-MG-OS concentrations (ppm) for three samples (144, 204, 208) calculated from standard addition, 2-MG-OS and 2-MT-OS external calibrations. | 55 |
| 2.5 | Comparison of concentrations of iSOA tracer concentrations and ratios in previous studies in the Amazon, SE USA and China. *Selected sample not an average concentration. Beijing (2017) values are taken from this study. | 57 |

| | | |
|-----|--|----|
| 2.6 | Isoprene CHO tracer concentrations measured via GC-MS using 24-hour samples between 22/05/2017 and 22/06/2017. 2-MTs is equal to the sum of 2-methylthreitol and 2-methylerythritol and the C5-alkene triols is equal to the sum of cis-2-methyl-1,3,4-trihydroxy-1-butene, 3-methyl-2,3,4-trihydroxy-1-butene and trans-2-methyl-1,3,4-trihydroxy-1-butene. | 76 |
| 3.1 | Matrix effect analysis results from 8 filter samples on three different organosulfate standards (CAM-OS – Camphorsulfonic acid, MG-OS – 2-methyl glyceric acid organosulfate, MT-OS – 2-methyl tetrol organosulfate). Alongside PM _{2.5} , NO ₃ and SO ₄ ²⁻ concentrations. The values in bold are the average ratios between a clean matrix and an ambient sample matrix. | 84 |
| 3.2 | Pollutant mean, median (Med), standard deviation (SD) and maximum values across the summer and winter campaigns. | 86 |
| 3.3 | Molecular formulae, retention times and time weighted means (ng m ⁻³) of nitrooxy organosulfates (NOS) and organosulfates (OS) from monoterpenes (MT) and isoprene (i) observed across summer and winter campaigns in Guangzhou. OSi species in bold had R correlation coefficients of less than 0.6 towards 2-MT-OS or 2-MG-OS and were therefore not used in the analysis of OSi formation. Isoprene OS is the sum of all potential isoprene OS species quantified in this study, while OSi is the sum of all isoprene OS species which had an R of greater than 0.6 towards either 2-Mt-OS or 2-MG-OS. Total BSOA is the sum of all quantified markers in this study. . . | 98 |

| | | |
|-----|---|-----|
| 4.1 | Matrix effect analysis results from 5 filter samples on three different organosulfate standards (CAM-OS – Camphorsulfonic acid, MG-OS – 2-methyl glyceric acid organosulfate, MT-OS – 2-methyl tetrol organosulfate). Alongside $PM_{2.5}$ and SO_4^{2-} concentrations. The values in bold are the average ratios between a clean matrix and an ambient sample matrix. | 120 |
| 4.2 | Average pollutant and meteorological values across the pre- and post-monsoon campaigns. | 122 |
| 4.3 | Molecular formulae, retention times and time weighted mean \pm SD ($ng\ m^{-3}$) of nitrooxy organosulfates (NOS) and organosulfates (OS) from monoterpenes (MT) and isoprene (i) observed across pre and post-monsoon campaigns in Delhi. | 136 |
| 4.4 | Comparison of $C_{10}H_{17}NO_7S$ concentrations across different locations. Locations and concentrations in bold were quantified by authentic standards. | 143 |
| 5.1 | Measured ($\log RIE_M$) and predicted ($\log RIE_P$) $\log RIE$ values for the 89 standards used for the development of the random forest model. Predicted $\log RIE$ values have an error range of ± 0.59 . Alongside their molecular formulas, retention times (RT) and the dominant functionality. | 152 |
| 5.2 | Contains descriptors obtained from Chemdes which had a R correlation greater than 0.3 to the $\log RIE$ values of the standards in Table 5.1. Package from which the descriptor as obtained and the description of the descriptor. | 159 |

| | | |
|-----|---|-----|
| 5.3 | Compound tag and reference predicted RIE factors and SMILE formulas for the structures of the previously proposed BSOA markers. Based on the RMSE uncertainty of 0.59, the predicted RIE values have an uncertainty range, as shown by the minimum and maximum RIE values. *Markers that have been structurally confirmed by comparison to an authentic standard or MS ² data in the BSOA chamber samples. | 162 |
| 5.4 | Comparison between marker concentrations quantified by a standard <i>cis</i> -pinonic acid calibration (PA) and corrected by the predicted RIE factors in Table 5.3. | 167 |
| 5.5 | Comparison of average aerosol metrics weighted by the number of markers, <i>cis</i> -pinonic acid calibration derived concentrations and RIE corrected concentrations. | 168 |
| 6.1 | Measured matrix effects of 5 organic acids with their respective retention times (RT) across 23 ambient samples collected across the Delhi, Guangzhou and Beijing campaigns. A value of 1 represents no matrix effect, below 1 is a matrix suppression and above 1 a matrix enhancement. Campaign mean \pm SD and overall mean \pm SD for each sampling site and all samples are shown in bold. . . | 178 |
| 6.2 | Mean \pm SD values for gas phase pollutants, inorganic ions and meteorological parameters across the 6 campaigns. | 180 |
| 6.3 | BSOA acid markers identified in chamber samples and screened for in ambient samples. | 182 |
| 6.4 | Mean \pm SD for the α -pinene derived organic acid markers identified across the Beijing, Guangzhou and Delhi campaigns with the number of observations in each campaign (n =). <i>Pinene</i> is abbreviated to <i>P</i> in the marker names. | 191 |
| 6.5 | Comparison of <i>cis</i> -pinonic and pinic acid concentrations between those measured in this study and previously. TS = This study . . | 192 |

| | | |
|-----|--|-----|
| 6.6 | Mean \pm SD for the Limonene derived acid markers identified across the Beijing, Guangzhou and Delhi campaigns with the number of observations in each campaign (n =). <i>Limonene</i> is abbreviated to <i>Lim</i> in the marker names. | 196 |
| 6.7 | Mean \pm SD for the β -caryophyllene derived acid markers identified across the Beijing, Guangzhou and Delhi campaigns with the number of observations in each campaign (n =). <i>β-caryophyllene</i> is abbreviated to <i>Bcary</i> in the marker names. | 199 |
| 6.8 | Comparison of β -caryophylinic acid concentrations between those measured in this study and previously. TS = This study | 200 |

List of Abbreviations

- 2-MG-OS** — 2-methylglyceric acid organosulfate
- 2-MT-OS** — 2-methyltetrol organosulfate
- AMS** — Aerosol Mass Spectrometry
- ASOA** — Anthropogenic Secondary Organic Aerosol
- BBCEAS** — Broadband Cavity Enhanced Absorption Spectroscopy
- BSOA** — Biogenic Secondary Organic Aerosol
- BVOC** — Biogenic Volatile Organic Compound
- CHOS** — Aerosol species containing at least one carbon, hydrogen, oxygen and sulfur atom
- CIMS** — Chemical Ionisation Mass Spectrometry
- DBE** — Double Bond Equivalent
- DC-GC-FID** — Dual Channel Gas Chromatography with Flame Ionisation Detector
- EESI** — Extractive Electrospray Ionisation
- FAGE** — Fluorescence Assay by Gas Expansion
- FIGAERO** — Filter Inlet for Gases and Aerosol
- GLV** — Green Leaf Volatiles
- HESI** — Heated Electrospray Ionisation
- HILIC** — Hydrophobic Interaction Chromatography
- HMML** — Hydroxy-Methyl-Methyl-alpha-Lactone
- HOM** — Highly Oxidised Molecule

HO_x — Sum of OH and HO₂

HRMS — High Resolution Mass Spectrometry

ICN — Isoprene Carbonyl Nitrate

IEPOX — Isoprene Epoxydiol

IHN — Isoprene Hydroxy Nitrates

INHE — Isoprene Nitrooxy Hydroepoxide

INP — Isoprene Nitrooxy Hydroperoxide

iSOA — Isoprene derived Secondary Organic Aerosol

ISOPOOH — Isoprene Hydroxy-Peroxides

MACR — Methacrolein

MAE — Methacrylic Acid Epoxide

ME — Matrix Effect

MVK — Methyl Vinyl Ketone

NO — Nitrogen Oxide

NO₂ — Nitrogen Dioxide

NOS — Nitrooxy Organosulfate

NOS_i — Isoprene derived Nitrooxy Organosulfate

NOS_{MT} — Monoterpene derived Nitrooxy Organosulfate

NO_x — Sum of NO and NO₂

NPF — New Particle Formation

OA — Organic Aerosol

OOA — Oxidised Organic Aerosol

OS — Organosulfate

OSi — Isoprene derived Organosulfate

OS_{MT} — Monoterpene derived Organosulfate

PAH — Poly Aromatic Hydrocarbon

PBLH — Planetary Boundary Layer Height

PM₁ — Aerosol with an aerodynamic diameter of less than 1 μm

PM_{2.5} — Aerosol with an aerodynamic diameter of less than 2.5 μm

PM₁₀ — Aerosol with an aerodynamic diameter of less than 10 μm

RH — Relative Humidity

RIE — Relative Ionisation Efficiency

RMSE — Root Mean Squared Error

RT — Retention Time

SD — Standard Deviation

SEUS — South East United States

SO₂ — Sulfur Dioxide

SOA — Secondary Organic Aerosol

SOAS — Southern Oxidant and Aerosol Study

UHPLC — Ultra High Pressure Liquid Chromatography

UHRMS — Ultra High Resolution Mass Spectrometry

VBS — Volatility Basis Set

VOC — Volatile Organic Compound

Acknowledgements

I never thought I would be where I am today, but I am extremely grateful to be. Attending the University of York and subsequently undertaking this PhD have been the best decisions I could have made. The last eight years have flown by and I have enjoyed every second of it.

I would firstly like to thank my supervisors Jacqui and Andrew for giving me the opportunities that they have, and for their patience and encouragement throughout. Thank you to everyone in the Hamilton and Rickard groups and everyone in WACL, both past and present, for making this experience even more enjoyable. A big shout out to Jack, David, Ryan, Luke and Jordan who have listened to all the trials and tribulations throughout my PhD, and continued to encourage me through endless amounts of pub trips. A special thank you to Jack, who's patience, encouragement and friendship means the world and I couldn't have done it without you. Thank you also to Jonny, who as an unexpected shower buddy on a summer school trip has become my 2nd dad and unofficial academic mentor. Thank you also to Ryan, Ben, Charlie and Kieran for your support and friendship throughout my life, I wouldn't be the person I am today without you.

This would all not have been possible without my partner, Jess. Thank you for listening, reassuring and motivating me through the struggles and celebrating with me through the highs. Jess, thank you for your love and partnership over the last four years, here is to many more years.

Finally, I would like to thank my family, without who, I wouldn't be where I am today, and I will be forever grateful for what you have given me and the sacrifices you have made for it.

Author's declaration

I declare that this thesis is a presentation of original work and I am the sole author. This work has not previously been presented for an award at this, or any other, University. All sources are acknowledged as References. Some of the contained work is based on peer reviewed publications with myself as the lead or co-author, the details of which are provided below:

- Bryant, D.J. et al. Strong anthropogenic control of secondary organic aerosol formation from isoprene in Beijing. *Atmospheric Chemistry and Physics*, 20(12):7531–7552, 6 2020.
- Hamilton, J.F., Bryant, D. J., et al. Key Role of NO₃ Radicals in the Production of Isoprene Nitrates and Nitrooxyorganosulfates in Beijing. *Environmental Science and Technology*, 55(2):842–853, 1 2021.
- Bryant, D. J. et al. Importance of Oxidants and Temperature in the Formation of Biogenic Organosulfates and Nitrooxy Organosulfates, *ACS Earth and Space Chemistry*, 5, 9, 2291-2306, 2021
- Bryant, D.J. et al. Biogenic and anthropogenic sources of isoprene and monoterpenes and their secondary organic aerosol in Delhi, India, to be submitted.
- Bryant, D.J. et al. Overcoming the lack of authentic standards for the quantification of biogenic secondary organic aerosol markers, to be submitted.

Chapter 1

Introduction

1.1 Motivation

Aerosols are solid or liquid particles suspended in the air. They are directly emitted to the atmosphere(primary), or formed in the atmosphere through chemical pathways via the oxidation of gases from both biogenic and anthropogenic sources (secondary).[1] Once aerosols are emitted or formed in the atmosphere, their chemical composition and size can change, through atmospheric processes such as oxidation, evaporation and gas to particle phase partitioning. Aerosol can be removed from the atmosphere via deposition onto a surface (dry deposition) or through precipitation (wet deposition). The source of aerosol forming species can be both natural and anthropogenic in nature, with recent research showing that biogenic aerosol formation can be significantly enhanced by anthropogenic activities. [1, 2]

High aerosol concentrations play an important role in the Earths climate[3–5], while having detrimental effects on the environment, air quality and human health[6]. Aerosol can affect the climate through both direct and indirect effects on radiative forcing, including the absorption and scattering of radiation and changing cloud properties.[7] The global effect of aerosol on radiative forcing is uncertain, but evidence suggests high concentrations of aerosol equate overall to a cooling effect on the atmosphere, due to increased cloud albedo and coverage.[7] Aerosol can also have a detrimental effect on both anthropogenic and natural environments. Recent studies have shown the effect of aerosol on cultural heritage sites within urban areas, through the degradation of materials and accumulation of pollutants on surfaces.[8–10] High aerosol concentrations can change lake acidity, in turn affecting water quality for human consumption [11, 12], effect plant growth and crop yields due to changing rainfall patterns,[13] and change animal behaviour[14].

Air pollution is considered by the World Health Organisation (WHO) as the greatest environmental threat to human health, with 9 out of 10 people breathing polluted air every day in 2019 and accounting for ca. 11.6 % of global premature deaths.[15] Respiratory illness, cardiovascular disease and cancer are the key causes

of premature mortality linked to poor air pollution.[6, 16–19] It is estimated that 4.2 million premature deaths occur a year globally and disproportionately affects low- and middle-income countries, who account for 92 % of the world’s pollution related deaths.[20, 21] Aerosol or fine particulate matter for regulatory purposes is divided into three sub categories, based on it’s aerodynamic diameter PM_{10} ($<10\ \mu\text{m}$), $PM_{2.5}$ ($<2.5\ \mu\text{m}$) and PM_1 ($<1\ \mu\text{m}$). $PM_{2.5}$ and PM_1 are able to get deep into the lungs, transporting carcinogenic species. Ultrafine species ($PM_{<1}$) can enter cells and the blood stream effecting cognitive abilities and implicated in Alzheimer’s disease.[22–25] Due to these health implications, policy mainly focuses on $PM_{2.5}$. All PM is damaging to health, but not all particles and constituents are equally toxic, with different sources presenting different toxicities based on their composition. [26]

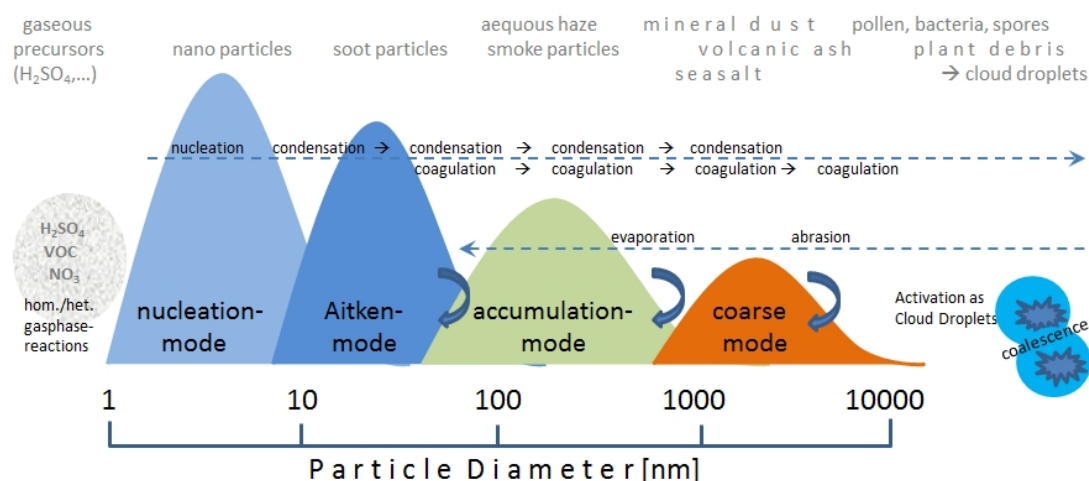


Figure 1.1: Particle size distributions and general sources. Taken from https://www.dwd.de/EN/research/observing_atmosphere/composition_atmosphere/aerosol/cont_nav/particle_size_distribution_node.html%7D

Secondary organic aerosol (SOA), formed from the oxidation of volatile organic compounds (VOCs), are a key class of aerosol. Owing to the wide range of VOCs and their respective reactivities, SOA represents an extremely complex mix of multi-functional compounds. As such, SOA formation and its respective composition in the real atmosphere remains uncertain due to the analytical challenges presented by the complexity of the system. Biogenic VOC (BVOC)

emissions outweigh those of anthropogenic emissions around 8:1 [27], and represent a complex mix of reactive gases, with differing volatilities and functionalities. The emission and composition of BVOCs in a given environment, is dependent on the number of plants, species and geographical location. Climate change is expected to have a large effect on BVOC composition and emission rates, due to more extreme weather events and increased temperature, changes in plant species and land cover, which in turn could increase biogenic SOA (BSOA) concentrations. As such BSOA composition is highly variable based on the emissions of BVOCs in a given environment, but BSOA formation has also been shown to be greatly influenced by anthropogenic pollutants such as sulfate, and NO_x , with urban BSOA composition greatly differing from cleaner environments. Due to increasing urbanisation, more and more people are living in urban areas, with high levels of air pollution, especially in developing countries.[28–32] While BSOA has been extensively studied in aerosol chamber studies, fewer studies have investigated BSOA formation in the real atmosphere, especially in highly polluted urban areas. Previous studies investigating BSOA in the real atmosphere have focused on isoprene SOA (iSOA) formation in the south east United States (SEUS), where high isoprene emissions lead to high iSOA concentrations[33–38] or monoterpene SOA in clean boreal forested areas across the northern hemisphere[39–41]. As such, we have a limited understanding of the concentrations and composition of BSOA across different environments especially highly polluted cities in developing countries. With limited studies having investigated the toxicity of BSOA, the effect of BSOA on human health is highly uncertain. [42–44]

1.2 Tropospheric Aerosol – composition and sources

Different sources dominate the different PM size ranges, with larger PM_{10} particles having a higher contribution of primary species, such as sea salt, sand and mineral

dusts as shown in 1.1.[45] Smaller size ranges are dominated by secondary organic and inorganic species, with organics generally being the dominant class worldwide, as shown in Figure 1.2.[29, 46]

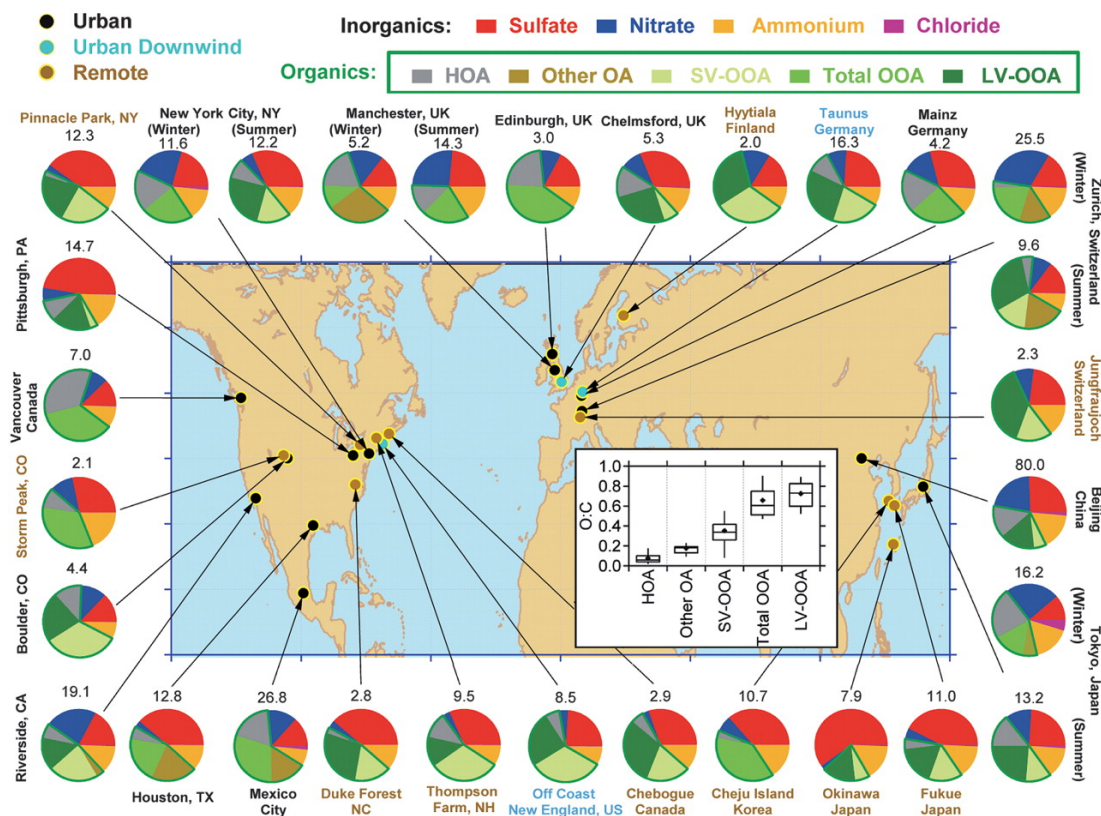


Figure 1.2: PM_{2.5} composition across selected sites across the world, taken from Jimenez et al., 2009. [47]

Organic compounds contribute a significant fraction (20-90 %) towards the total mass of tropospheric PM_{2.5}, with approximately 300 Tg / yr of OA emitted to or formed in the atmosphere.[46, 48, 49] There are many sources of organic compounds found in PM_{2.5}, including primary emissions (e.g. primary OA, engine exhaust and biomass burning) or formed in the atmosphere through gas-particle partitioning processes to form SOA, which often accounts for a large, sometimes dominant fraction of organic mass found in tropospheric PM_{2.5}. [29] The composition of SOA is highly complex and variable, in part this is due to the number of VOC precursors which is estimated to be on the order of 1000's, with the oxidation of each VOC producing its own unique SOA markers, which can

then undergo further transformations.[50]

SOA can be formed from the oxidation of both anthropogenic and biogenic VOCs, although many VOCs have mixed sources. Anthropogenic SOA (ASOA) is formed from the oxidation of VOCs emitted from industrial combustion sources, vehicle emissions, solvent and paint usage and include long chain aliphatics, poly aromatic hydrocarbons (PAHs) and other aromatic compounds. Biomass and domestic fuel burning can lead to the formation of phenolic compounds, furans as well as compounds more commonly referred to as BSOA. $C_5 - C_{15}$ terpenoid compounds alongside a range of other BVOCs from a wide range of vegetation can lead to the formation of BSOA (discussed in more detail in later chapters).

Global SOA production estimates have been made by two different approaches: bottom up and top down. A bottom up estimation uses known or modelled VOC precursor fluxes combined with SOA yields from oxidation chamber experiments in global models giving a global SOA production. Top down estimation constrains to the eventual fate of known precursor emissions to estimate SOA production.[1] The two approaches give very different results. Bottom up approaches estimating global SOA production range from 12 to 480 Tg yr⁻¹[49, 51–55], while top down estimates give an uncertain range of 50-1820 Tg yr⁻¹(Goldstein and Galbally, 2007)[50, 56, 57]. Using bottom up approaches, global production of BSOA is estimated at 14.9 - 55 Tg yr⁻¹, compared to 1.6-24.6 Tg yr⁻¹ for anthropogenic SOA.[51] Figure 1.3 gives an estimated breakdown of the sources of aerosol to the atmosphere, and the estimated losses and processes, and highlights the large contribution from BSOA.

1.3 Emission of Biogenic Volatile Organic Compounds

Globally, total BVOC emissions are estimated to be 1000 Tg yr⁻¹[27], roughly 8 times higher than those from anthropogenic sources(127 Tg yr⁻¹)[58].However

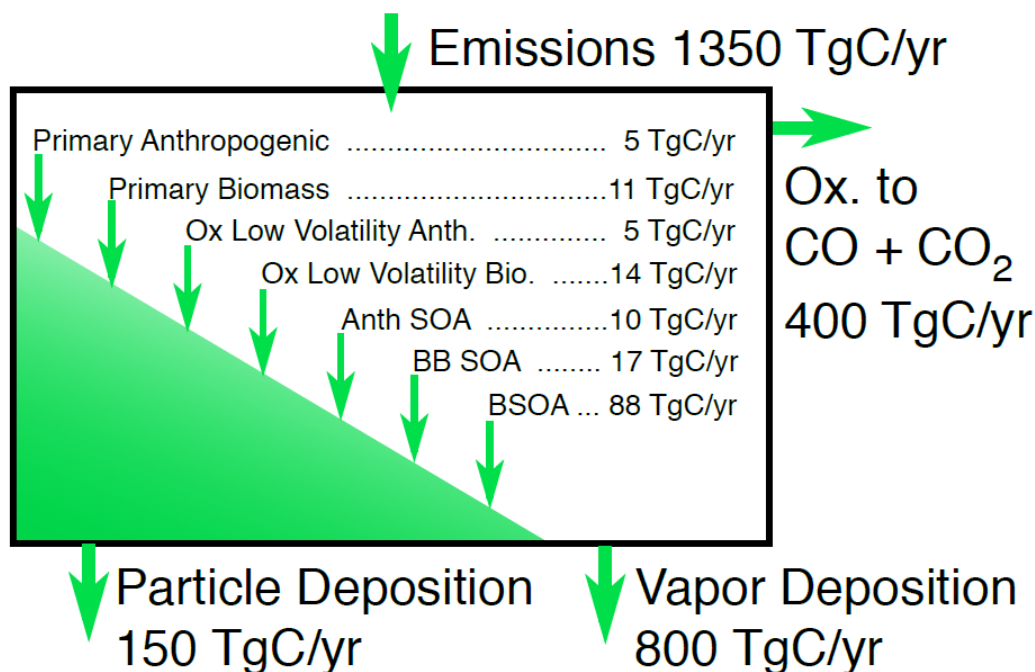


Figure 1.3: Global flux estimates of VOC and OA, taken from Hallquist et al., 2009. [1]

due to the distribution of anthropogenic sources, anthropogenic VOC's generally dominate in urban environments. BVOCs cover a diverse range of compounds over a broad range of reactivities and functionalities. Terpenoids are the most abundant BVOC class, estimated to consist mainly of isoprene (C_5H_8 , 50 %), monoterpenes ($C_{10}H_{16}$, 15%) such as limonene and α/β -pinene as well as sesquiterpenes ($C_{15}H_{24}$ 3%) such as β -caryophyllene. Isoprene is the dominant BVOC in terms of emissions to the atmosphere, with estimated global emissions of 412-601 Tg yr⁻¹, compared to monoterpene emissions of 33-480 Tg yr⁻¹. [27]

As shown in figure 1.4, BVOC emissions are highest around the equator, due to large fluxes from rainforests, however moderate emissions are observed across boreal forests during the norther hemisphere summer.

Around 1700 BVOCs have been identified from more than 90 plant families. BVOCs are released by almost any kind of vegetation and are involved in a wide range of ecological functions such as defence, pollinator attraction, communication and environmental stress adaptation. [59] BVOC emissions depend strongly on the

species of plant, which different species evolving different chemical solutions for the same challenges.[60] Terpenes such as α -pinene and limonene are the largest and most diverse group of BVOCs[61] which are used to attract organisms such as pollinators[62–64], repel potential herbivores[65, 66] and protect themselves against pathogens[67]. While Green leaf volatiles (GLVs) which are C₆ aldehydes, alcohols and their esters are released by nearly all plants upon damage[68, 69], or when infested[70, 71]. GLVs have been shown to be important communicators between plants, either activating nearby plant defences to stresses or prime for faster response.[72, 73] Studies have shown that isoprene is released as a response to high temperatures[74], with high isoprene emissions measured during heat waves.[75] The release of isoprene is hypothesised to be linked to an enhanced tolerance of photosynthetic processes to high temperatures.[76]

Higher global temperatures and increased intensity and frequency of heatwaves are expected due to climate change which could increase localised isoprene emissions in the future.[77] While environmental changes will change the geographical distribution of isoprene emissions, but is not expected to change the overall total flux.[78, 79] Over the 21st century it has been modelled that global isoprene emissions are likely to remain stable or decrease, with the main driver being anthropogenic land use changes.[78]

Due to the expansion of agriculture and pastures in response to rapidly growing populations and higher consumption rates, humans have now converted around a third of the global land surface from natural vegetation in just six decades (1960 - 2019).[80] Crops typically have low isoprene emission rates, compared to natural landscapes, which will in turn lead to lower global isoprene emissions.[81] However global efforts for afforestation both regenerating forests lost to agriculture but also the greening of cities may increase BVOC emissions in some areas.[82] Global demand for specific crops such as oil palm may also have an effect on isoprene emissions, owing to the extremely high isoprene emissions, which exceed those of natural forests cut down for its production.[83]

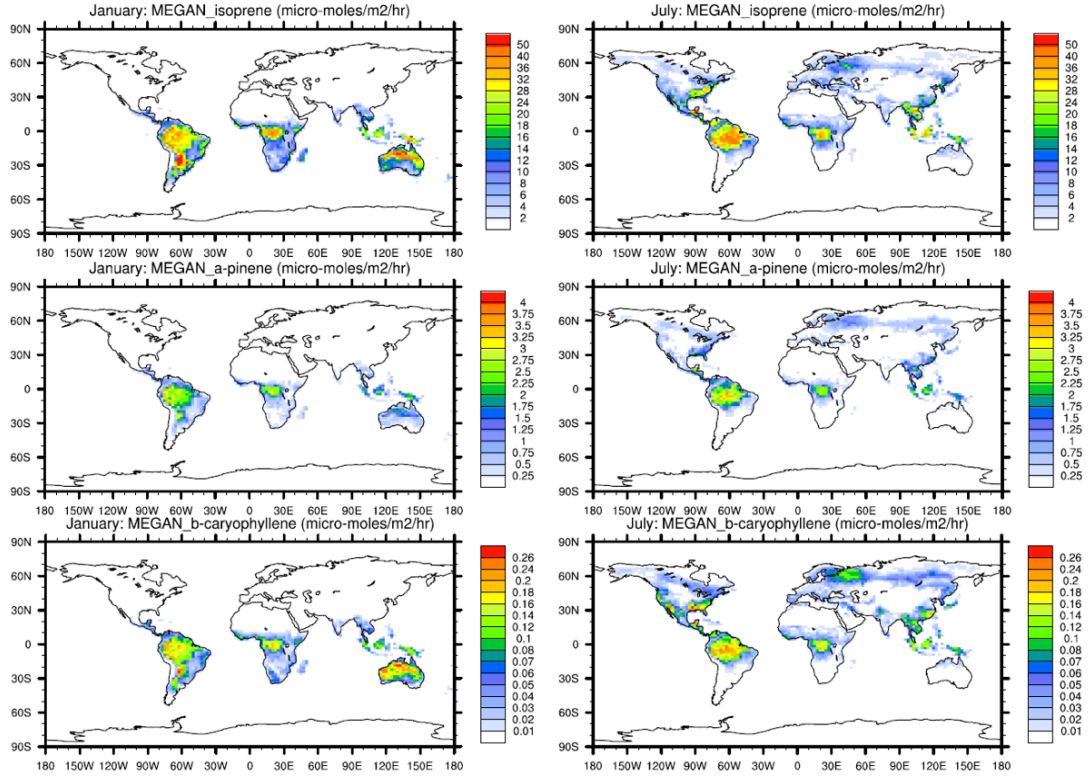


Figure 1.4: January and July 2000 global emissions of isoprene, α -pinene and β -caryophyllene simulated with MEGAN 2.1, taken from Guenther et al., 2012.

1.4 Secondary Organic Aerosol

Gas-phase VOCs can undergo oxidation to form species with lower volatilities, some of which are sufficiently low to partition into the aerosol phase, through either new particle formation (NPF) or condensation onto pre-existing aerosol. [1] A species ability to partition into the aerosol phase, forming SOA, can be described by gas-particle transition theory introduced by Pankow., 1994 and Odum., 1996. The partitioning is based on the absorptive partitioning coefficient, K_p or its inverse, the saturation vapour concentration C_i^* (equation 1.1).[84–87]

$$\frac{C_i^p}{C_i^g} = K_{p,i} C_{OA} = \frac{C_{OA}}{C_i^*} \quad (1.1)$$

Where C_i^g is the mass concentration of species i per unit volume of air ($\mu\text{g m}^{-3}$) in the gas phase, C_i^p is the mass concentration per unit volume of air in the aerosol

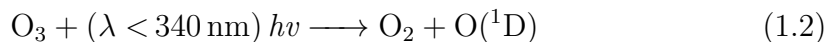
phase ($\mu\text{g m}^{-3}$), and C_{OA} is the mass concentration per unit volume of air of the total absorbing organic particle mass ($\mu\text{g m}^{-3}$). The lower the C_i^* of a species, the lower the volatility, which increases the extent to which it will partition. C_i^* tends to decrease with increasing oxidation, with species with the same carbon number having lower C_i^* values with increasing numbers of oxygenated functional groups (-OH, -OOH, C(O)OH).[86] Understanding the volatilities of all SOA species is not practical, due to the number of species. As such, volatility measurements of select functionalities have been made, and the volatility basis set (VBS) approach developed.[85] The VBS is based on grouping compounds with fixed C_i^* values, each separated by one order of magnitude of $\log(C_i^*)$. These range from VOCs, which exist almost entirely in the gas phase, having not undergone oxidation, through to extremely low volatility organic compounds (ELVOC), which exist almost entirely in the particulate phase.[85, 88–90] Gas-particle transitions usually occurs for species condensing onto the surface of pre-existing aerosols, leading to aerosol growth, although NPF can also occur. NPF has been observed across several environments, including urban and clean sites.[91, 92] NPF occurs in two stages, the first step involves the formation of a critical nucleus during the gas-particle transitioning of species with sufficiently low volatility, followed by growth by condensation. Sulfuric acid is considered to be the most prevalent nucleating species because of its low vapour pressure, while highly oxidised molecules (HOMs) which form from extensive auto-oxidation of VOCs have also been observed to undergo NPF. [93–95]

1.5 Tropospheric VOC oxidants

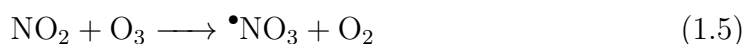
VOCs undergo oxidation in the atmosphere, with oxidation initiated via hydroxyl radicals (OH), ozone (O_3) and nitrate radicals (NO_3).[96, 97] The concentrations of the oxidants vary by time of day, season and location. For example, OH and O_3 are elevated during the day, while NO_3 generally becomes increasingly important at night. These oxidants alongside NO_x ($\text{NO} + \text{NO}_2$) are regulated by

the HO_x catalytic radical propagation cycle as shown in Figure 1.5.[98] Through this cycle, tropospheric NO₂ and O₃ is created through the reactions of peroxy (RO₂) and hydroperoxy (HO₂) radicals with NO. O₃ and NO₂ are important secondary pollutants as a result of this HO_x cycle, which have detrimental affects on human health. This cycle is key to photochemical smog formation, through the formation of PM from the oxidation of VOCs and NO₂ and O₃ as secondary pollutants from this process.

OH is the most important tropospheric oxidant, and is formed through the photolysis of O₃ in the presence of water vapour. O₃ photolysis occurs at wavelengths < 340 nm, resulting in the formation of a excited oxygen atom O(¹D) (1.2) and is rapidly stabilised by N₂ or O₂ (M) to O(³P) (1.3), with a relatively minor fraction of O(¹D) reacting with water vapour to produce two molar equivalents of OH radicals (1.4). OH radicals can then react with a range of VOCs to produce RO₂ radicals, which can then react with NO to form alkyl nitrates which will be discussed in more detail later. RO₂ radicals can also form HO₂ radicals through reaction with NO, in turn producing secondary NO₂ forming O₃ as shown in Figure 1.5. OH radicals can then be regenerated or recycled through HO₂ further reacting with NO, again in turn forming NO₂ and subsequently O₃. This recycled OH radical is then able to restart the radical propagation cycle. OH concentrations vary across locations, with the highest concentrations around the equator due to higher UV intensity. Urban areas report high OH concentrations due to high VOC concentrations and NO leading to rapid recycling of OH radicals as well as the photolysis of nitrous acid (HONO).[99, 100] OH can also be formed from the ozonolysis and photolysis of O₃ and carbonyls, and the photolysis of HONO (Figure 1.7), which are key night-time sources of radicals (OH, HO₂, RO₂). OH radicals can also result from the reaction of nitrate radicals with unsaturated VOCs, through the subsequent reaction of RO₂ radicals with NO.[101] Due to the recycling of OH radicals through the interactions of RO₂ and HO₂ with NO, an anthropogenic pollutant, the oxidation of biogenic VOCs by OH radicals is an example of a biogenic-anthropogenic interaction.



Nitrate radicals (NO_3) are generated throughout the day via the reaction of NO_2 and O_3 (1.5). The oxidation of VOC's via NO_3 becomes increasingly important at night due to day-time photolysis of NO_3 back to NO_x , giving a daytime lifetime of $\sim 5\text{s}$ (1.6, 1.7).[96, 102] NO_3 and NO_2 react further to establish a chemical equilibrium through the formation of N_2O_5 , which can then decompose back to NO_3 and NO_2 , or is readily taken up into aqueous inorganic aerosol or water droplets. Once in the aqueous phase, it can be hydrolysed to form nitric acid, affecting the pH of aerosol species. The reaction of NO_3 with NO (1.8) to form NO_2 is a large loss of NO_3 , especially in urban environments. However, high levels of NO titration by O_3 can lead to nitrate radical oxidation becoming more competitive during the afternoon.[103] It should be noted that due to the anthropogenic sources of NO_2 and O_3 in urban areas, reactions of BVOCs and NO_3 represent another key anthropogenic-biogenic interaction.



Tropospheric ozone is formed through the photolysis of NO_2 (1.10), followed by the reaction of $\text{O}({}^3\text{P})$ with molecular oxygen in the presence of air (M) (1.11). In polluted environments, titration of NO can occur, especially during the afternoon during peak ozone, along with peak photolysis of NO_2 (1.12).

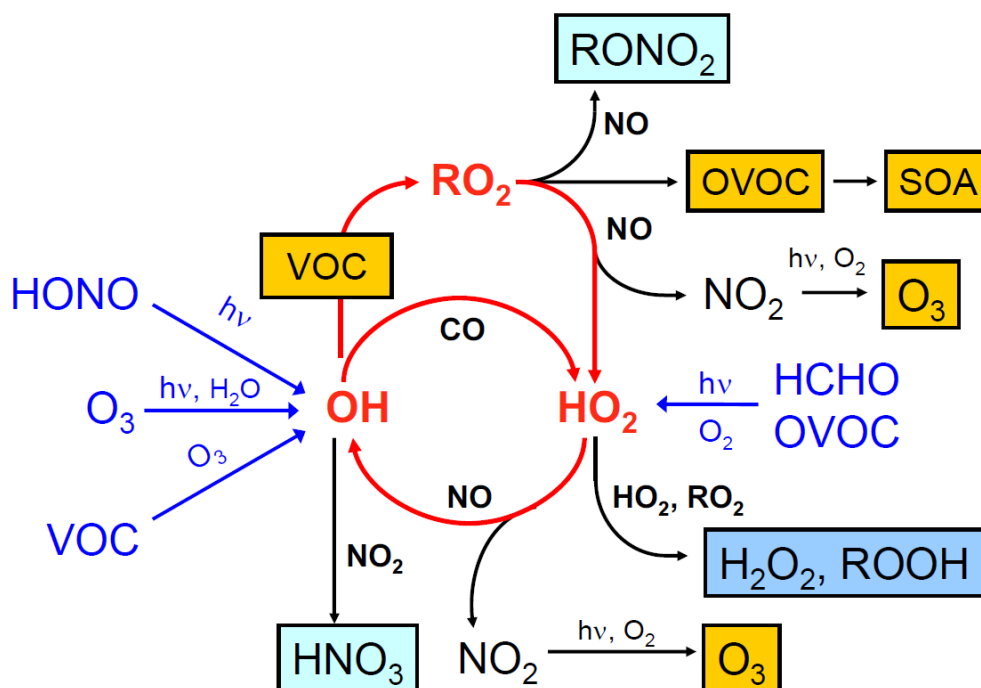
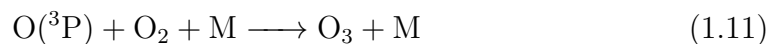


Figure 1.5: HO_x cycle taken from Lu et al.,2012. Primary radical production is shown via the blue arrows, while radical chain reactions are shown via the red arrows.

1.6 SOA Formation Pathways

SOA is formed from the oxidation of VOCs (section 1.5), and subsequent partitioning to the aerosol phase (section 1.4). Reactions of VOCs with OH and O₃ are dominant during the day, whereas at night and under some highly polluted conditions, into the afternoon and early evening, NO₃ oxidation can become more important (section 1.5).[104] VOC reactivity towards these oxidants can vary massively, based on the functionality and structure of the VOC.[96] Terpenes

which contain carbon-carbon double bonds, are reactive towards OH, NO₃ and O₃, with OH radical degradation of VOCs the most important loss route due to the fast relative rates of reaction.[105] Other atmospheric species can influence these formation pathways, for example the availability of NO can change the fate of secondary intermediates.

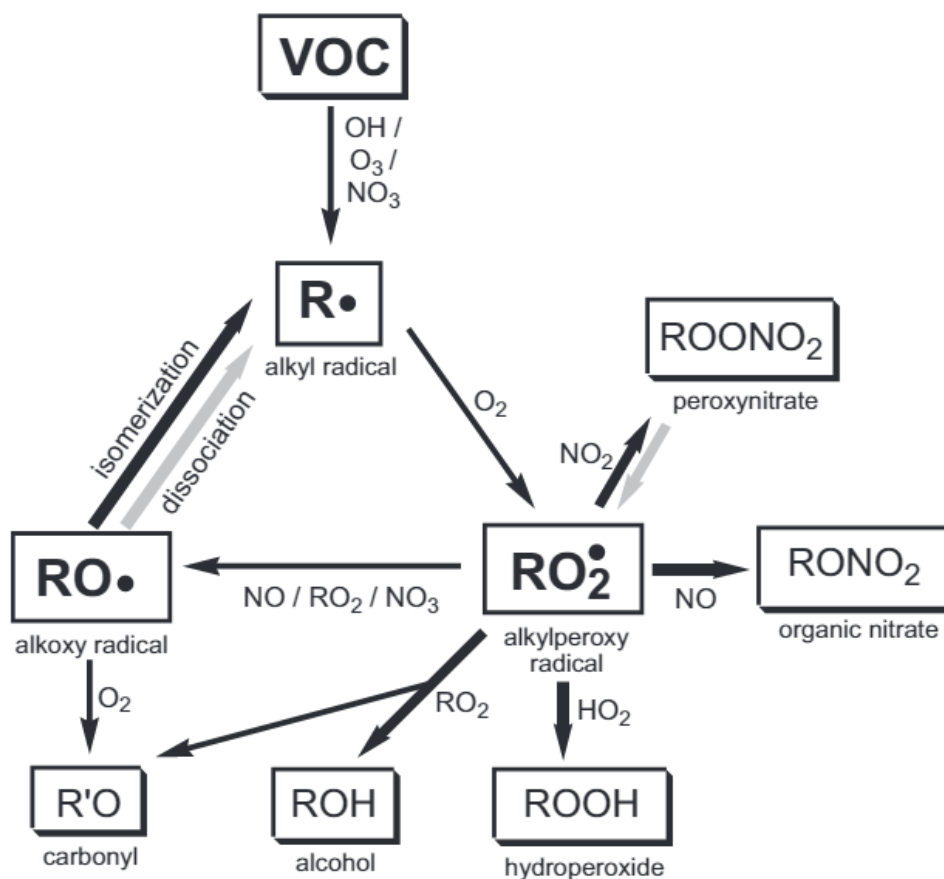


Figure 1.6: Simplified VOC degradation mechanism, taken from Kroll and Seinfeld., 2008.

The oxidation of VOCs such as terpenes, via OH radicals undergo an initial oxidation of the VOC producing an alkyl radical (figure 1.6), through the preferential addition to a C=C double bond, which is quickly stabilised via reaction with molecular oxygen to form a RO₂ radical. RO₂ radicals can then undergo several different reaction routes, based on the environment it is in. RO₂ radicals can react with HO₂ radicals under low NO conditions to form hydroperoxides or

undergo self reactions with other RO_2 radicals to form alcohols or carbonyls. NO_x plays a key role in SOA formation. RO_2 radicals can react with NO_2 under high NO_x conditions to form peroxyxynitrate species, or with NO to form an alkoxy radical or organic nitrate. Alkoxy radicals can then undergo further oxidation reactions or chain terminating reactions before partitioning to form SOA.[1, 86]

NO_3 radical oxidation of VOCs occurs in a similar way to that of OH radicals (Figure 1.6), although the nitrate group has been shown to have a key effect on reaction kinetics of the RO_2 and RO radicals. NO_3 radicals undergo a preferential addition to $\text{C}=\text{C}$ double bond, with the structure of the VOC determining the position of attachment. Under subsequent reaction with O_2 , nitrooxy peroxy radicals are formed. At night, these nitrooxy peroxy radicals are likely to undergo isomerisation or further reactions with RO_2 , HO_2 , NO_3 or OH radicals. These species can then undergo partitioning to form SOA.[106–109]

The ozonolysis of $\text{C}=\text{C}$ double bond containing species proceeds via a different route, through the formation of stabilised criegee intermediates, as shown in Figure 1.7. The $\text{C}=\text{C}$ double bond is cleaved through the reaction with ozone, to form a carbonyl and excited criegee intermediate, via the formation of a primary ozonide. This species can be both in the syn and anti- conformers, with syn being the most stable.[110] This excited criegee intermediate can then decompose via the hydroperoxide channel or be stabilised to form a stabilised criegee intermediate (SCI), which can then go on to react with water or other species. The extent of SOA formation from alkene ozonolysis is dependant on the alkenes initial structure, with ozonolysis of exo cyclic alkenes forming smaller species, which are more volatile, compared to endo alkenes which form either the same or increased carbon numbered species, leading to more SOA formation. The OH/O_3 pathways are in competition, with the oxidation route highly dependent on VOC structure and functionality.[1, 86]

More recently it was discovered that some larger VOCs such as monoterpenes, are able to rapidly generate low-volatility species [111], through a process known as auto-oxidation [112, 113]. These low-volatility species that are formed are

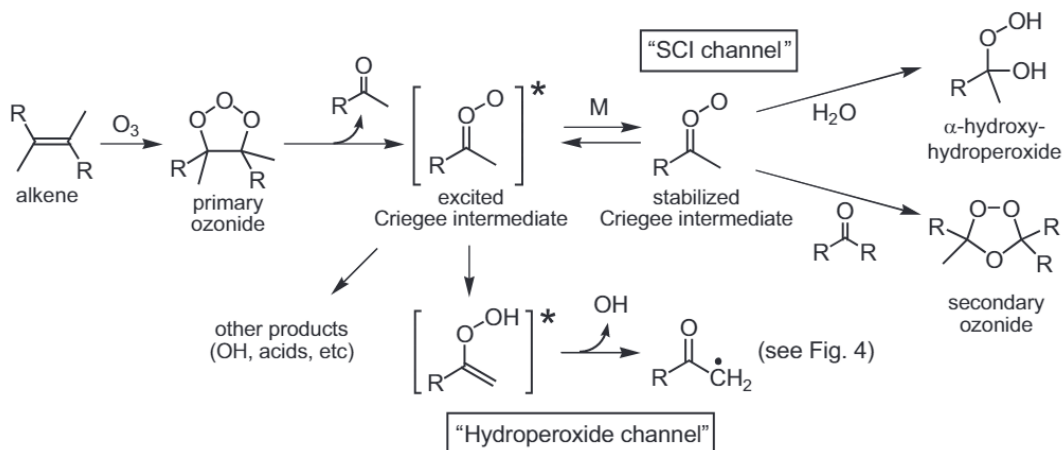


Figure 1.7: Simplified ozonolysis schematic of an alkene, taken from Kroll and Seinfeld., 2008.

known as highly oxidised molecules (HOMs) and have sufficiently low-volatility for NPF. HOM formation has been observed via photo-oxidation and ozonolysis of monoterpenes. Auto-oxidation has been suggested to proceed via H-shift isomerization in the oxygenated RO_2 species formed from the breakdown of the primary ozonide to form a HO_2 species (Figure 1.8). Subsequent loss of OH and addition of O_2 produces a more oxidised RO_2 species, which can then undergo further oxidation steps or terminating via the loss of an OH radical.[112–114] Recently, auto-oxidation reactions of α -pinene have been shown to increase with increasing NO_x , due to higher O_3 and OH concentrations, and only under extremely high NO concentrations do estimates show suppression of auto-oxidation.[115]

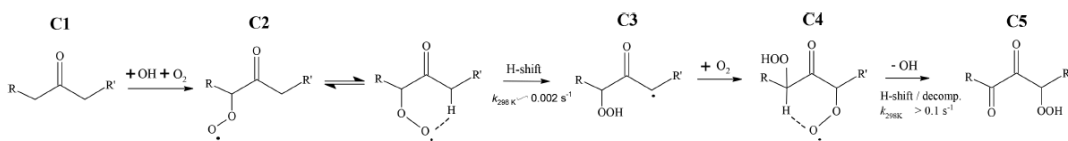


Figure 1.8: Auto-oxidation of the O_3 initiated degradation of α -pinene, taken from Iyer et al., 2021.[113]

1.6.1 Isoprene Derived SOA

Due to the large global emissions of isoprene, even small SOA formation yields can lead to significant concentrations.[116] Early isoprene studies suggested that iso-

prene was not a significant producer of SOA, due to the formation of highly volatile first generation products, with experiments showing limited aerosol growth.[117] It was over a decade before until SOA from isoprene (iSOA) was observed over the Amazon.[118] It is now widely accepted that isoprene is a significant source of OA, through the formation of a variety of multifunctional gas-phase first and second generation products, before uptake into the aerosol phase on the surface of pre-existing aerosol species.[1, 106, 119] OH radical oxidation of isoprene is the predominant oxidation reaction in the atmosphere, followed by O_2 addition, to form a RO_2 radical. Due to the conjugated nature of isoprene, a range of initial RO_2 species can be formed, with their subsequent degradation chemistry dependent on structure.[106] The fate of these RO_2 species can then proceed via a “lower” NO_x route (Figure 1.9) or “higher” NO_x route (Figure 1.10), with unique chemical markers identified to investigate each route.[120]

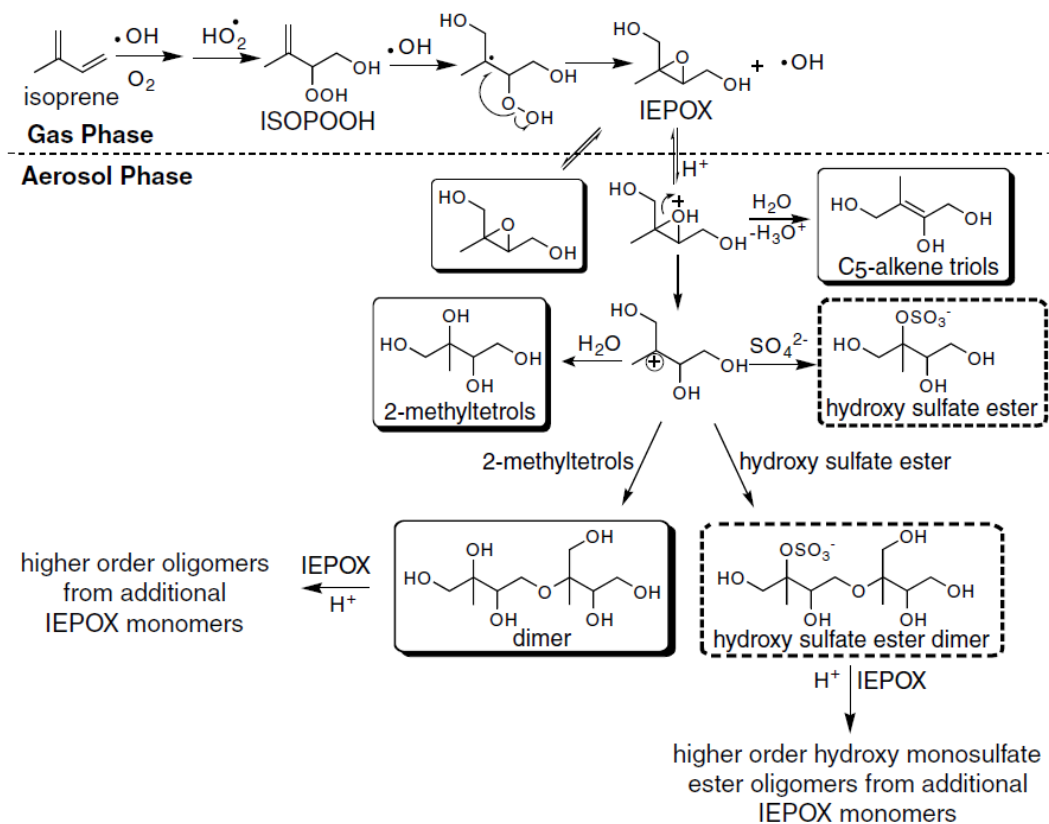


Figure 1.9: Low NO_x Isoprene OH degradation pathway, taken from Surratt et al., 2010.

Isoprene oxidation can proceed under low or high NO concentration formation pathways, depending on local atmospheric conditions. While no exact definition of low and high NO concentrations are given, higher-NO concentrations will suppress low-NO products and promote the formation of high-NO species.[121] Typical low-NO locations include remote sites such as boreal forests or rainforests, far from anthropogenic sources of NO and SO₂. [37, 122–124] Typical high-NO locations include urban areas [33, 36, 125, 126], but also locations downwind of NO sources [124]. Low-NO conditions have also been observed in urban areas due to ozone titration during the afternoon. [103]

Under the low NO route, the reaction pathway mainly proceeds via HO₂ + RO₂ producing hydroxy-hydroperoxides (ISOPOOH), while the RO₂ + RO₂ route can lead to the formation of RO, alcohols or peroxides but are suggested to be minor due to high HO₂ concentrations and faster rates of reaction between HO₂ + RO₂. [102, 106]

ISOPOOH can be oxidised again by OH to form an epoxydiol (IEPOX). [121] IEPOX has been established to undergo reactive uptake into the aerosol phase through the acid-catalysed ring opening of the epoxide, followed by the subsequent addition of a range of nucleophiles to produce different products. [127–130] Reaction with H₂O forms C₅-alkene triols and 2-methyl tetrol (2-MT), and reaction with inorganic sulfate forms a hydroxy sulfate ester (2-methyl tetrol organosulfate, 2-MT-OS). Dimer formation has also been identified, with carbocation reactions with 2-methyl tetrols and hydroxy sulfate esters, with higher order oligomers formed from additional IEPOX monomers. [127]

Under “higher” NO_x conditions, RO₂ + NO is in competition with RO₂ + HO₂, with products including mainly methyl vinyl ketone (MVK) and methacrolein (MACR), but also hydroxynitrates. [106, 119, 120] MVK and MACR have branching ratios of between 30–45 % and 20–30 %. [106] Second generation products from the OH oxidation of MACR in the presence of NO include alkoxy radicals, which are thought to be a minor route to SOA formation due to their volatile fragmentation products. [131] The dominant MACR degradation is thought to

proceed through further OH oxidation, followed by reaction with NO_2 to form methacryloylperoxynitrate (MPAN) under high NO_2/NO ratios.[127, 132] MPAN is further oxidised by OH to form hydroxymethylmethyl- α -lactone (HMML) or methacrylic acid epoxide (MAE).[127, 130] Due to the epoxide functionality of MAE, the reactive uptake mechanism is the same as that for IEPOX, via acid catalysed uptake followed by reaction with nucleophiles such as water to form 2-methyl glyceric acid (2-MG), inorganic sulfate to form 2-methyl glyceric acid organosulfate (2-MG-OS) or nitrate radicals to form organic nitrates. HMML does not require acid activation of the epoxide ring, and undergoes nucleophilic ring opening reactions. Although HMML has been suggested to form in lower yields than MAE[130], significant HMML concentrations have been observed compared to MAE.[133]

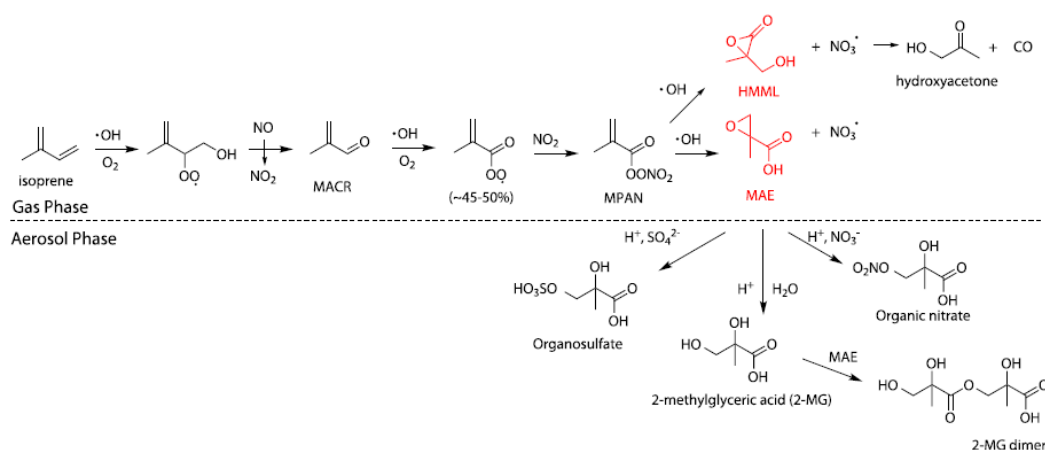


Figure 1.10: High NO Isoprene OH degradation pathway, taken from Lin et al., 2013.

Organosulfates (OS) are a key class of iSOA and the sulfated versions of 2-MT and 2-MG (2-MT-OS and 2-MG-OS) are some of the most commonly identified SOA tracers in ambient samples and are key contributors to OA mass.[34, 35, 134, 135] It is generally expected that the heterogeneous reaction of epoxides is the dominant pathway for OS formation related to MT [127] and MG [130], however reaction of alkenes with sulfate radicals in aqueous solutions have recently been proposed for isoprene OS (OSi) formation.[136] However, 2-MG-OS/2-MT-OS are

not the only OSi markers identified in isoprene oxidation. Surratt et al., 2008 conducted extensive chamber experiments to characterise products from isoprene oxidation, with 16 organosulfates identified. The formation pathways of these “other” OSi species are less well understood, with studies suggesting that several of these other OSi species can form from further heterogenous oxidation or ageing of 2-MT-OS/2-MG-OS.[137] These markers will be discussed in later chapters.

Since IEPOX is such a dominant route of SOA formation from isoprene, recent studies have started to look at the effect of organic coatings and aerosol viscosity changes on the multiphase processes of IEPOX. The majority of chamber studies studying IEPOX uptake use “pure” inorganic seed aerosol, while in the real atmosphere, pre-existing sulfate particles are likely to contain organic compounds, which could inhibit further uptake of IEPOX.[138] These organic compounds can undergo phase separation, forming a layer around an inorganic core, known as core-shell morphology as shown in figure 1.11.[139–142] This separated shell can then reduce the reactive uptake of species into the aqueous inorganic core, with some studies highlighting a potential self-limiting effect during the reactive uptake process.[138, 143–145] Aerosol viscosity can also play a role in reactive uptake, with increased viscosity from multi-phase or particle phase reactions further reducing multi-phase reactions.[146, 147] A recent modelling study estimated that organic coatings could reduce IEPOX-derived SOA by up to 33% during the Southern Oxidant and Aerosol Study (SOAS) in 2013 around Atlanta, US.[148] This limiting effect is likely to also be taking place in urban areas, with high concentrations of OA and potential evidence of this will be discussed in later chapters.

In addition to OSi species, isoprene related nitroxy OSs have also been identified (NOSi) in chamber studies of isoprene photo-oxidation in the presence of NO_x or nitrate radical chemistry.[134, 135, 149] During the day, ISOPOO can react with NO to form isoprene hydroxy nitrates (IHN), with further reactions leading to multi-functional isoprene nitrate species.[106] Due to low OH concentrations at night, at locations with sufficient NO_x concentration, NO_3 chemistry becomes an important loss route of isoprene.[150] Although NO_3 radicals are formed throughout

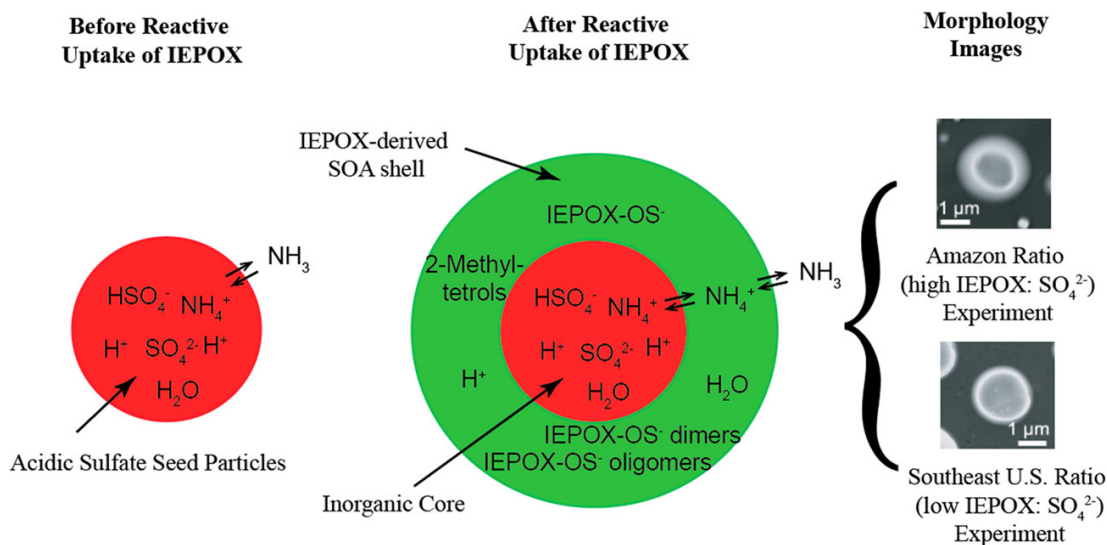


Figure 1.11: Schematic highlighting the effect of core-shell morphology on IEPOX uptake, taken from Zhang et al., 2019.

the day, rapid photolysis and reaction with NO limit's concentrations, although recent studies have suggested daytime nitrate radical isoprene degradation is more prominent than thought, with low NO concentrations observed in highly polluted urban areas due to ozone titration.[103, 104] While the rate of isoprene emissions at night is far lower than during the day, isoprene can build up during the late afternoon outside of peak OH concentrations, with anthropogenic sources of isoprene also a key nocturnal source in urban areas.[151] The main first-generation products formed from NO_3 oxidation are C_5 nitrooxy hydroperoxide (INP), C_5 carbonyl nitrate (ICN) and C_5 hydroxy nitrate (IHN) as shown in figure 1.12.[109, 152] These first-generation nitrates can then undergo further oxidation via OH or NO_3 radicals. Schwantes et al.,2015 suggests that INP reacts with OH to form (C_5) nitrooxy hydroxyepoxide (INHE), which can then undergo reactive uptake to acidified aerosol, similar to IEPOX. Several NOSi markers have been identified in chamber studies, including mono-, di- and tri- nitrated species and have been identified and quantified in several ambient studies.[125, 126] These species and their potential formation mechanisms will be further discussed in more detail in chapter 2.

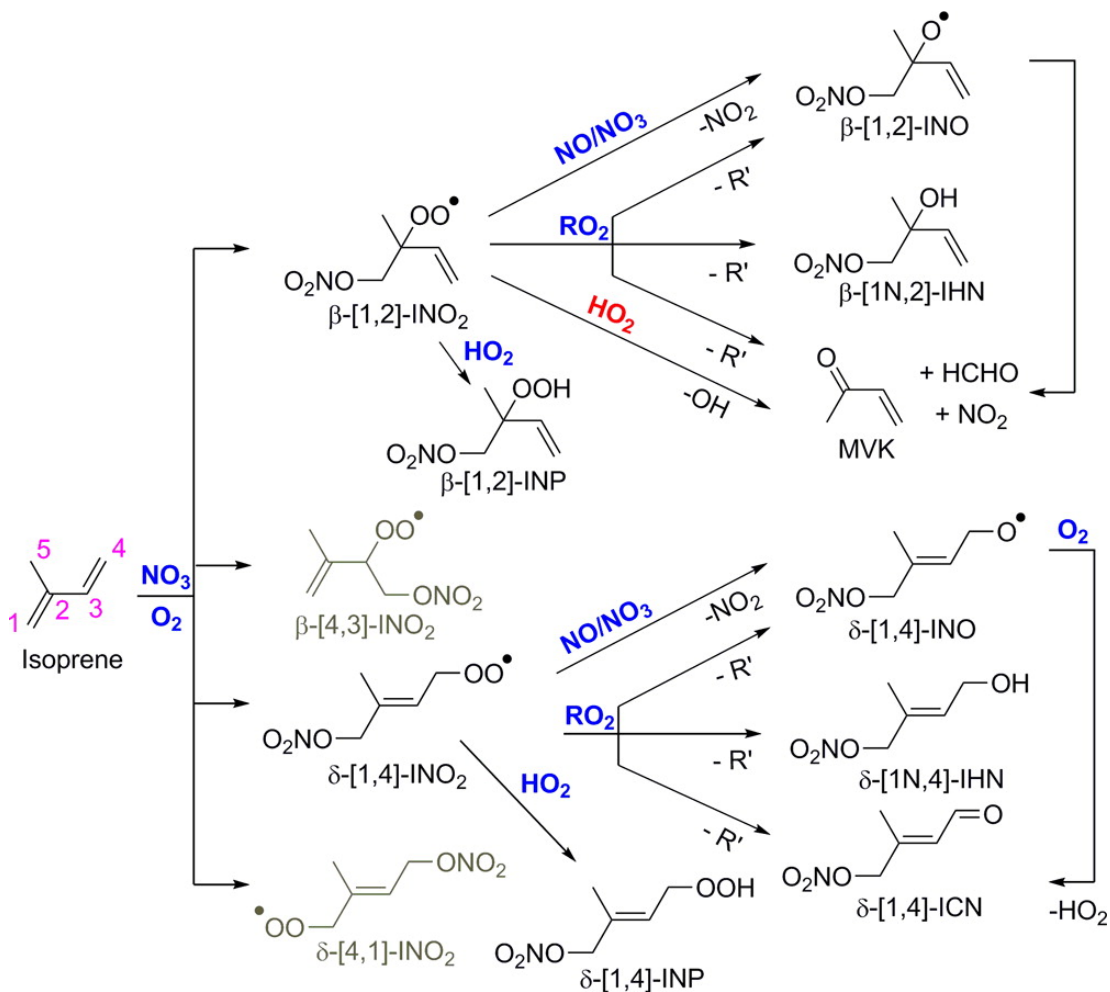


Figure 1.12: Diagram of the Main Products Formed from NO_3 Oxidation of Isoprene, taken from Schwantes et al., 2015.

1.7 Effect of Anthropogenic Emissions on biogenic SOA formation

Anthropogenic pollutants have been shown to impact the formation of BSOA formation through anthropogenic-biogenic interactions.[38, 153, 154] Anthropogenic species tend to have an enhancement effect on BSOA formation. Therefore, while BVOCs dominate over anthropogenic VOCs and are hard to control, the reduction of anthropogenic pollutants could in turn help reduce BSOA concentrations.[155]

1.7.1 Sulfate concentrations and aerosol acidity

As discussed in section 1.6, the isoprene epoxide OS formation pathway is widely regarded as the dominant pathway in OS formation in the presence of sulfate particles. Eddingass et al., 2010 proposed two possible acid catalysed ring opening mechanisms of epoxides, both mechanisms proceed via protonation of the oxygen on the epoxide ring.[156] The A1 mechanism proceeds via the formation of a carbocation through the breaking of one of the C-O bonds, while the A2 mechanism (Figure 1.13) undergoes a nucleophilic addition to the epoxide ring. However the A-2 mechanism has been shown to be more kinetically favourable than the A-1 mechanism.[156] Other formation mechanisms have been investigated (Figure 1.13), including sulfate esterification (b), nucleophilic substitution (c), radical reactions (d) and heterogeneous reactions with SO₂ (e). The formation of NOS species and the effect of aerosol acidity and sulfate concentrations is less well understood. Nucleophilic substitutions of hydroxyl groups by sulfate anions have however been shown to be unlikely. Recent studies have shown the strong correlation between NOS species and sulfate concentrations, with proposed NOSi formation mechanisms proceeding via the formation of hydroxy nitrate epoxides, which then undergo acid catalysed reactive uptake like IEPOX.[104, 152]

Aerosol acidity is mainly derived from H₂SO₄ and HNO₃ formed from the oxidation of SO₂ and NO_x. SO₂ is a common air pollutant, released through coal combustion and manufacturing, and while North America and Europe by moving away from coal combustion have reduced SO₂/SO₄²⁻ concentrations[157], developing countries still experience high concentrations. The pH of aerosol has been measured at multiple locations[158, 159], with the SEUS experiencing much more acidic aerosol than China.[160] A multitude of studies have shown enhanced SOA yields from isoprene, monoterpenes and sesquiterpenes, with higher acidity levels. Low NO_x formation of OSi was shown to increase from 1.3 % to 28.6 % yield moving from neutral seed to acidic.[127] While strong correlations between aerosol acidity and SOA yield in chamber experiments are observed, weaker correlations in

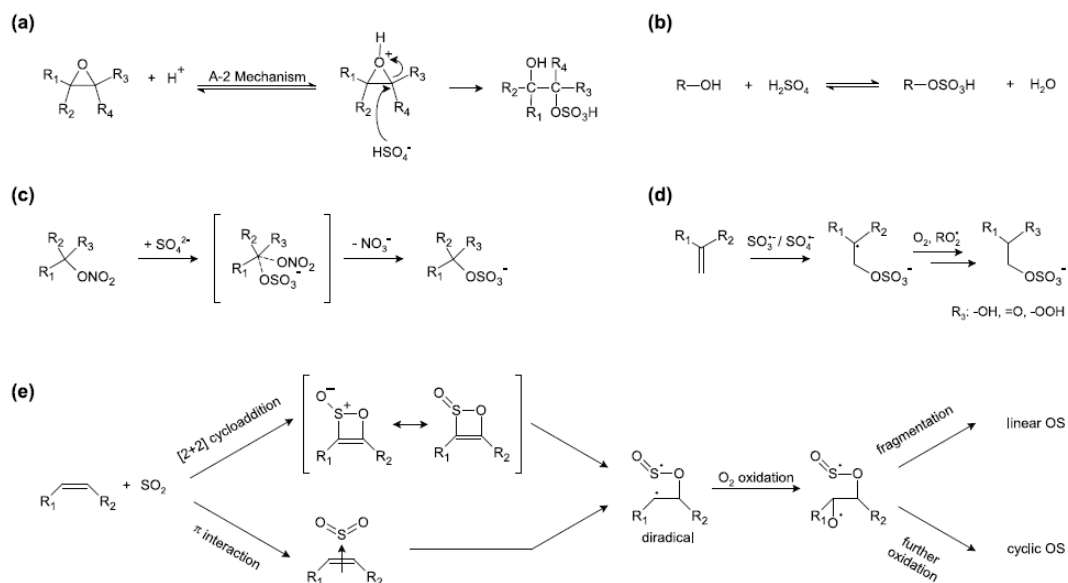


Figure 1.13: Potential formation mechanisms of organosulfates, taken from Brüggemann et al., 2020.

ambient studies have been observed, with stronger correlations towards inorganic sulfate concentrations. This is likely due to sulfate aerosol providing a large surface area, due to its ability to undergo NPF, and SO_4^{2-} acting as a nucleophile in OS formation.[33, 34] Increased sulfate concentrations could also affect OS formation through a process known as “salting in”. Salting in refers to the increased solubility of polar compounds in an aqueous solution with higher salt concentrations (in this case sulfate) i.e. increased ionic strength.[2]

1.7.2 NO_x

NO_x can influence the formation of iSOA through altering the fate of the RO_2 radical, with $\text{RO}_2 + \text{NO}$ reactions leading to organic nitrates and alkoxy radicals. As discussed, isoprene SOA has distinct “lower” and “higher” NO_x formation pathways, with chamber studies generally showing the “lower” NO_x pathway produces higher SOA yields than the “higher” NO_x route. This is due to the decomposition of the RO radical produced, forming more volatile species during the “higher” NO_x route, leading to less gas-particle partitioning.[120] However,

these are primarily based on lower NO concentrations, rather than NO₂. Recent studies have shown that under high NO_x conditions with higher [NO₂]/NO ratios, NO₂ + RO₂ can yield substantial SOA yield, through the formation of MPAN. [2, 127, 132]

NO_x levels also have an effect on the formation of SOA from monoterpenes, and like isoprene, higher yields have been observed under “lower” NO_x concentrations. This decrease in SOA with increasing NO_x has been attributed to the suppression of NPF, limiting the further uptake of semi-volatile species.[161] New particle formation of monoterpene derived species has been found to be suppressed under higher NO_x conditions, due to the suppression of low-volatility products such as hydroperoxides.[161, 162] This then has a knock on effect, due to limiting the amount of particle surface for further condensation.[163] In contrast to isoprene and monoterpenes, SOA yields from β -caryophyllene photo-oxidation have been shown to be larger under higher NO_x conditions than low, although there are limited studies.[164, 165] This was proposed to be due to the formation of less volatile multifunctional species, but further work is required to fully understand the enhancement.

1.8 BSOA characterisation and quantification

Due to the complex nature of aerosol formation, and the chemically diverse functionality of the compounds, there is no one instrument capable of investigating the molecular composition of individual markers in real time.[1] As such, different techniques and instruments are used collaboratively to investigate aerosol formation and concentrations in the ambient atmosphere.

Mass spectrometry (MS) is the dominant technique for aerosol characterisation and mass spectrometers broadly fall into two categories; online and offline. Online mass spectrometers such as aerosol mass spectrometry (AMS), are able to elucidate aerosol concentrations based on broad definitions such as sulfate, nitrate, ammonium, chloride and total OA, at high time resolutions.[47, 166]

Recently positive matrix factorisation (PMF) has been used to provide further information from the OA constituents, splitting the OA into factors based on their time series and labelled according to their O:C ratio.[47] AMS has been utilised in a multitude of environments to improve our understanding of aerosol formation[167, 168], ageing [169, 170] and concentrations[46, 171]. While AMS provides high resolution aerosol composition, the molecular composition on an individual compound basis is not achievable with AMS. Offline techniques are able to fill this gap, at the expense of time resolution.[1] For offline techniques, aerosol samples are collected, generally on pre-conditioned filter paper using high volume samplers (Figure 1.14). Chemical Ionization Mass Spectrometry with a Filter Inlet for Gases and AEROSols (FIGAERO-HRToF-CIMS) allows for both gas and particle phase chemical constituents to be measured at the same time. Collected particles are thermally desorbed to form a thermogram, where individual compound signals appear at distinct temperatures, allowing the analysis of volatile and semi-volatile species.[172] Aerosol is more commonly analysed using electrospray ionisation high resolution mass spectrometry which is usually linked to high performance liquid chromatography (ESI-HPLC-UHRMS). HPLC-UHRMS has been used extensively for aerosol chemical composition and allows for the structure of individual species and their isomers to be identified.[134, 149, 173]

ESI is the most common ionisation techniques for aerosol samples using offline MS analysis.[1, 48] One of the main advantages to ESI is the lack of fragmentation of analytes, making molecular identification easier. While ESI can be used in both the positive and negative modes, negative mode is more commonly used due to the functionality of common aerosol markers. To overcome the low time resolution of offline filter samples, some studies have started to use extractive electrospray ionisation (EESI) which allows online analysis of particle without significant fragmentation.[174]

It was the recent advances in MS technology, such as the development of the Orbitrap mass analyser, due to the compact size and the relative reductions in prices that has fueled an increase in UHRMS studies of aerosol markers. Owing to



Figure 1.14: Filter sample collected in Delhi.

the high mass resolutions of several 100s of thousands, prior chromatographic separation is not necessary for detailed compositional information to be obtained.[175, 176] Due to this, a large number of studies use direct injection UHRMS to investigate the broad molecular characteristics of aerosol samples collected in both rural and urban areas. These studies give general overviews of aerosol metrics such as average H:C and O:C, average number of carbons, oxidation state (OSs) and double bond equivalent (DBE). These studies can give an insight into general sources of aerosol through the production of Van Krevelen diagrams (Figure 1.15), which plot H/C and O/C ratios for each molecular formula in a sample. As well as Kendrick mass defect plots (Figure 1.16), which plot the Kendrick mass defect against the nominal Kendrick mass and can highlight changes in aerosol sources.

[177–182]

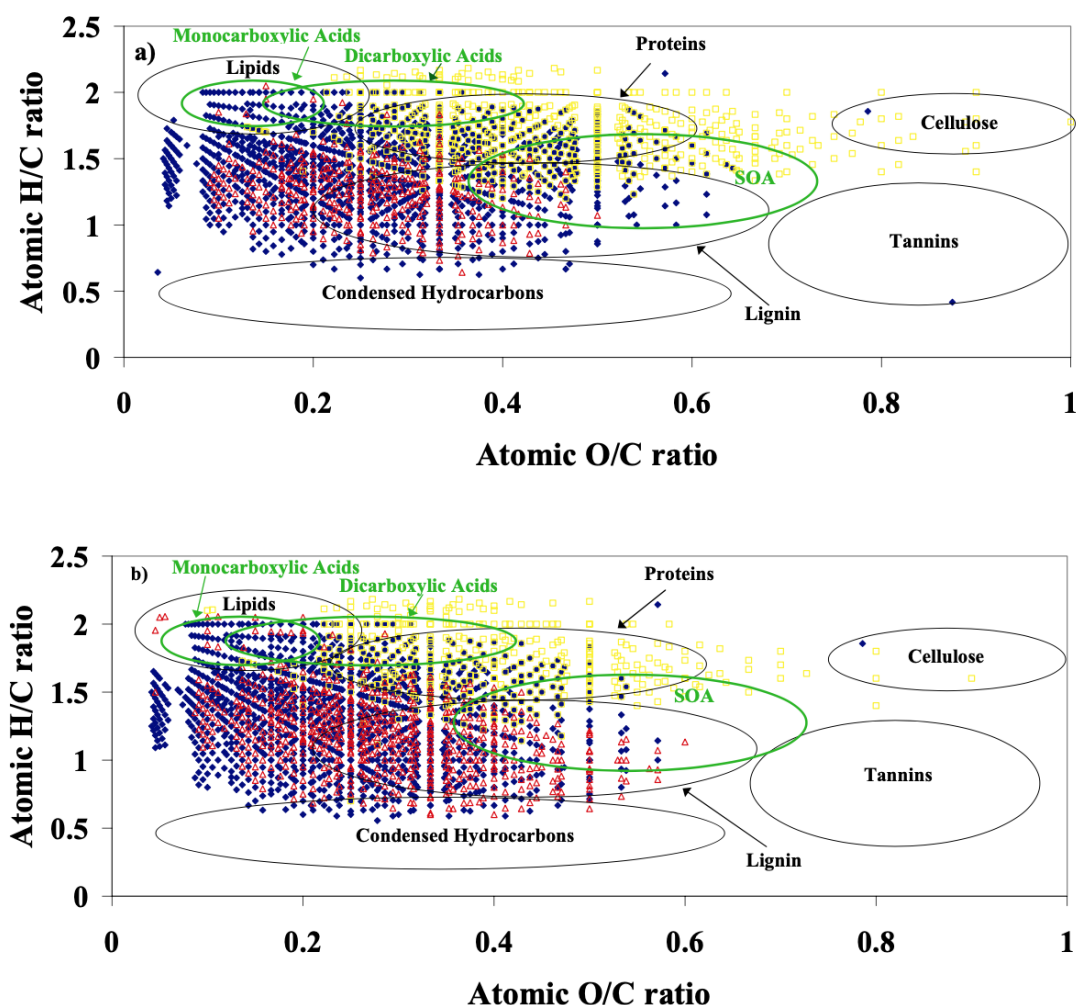


Figure 1.15: van Krevelen plots for molecular formulas assigned to FT-ICR mass spectra peaks in aerosol WSOC samples from a) New York and b) Virginia. Blue diamonds represent compounds containing only C, H, and O, yellow squares represent S-containing compounds, and red triangles are N-containing compounds. Black ovals represent traditional potential source molecular classes. Taken from Wozniak et al., 2008. [183]

These studies however are limited by the lack of quantification and isomer identification, and one of the major challenges going forward for SOA studies is the accurate quantification of individual markers in the ambient atmosphere.[48] HPLC allows the separation of individual markers for structural elucidation or identification. As such, HPLC-UHRMS has been used extensively for the quantification of individual BSOA markers in ambient samples [41, 126, 184, 185],

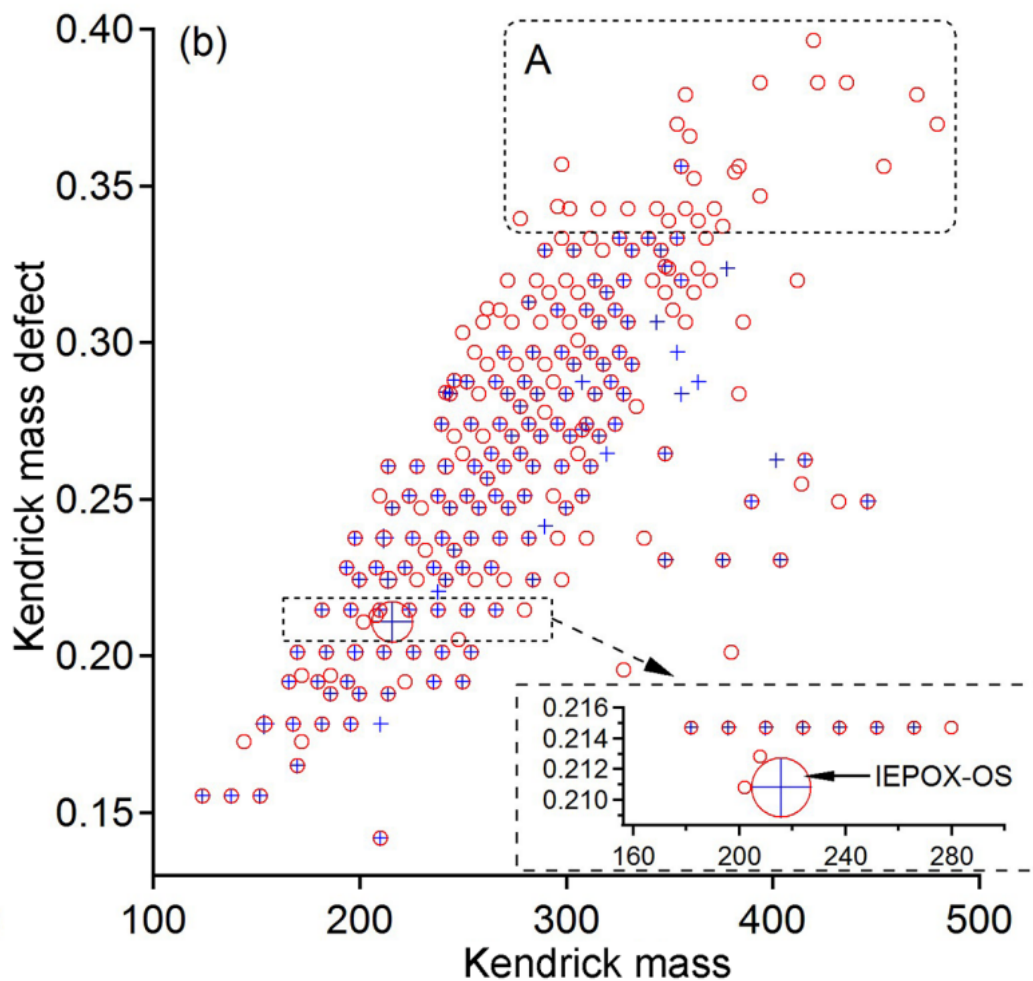


Figure 1.16: Kendrick mass defect plot of CHOS-containing formulae from samples collected in central Amazonia. Periods with low and very high incidents of fires are marked as blue and red markers respectively. Taken from Kourtschev et al., 2016.[180]

but does provide some analytical challenges.[48, 186]

Aerosol samples have been shown to contain thousands for individual markers[179], and as such separation of all these species at once is not possible due to the broad range of polarities. LC can be split into reverse phase (non-polar stationary phase) and normal phase (polar stationary phase) separations, with reverse phase the dominant technique for BSOA studies utilising C_{18} columns. More recently however, studies focusing solely on small, highly polar OSi species have started to use normal phase in particular hydrophobic interaction liquid

chromatography (HILIC) columns for separation.[35, 137, 187] C₁₈ columns allow for a wider range of polarities to be investigated, at the cost of better separation. However, higher mass resolution from HRMS allows for this to be overcome.

There are several challenges associated with the quantification of molecular level markers in ambient samples.[48, 186] Firstly, matrix effects (ME's) are a common analytical chemistry challenge when using MS, where the sample being analysed perturbs the signal of the markers within the sample being identified, this can either be an enhancement or suppression of signal intensity. There are several reasons for matrix effects, all of which are likely to occur in the analysis of aerosol samples. Target markers may react with other species within the matrix, either increasing or decreasing concentrations, co-elution of markers may change ionisation efficiencies due to changes in the droplet properties, competition between compounds for the limited number of charged sites on the surface of the electrospray droplet and/or the matrix can alter adduct formation.[188] It was only recently that ambient studies have started to account for and investigate the ME's associated with ambient aerosol samples, and how the ME's affect quantified BSOA concentrations.[125, 184, 189] Owing to the limited number of studies, a consensus cannot yet be drawn. However studies suggest significant matrix effects for early eluting species when using reverse phase C₁₈ chromatography for OSi quantification, with smaller ME for later eluting species. No study has looked at the ME associated with HILIC separation of the same compounds.

Secondly, accurate quantification relies on use of authentic standards which for aerosol markers are not widely available. Without authentic standards, many studies employ the use of proxy standards such as camphorsulfonic acid (C₁₀H₁₆O₄S) for organosulfates and *cis*-pinonic acid (C₁₀H₁₆O₃) for terpenoic acids, which are species with a similar structure and functionality to the marker being quantified. However, this assumes that the proxy standard has the same or similar ionisation efficiency as the marker of interest. Recently, studies have started to synthesise aerosol markers, and compared them to the proxy standards which are in wide use. For example, Kenseth et al., 2020 synthesised a series of α -pinene-derived

carboxylic acid and dimer species, and compared their ionisation efficiencies to *cis*-pinonic acid. They found that the ionisation efficiencies of the synthesised species were 19-36 times higher than *cis*-pinonic acid, meaning a potential error of 3600 %.[190] OS and NOS standards for isoprene[191], monoterpenes[185, 192–194] and sesquiterpenes[195] have also been synthesised. For the synthesised organosulfates, a smaller range of ionisation efficiencies were established, with a factor of 6.4 between the least ionising and most ionising, with camphorsulfonic acid being established as the most accurate proxy standard.[192] However, unless these authentic standards are made more widely available, through the sharing of standards, or produced commercially, the synthesis of standards is limited to larger labs who can cover the associated costs. An emerging area of analytical chemistry, which would heavily benefit aerosol science is the quantification of markers without authentic standards using modelled ionisation efficiencies to correct the quantification of a marker using a non-authentic standard.[196–198]

1.9 Thesis Outline

The overall aim of this thesis is to investigate BSOA formation and concentrations in mega-cities using HPLC-UHRMS. This study involves the use of offline filters collected in Beijing, Delhi and Guangzhou as well as the development of more accurate quantification techniques for BSOA. A brief summary of each chapter is given below.

Chapter 2

This chapter utilises offline filter samples collected in summertime Beijing, China alongside a suite of complementary measurements. Isoprene organosulfate and nitrooxy organosulfate markers were quantified, alongside the investigation of matrix effects on quantification. Strong biogenic-anthropogenic interactions were identified through the uptake of epoxide intermediates to the gas phase via inorganic sulfate, and nitrate radical oxidation.

Chapter 3 This chapter focuses on offline filter samples collected at one of

the highest time-resolutions to date, with on average 8 filters collected per day, in winter and summer-time campaigns in Guangzhou, China. This allowed diurnal information on the formation of isoprene and monoterpene SOA markers using offline high resolution mass spectrometry for the first time. Guangzhou represents an interesting case study for biogenic-anthropogenic interactions, due to its subtropical climate, while situated in one of the most populous regions of the Earth.

Chapter 4 This chapter utilises offline filter samples collected in pre- and post-monsoon campaigns in Delhi, India and represents the first investigation of BSOA using HPLC-UHRMS in India. Organosulfates and nitrooxy-organosulfates from isoprene, monoterpenes and sesquiterpenes were quantified using a mixture of authentic and proxy standards. Delhi is an interesting case study for BSOA formation due to being one of the most polluted cities in the world, leading to unusual chemistry and sources of VOCs.

Chapter 5 This chapter outlines a new quantification technique for biogenic organic acid SOA markers. The method combines relative ionisation efficiency measurements and machine learning for the prediction of ionisation efficiency factors for markers without authentic standards. This is to overcome the large identified differences in ionisation efficiencies between different SOA compounds and the significant lack of readily available authentic standards for quantification.

Chapter 6 This chapter utilises the predicted relative ionisation efficiency factors from Chapter 5 and applies them to the quantification of biogenic organic acids using samples from Beijing, Delhi and Guangzhou. This study represents one of the largest ambient studies of BSOA in terms of number of samples. Biogenic organic acid SOA markers from α -pinene, limonene and β -caryophyllene were identified in ambient samples from a library of markers generated from chamber studies. Concentrations, time series and diurnal variations were investigated for the first time for some markers. Overall marker formation pathways were investigated, in terms of temperature and ozone concentrations.

Chapter 7

A summary of the work presented across chapters 2-6, and a discussion of future work.

Chapter 2

Isoprene secondary organic aerosol in Beijing: Formation of Organosulfates and Nitrooxy organosulfate

This work was originally published in *Atmospheric Chemistry and Physics*[125] and *Environmental Science and Technology*[104]. My role included the extraction and analysis of the filter samples using UHPLC/ESI-HR-MS. UHPLC/ESI-HR-MS data was collected by myself and collated with measurements made by collaborators. All subsequent analysis and write up was undertaken by myself.

2.1 Introduction

Rapidly developing countries such as China often experience very poor air quality. Beijing regularly experiences periods of very high particle pollution, with annual and 24-hourly levels well above World Health Organisation guidelines.[28, 199] Premature mortality, as a result of respiratory illness, cardiovascular disease and cancer, has been associated with exposure to poor air quality.[6, 19, 200–204] Lelieveld et al. (2015) estimated that 1.36 million premature deaths in China in 2010 were a result of exposure to outdoor air pollution.[16] By far the most dangerous pollutant to health in China are particles less than 2.5 microns in diameter ($PM_{2.5}$), with a recent study suggesting that a 50 % reduction in excess mortality requires a 62 % reduction in $PM_{2.5}$ in the Beijing-Tianjin-Hebei (BTH) region.[205]

Previous measurements using aerosol mass spectrometry (AMS) indicate that PM_1 in Beijing is mainly composed of sulfate, nitrate, ammonium and organics.[206, 207] Positive Matrix Factorisation of AMS measurements indicate that oxidised or secondary organic aerosol (SOA) can make up a substantial fraction of the PM_1 mass ($> 25\%$), even in urban areas, but the sources of this material are still poorly understood.[208, 209] Hu et al., 2017 estimated that exposure to SOA was responsible for 0.14 million deaths in China in 2013 based on mass contribution alone, ranging from $< 1\%$ to 23 % source contributions to $PM_{2.5}$ depending on location.[205] Zhang et al., 2017 used ^{14}C measurements to determine that non-fossil emissions are generally a dominant contributor of secondary organic carbon (SOC) in Beijing, with a larger contribution in summer as a result of

increased biogenic volatile organic compounds (VOCs) emissions.[210]

Hu et al., 2017 updated the Community Multi-scale Air Quality (CMAQ) model with updated SOA yields and a more detailed description of SOA formation from isoprene oxidation.[211] Removing all anthropogenic pollutants from the model resulted in a huge drop in isoprene SOA (iSOA) concentrations, indicating that controlling anthropogenic emissions would result in reduction of both anthropogenic and biogenic SOA. The predicted SOA was dominated by isoprene in summer across China and in four cities (Beijing, Guangzhou, Shanghai, Chengdu) with concentrations up to $30 \mu\text{g m}^{-3}$ in Beijing. However, there is currently very little observational evidence to support such high SOA mass concentrations from isoprene oxidation in these Chinese cities. The widely used SOA tracer method [212] has been used extensively to estimate the fraction of iSOA across China. Ding et al., 2014 studied SOA at 14 Chinese sites and found that iSOA dominated the apportioned SOA mass ($46 \pm 14 \%$), with it contributing between $0.4 - 2.17 \mu\text{g m}^{-3}$ and an average of $1.59 \mu\text{g m}^{-3}$ in Beijing.[213] However, only a very limited subset of VOC precursors was included, and this method fails to account for heterogeneous formation processes. To overcome some of these limitations, Wang et al., 2017 used tracer-based source apportionment of $\text{PM}_{2.5}$ with positive matrix factorisation in the Pearl River Delta region during summer. They identified an iSOA factor that contributed up to $4 \mu\text{g m}^{-3}$ in Guangzhou, and up to 11 % of the total SOC.[214]

Observations using AMS indicate that IEPOX-derived SOA can make up a significant fraction of OA in isoprene-rich environments, such as Borneo (23 %)[215], the Amazon (34 %) [123] and the South East US (33-40 %)[33, 34, 191]. Hu et al., (2015) compared previous AMS studies and found a magnitude lower average IEPOX-SOA signal in urban studies ($f_{\text{C}_5\text{H}_6\text{O}} = 0.17 \%$) compared to those in isoprene-rich regions ($f_{\text{C}_5\text{H}_6\text{O}} = 2.2 \%$).[216] The average IEPOX-SOA concentration measured in Nanjing, a polluted city in Eastern China, in August 2013 was $0.33 \mu\text{g m}^{-3}$.[217] This represented only 3.8 % of the total OA, indicating there is limited formation of IEPOX under high- NO_x conditions (average $\text{NO}_x =$

21 ppb). He et al., 2018 found higher concentrations of the low-NO iSOA tracers (average = 121 ng m⁻³) than the high-NO iSOA tracers (average = 9 ng m⁻³) at a regional background site (Wanqingsha) situated within the heavily polluted Pearl River Delta Region.[218] Only two high-NO iSOA tracers were measured (2-MG and 2-MG-OS), which could lead to a significant underestimate of the strength of the high NO_x pathway. Wang et al., 2018 measured a range of OSi species at a regional site 38 km north east of Beijing during May-June 2016. OSi concentrations ranged from 0.9-20 ng m⁻³, with a mean OSi concentration of 14.8 ng m⁻³. In both these studies, the ratio of the average concentration of the commonly used OS tracers from the low NO versus the high NO pathways was close to 1.5 (2-MT-OS:2-MG-OS; Beijing = 1.47, Wanqingsha = 1.57) indicating that even in polluted environments low-NO oxidation chemistry can play a significant role in iSOA formation.

SOA formed from anthropogenic and other biogenic (monoterpenes and sesquiterpenes) sources have also been studied. Thousands of organic species including hundreds of OS and NOS species have been identified in studies from a range of precursors using UHPLC/ESI-HR-MS from ambient aerosol samples.[214, 219] Brüggemann et al., 2019 quantified with authentic standards both monoterpene OS (OS_{MT}) and sesquiterpene (OS_{SQT}) species in Melpitz, Germany and Wangdu, China. They found median daytime concentrations for Melpitz and Wangdu for 52 OS_{MT} species of 12.15 ng m⁻³ and 38.19 ng m⁻³ respectively. For the 5 OS_{SQT} species, median concentrations were 0.3 ng m⁻³ and 3.90 ng m⁻³ for daytime concentrations respectively, much lower than the OSi species quantified in this study. Riva et al., 2016 identified OS species from the photo-oxidation of C₁₀ – C₁₂ alkanes, which were then characterised in ambient aerosol samples collected in Lahore, Pakistan and Pasadena, CA, USA. High concentrations of OS species were identified in Lahore, with the largest observed concentration arising from a cyclodecane OS species (C₁₀H₁₆O₇S) with a concentration of 35.93 ng m⁻³.

The lack of molecular-level measurements of iSOA in highly polluted urban areas makes it difficult to determine the role of isoprene in summer haze episodes in

Beijing. To investigate the formation of iSOA in Beijing, offline PM_{2.5} filter samples were collected during summer 2017 as part of the Atmospheric Pollution and Human Health program (APPH).[220] The filters were extracted and then screened using a sensitive and selective high throughput method based on UHPLC/ESI-HR-MS. High-time resolution filter sampling allowed the formation and evolution of iSOA to be studied, with observed concentrations strongly controlled by levels of anthropogenic pollutants.

2.2 Experimental

2.2.1 PM_{2.5} filter sampling and extraction

Aerosol samples were collected between the 18th May and 24th June 2017 at the Institute of Atmospheric Physics (IAP) in Beijing, China. This sampling was part of the Sources and Emissions of Air Pollutants in Beijing (AIRPOLL-Beijing) project, as part of the wider Atmospheric Pollution and Human Health in a Chinese Megacity (APHH-Beijing) programme.[220] PM_{2.5} filter samples were collected using an ECOTECH HiVol 3000 (Ecotech, Australia) high-volume air sampler with a selective PM_{2.5} inlet, with a flow rate of 1.33 m³ min⁻¹. Filters were baked at 500 °C for five hours before use. After collection, samples were wrapped in foil, and then stored at -20 °C and shipped to York for offline analysis. Samples were collected at a height of 8 m, on top of a building in the IAP complex. Samples were collected roughly every 3 hours during the day, approximately between 08:30 and 17:30 and then one sample was collected overnight between 17:30 and 08:30. Hourly samples were also taken on certain days towards the end of the sampling period on high pollution days. 24-hour samples were also collected using a Digitel high volume PM_{2.5} sampler at the same location.

The extraction of the organic aerosol from the filter samples was based on the method outlined in Hamilton et al., 2008.[221] Initially, an 8th of the filter was cut up into roughly 1 cm² pieces and stored in a vial. 4 ml of LC-MS grade H₂O was

then added to the sample and left for two hours. The samples were then sonicated for 30 minutes. A small subset (3) of the filter samples were also extracted via orbital shaker and no appreciable difference was found in the concentrations of the iSOA tracers compared to sonication. Using a 2 ml syringe, the water extract is then pushed through a 0.22 μm filter (Millipore) into another sample vial. An additional 1 mL of water was added to the filter sample, then extracted through the filter, to give a combined aqueous extract. This extract was then reduced to dryness using a vacuum solvent evaporator (Biotage, Sweden). The dry sample was then reconstituted in 1 mL 50:50 MeOH:H₂O solution for offline chemical analysis.

2.2.2 Ultra-high performance liquid chromatography tandem mass spectrometry (UHPLC-MS²)

The water-soluble fraction of the filter samples were analysed using UHPLC-full scan-ddMS², using an Ultimate 3000 UHPLC (Thermo Scientific, USA) coupled to a Q-Exactive Orbitrap MS (Thermo Fisher Scientific, USA) with a heated electrospray ionisation (HESI). The UHPLC method uses a reverse phase 5 μm , 4.6 x 100mm, Accucore column (Thermo Scientific, UK) held at 40 °C. The mobile phase consists of LC-MS grade water and 100 % MeOH (Fisher Chemical, USA). The water was acidified using 0.1 % formic acid to improve peak resolution. The injection volume was 2 μL . The solvent gradient was held for a minute at 90:10 H₂O:MeOH, then changed linearly to 10:90 H₂O:MeOH over 9 minutes, then held for 2 minutes at this gradient before returning to 90:10 H₂O:MeOH over 2 minutes and then held at 90:10 for the remaining 2 minutes, with a flow rate of 300 $\mu\text{L min}^{-1}$. Due to the wide range of compounds studied, poor retention was observed for some species (RT < 0.8 min). These species closely eluted to the dead time of the column where inorganic sulfate ions eluted (0.67 min). To check for ionisation artefacts, an aqueous solution containing 20 ppm ammonium sulfate, 1ppm 2-methyltetrol and 1ppm 2-methylglyceric acid was run under the same

conditions as the filter samples to check for organosulfate formation (2-MT-OS and 2-MG-OS respectively). No MG-OS formation was observed and <0.5% conversion was seen for the 2-MT. This therefore rules out adduct formation for the two most important OSi species, 2-MT-OS and 2-MG-OS, however due to the lack of authentic standards and the complexity of the samples, adduct formation throughout the entire chromatogram could still be occurring. At this stage, there is not enough evidence to say either way if adducts are forming or not. The mass spectrometer was operated in negative mode using full scan ddMS². The scan range was set between 50 - 750 m/z, with a resolution of 70,000. The ESI voltage was 4 kV, with capillary and auxiliary gas temperatures of 320 °C. The number of most abundant precursors for MS² fragmentation per scan was set to 10. The samples were run in batches of 70, in a repeating sequence of 5 samples followed by one blank, each filter sample was run only once. The calibrations were run separately after the samples were finished, in the following sequence; (3 X same concentration) X number of standards in calibration curve from the lowest concentration to the highest followed by 2 blanks. The quantification method will be discussed in the results section.

2.2.3 Construction of accurate mass library

A mass spectral library was built using the compound database function in TraceFinder 4.1 General Quan software (Thermo Fisher Scientific, USA). Each compound was input into the compound library in the generic form: C_cH_hO_oN_nS_s (where c, h, o, n, and s represent the number of carbon, hydrogen, oxygen, nitrogen and sulfur atoms respectively). From literature, species were identified, searched for in the ambient samples according to their accurate mass, and then the retention time (RT) of each isomer was obtained. Using previously observed iSOA products from literature, extracted ion chromatograms were plotted for each m/z value from a small subset of ambient samples and the retention time (RT) of observed species/isomer were obtained. For most of the OSi species in this study the

separation was not good enough to see individual isomers and only one peak was observed, which was added to the library. For the NOSi species, individual isomers could be resolved, and each isomer was added to the library based on its retention time. The accurate masses, RT and literature references for iSOA tracers are shown in Table 2.2.

2.2.4 Automated method for SOA tracer analysis

The UHPLC/ESI-HR-MS data for each ambient sample and standard was analysed using TraceFinder™. Tracefinder extracted the OSi/NOSi tracer peak areas from each ambient sample chromatogram using the library based on RT and accurate mass. The mass tolerance of the method was set to 2 ppm and the retention time window was set to 30 s, although for species with multiple isomers present, the integration was checked to make sure the same peaks were not being integrated twice, and the window changed accordingly. The peak tailing factor was set to 2.0 to reduce the integration of the peak tails. The minimum signal to noise (S/N) for a positive identification was set to 3.0. Using the output from TraceFinder, an in-house R code script was developed to combine the identified species and peak areas with the correct filter sampling date/time midpoint and volume of air sampled. Calibration curves from the standards were then obtained, and the intercept and gradient inputted to quantify the iSOA tracer concentrations in the extract. These quantified values were then converted to the mass on the whole filter and divided by the volume of air sampled for that filter sampling period and converted to units of ng m^{-3} . Higher time resolution data were averaged to the filter sampling times. It should be noted that MS^2 was used to check that the iSOA species fragmented to give typical OS fragment ions.

2.2.5 Hydrophilic Liquid Interaction Chromatography

A subset of filters (n=15) were also analysed at the University of North Carolina (UNC) using a newly developed HILIC method interfaced to high-resolution

quadrupole time-of-flight mass spectrometry equipped with ESI (i.e., HILIC/ESI-HR-QTOFMS) by Will Dixon.[187] Briefly, filters were extracted with 22 mL of LC/MS-grade methanol by 45 min of sonication; the samples were first extracted for 23 min, the water bath replaced with cool water, and then extracted again for 22 min. This was done to make sure the water bath contained within the sonicator did not reach above 30 °C. Extracts were filtered through polypropylene membrane syringe filters in order to remove insoluble filter fibres and soot particles. The extracts were dried under a gentle stream of nitrogen gas. Dried methanol extracts were reconstituted with 150 μ L of 95:5 (v/v) LC/MS-grade acetonitrile/Milli-Q water. Operating details of the HILIC/ESI-HR-QTOFMS used for these samples is also summarized by Cui et al., 2018.

2.2.6 Gas Chromatography – Mass Spectrometer

Details of the measurement procedure used can be found elsewhere.[222] Briefly, filter samples were extracted with dichloromethane/methanol (2:1 v/v), filtered through quartz wool packed in a Pasteur pipette, concentrated using a rotary evaporator under vacuum, and blown down to dryness with pure nitrogen gas. The extracts were derivatized and diluted with n-hexane containing the internal standard prior to GC-MS analysis. Separation was performed on a fused silica capillary column (DB-5MS: 30 m \times 0.25 mm \times 0.25 μ m). The MS detection was conducted in electron ionization (EI) mode at 70 eV, scanning from 50 to 650 Da. Individual compounds were identified by comparison of mass spectra with those of authentic standards or literature data. 2-methylglyceric acid, C₅-alkene triols (the sum of cis-2-methyl-1,3,4-trihydroxy-1-butene, trans-2-methyl-1,3,4-trihydroxy-1-butene, and 3-methyl-2,3,4-trihydroxy-1-butene), and 2-methyltetrols (the sum of 2-methylthreitol and 2-methylerythritol) were quantified using the response factor of meso-erythritol. Field blank filters were treated as the real samples for quality assurance. Target compounds were not detected in the blanks.

2.2.7 High-Resolution Aerosol Mass Spectrometry measurements

AMS measurements were undertaken by the University of Manchester. The size-resolved non-refractory submicron aerosol species at the same site were measured by an Aerodyne high-resolution time-of-flight aerosol mass spectrometer (HR-ToF-AMS) at a time resolution of 5 min. The elemental ratios of hydrogen-to-carbon (H:C) and oxygen-to-carbon (O:C) of OA were determined, and the sources of OA were analysed with positive matrix factorisation. Six OA factors were identified in summer including two primary factors; hydrocarbon like OA (HOA), cooking OA (COA), and three oxidised OA factors with increasing degrees of oxidation, OOA1 (O:C = 0.53), OOA2 (O:C = 0.74), OOA3 (O:C = 1.18).

2.2.8 Iodide CIMS

A time of flight chemical ionisation mass spectrometer (ToF-CIMS)[223, 224] using an iodide ionisation system coupled with a filter inlet for gases and aerosols (FIGAERO) was deployed to make near simultaneous, real-time measurements of both the gas- and particle-phase chemical composition. The instrument was originally developed by Lopez-Hilfiker et al., 2014 and is described and characterised in more detail by Bannan et al., 2019.[225, 226] The experimental set up employed by the University of Manchester ToF-CIMS is described in Zhou et al., 2019.[227] Only gas phase data is presented herein.

Field calibrations were regularly carried out using known concentration of formic acid in gas mixtures made in a custom-made gas phase manifold. A range of other species were calibrated for after the campaign, and relative calibration factors were derived using the measured formic acid sensitivity during the in-situ calibrations.[228] Offline calibrations after the field work campaign were performed specific to the isoprene oxidation species observed here. IEPOX ($C_5H_{10}O_3$) synthesized by the University of North Carolina, Department of Environmental Sciences & Engineering was specifically calibrated for. Known concentrations were

deposited on the FIGAERO filter in various amounts and thermally desorbed using a known continuous flow of nitrogen over the filter. For the isoprene nitrate; $C_5H_9NO_4$ there was no direct calibration source available and concentrations using the calibration factor of $C_5H_{10}O_3$ are presented here.

2.2.9 Gas-phase measurements

Additional gas-phase measurements were collected at the site from an elevated inlet at 8 m. Data included Nitrogen oxide, NO, measured by chemiluminescence with a Thermo Scientific Model 42i NO_x analyser and Nitrogen dioxide, NO_2 , was measured using a Teledyne Model T500U Cavity Attenuated Phase Shift (CAPS) spectrometer. The sum of the NO_y species was measured using a Thermo Scientific Model 42C NO_x analyser and a heated molybdenum converter at the sample inlet. The molybdenum converter reduces NO_y compounds to NO allowing measurement by chemiluminescence. Ozone, O_3 , was measured using a Thermo Scientific Model 49i UV photometric analyser. All instruments were calibrated throughout the measurement period, with a 'zero' or 'background' calibration using a Sofnofil/charcoal trap. Span (high concentration) calibrations were carried out using gas standards. Both the Thermo Scientific 42i and 42C instrument calibrations are traceable to the National Physical Laboratories (NPL) NO scale. The meteorological variables of wind speed, wind direction, relative humidity (RH), and temperature were measured at 102 m on the IAP 325 m meteorological tower.

Observations of VOCs were made using a dual-channel GC with flame ionisation detectors (DC-GC-FID). Air was sampled at 30 L min^{-1} at a height of 5m, through a stainless-steel manifold $1/2$ " internal diameter. 500 mL subsamples were taken, dried using a glass condensation finger held at -40°C and then pre-concentrated using a Markes Unity2 pre-concentrator on a multi-bed Ozone Precursor adsorbent trap (Markes International Ltd). These samples were then transferred to the GC over for analysis following methods described by Hopkins et al., 2011.[229]

Further details of the following additional gas phase instrumentation can be found in Shi et al., 2019. Isoprene was also measured at a height of 102 m using a Voice200 Selected ion flow tube mass spectrometer (SIFT-MS, Syft Technologies, Christchurch, New Zealand). OH, HO₂ and RO₂ concentrations were measured using Fluorescence Assay by Gas Expansion (FAGE)[230] and NO₃ concentrations were measured using Broadband cavity enhanced absorption spectrometry.[231]

2.3 Results and discussion

The field campaign was conducted at the Institute of Physics, Beijing, situated between the third and fourth ring roads.[220] The site is typical of central Beijing, surrounded by residential and commercial properties and is near several busy roads. It is also close to several green spaces including a tree-lined canal to the south and the Olympic forest park to the north-east, providing sources for local isoprene emissions.

2.3.1 Isoprene gas phase concentrations and loss processes

Isoprene was measured hourly using the DC-GC-FID between 18/05—20/06/2017 and the observed concentrations are shown in Figure 2.1, alongside NO, NO₂ and O₃. The mean mixing ratio of isoprene was 0.53 ppb, with a maximum of 2.9 ppb on the 16/06/2017. The ambient temperature ranged from 16 to 38 °C. Day-time isoprene mixing ratios increased with temperature, with all isoprene mixing ratios above 1 ppb occurring when the temperature was > 25 °C.

The average diurnal profile of isoprene in Figure 2.2 shows low values overnight (< 50 ppt), with a rapid increase at 6 am reaching a maximum of around 1 ppb by the afternoon. The mixing ratio rapidly decreased after 18:00 and returned to very low values by around 22:00. There was strong a correlation between the isoprene mixing ratio measured at 8 m by the DC-GC and at 102 m using the SIFT-MS ($R^2 = 0.77$). The SIFT-MS measurements were therefore used to investigate the correlation with iSOA tracers when no DC-GC data was available. The slope of

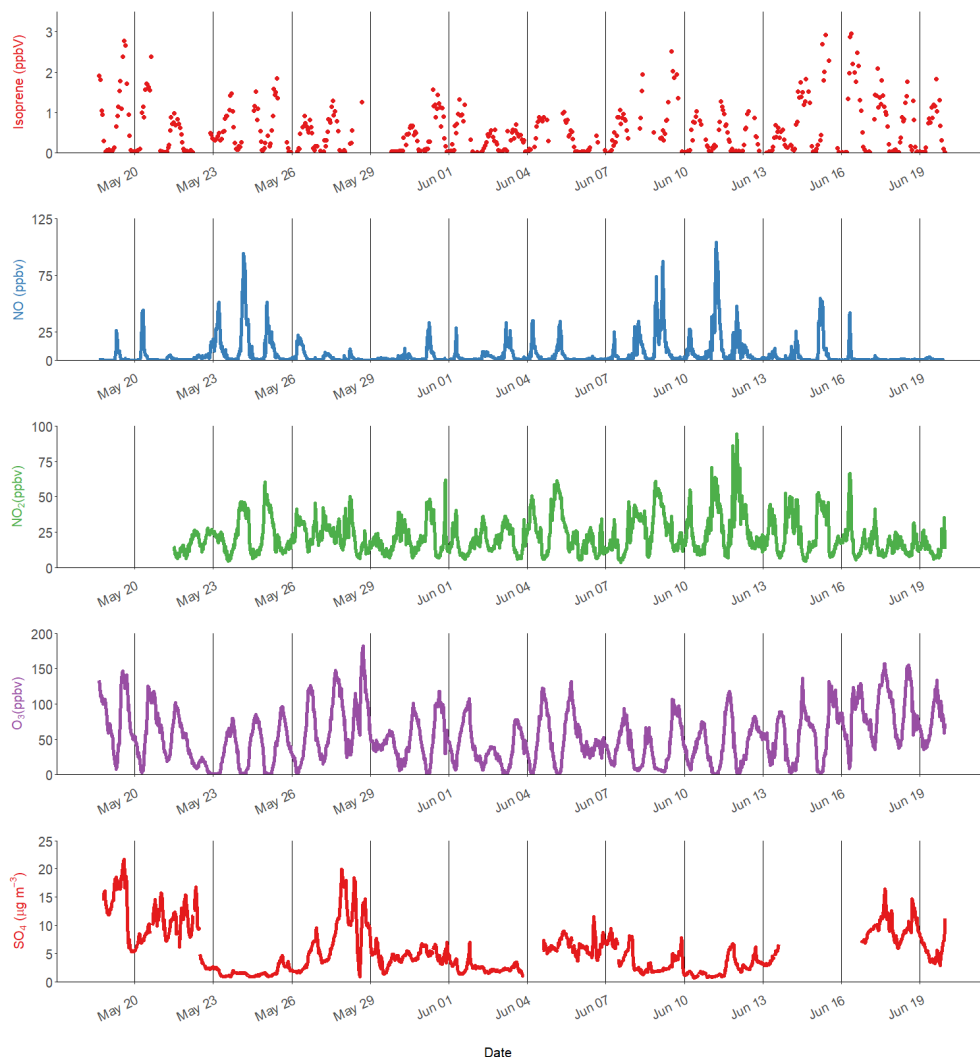


Figure 2.1: Time series of isoprene, nitric oxide (NO), nitrogen dioxide (NO₂), ozone (O₃) and particulate sulfate (SO₄). The black lines are at midnight every 72 hours.

the linear fit between the two data sets was 0.67, indicating a loss of around 30% of the isoprene during transport from the ground to the tower (100m).

Using the average observed diurnal profiles of the main atmospheric oxidants, OH, O₃ and NO₃ (shown in Figure 2.3), and isoprene (Figure 2.2), the isoprene loss rate was calculated (rate of loss = $\kappa_{\text{ox}}[\text{Oxidant}][\text{Isoprene}]$) and is shown in Figure 2.4A. The percentage contribution of each oxidant to the average diurnal isoprene loss rate is shown in Figure 2.4B.

During the day, OH is responsible for over 90 % of isoprene loss, with NO₃

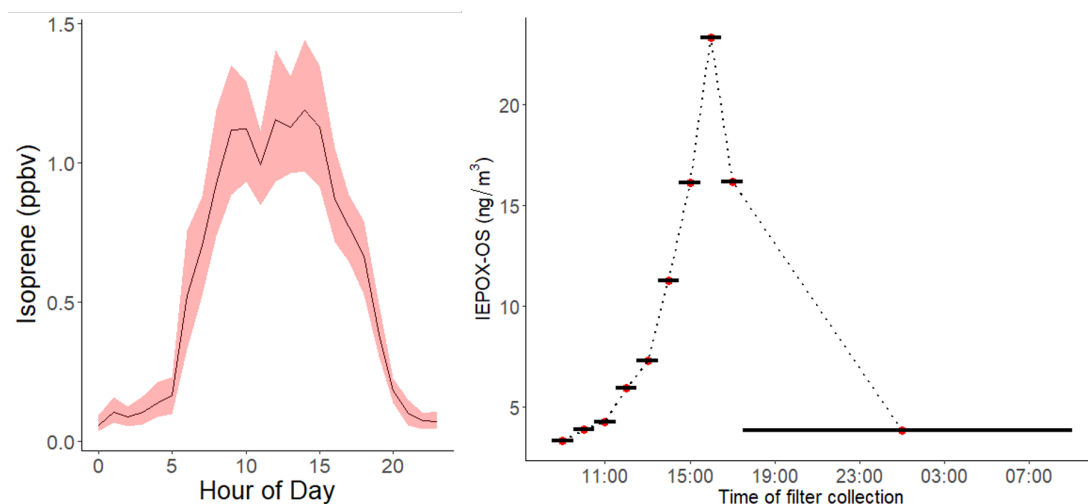


Figure 2.2: (A) Average diurnal profile of isoprene mixing ratio measured using DC-GC-FID. (B) Diurnal profile of 2-methyltetrol sulfate (2-MT-OS) in PM_{2.5} collected on filters hourly over the 11th to 12th June 2017. Black lines indicate length of filter sampling period.

becoming more important from 18:00 until around 03:00, although the amount of isoprene available to react rapidly decreased during this time period. OH chemistry is still an important loss route at night (>30 %) owing to night-time OH sources, such as the ozonolysis of alkenes.[232] Loss of isoprene via ozonolysis however is a minor route, contributing <15 %. During the daytime (10:00-15:00), the lifetime of isoprene was on average around 20 minutes, increasing to a maximum of around 6 hours at 03:00. While the high levels of oxidants lead to a short isoprene lifetime during the day, the ambient concentrations of isoprene are still maintained at the ppb level. This indicates that there are significant local emissions of isoprene impacting the measurement site and therefore a high potential for the formation of iSOA in this urban environment.

2.3.2 Anthropogenic tracers

A range of gas phase anthropogenic tracers were measured during the campaign as discussed in Shi et al., 2019. Figure 2.1 shows the time series of NO, NO₂, O₃ and particulate sulfate during the part of the campaign analysed in this study. Table 2.1 shows the average, maximum and minimum concentrations for these

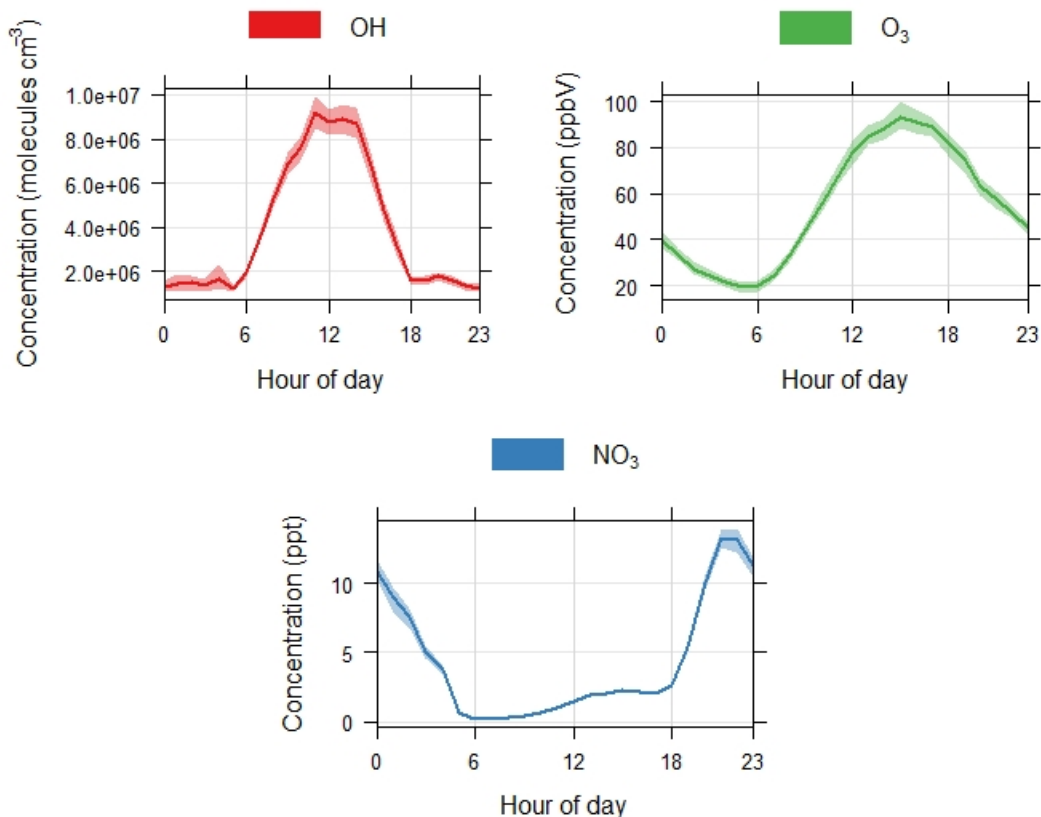


Figure 2.3: Campaign average diurnal profiles of OH measured by FAGE, O₃ measured by UV spectroscopy and NO₃ measured by BBCEAS.

anthropogenic pollutants. NO mixing ratios ranged from less than 0.1 ppbv to 104 ppbv, and a mean concentration during the filter sampling period of 5.1 ± 11.5 ppbv. The highest concentrations generally occurred in the morning 04:00-07:00 and steadily decreased during the day. On some days, the mixing ratio of NO was very low in the afternoon, likely as a result of reaction with ozone and other unknown sinks.[103] The mean mixing ratio of NO₂ was 22.3 ± 13.0 ppbv, much higher than NO, with a range of 3.7 to 95 ppbv. NO₂ peaked between 06:00-07:00 and decreased to a minima at 14:00 and then steadily increased until about 20:00. High afternoon concentrations of O₃ (>80 ppb) were observed on most days, with a maximum observed mixing ratio of 182 ppbv. Night time O₃ levels were much lower due to reduced photochemistry and reaction with NO, although on some nights O₃ levels were maintained above 40 ppbv, as shown in Figure 2.1.

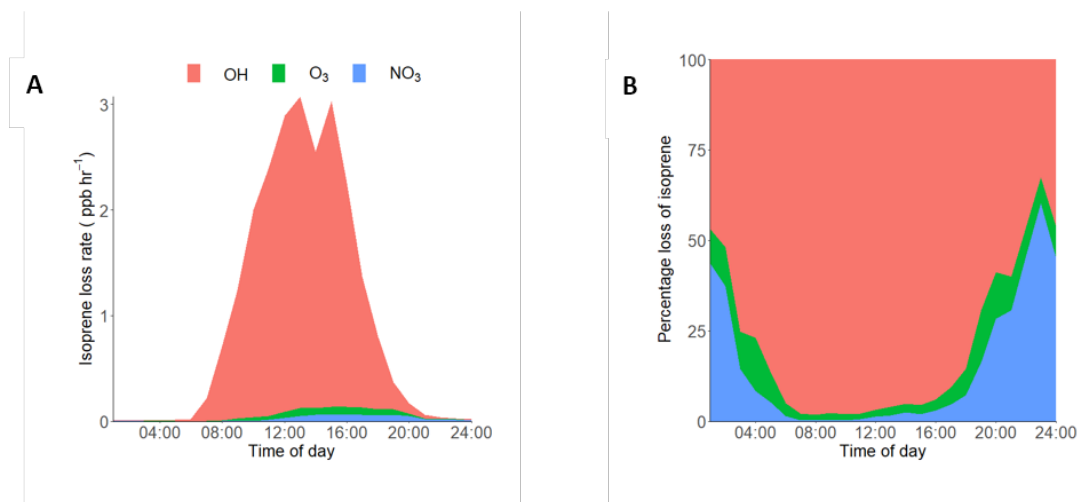


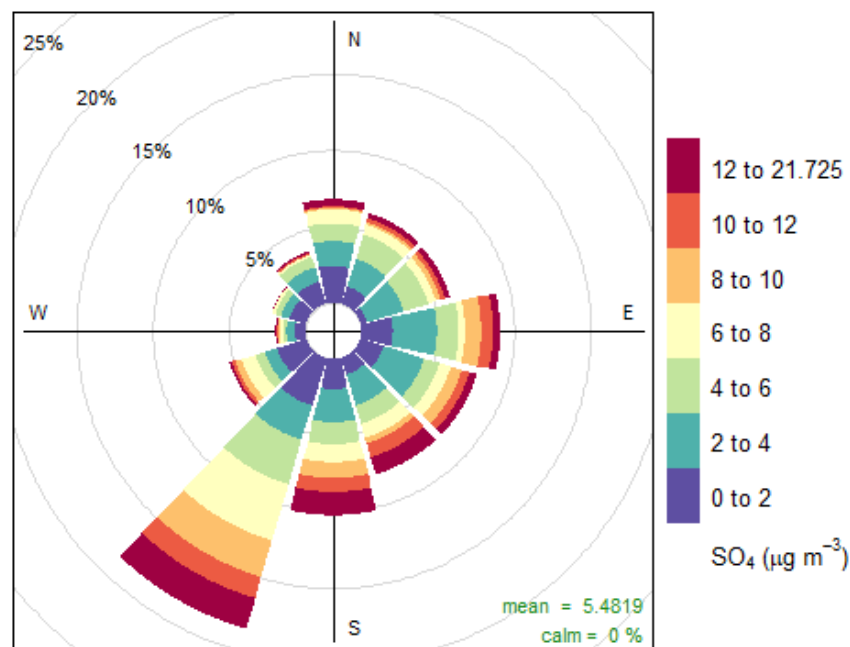
Figure 2.4: (A) Diurnal loss rate of isoprene calculated using measured average diurnal profiles of isoprene, OH, NO₃ and O₃. (B) Average diurnal of the percentage loss of isoprene from reactions with OH, O₃ and NO₃ radicals. The IUPAC rate constants used for the calculations are as follows, NO₃: 7×10^{-13} , O₃: 1.27×10^{17} , OH: $1 \times 10^{10} \text{ cm}^3 \text{ molecule}^{-1} \text{ s}^{-1}$. [102]

Table 2.1: Anthropogenic pollutants measured during the sampling period analysed in this study.

| Pollutant | Mean \pm SD | Max | Min |
|--|-----------------|-------|-----|
| O ₃ (ppbv) | 54.0 ± 37.5 | 181.8 | 2.0 |
| NO (ppbv) | 5.1 ± 11.3 | 104.1 | 0.1 |
| NO ₂ (ppbv) | 22.3 ± 13.0 | 94.5 | 3.7 |
| SO ₄ ($\mu\text{g m}^{-3}$) | 5.5 ± 4.1 | 21.7 | 0.7 |

Particulate sulfate concentrations, measured by AMS are also shown in Figure 2.1.

Sulfate ranged from 0.7 to 21.7 $\mu\text{g m}^{-3}$, with an average of $5.5 \pm 4.1 \mu\text{g m}^{-3}$. The time series shows a number of periods of high sulfate concentrations and these generally matched periods of increased PM_{2.5}. Figure 2.5 shows the wind direction dependent concentrations of particulate sulfate for the sampling period in a pollutionRose plot (R, Openair package). There is a strong source of sulfate from the south of the sampling site, which is enhanced under the highest wind speeds. Previous studies have shown a strong source of pollution from the south west of Beijing, which is where many industrial factories are located. [233]



Frequency of counts by wind direction (%)

Figure 2.5: PollutionRose plot (Openair) of particulate sulfate measured by AMS, for the sampling period. Highlighting under what wind conditions the highest concentrations of sulfate occur.

2.3.3 Isoprene SOA in Beijing

Using the high throughput screening method described, the peak areas of 31 potential isoprene-derived OSs and NOSs, were measured in 132 PM_{2.5} filter extracts. The full list of iSOA tracers, along with their measured m/z and molecular formula is shown in Table 2.2, ordered by descending average concentration (weighted by filter sampling time and reported in ng m⁻³) during the campaign. The iSOA tracers identified in this study are correlated towards themselves as well as common anthropogenic tracers in a correlation plot (R, Openair, CorPlot), shown in Figure 2.6. The correlation plot highlights the correlations of the iSOA tracers to each other as well as the moderate to strong correlations towards some

Table 2.2: Molecular formulas, negative ion masses, retention times (RT), time weighted means (ng m^{-3}) for the entire sampling period and original reference to where the tracer was found of each proposed iSOA tracer. BD = Below detection. The estimated uncertainties calculated as 60 %, accounting for the use of the matrix correction factors.

| Isoprene Tracer | [M-H] ⁻¹ | RT (min) | Time weighted mean (ng m^{-3}) | Maximum (ng m^{-3}) | Minimum (ng m^{-3}) | Ref. |
|---|---------------------|----------|---|--------------------------------|--------------------------------|-------|
| C ₂ H ₄ O ₆ S | 154.9656 | 0.73 | 38.4 | 366.1 | BD | [134] |
| C ₅ H ₁₀ O ₆ S | 197.0125 | 0.79 | 28.7 | 336.2 | 0.25 | [173] |
| C ₅ H ₁₀ O ₅ S | 181.0176 | 0.93 | 26.5 | 448.5 | 2.91 | [234] |
| C ₄ H ₈ O ₆ S | 182.9969 | 0.73 | 21.7 | 229.1 | 0.50 | [235] |
| C ₄ H ₈ O ₇ S | 198.9918 | 0.73 | 21.5 | 180.5 | 0.32 | [173] |
| C ₃ H ₆ O ₅ S | 152.9863 | 0.73 | 20.5 | 327.9 | 0.98 | [134] |
| C ₃ H ₆ O ₆ S | 168.9812 | 0.73 | 14.5 | 137.7 | 0.25 | [134] |
| C ₅ H ₈ O ₇ S | 210.9918 | 0.73 | 14.0 | 136.4 | 0.27 | [134] |
| C ₅ H ₁₁ O ₉ NS | 260.0082 | 0.86 | 12.6 | 154.1 | 0.10 | [134] |
| C ₅ H ₁₂ O ₇ S | 215.0231 | 0.71 | 11.8 | 110.9 | 0.77 | [134] |
| C ₅ H ₁₀ O ₇ S | 213.0075 | 0.73 | 10.6 | 104.7 | 0.38 | [134] |
| C ₅ H ₉ O ₁₀ NS | 273.9874 | 0.94 | 9.17 | 53.8 | BD | [149] |
| C ₄ H ₈ O ₅ S | 167.0019 | 0.73 | 9.10 | 114.5 | 0.68 | [173] |
| C ₅ H ₈ O ₅ S | 179.0020 | 0.85 | 6.59 | 144.2 | 0.43 | [235] |
| C ₅ H ₁₀ O ₅ S | 181.0176 | 1.24 | 4.90 | 36.3 | 1.21 | [235] |
| C ₅ H ₁₀ O ₈ S | 229.0024 | 0.75 | 4.59 | 40.9 | BD | [149] |
| C ₅ H ₈ O ₉ S | 242.9816 | 0.64 | 1.55 | 13.9 | BD | [149] |
| C ₅ H ₁₀ O ₁₁ N ₂ S | 304.9783 | 2.18 | 1.04 | 8.62 | BD | [134] |
| C ₁₀ H ₂₀ O ₈ S | 299.0806 | 1.65 | 1.01 | 8.38 | BD | [235] |
| C ₅ H ₁₀ O ₁₁ N ₂ S | 304.9783 | 1.89 | 0.83 | 7.69 | BD | [134] |
| C ₈ H ₁₄ O ₁₀ S | 301.0235 | 0.73 | 0.57 | 4.16 | BD | [173] |
| C ₅ H ₁₀ O ₁₁ N ₂ S | 304.9783 | 1.56 | 0.42 | 2.90 | BD | [134] |
| C ₁₀ H ₁₈ O ₇ S | 281.0701 | 1.03 | 0.33 | 6.76 | BD | [235] |
| C ₅ H ₁₀ O ₁₁ N ₂ S | 304.9783 | 3.60 | 0.31 | 3.32 | BD | [134] |
| C ₅ H ₉ O ₁₃ N ₃ S | 349.9783 | 5.90 | 0.19 | 2.04 | BD | [152] |
| C ₁₀ H ₁₈ O ₈ S | 297.0650 | 0.75 | 0.14 | 5.25 | BD | [235] |
| C ₅ H ₁₁ O ₈ NS | 244.0133 | 1.93 | 0.11 | 1.46 | BD | [149] |
| C ₅ H ₉ O ₁₃ N ₃ S | 349.9783 | 5.49 | 0.02 | 0.17 | BD | [152] |
| C ₅ H ₉ O ₁₃ N ₃ S | 349.9783 | 5.34 | 0.008 | 0.10 | BD | [152] |
| C ₅ H ₁₂ O ₈ S | 231.0180 | 0.75 | 0.005 | 0.50 | BD | [235] |
| C ₁₀ H ₂₀ O ₉ S | 315.0755 | 1.46 | 0.002 | 0.21 | BD | [235] |

of the anthropogenic pollutants as discussed in further sections.

2.3.4 Quantification of isoprene OS tracers

Initially, two synthesised OSi standards (2-MT-OS and 2-MG-OS)[187, 191] were used to produce calibration curves. Both standards gave strong linear calibration curves ($R^2 = 0.980$ and 0.996 respectively) across an appropriate range of concentrations for the peak areas in the samples. The gradient obtained for the 2-MT-OS standard was 4 times higher than that of the 2-MG-OS, as shown in Figure 2.7.

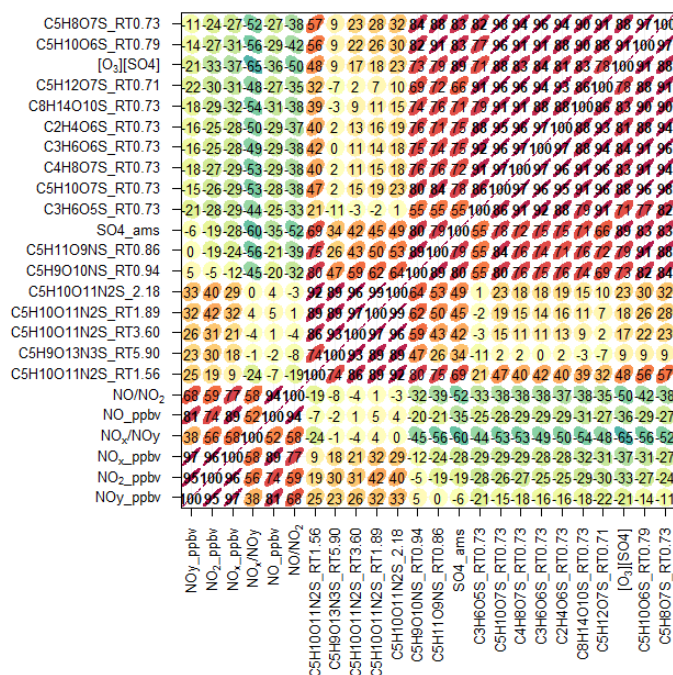


Figure 2.6: Correlation plot (R, Openair, CorPlot) highlighting the correlations between known iSOA tracers and anthropogenic pollutants. The number represents the R correlation between the two species. With redder more elongated circles highlighting a higher correlation.

To investigate the potential for matrix effects from the large amounts of inorganic sulfate, nitrate and other particulate components that co-elute due to the poor retention of OS in reverse phase UHPLC, standard addition calibrations were used. Five-point standard addition calibrations were run on 6 different filter extracts, covering both day and night-time, samples, during periods of both high and low concentrations of iSOA species. This therefore gives a representative sample of filters for the entire sampling period. 50 μL of filter sample extract and 50 μL of the calibrant solution were combined, giving a dilution factor of 2. The five-point calibration range of standard added to each sample was between 0-3 ppm for 2-MGOS and 0-1 ppm for 2-MT-OS. Two examples of the standard addition calibrations are shown in figure Figure 2.8A (2-MG-OS) and Figure 2.8B (2-MT-OS), with good linear fits observed ($R^2 = 0.997$ and 0.997 respectively).

A strong matrix effect was observed for the 2-MT-OS, with the concentration

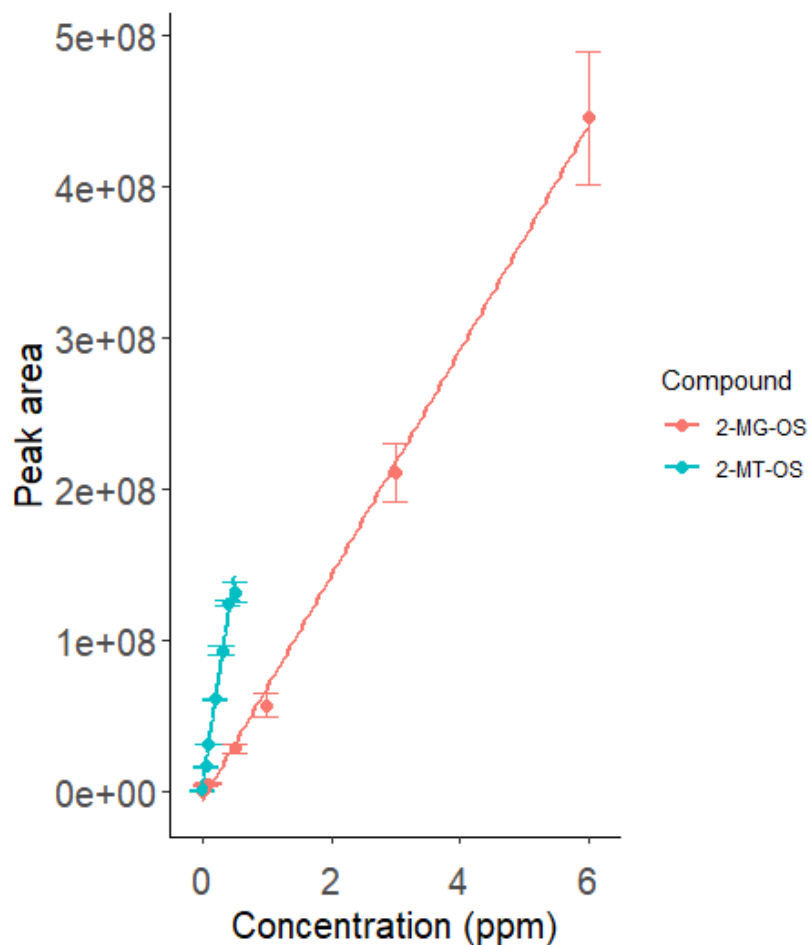


Figure 2.7: Comparison of 2-MT-OS calibration ($R^2 = 0.9804$) (Blue) and 2-MG-OS calibration ($R^2 = 0.9978$) (Red). Highlighting the difference in gradients between the two species. The error bars highlight the standard error for each concentration.

measured by standard addition calibration 8.6 to 10 times higher than when using the external calibration carried out on the same day. In contrast, the 2-MG-OS showed a much lower matrix effect, with the concentrations only 1.1-1.5 times higher when using the standard addition calibration. A further comparison using camphorsulfonic acid, which has a longer retention time (3.74 min) and so does not experience high inorganic ion concentrations in the source, showed no matrix effects when using standard addition. Table 2.3 and Table 2.4 show a comparison of the concentrations calculated from the standard additions and the two external calibrations. Table 2.3 shows the concentration of 2-MT-OS in three

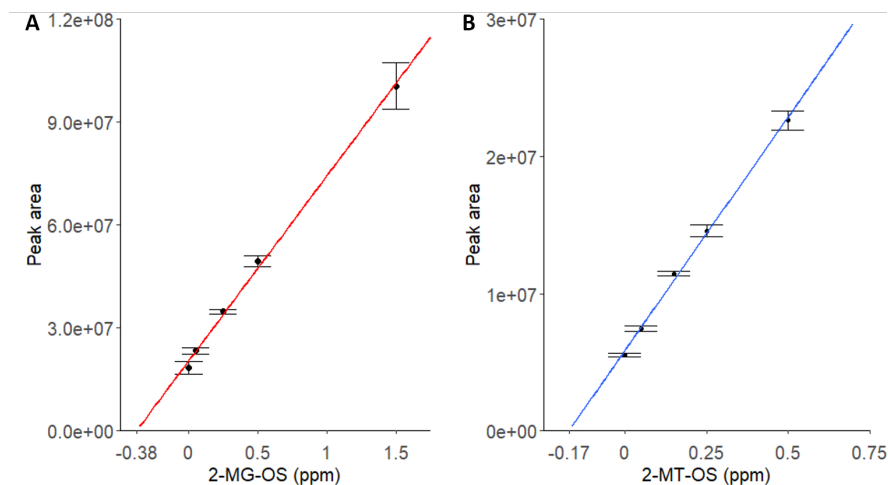


Figure 2.8: (A) 2-MG-OS standard addition calibration of filter extract 205 in Table 2.4. The error bars highlight the standard error for each concentration. (B) 2-MT-OS standard addition calibration of filter extract 204 in Table 2.3. The error bars highlight the standard error for each concentration.

filter sample extracts (144, 204, 208) calculated via standard addition of 2-MT-OS to the filter sample extract and via external calibrations using both 2-MT-OS and 2-MG-OS. The ratio of the standard addition to the external calibrations then gives an estimate of the under or overestimate the external calibrations make to calculating the concentration of 2-MT-OS in the samples. Both the external calibrations would lead to an underestimation of concentration of 2-MT-OS in the filter samples. 2-MG-OS provided a closer quantification of 2-MT-OS in the samples, with an average factor of 2.3 underestimation, while the 2-MT-OS external calibration gives a sample concentration a factor of 10 lower than the standard addition determined concentration.

Table 2.3: 2-MT-OS concentrations (ppm) for three samples (144, 204, 208) calculated from standard addition, 2-MG-OS and 2-MT-OS external calibrations.

| Sample | Filter extract concentration (ppm) | | | |
|--|------------------------------------|------|------|---------|
| | 144 | 204 | 208 | Average |
| Standard addition | 0.078 | 0.17 | 0.18 | - |
| External calibration (2-MG-OS) | 0.03 | 0.07 | 0.07 | - |
| External calibration (2-MT-OS) | 0.009 | 0.06 | 0.02 | - |
| Ratio of standard addition to 2-MG-OS | 2.2 | 1.5 | 2.5 | 2.3 |
| Ratio of standard addition to 2-MT-OS | 8.6 | 6 | 10 | 9.2 |

Table 2.4: 2-MG-OS concentrations (ppm) for three samples (144, 204, 208) calculated from standard addition, 2-MG-OS and 2-MT-OS external calibrations.

| Sample | Filter extract concentration (ppm) | | | |
|--|------------------------------------|-------|-------|---------|
| | 143 | 205 | 209 | Average |
| Standard addition | 0.0097 | 0.38 | 0.28 | - |
| External calibration (2-MG-OS) | 0.0091 | 0.25 | 0.19 | - |
| External calibration (2-MT-OS) | 0.0023 | 0.064 | 0.049 | - |
| Ratio of standard addition to 2-MG-OS | 1.1 | 1.5 | 1.4 | 1.3 |
| Ratio of standard addition to 2-MT-OS | 4.2 | 6 | 5.6 | 5.3 |

It is not realistic to carry out standard addition calibrations for all samples and all SOA tracers. When the 2-MG-OS external calibration was used to predict the 2-MT-OS concentrations during the standard addition experiments, the concentrations were within a factor of 1.5-2.5. Therefore, the 2-MG-OS external calibration was used as a proxy for all isoprene SOA tracers, with scaling factors applied to account for matrix effects (1.33 for 2-MG-OS, 2.33 for 2-MT-OS, and an average of 1.83 used for all other OSs). Therefore, we estimate an uncertainty on our measured concentrations of 60%, this uncertainty was calculated to account for the difference in the measured correction factors used when correcting for the matrix effects. The uncertainty was calculated as 2σ of the 6 values used to calculate the average correction factor of 1.83. The matrix effects identified in this study are likely due to the extracted samples being a complex mixture of different compounds, including a high proportion of inorganic ions that are extracted into water. This is likely to change the surface tension of the droplet produced in the ionisation source and the ion distribution. Further work is needed to fully understand the reasons. Without these additional standard addition calibrations, the iSOA concentrations would have been largely underestimated. The dinitrate and trinitrate NOS species eluted after the sulfate peak ($R_t > 1.6$ min), suggesting these species are less likely to be influenced by ME's. In the absence of authentic standards for these species, camphorsulfonic acid was used as a proxy for calibration. This work highlights an additional difficulty of calibration when using ESI-MS to study OSi and NOSi and indicates that future studies using reversed phase LC (RPLC) should consider the impacts of matrix effects.

2.3.5 Organosulfates

2.3.5.1 2-methyltetrol OS (2-MT-OS)

2-MT-OS ($C_5H_{12}SO_7$) formed from the uptake of IEPOX into the particle phase is often used as a marker of low-NO isoprene photochemistry.[106] The time series of 2-MT-OS is shown in Figure 2.9A. The particle concentration ranged from 0.7 $ng\ m^{-3}$ to a maximum of 111 $ng\ m^{-3}$, with a mean concentration of 11.8 $ng\ m^{-3}$. The mean concentrations of 2-MT-OS and 2-MG-OS are compared to observations in previous studies in Table 2.5. The mean concentration observed in Beijing was much lower than those observed in the Amazon[143] and the SE US[34, 35] but are higher than summer time observations at polluted regional sites in China [126, 218]. The lower amounts of IEPOX-derived SOA results in an average AMS $f_{C_5H_6O}$ in Beijing during the APHH project of only 0.2 %, similar to observations in other urban studies.[216]

Hourly samples were collected on selected high pollution days and used to obtain information on the diurnal evolution of the iSOA tracers. The findings on these days are consistent with the three-hourly data. The particulate 2-MT-OS measured by UHPLC-MS, on the 11th - 12th June 2017, had a strong diurnal profile (Figure 2.2), peaking in the late afternoon, between 15:30 and 18:30, with a minimum over-night. This is consistent with the average diurnal profile of the gas phase precursors IEPOX+ISOPOOH ($C_5H_{12}O_3$) measured using the I-CIMS (Figure 2.10).

High levels of ozone were observed in the afternoon (up to 180 ppb), leading to relatively low levels of NO observed for a highly polluted environment, in some cases below 500 ppt. Thus, although the mixing ratio of NO_x was high, on most afternoons less than 2 % was in the form of NO. High levels of peroxy radicals were observed, with mean afternoon concentrations of HO_2 and RO_2 of around 3×10^8 molecule cm^{-3} and 1.5×10^9 molecule cm^{-3} , respectively. Zero-dimensional box modelling undertaken by Dr Mike Newland, University of York indicates on some days up to 35 % of the isoprene-derived RO_2 radicals can react with HO_2 in the

Table 2.5: Comparison of concentrations of iSOA tracer concentrations and ratios in previous studies in the Amazon, SE USA and China. *Selected sample not an average concentration. Beijing (2017) values are taken from this study.

| Mean Concentration (ng m ⁻³) | | | | Low:High NO | | CHO:CHOS | |
|---|----------|------|----------|-------------|-----------------|--------------|--------------|
| 2-MT | 2-MT-OS | 2-MG | 2-MG-OS | 2-MT:2-MG | 2-MT-OS:2-MG-OS | 2-MT:2-MT-OS | 2-MG:2-MG-OS |
| Amazon, Manuas (2016) [187] | | | | | | | |
| 137* | 390* | – | – | – | – | 0.35 | – |
| Amazon, T3 (2014) [124] | | | | | | | |
| – | 83(wet) | – | 0.7(wet) | – | 118(wet) | – | – |
| – | 399(dry) | – | 30(dry) | – | 13(dry) | – | – |
| SE US, Centreville (2013) [143] | | | | | | | |
| – | 217 | – | 10.7 | – | 20.3 | – | – |
| SE US, Look Rock (2013) [34] | | | | | | | |
| 163.1 | 169.5 | 7.5 | 10 | 21.7 | 17.0 | 0.96 | 0.75 |
| SE US, Look Rock (2013) [187] | | | | | | | |
| 861* | 2334* | – | – | – | – | 0.37 | – |
| SE US, Atlanta (2015) [35] | | | | | | | |
| – | 1792 | – | 53 | – | 33.8 | – | – |
| China Regional, PRD (2008) [218] | | | | | | | |
| 91.5 | 2.2 | 7.7 | 1.4 | 11.9 | 1.57 | 41.6 | 5.51 |
| China Regional, Beijing (2016) [126] | | | | | | | |
| – | 5.3 | – | 3.6 | – | 1.47 | – | – |
| China Rural, NCP (2013) [236] | | | | | | | |
| 44 | – | 19.3 | – | 2.30 | – | – | – |
| China Urban, Beijing (2017) | | | | | | | |
| 17.3 | 11.8 | 7.2 | 21.5 | 2.40 | 0.55 | 1.47 | 0.33 |

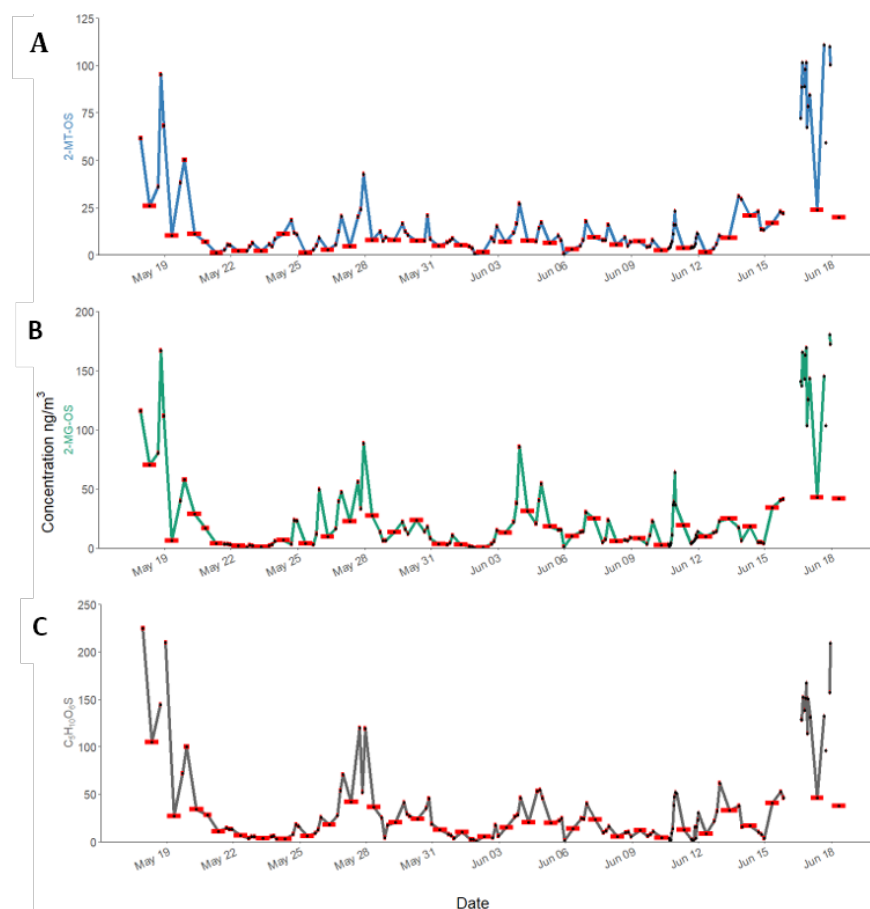


Figure 2.9: Time series of observed concentrations of iSOA tracers in Beijing during APHH. (A) 2-MT-OS ($C_5H_{12}O_7S$) (B) 2-MG-OS ($C_4H_8O_7S$) (C) $C_5H_{10}SO_6$. The red bars indicate the length of the sampling time.

afternoon.[103] Thus, the diurnal profile seen in Figure 2.2, measured in samples during the measurement period suggests that IEPOX was formed at this urban location by the reaction of OH with local isoprene emissions, with a fraction of the RO_2 radicals formed reacting with HO_2 rather than NO, and subsequent uptake to aerosol forming 2-MT-OS. OH + isoprene hydroxynitrate also has a small yield of IEPOX.[237] The average diurnal profile of isoprene hydroxynitrates ($C_5H_9NO_4$) in the gas phase measured using the I-CIMS peaks at around 11:00-12:00 followed by a reduction during the afternoon into the evening/night (Figure 2.11).

This is likely to be a result of the relatively low levels of NO during the afternoon, which will reduce isoprene nitrate formation from $RO_2 + NO$ reactions, thus isoprene hydroxynitrates are unlikely to be a significant source of 2-MT-OS

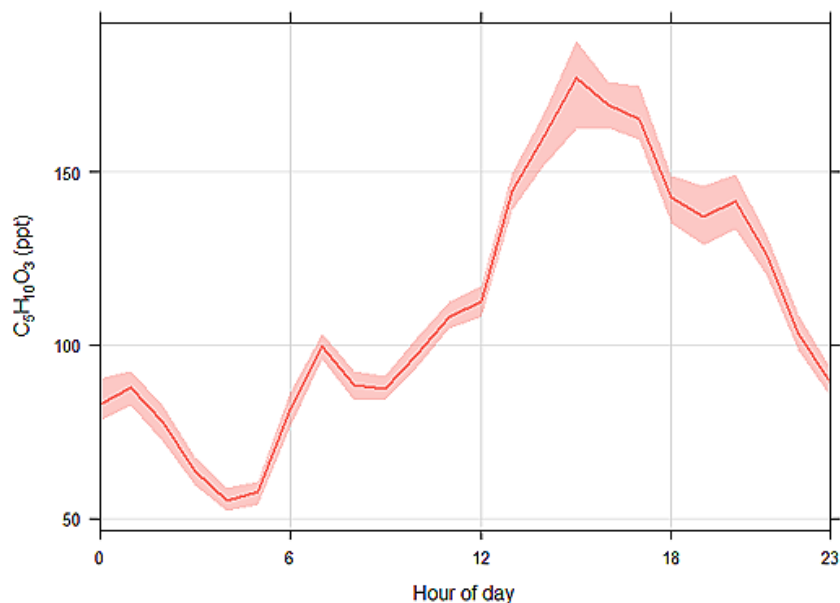


Figure 2.10: Campaign average diurnal variation with 95% confidence interval of $C_5H_{10}O_3$ measured in the gas phase using I-CIMS.

in Beijing. The 2-MT-OS showed a moderate correlation with particulate sulfate ($R^2 = 0.44$), and a weak anti-correlation with photochemical age, estimated using the ratio of NO_x/NO_y ($R^2 = 0.23$) as shown in Figure 2.6. All correlations between species are shown in Figure 2.6. By taking the product of the concentration of O_3 , as a proxy of photochemistry, with the amount of particulate sulfate measured using AMS, $[O_3][pSO_4]$, a much stronger correlation with 2-MT-OS was observed ($R^2 = 0.61$) as shown in Figure 2.12. This observation highlights the role of both local photochemistry and particulate sulfate mass in the formation of 2-MT-OS. The correlation of $[O_3][pSO_4]$ with 2-MT-OS is likely to be weaker at longer photochemical ages when the O_3 concentration is not directly related to the photochemical formation of the OS. Again, this highlights the strong role of local photochemistry in the production of low-NO iSOA (2-MT-OS) in Beijing. Elevated levels of 2-MT-OS were observed at the start and end of the measurement period which were influenced by strong south-westerly winds. There were also elevated isoprene concentrations (up to 2.9 ppb) and high particulate SO_4^{2-} levels. Therefore, these spikes in 2-MT-OS could be a result of either higher

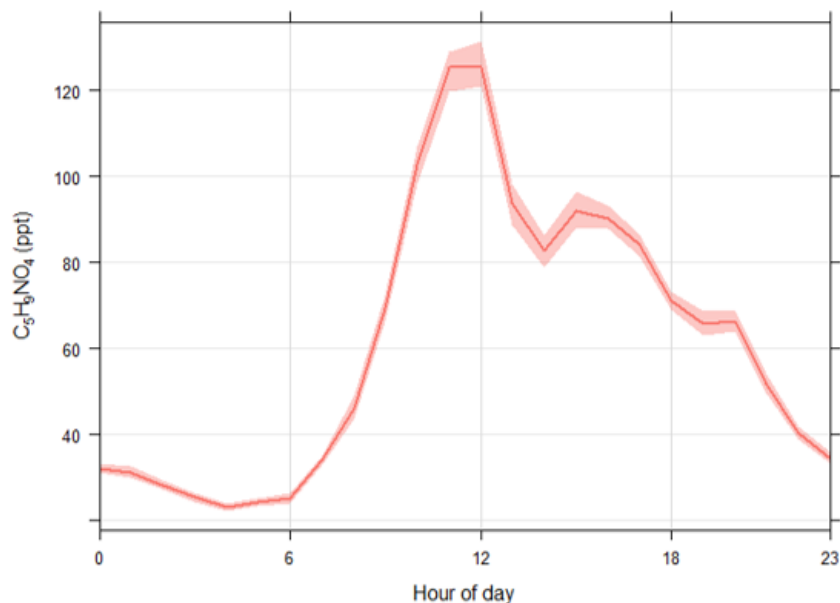


Figure 2.11: Campaign average diurnal variation with 95% confidence interval of $C_5H_9NO_4$ measured in the gas phase using I-CIMS.

2-MT-OS in regional aerosol transported to the site or a high isoprene emission source to the south west of the site (i.e. producing IEPOX locally) that then reacts with increased regional sulfate pollution. The I-CIMS data shows that the IEPOX/ISOPOOH (Figure 2.10 and Newland et al., 2020) signal increases during the afternoon as the NO levels drop to below 1 ppb. The low NO levels mean that up to 30 % of the isoprene peroxy radical from OH oxidation can react with HO₂ rather than NO at this site, meaning IEPOX can be formed locally.[103] There is also likely to be a regional source of IEPOX and 2-MT-OS, suggesting both local and regional anthropogenic influences.

Analysis of the 2-MT-OS isomer distribution using HILIC/ESI-HR-QTOFMS, on a subset of 15 samples, indicates that β -IEPOX is the dominant ambient IEPOX isomer, in line with other recent observations see as shown in Figure 2.13).[187, 238] The MT-OS derived exclusively from δ -IEPOX-OS isomers could not be observed in any of the samples. The 4 IEPOX-OS isomers in Figure 2.13 showed similar temporal trends although small changes in the relative proportions were observed. The sum of peak areas from the 2-MT-OS isomers measured by HILIC

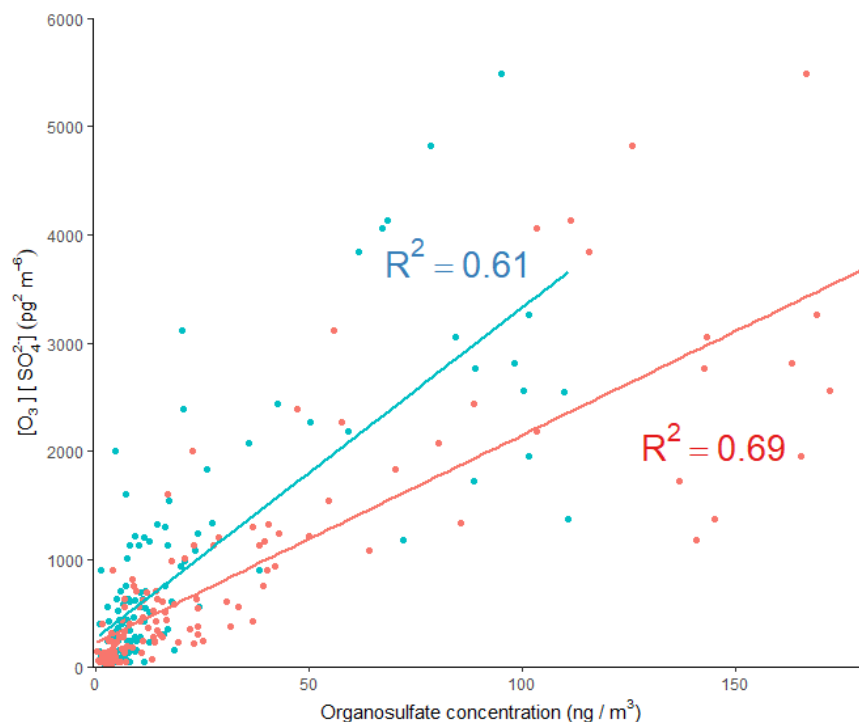


Figure 2.12: Plot of 2-MT-OS ($C_5H_{12}O_7S$, blue) and 2-MG-OS ($C_4H_8O_7S$, red) concentrations versus $[O_3][SO_4]$. The high time resolution data (O_3 and AMS SO_4) has been averaged to the filter sampling time.

and the quantified 2-MT-OS (sum of isomers) measured via UHPLC/ESI-HR-MS were compared and showed a high degree of correlation ($R^2 = 0.84$), even though the two methods used different solvents. The agreement indicates that the UHPLC/ESI-HR-MS method captures the sum of the isomers and there is no evidence of ion source induced artefacts.

2.3.5.2 2-methyl glyceric acid OS (2-MG-OS)

The most common targeted iSOA tracer for high-NO isoprene chemistry is 2-methylglyceric acid (2-MG) and its derivatives. As such, this tracer is the result of a direct biogenic-anthropogenic interaction. Two observed iSOA tracers related to this chemistry are the OS derivatives of 2-methylglyceric acid (2-MG-OS) and the unresolved C_8 dimers of 2-MG-OS ($C_8H_{14}SO_{10}$) that have been identified previously in chamber-derived iSOA.[127, 239] 2-MG-OS had an average concentration during the campaign of 21.5 ng m^{-3} , ranging from 0.3 to 180.5

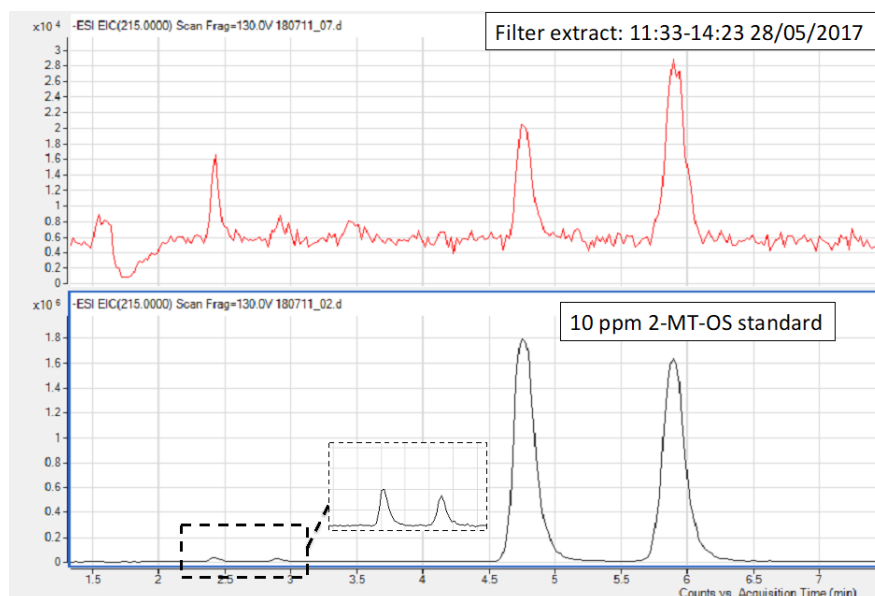


Figure 2.13: Extracted ion chromatograms (m/z 215.0) using hydrophobic interaction liquid chromatography (HILIC) of 2-methyltetrol OS (2-MT-OS) isomers, highlighting improved separation of isomers using this technique. Upper: Extract of filter collected on the 28/05/2017 between 11:33 and 14:23. Lower: 10 ppm 2-MT-OS standard.[187]

ng m^{-3} , with the time series shown in Figure 2.9B. These values are within the range of 2-MG-OS measured in other urban locations.[35, 191, 240] However, these concentrations are considerably higher than previously observed at two Chinese regional background sites.[126, 218] At these locations, the ratio of the low-NO to high-NO OSi tracer average concentrations was close to 1.5 (2-MT-OS:2-MG-OS; Beijing = 1.47, Wanqingsha = 1.57). However, in central Beijing, this ratio was considerably lower (2-MT-OS:2-MG-OS = 0.55), reflecting the higher proportion of RO_2 radicals reacting with NO at this location compared to the regional measurements. The ratio of 2-MT-OS:2-MG-OS observed in Beijing is compared to previous studies in Table 2.5 and is considerably lower than measurements taken in a range of isoprene dominated environments (South East US, 2-MT-OS:2-MG-OS = 17[34]; Amazon, 2-MT-OS:2-MG-OS = 13-118[124]; Atlanta, 2-MT-OS:2-MG-OS = 33[35]) reflecting the strong impact of urban NO emission on iSOA formation. Future work should investigate how to use these ratios to quantify the effect of NO emission on iSOA formation in different regions.

The mean concentration of the 2-MG-OS dimer ($C_8H_{14}SO_{10}$) was 0.57 ng m^{-3} . A strong linear relationship was observed between the 2-MG-OS monomer and dimer concentrations ($R^2 = 0.83$) with a dimer:monomer ratio of 0.02. Formation of oligomers from reactions of 2-MG and HMML has been shown to be reduced in chamber experiments under humid conditions.[149, 241] The average RH during the afternoon of the campaign was 40 %, which may account for the relatively low formation of the dimer OS compared to the monomer as shown in Figure 2.14.

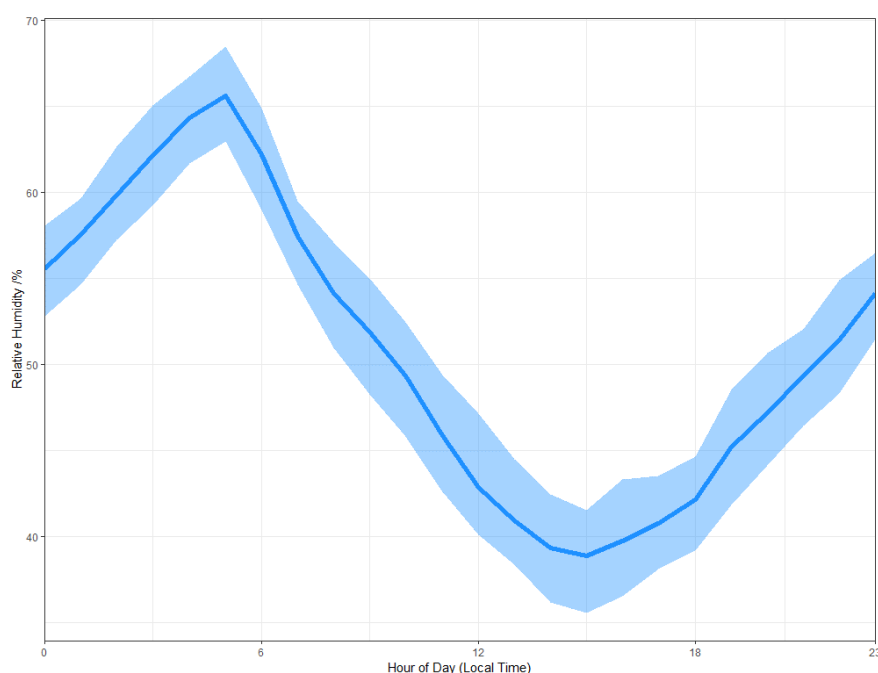


Figure 2.14: Campaign average diurnal of relative humidity (%).

The diurnal profile of the 2-MG-OS as shown in Figure 2.15 was similar to the 2-MT-OS peaking during the early afternoon samples but with an enhanced signal at night. There was also a strong correlation between these two species ($R^2 = 0.92$) during the campaign. The 2-MG-OS showed a stronger correlation with particulate sulfate ($R^2 = 0.52$) than 2-MT-OS ($R^2 = 0.44$), and there was also a weak anti-correlation with photochemical age ($R^2 = 0.28$). A strong correlation was also observed for 2-MG-OS with $[O_3][pSO_4]$ ($R^2 = 0.69$), as shown in Figure 2.12, highlighting that formation is dependent on both photochemistry and sulfate aerosol availability.

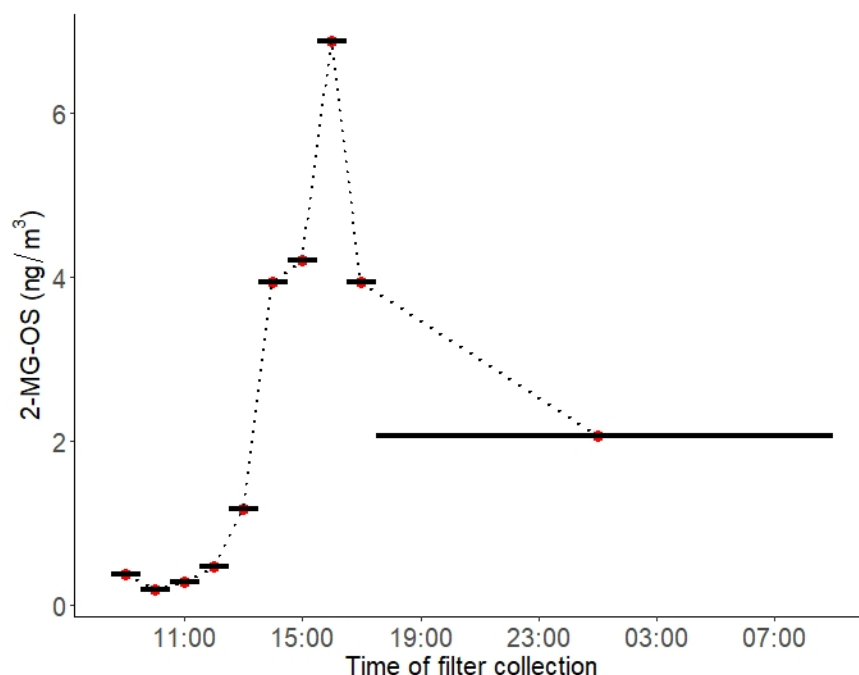


Figure 2.15: Diurnal profile of 2-methylglyceric acid sulfate (2-MG-OS) in particulate matter collected on filters hourly over the 11th to 12th June 2017. Black lines indicate length of sampling.

2.3.5.3 Other isoprene-related OSs

24 additional OSs species, with molecular formulae consistent with iSOA tracers seen in previous chamber experiments, were also observed in Beijing as shown in Table 2.2. For C₅ compounds, the most abundant species were C₅H₁₀SO₆ and C₅H₁₀SO₅, with mean concentrations of 28.7 ng m⁻³ and 26.5 ng m⁻³, respectively. The identity of the OS at m/z 182 (C₅H₁₀SO₅) is currently unknown and the product ion MS provides little additional information other than sulfate-related fragment ions at m/z 97 and m/z 80. The OS at m/z 198 (C₅H₁₀SO₆) was identified as an IEPOX-related OS in chamber experiments by Nestorowicz et al., 2018, but at relatively low concentrations compared to the 2-MT-OS (1-4 %). This is very different to the observed ratio in Beijing, where the C₅H₁₀SO₆ average concentration was more than double that of 2-MT-OS, as shown in Figure 2.9. This compound showed a strong correlation with 2-MT-OS (R² = 0.77) but it is currently unclear why this compound is the most abundant C₅ species. The

molecular weight of this species is 18 Da ($-\text{H}_2\text{O}$) lower than 2-MT-OS, which may indicate it is a dehydration product enhanced under acidic aerosol conditions. In addition, this species may also be enhanced if it is formed from additional VOC precursors.

Potential low-NO iSOA tracers, seen in chamber experiments, correlated strongly with the 2-MT-OS including unresolved isomers of cyclic hemiacetals [$\text{C}_5\text{H}_{10}\text{SO}_7$ ($R^2 = 0.92$)], and lactones [$\text{C}_5\text{H}_8\text{SO}_7$ ($R^2 = 0.83$)]. [242] These compounds were similar in concentration to the 2-MT-OS, with the lactones at MW 212 having a mean concentration of 14 ng m^{-3} and the cyclic hemiacetals at MW 214 a mean of 10.6 ng m^{-3} . These compounds were also observed to be the dominant type of OSi in Atlanta, Georgia, although they had concentrations a factor of 15 times lower than the observed 2-MT-OS. [35]

Additional small OS compounds, previously identified during high-NO chamber experiments, were also observed in Beijing, including in order of decreasing concentration, glycolic acid sulfate ($\text{C}_2\text{H}_4\text{SO}_6$, mean = 38.4 ng m^{-3}), hydroxyacetone sulfate ($\text{C}_3\text{H}_6\text{SO}_5$, mean = 20.5 ng m^{-3}) and lactic acid sulfate ($\text{C}_3\text{H}_6\text{SO}_6$, mean = 14.5 ng m^{-3}). [134, 173] These concentrations are in line with measurements made in other urban locations. [36, 191, 193] While all three $\text{C}_2 - \text{C}_3$ -OS compounds had strong correlations with the other OSi tracers ($R^2 = 0.6-0.94$), the relative strength of isoprene versus other VOC precursors, such as aromatics, cannot be determined. As such, they cannot be definitively assigned as iSOA tracers, and are therefore included in the potential iSOA portion of Figure 2.16. The sum of the C_2 and C_3 OSi had an average concentration of 73 ng m^{-3} , with a range of $2.0-831 \text{ ng m}^{-3}$.

2.3.6 Isoprene nitrooxy organosulfates

Nine NOSi compounds were observed in the Beijing samples and their mean, median and maximum observed concentrations are shown in Table 2.2. Two mono-nitrated tracers ($\text{C}_5\text{H}_{11}\text{NO}_9\text{S}$, MW 261 and $\text{C}_5\text{H}_9\text{NO}_{10}\text{S}$, MW 275) followed

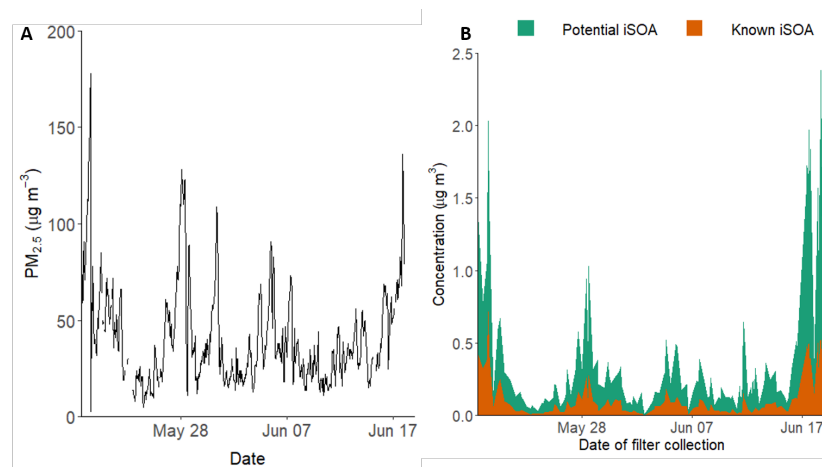


Figure 2.16: A) Time series of $PM_{2.5}$ over the sampling period. B) Time series of the total known isoprene SOA signal (2-MT-OS, 2-MG-OS, $C_5H_{10}SO_7$ (MW 214), $C_5H_8SO_7$ (MW 212), $C_5H_{11}NSO_9$ (MW 261), $C_5H_9NSO_{10}$ (MW 275), $C_5H_{10}O_{11}N_2S$ (MW 306), $C_5H_9O_{13}N_3S$ (MW 351) and the total signal from the other iSOA tracers quantified in this study.

similar temporal trends as other OSi, peaking generally during the day, and with a strong correlation with particulate sulfate as discussed above. Four di-nitrated isomers ($C_5H_{10}N_2O_{11}S$, MW 306) and three tri-nitrated isomers ($C_5H_9N_3O_{13}S$, MW 351) were also observed, all showing a strong enhancement during the night.

2.3.6.1 Mono-nitrate NOS

A NOS ($C_5H_{11}NO_9S$, MW 261) consistent with 2-methyltetrol nitrooxyorgano-sulfate, was observed and the time series is shown in Figure 2.17A. This species had a mean concentration of 12.6 ng m^{-3} , a standard deviation of 19.6 ng m^{-3} , and a maximum of 154 ng m^{-3} . This mean concentration is similar to that of 2-methyltetrol-OS (2-MT-OS, MW 216) in $PM_{2.5}$, observed during the same period (mean = 11.8 ng m^{-3} , a standard deviation of 26.3 ng m^{-3}). This species generally peaked in the samples taken during the late afternoon, as shown in the box whisker plots in Figure 2.18A, although there is not a very strong diurnal profile. This NOSi species was observed to have a moderate correlation with particulate sulfate ($R^2 = 0.61$) shown in Figure 2.6. This NOSi species also correlated moderately to strongly with other OS species formed from isoprene oxidation by

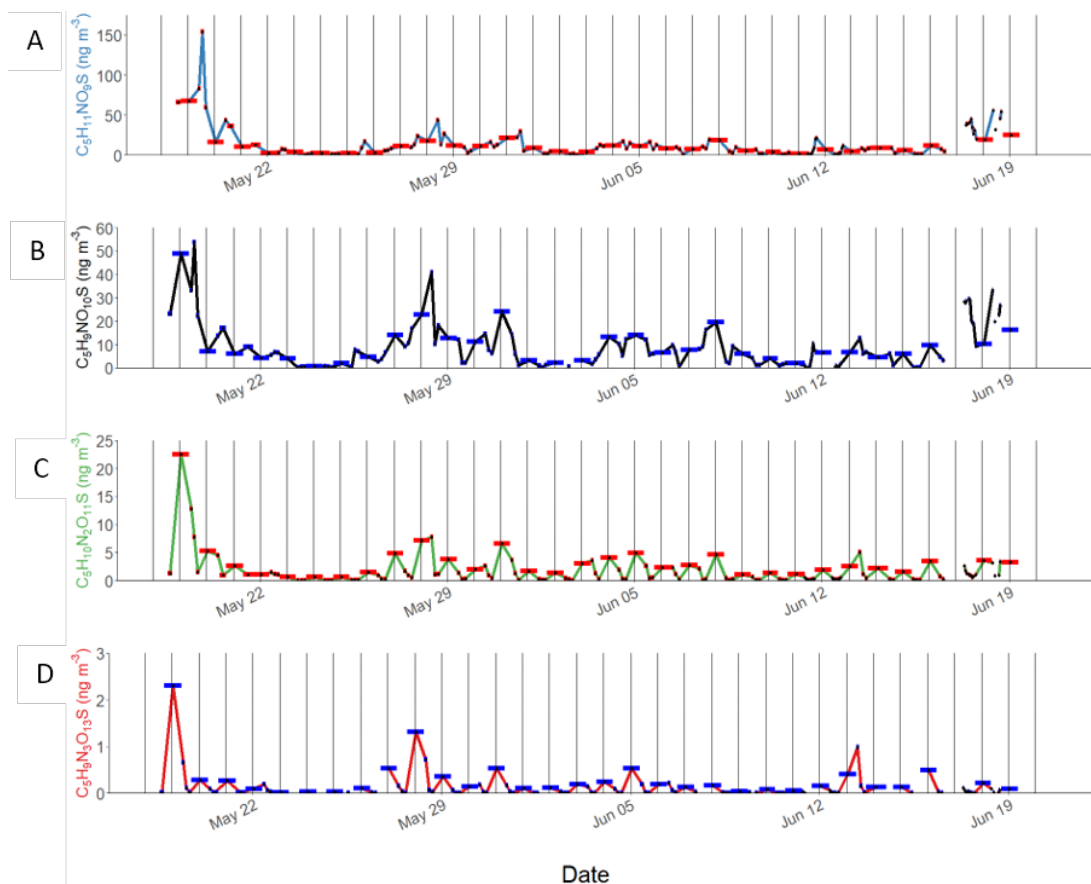


Figure 2.17: Time series of the measured concentrations of NOS in Beijing aerosol. The vertical lines are at midnight of each day of sampling. A) $C_5H_{11}NO_9S$ (MW 261). B) $C_5H_9NO_{10}S$ (MW 275). C) Sum of $C_5H_{10}N_2O_{11}S$ species (MW 306). D) Sum of $C_5H_9N_3O_{13}S$ (MW 351) species. The blue and red bars on each point show the full filter sampling time. The mid-sample points are connected with a line to show the temporal trend.

OH, observed in Beijing (2-MT-OS, $R^2 = 0.51$; 2-methylglyceric acid-OS, $R^2 = 0.58$; $C_5H_{10}O_6S$, MW 198, $R^2 = 0.80$). Wang et al., 2018 also observed that this NOS species correlated well with other OSi at Changping, a site 38 km northeast of Beijing.[126] Figure 2.19 shows a new proposed route of formation, via the acid-catalysed heterogeneous uptake of isoprene nitrooxy hydroxyepoxide (INHE). The reaction of isoprene with NO_3 radicals leads to isoprene nitrooxy peroxy radicals (INO_2). Under the low concentrations of NO observed in this study, INO_2 can react with HO_2 , leading to the formation of isoprene nitrooxy hydroperoxide (INP), as shown in the central section of Scheme 1. There are six possible INP

isomers and only the most abundant isomer (δ -[1,4]-INP) observed by Schwantes et al., 2015 is shown.[109] The reaction of INP with OH radicals, followed by OH recycling, can lead to INHE (β -[4,1]-INHE and β -[1,2]-INHE) in a similar way to the formation of IEPOX from the reaction of OH with ISOPOOH.[121] Schwantes et al.,2015 also showed that INHE could undergo reactive uptake to highly acidified aerosol, similar to IEPOX.[109]

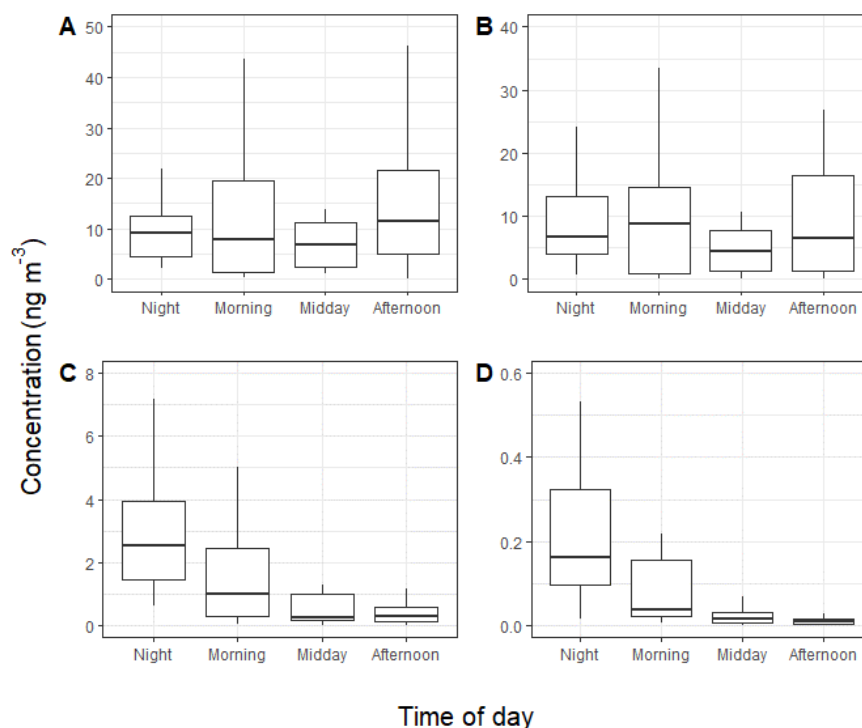


Figure 2.18: Box and whisker plots of observed NOS concentrations separated by the time of day the filter was collected. A) $C_5H_{11}O_9NS$, B) $C_5H_9O_{10}NS$, C) $C_5H_{10}O_{11}N_2S$, D) $C_5H_9O_{13}N_3S$. The filter mid-points were split into different times of day, 00:00-07:00, 07:00-11:00, 11:00-13:00 and 13:00 -17:00 based on the general sampling times of the filters and labeled as night, morning, midday and afternoon respectively. The thick black line represents the median value, the upper and lower hinges represent the 75th and 25th percentiles respectively, with the upper and lower whiskers representing the largest value in the set. Outliers were removed so the diurnal profiles could be seen more clearly.

INP, the precursor to INHE, only forms from NO_3 oxidation of isoprene. In Schwantes et al., 2015 it was proposed that any INP formed overnight and any still remaining at sunrise could undergo OH oxidation to form INHE. Ambient observations indicate that the suppressed NO conditions often experienced in

Beijing during the afternoon[103] could enhance the production of daytime INHE in this polluted environment owing to two factors. First, the loss rate of NO_3 via the reaction with NO is reduced due to low afternoon NO concentrations leading to a longer NO_3 daytime lifetime. Second, the INO_2 radicals that form from $\text{NO}_3 + \text{isoprene}$ chemistry will have a longer lifetime under low- NO conditions and thus a higher fraction will react with HO_2 to form INP. INP produced in the daytime can then readily react with OH to form INHE.

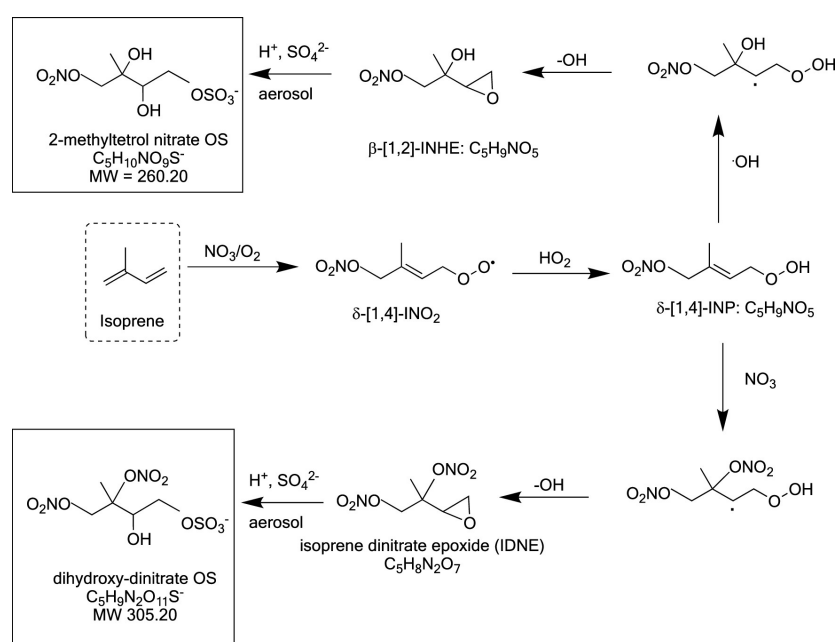


Figure 2.19: Proposed Formation Pathways of Mono-Nitrated OS and Di-Nitrated OS Species Observed in the Aerosol from the NO_3 Initiated Oxidation of Isoprene. Note that only one of six possible INP isomers is shown, for simplicity, with δ -[1,4]-INP and β -[1,2]-INHE the dominant isomers observed in Schwantes et al., 2015.

A second mono-NOSi marker ($\text{C}_5\text{H}_9\text{NO}_{10}\text{S}$, MW 275) was observed, and the time series is shown in Figure 2.17B. This species had a mean concentration during the campaign of 9 ng m^{-3} , a standard deviation of 10.1 ng m^{-3} , and a maximum of 53.8 ng m^{-3} . This species had no obvious diurnal profile, as shown in Figure 2.18B. Of all the iSOA tracers observed, this compound correlated most strongly with the 2-methyltetrol NOS ($\text{C}_5\text{H}_{11}\text{NO}_9\text{S}$) ($R^2 = 0.79$). Nestorowicz et al., 2018 identified this species as a highly oxidized NOS tracer formed from

2-methylthreonic acid in iSOA collected during photo-oxidation experiments in the presence of NO.[149]

This NOSi species could be produced from two alternative routes. First, from the oxidation of isoprene nitrooxy aldehyde (a C₅ carbonyl nitrate species (ICN))[109, 243, 244] formed from the reaction of INO₂ with NO, NO₃, and/or another RO₂ species, or from the reaction of INP with OH (in an alternative reaction pathway to the formation of INHE). This ICN species can then react with NO₃ or OH, leading to the formation of the observed NOS species via an isoprene nitrooxy hydroxy- α -lactone (INHL) species, as shown in figure 2.20. This route is similar to the formation of 2-MG from isoprene + OH derived hydroxymethyl-methyl- α -lactone (HMML).[133] The second proposed route is the formation of this species as a result of heterogeneous oxidation of 2-methyltetrol nitrate (C₅H₁₁NO₉S). This route has recently been shown to be an important pathway to form the non-nitrated OS analogues, with 2-MT-OS undergoing salting-out to the surface of particles making it susceptible to heterogeneous OH oxidation.[149] The carbonyl species formed may then undergo cyclization to form a NOS hemiacetal species.

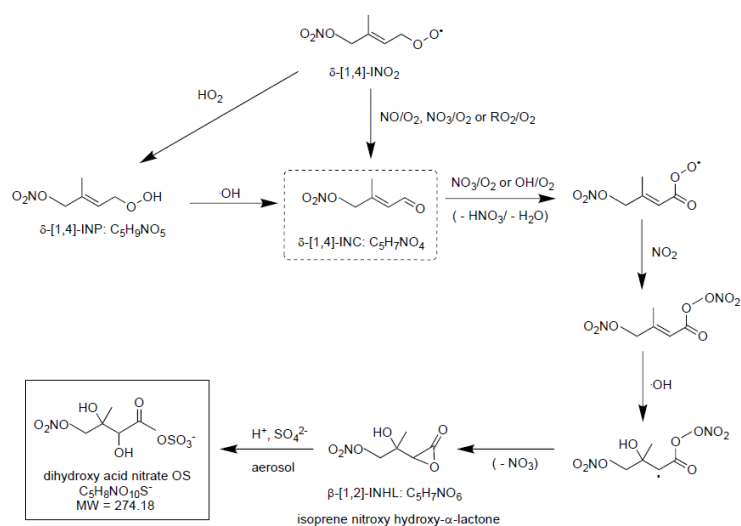


Figure 2.20: Proposed Formation Pathway of the Mono-Nitrated OS C₅H₉NO₁₀S species.

2.3.6.2 Di- and Tri-Nitrated NOS

Four of the NOSi species observed are di-nitrated isomers ($C_5H_{10}N_2O_{11}S$, MW 306, with retention times 1.56, 1.86, 2.18, and 3.6 min) and three are tri-nitrated isomers ($C_5H_9N_3O_{13}S$, MW 351, with retention times 5.34, 5.49, and 5.90 min). These structural isomers result from the different INO_2 radicals that can form during isoprene + NO_3 oxidation. However, the product-ion mass spectra (MS^2) provided only a few ions related to the loss of sulfate and nitrate and could not be used to determine the position of the groups. The time series of the sum of the di- and tri-nitrated NOSi is shown in Figure 2.17C,D, respectively. The sum of the four di-nitrated NOSi isomers had an average concentration of 2.6 ng m^{-3} , a standard deviation of 2.6 ng m^{-3} , and a maximum of 23 ng m^{-3} . The tri-nitrated NOSi species were observed at much lower concentrations, with an average sum of 0.2 ng m^{-3} , a standard deviation of 0.3 ng m^{-3} , and a maximum of 2.3 ng m^{-3} . These NOSi exhibited moderate to strong correlations with each other, as shown in Figure 2.6 ($R^2 = 0.76\text{--}0.99$). The di-nitrated NOSi (MW 306) species show a strong enhancement at night, as shown in Figure 2.18C, with the mean nighttime concentration (3.43 ng m^{-3}), around 7 times higher than during the afternoon (0.47 ng m^{-3}). These NOS tracers have all previously been observed in chamber studies of NO_3 oxidation of isoprene.[109, 134, 149, 152] The same di-nitrates have also been observed during the oxidation of isoprene by OH in the presence of NO[134], but this is assumed to be a minor NOS formation pathway under the conditions observed in Beijing owing to their significant enhancement in the night-time samples. The tri-nitrated NOSi is also elevated at night, as shown in Figure 2.18D, with very low concentrations observed in the afternoon.

Ng et al., 2008 proposed the formation of di- and tri-nitrated NOSi via the formation of an isoprene hydroxynitrate (IHN) from $INO_2 + INO_2$ self-reactions after the initial NO_3 attack. A second NO_3 oxidation step at the other double bond then leads to the formation of dihydroxy-dinitrates, again via the reaction with INO_2 radicals. A subsequent unknown reaction step with particulate sulfate

is then postulated to lead to NOS formation. Here an alternative mechanism is proposed where this species is formed via heterogeneous uptake of a di-nitrated epoxide, as shown in the lower section of figure 2.19. Similar to the mono-nitrate formation, the NO_3 reaction with isoprene leads to INO_2 , and the reaction with HO_2 leads to the isoprene nitrooxy hydroperoxide (INP). Subsequent addition of a second NO_3 at the C_2 position of the remaining double bond leads to an alkyl radical on the C_3 position. This radical then eliminates OH to form isoprene di-nitrated epoxide (IDNE), as proposed in Kwan et al., 2012.[244] The resulting IDNE species can then undergo heterogeneous uptake to acidic aerosols to form either di-hydroxy-di-nitrates via the reaction with H_3O^+ or di-nitrooxy hydroxy OS from the reaction with sulfate.

The isoprene-derived di- and tri-nitrated NOSs exhibited a strong diurnal profile as shown in Figure 2.18C,D, peaking in the night-time samples, suggesting their formation is a result of multiple steps of NO_3 oxidation. This is in contrast to the INHE-derived mono-nitrate outlined above that formed as a result of NO_3 oxidation followed by OH oxidation. The correlation of the di- and tri-nitrated NOSi with particle sulfate is much weaker than the mono-nitrated NOS, as shown in Figure 2.6 ($R^2 = 0.07\text{--}0.45$). There is no correlation with the average night-time NO_3 mixing ratio ($R^2 = 0.10$), but there is a weak correlation with the maximum production rate of NO_3 (P_{NO_3} , $R^2 = 0.29$) calculated during each filter sampling period. Production of these NOS species is predicted to be highest just after sunset (ca. 19:15–19:30), where residual isoprene can react with increased levels of NO_3 , resulting from lower levels of photolysis. The production will then reduce rapidly as the isoprene and NO_3 are consumed. The strong enhancement of the observed di- and tri-nitrated NOSi at night, in comparison to the INHE-related mono-nitrate, may indicate that their common precursor INP reacts with OH radicals during the day, and the products that require two NO_3 oxidation steps therefore only form when OH levels drop after sunset. The formation route of the tri-nitrated species remains uncertain.

The diurnal profile of the di- and tri-nitrated NOSi species both show a sur-

prisingly rapid drop in the concentration during the daytime. In a previous study of highly oxidized organic nitrates using CIMS, the optimum model-observation agreement was achieved using a short atmospheric lifetime of the order of 2-4 h.[245] Therefore, the diurnal profile seen in Beijing is likely the result of a rapid in-particle loss of di- and tri-nitrated NOS, through processes such as hydrolysis or oxidation.[246, 247] This may lead to particle-phase inorganic nitrate formation and act as a minor sink of atmospheric NO_x in Beijing. The drop in concentration of these species during the day may be partly due to the expansion of the boundary layer in the morning; however, this is not sufficient to explain the trends. On most days, there was also an appreciable amount of these NOS species in the morning samples, as shown in Figure 2.18 and Figure 2.17; and on a few days, the concentration of di-nitrated OS (MW 306) increased in the morning sample. The average diurnal profile of the observed mixing layer height during the campaign (Figure 2.21) shows a shallow nocturnal boundary layer with a minimum of around 250 m at midnight, then increasing from around 08:00 to a maximum of around 1000 m at 15:00. A recent study has shown the efficient formation of isoprene nitrates (IsN) in a polluted residual layer over Sacramento, California.[248] This suggests that the relatively high abundance of these species during the early morning sample may be the result of mixing down of regionally produced NOS from the nocturnal residual layer during the collapse of the nocturnal boundary layer.

These observations show that the reaction of isoprene with NO_3 leads to the formation of isoprene-derived nitrates in both the gas and particle phases in Beijing and that the nitrate radical plays a key role in the formation of IsN both during the day and at night. The mono-nitrated NOSi identified are predominately formed in the late afternoon from the reaction with NO_3 and then OH radicals, with their concentration also influenced strongly by particulate sulfate availability. In contrast, the abundance of the di- and tri-nitrated NOSi species, in summertime, is driven by both local night-time NO_3 chemistry, most likely in the early evening when the NO_3 concentrations are increasing (and OH decreasing) as the sun goes

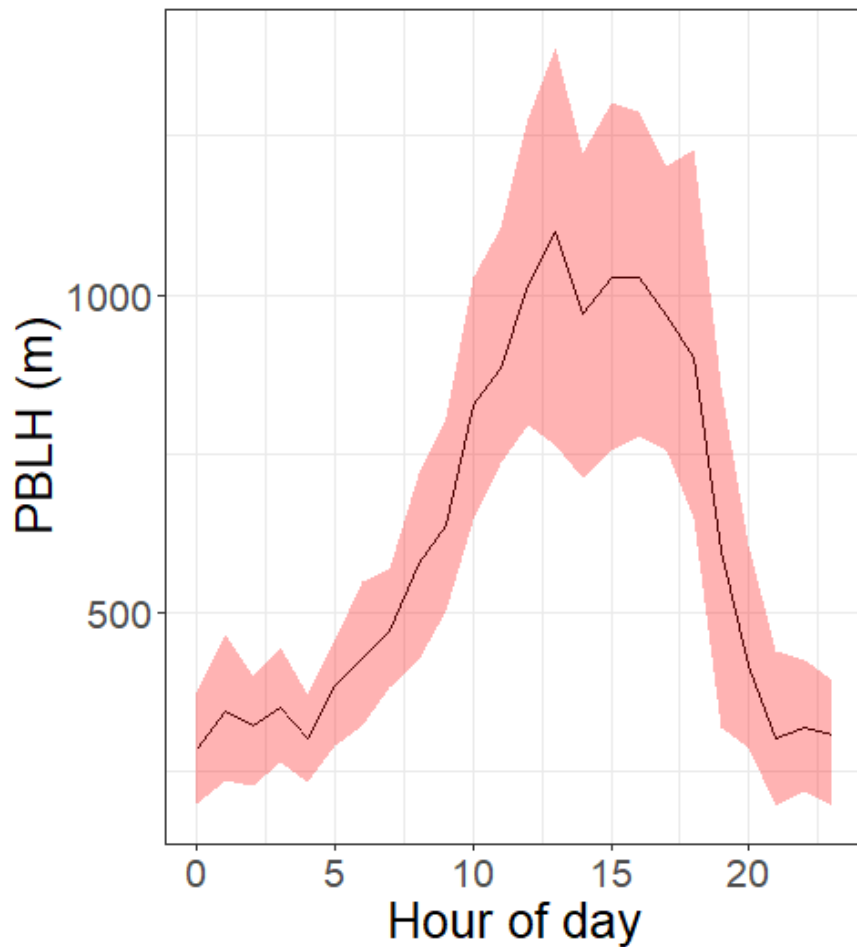


Figure 2.21: Boundary layer height (m) diurnal across the Beijing summer campaign.

down and isoprene is still present in reasonable amounts, and the mixing down of aged aerosol in the morning from more regional sources as the nocturnal boundary layer collapses. Unfortunately, the long nocturnal filter sampling time (15 h) in this study does not allow the full dynamics of the night-time formation of NOS to be observed and increased temporal resolution is needed to determine the relative role of isoprene, NO_3 , and sulfate aerosol to and NOS formation in Beijing and other megacities. The measurements were taken at 8 m and so represent surface processes close to the emission of both isoprene and NO .

2.3.7 Contribution of Isoprene SOA in Beijing

In order to estimate the total amount of OSi and NOSi, labelled here as iSOA, 13 species were chosen that could be confidently identified as being predominately from isoprene (2-MT-OS, 2-MG-OS, C₅H₁₀SO₇, C₅H₈SO₇, C₅H₁₁NSO₉, C₅H₉NSO₁₀, C₅H₉N₂SO₁₁, C₅H₈N₃SO₁₃). Although there were a number of other compounds with formula similar to iSOA tracers, their trends compared to previous studies and potential for alternative sources made a confident assignment of VOC precursor difficult. Therefore, the estimated contribution of iSOA to the observed total particulate mass determined here should be taken as a lower limit. Figure 2.16 shows the time series of the iSOA observed in Beijing. The average concentration was 82.5 ng m⁻³ during the campaign, ranging from 718 ng m⁻³ on the 19/05/2017 (11:38 – 14:30) to 1.9 ng m⁻³ on the 02/06/2017 (14:36-17:28). The contribution of iSOA to the OOA (Σ [OOA1-3]) factors measured by the AMS was obtained by assuming all OSi and NOSi species fragment in the ion source to lose the sulfate and nitrate groups. Across the whole measurement period, the iSOA tracers represented only a small fraction of the total OOA measured by AMS (0.62% of OOA). However, towards the end of the measurement period, this increased up to a maximum of 3 % on the 17/06/2017 (13:32-14:23).

Additional iSOA tracers containing only CHO (Table 2.6), including 2-methyltetrols, 2-methylglyceric acid and C₅-alkene triols, were measured in separate 24-hour filter samples, with the commonly used derivatization GC-MS method.[118, 233] The average ratio of the 2-methyltetrols to its corresponding OS (2-MT:2-MT-OS) was 1.4, indicating extensive heterogeneous conversion of isoprene oxidation products within the particles. The observed ratio is slightly larger than those measured in the SEUS (0.37-0.96 as shown in Table 2.5) but much lower than that measured in the Pearl River Delta region (40) where the 2-methyltetrols dominated. In contrast, the average ratio of the high-NO iSOA tracer, 2-MG and its corresponding organosulfate (2-MG:2-MG-OS) observed in Beijing was 0.33, indicating more extensive transformation to products from heterogeneous

reactions. This ratio may also reflect the more volatile nature of 2-MG compared to 2-MT. Overall, the combined concentrations of these isoprene CHO compounds were generally low (mean 25 ng m⁻³, max 69 ng m⁻³) in comparison to the heterogeneous iSOA compounds (i.e., OSi and NOSi) targeted in this work.

In addition, the concentrations of these CHO species may be overestimated based on recent studies demonstrating that thermal decomposition leads to these products being detected by GC-MS and FIGAERO-CIMS methods[249], and so the conversion to products from heterogeneous reactions (i.e., OSi and NOSi) may in fact be larger (2MT:2MT-OS = 0.5-0.91 using the overestimates of 160-288 % observed in Cui et al., 2018).

Table 2.6: Isoprene CHO tracer concentrations measured via GC-MS using 24-hour samples between 22/05/2017 and 22/06/2017. 2-MTs is equal to the sum of 2-methylthreitol and 2-methylerythritol and the C₅-alkene triols is equal to the sum of cis-2-methyl-1,3,4-trihydroxy-1-butene, 3-methyl-2,3,4-trihydroxy-1-butene and trans-2-methyl-1,3,4-trihydroxy-1-butene.

| Isoprene Tracer | Min (ng m⁻³) | Max (ng m⁻³) | Average (ng m⁻³) |
|------------------------------------|--------------------------------|--------------------------------|------------------------------------|
| 2-MTs | 4.55 | 52.67 | 17.29 |
| MG | 1.38 | 15.53 | 7.24 |
| C₅-alkene triols | 0.23 | 1.08 | 0.51 |

The study presented here shows for the first time that OS and NOS species derived from isoprene oxidation can make a significant contribution to oxidized organic aerosol in Beijing in summer. There is significant anthropogenic control, from both NO_x and sulfate aerosols, on the products and concentrations of iSOA in Beijing. The majority of the OS species showed a strong correlation towards the product of [O₃][pSO₄], highlighting the role of both photochemistry and the availability of particulate sulfate in heterogeneous reactions. When the observed concentrations of all of the OSi and NOSi species measured in this study (including the additional 19 compounds not confidently assigned to iSOA) are combined, they contribute 2.2 % to the total OOA on average, increasing to a maximum of 10.5 %, indicating the extensive heterogeneous conversion of VOC oxidation products in Beijing in summer.

Chapter 3

Importance of Oxidants and Temperature in the Formation of Biogenic Organosulfates and Nitrooxy Organosulfates

This work was originally published in *ACS Earth and Space Chemistry* [250].

3.1 Introduction

Organosulfates (OSs) are key contributors of atmospheric secondary organic aerosol (SOA) and have been detected in ambient aerosols in both clean and polluted sites around the world.[34, 35, 125, 126, 184, 185, 235, 251–253] OSs have been shown to make up significant portions of organic aerosol (OA) and PM_{2.5} (particulate matter less than 2.5 μm in diameter) mass [186, 254, 255], with isoprene derived OSs (OSi) accounting for up to 8% of organic matter.[130] Radiocarbon measurements have shown that OA is dominated by modern carbon even in urban areas [210, 256–258], suggesting that biogenic sources could be playing a key role in OA and PM_{2.5} formation. Chamber studies have shown the formation of particle bound OSs from gas-phase oxidation of biogenic volatile organic compounds (BVOCs) such as isoprene [134, 135, 239], monoterpenes [134, 259], sesquiterpenes [260] and green leaf volatiles [261] via OH, NO₃, and O₃ oxidation pathways in the presence of sulfate aerosol or SO₂. Many of the species identified in these chamber studies have also been detected in ambient samples, with OSi as some of the most abundant biogenic OS markers quantified.[35, 38] It should be noted that while these OS species are termed as BSOA due to their VOC precursors which are predominantly biogenic, they are formed through interactions with anthropogenic pollutants. The formation mechanisms of OSs have been studied extensively [186], with OS formation through an acid catalyzed ring opening of epoxides considered to be the most important route [127, 134, 173, 252, 259], especially for those derived from isoprene. However, several other routes have been proposed such as sulfate radical addition to an unsaturated precursor in the aqueous phase [262, 263], direct sulfate esterification of an alcohol precursor [134], or the replacement of nitrate groups within organonitrate species with sulfate.[247, 264] Recent studies have reported the formation of OSs both directly and indirectly from the reaction of unsaturated species with SO₂. [265–267] Nitrooxy-OSs (NOSs) are a sub class

of OS and have been observed in several locations [125, 126, 184, 219, 240, 253, 268–272], but their formation pathways are less well-studied.[109, 134, 273, 274] NOS species have been shown to form from the reaction of sulfate with organic nitrate species, formed during OH photo-oxidation of VOCs via a reaction of the peroxy radicals with NO. Organic nitrates can also be formed from nitrate radical initiated oxidation of VOCs [152, 274], which becomes increasingly important at night when the concentration of NO₃ radicals is higher and concentrations of OH are reduced.[104] Recent studies by Liebmann et al. in 2019 and Hamilton et al. in 2021 indicate that, under low-NO conditions, nitrate radical chemistry can also play an important role in organic nitrate production during the daytime.[104, 275] Several factors make the accurate identification and quantification of individual OS species in ambient aerosol challenging [276], but it is important for understanding aerosol formation, properties, and the factors that affect the OS contribution to PM_{2.5}. First, the compositionally complex samples, which contain thousands of multifunctional compounds, can lead to significant matrix effects as seen for OSi species.[125, 184] Second, BSOA suffers from a lack of authentic standards, meaning proxy standards must be used. Recently, several studies have synthesized a number of authentic OS standards derived from isoprene and monoterpenes and quantified them in ambient samples.[185, 192, 193] These studies have shown that differences in ionization efficiencies between several authentic monoterpene OSs and proxy standards can be significant, with Wang et al. in 2017 showing a factor 6.4 difference between the two extremes on the ionization scale, highlighting the need for future studies to focus on more accurate quantification.[192]

Guangzhou is a megacity in South China situated in the Pearl River Delta (PRD) region, with an approximate population of 15 million. To the south are the densely populated cities of Macao, Shenzhen, and Hong Kong, while there is relatively less urbanization to the north of Guangzhou. Guangzhou like the rest of China historically experiences high levels of pollution but less extremely than northern cities. Recently introduced pollution controls have started to take effect, reducing the concentrations of some pollutants.[199, 277]

Unlike in some other cities in China, nonfossil secondary species account for higher fractions of OA during both high and low-PM episodes in Guangzhou even during the winter.[255] Guangzhou has a subtropical climate, with mild winters and hot rainy summers due to Asian monsoons. This promotes high emissions of BVOCs [278] into a region that is heavily influenced by anthropogenic emissions, providing a good case study of biogenic–anthropogenic interactions. Multiple studies have now identified and quantified OSs in ambient samples, however many of these used long sampling times, [35, 126, 184, 185] which does not allow for ambient diurnal variations to be resolved, thus hindering the determination of formation mechanisms and sources. This study employs one of the highest time resolution filter collection regimes for OS and NOS to date, with eight filters collected per day in Guangzhou. Over 300 ambient PM_{2.5} samples were collected over two intensive campaigns during the summer and winter and were analyzed using ultrahigh-performance liquid chromatography tandem mass spectrometry (UHPLC–MS²). Over 40 biogenic OS and NOS species were quantified using a mixture of authentic and proxy standards. Diurnal variations of different tracers were comprehensively investigated and linked to different formation pathways. Biogenic—anthropogenic interactions were also investigated to better assess the formation pathways of OSs and NOSs under real atmospheric conditions.

3.2 Experimental

3.2.1 Filter collection

Ambient aerosol filter samples were collected in Guangzhou, China at the Guangzhou Institute for Geochemistry (GIG) as part of the Natural Environmental Research Council’s (NERC) NITRO-PM project. The sampling took place on top of a 12-story mixed use office and laboratory building (23.145 N, 113.364 E). The site was surrounded by residential buildings, with a six-lane road ~500 m to the south and a forest park ~4 km to the north. PM_{2.5} samples were

collected during the summer (31/07/2019–23/08/2019, $n = 147$) and winter (20/11/2019–12/12/2019, $n = 167$) by Atallah Elzein, using an Ecotech HiVol (Ecotech, Knoxfield, Australia) with a selective $\text{PM}_{2.5}$ inlet and a flow rate of $1.1 \text{ m}^3 \text{ min}^{-1}$. Filters were pre-baked to remove residual organics at $500 \text{ }^\circ\text{C}$ for 5 h before use. After collection, samples were wrapped in foil and stored at $-20 \text{ }^\circ\text{C}$ until analysis. Filter samples were collected eight times a day on most days: 06:00–08:00, 08:00–10:00, 10:00–13:00, 13:00–15:00, 15:00–17:00, 17:00–19:00, 19:00–21:00, 21:00–06:00. On some days, lower time resolution samples were collected due to extreme weather conditions, including Tropical Cyclone Wipha between the first and third of August 2019.

3.2.2 Extraction

The extraction of the filter is similar to that used previously by Bryant et al. in 2020. Initially, using a standard square filter cutter, an aliquot of the filter was taken, with an area of 47.61 cm^2 ($6.9 \text{ cm} \times 6.9 \text{ cm}$), which was then cut into roughly 1 cm^2 pieces and stored in a 20 mL glass vial. Next, 8 mL of LC–MS grade MeOH (Optima, Fisher Chemical) was added to the sample and sonicated for 45 min. Ice packs were used to keep the bath temperature below room temperature, with the water swapped midway through. Using a 5 mL plastic syringe, the MeOH extract was then pushed through a $0.22 \text{ }\mu\text{m}$ filter (Millipore) into another sample vial. An additional 2 mL ($2 \times 1 \text{ mL}$) of MeOH was added to the filter sample and then extracted through the filter to give a combined extract of $\sim 10 \text{ mL}$. This extract was then reduced to dryness using a Genevac vacuum concentrator. The dry sample was then reconstituted in 50:50 MeOH/ H_2O (Optima, Fisher Chemical) for analysis. Extraction efficiencies of 2-methyl glyceric acid organosulfate, camphorsulfonic acid, and pinonic acid were determined using authentic standards spiked onto a prebaked clean filter and recoveries were calculated to be 71%, 99%, and 85%, respectively.

3.2.3 Ultrahigh-Performance Liquid Chromatography Tandem Mass Spectrometry (UHPLC–MS²)

The extracted fractions of the filter samples were analyzed using an Ultimate 3000 UHPLC (Thermo Scientific) coupled to a Q Exactive Orbitrap MS (Thermo Fisher Scientific) using data dependent tandem mass spectrometry (ddMS²) with a heated electrospray ionization source (HESI). The UHPLC method uses a reversed-phase 5 μm , 4.6 mm \times 100 mm, polar end-capped Accucore column (Thermo Scientific, 17326-102130) held at 40 °C. The mobile phase consisted of water (A) and methanol (B), both with 0.1% (v/v) of formic acid (98% purity, Acros Organics). A gradient elution was used, starting at 90% (A) with a 1 min postinjection hold, decreasing to 10% (A) at 26 min, returning to the starting mobile-phase conditions at 28 min, followed by a 2 min hold, allowing the re-equilibration of the column. The flow rate was set to 0.3 mL min⁻¹. A sample injection volume of 4 μL was used. The capillary and auxiliary gas heater temperatures were set to 320 °C, with a sheath gas flow rate of 45 (arb.) and an auxiliary gas flow rate of 20 (arb.). Spectra were acquired in the negative ionization mode with a scan range of mass-to-charge (m/z) 50–750. Tandem mass spectrometry was performed using higher-energy collision dissociation with a stepped normalized collision energy of 65, 115. The isolation window was set to m/z 2.0 with a loop count of 10, selecting the 10 most abundant species for fragmentation in each scan.

3.2.4 Data Processing and Compound Library

A mass spectral library was built using the compound database function in Tracefinder 4.1 General Quan software (Thermo Fisher Scientific). To build the library, compounds from previous studies [134, 149, 152, 235, 263, 279] were searched for in an afternoon and a nighttime filter sample extract analysis using the Xcalibur software. Identified compounds were input into the compound library in the generic form: C_cH_hO_oN_nS_s (where c, h, o, n, and s represent the number of carbon, hydrogen, oxygen, nitrogen, and sulfur atoms, respectively).

Where multiple isomers were observed, each isomer was added to the library independently, on the basis of its retention time (RT). The UHPLC/ESI-HRMS data for each standard and ambient sample were analyzed using Tracefinder general Quan software (Thermo Fisher Scientific). Blank subtractions were undertaken for all ambient samples, using a field blank. Tracefinder extracted compound peak areas from each sample on the basis of the assigned library. The mass tolerance of the method was set to 3 ppm, with the RT window set to 10 s. The peak tailing factor was set to 2.0 and the detection algorithm used was ICIS, with a nearest RT detection strategy. The minimum signal-to-noise (S/N) for a positive identification was set to 3.0. The suitability of the peak was also assessed for a positive identification, with the peak height at which to compare the symmetry of the left and right sides of the peaks set to 40% and symmetry threshold, which is the minimum percentage difference considered symmetrical set to 70%.

3.2.5 Calibration and Matrix Effects

The accurate quantification of BSOA is difficult owing to a lack of authentic standards. This study employs one proxy (camphorsulfonic acid, Sigma- Aldrich) and two authentic standards (2-methyl tetrol organosulfate (2-MT-OS) and 2-methyl glyceric acid organosulfate (2-MG-OS)). The authentic standards were obtained from Surratt's group at The University of North Carolina at Chapel Hill.[187] Standards were run across a 9-point calibration curve (2 ppm–7.8 ppb, $R^2 > 0.99$). We also evaluated the matrix effect of the ambient samples on the signal response of the three standards used for quantification. The measured signal intensity of the standards in a blank solvent matrix were compared to the ambient aerosol matrix. A 10 μL mixture containing camphorsulfonic acid, 2-MG-OS, and 2-MT-OS at 10 ppm was spiked into either 100 μL of ambient filter sample extract or into 100 μL of blank 50:50 (MeOH/H₂O) solvent. The samples were run as described above. The matrix effect factors were then calculated by taking the compound areas from the spiked ambient samples, subtracting the areas of

Table 3.1: Matrix effect analysis results from 8 filter samples on three different organosulfate standards (CAM-OS – Camphorsulfonic acid, MG-OS – 2-methyl glyceric acid organosulfate, MT-OS – 2-methyl tetrol organosulfate). Alongside PM_{2.5}, NO₃ and SO₄²⁻ concentrations. The values in bold are the average ratios between a clean matrix and an ambient sample matrix.

| Start date | Time of day | Conc. ($\mu\text{g m}^{-3}$) | | | CAM -OS | MG -OS | MT -OS |
|------------|-------------|--------------------------------|-----------------|-------------------------------|--------------|--------------|--------------|
| | | PM _{2.5} | NO ₃ | SO ₄ ²⁻ | | | |
| 01-Aug | All day | 7.48 | 0.32 | 1.25 | 0.40 | 0.78 | 0.23 |
| 20-Aug | 17:00–19:00 | 18.5 | 0.57 | 1.02 | 0.43 | 0.78 | 0.38 |
| 21-Aug | 06:00–08:00 | 41.5 | 2.54 | 2.54 | 0.42 | 0.89 | 0.31 |
| 22-Nov | 13:00–15:00 | 21.0 | 4.66 | 6.87 | 0.92 | 0.70 | 0.24 |
| 24-Nov | 21:00–06:00 | 29.9 | 6.52 | 7.00 | 0.53 | 1.15 | 0.62 |
| 01-Dec | 13:00–15:00 | 19.0 | 7.34 | 14.13 | 0.91 | 0.67 | 0.19 |
| 03-Dec | 21:00–06:00 | — | 6.28 | 8.32 | 0.89 | 1.11 | 0.17 |
| 05-Dec | 06:00–08:00 | 22.5 | 5.30 | 5.47 | 0.90 | 0.64 | 0.20 |
| Average | | | | | 0.68 | 0.84 | 0.29 |
| | | | | | ±0.23 | ±0.18 | ±0.14 |

compounds that were already present in the ambient sample, and then dividing by the compound areas in the blank matrix. If no matrix effect was present, the ratio would equal 1. Table 3.1 shows the ratios across eight ambient samples collected during both campaigns, which represent a mixture of high and low PM_{2.5} concentrations across different times of day. 2-MT-OS showed a significant matrix effect, with an average matrix ratio of 0.29 ± 0.23 , suggesting a 71% suppression in signal response. In contrast, 2-MG-OS showed little matrix suppression with an average of 0.84 ± 0.18 .

Matrix correction factors were applied alongside calibrations to different compound classes and for compounds eluting at different times. Species eluting before 2 min (mainly OSi species) were quantified using an average gradient of 2-MG-OS and 2-MT-OS across the 9-point calibration curve, and a matrix correction factor of 0.57 ± 0.16 was applied on the basis of the average matrix effect factors for 2-MG-OS and 2-MT-OS. 2-MG-OS and 2-MT-OS identified in the ambient samples were quantified using their own authentic standards and corrected with their own specific factors of 0.84 ± 0.18 and 0.29 ± 0.14 , respectively. For species eluting

after 2 min, camphorsulfonic acid was used a proxy and corrected with a matrix effect factor of 0.68 ± 0.23 . Camphorsulfonic acid has been shown to be the most accurate proxy standard by comparison with synthesized authentic monoterpene OS standards from α -/ β -pinene and limonene.[192] Due to the limited number of studies investigating the matrix effects of aerosol samples, conclusions of the underlying causes cannot be drawn. However, the suppression is likely due to the large numbers of co-eluting inorganic and organic species, reducing the ionization efficiency of the marker compounds.[280]

Uncertainties for the calibration of 2-MG-OS and 2-MT-OS were calculated from the standard deviation uncertainty in the repeated measurements of the nine calibration points and the standard deviation of the matrix effects calculated in Table 3.1. The uncertainties associated with 2-MG-OS and 2-MT-OS were calculated to be 25% and 48%, respectively, mainly due to the large uncertainties in the matrix correction factors. For species quantified by the average of 2-MG-OS and 2-MT-OS, we estimated the error to be the sum of the errors associated with 2-MG-OS and 2-MT-OS (56%). For OS/NOS species eluting after 2 min, the uncertainty (36.5%) was estimated on the basis of the standard deviation of the camphorsulfonic acid calibration and the difference in matrix effect factors as well as the use of proxy standards. Recently, a study that synthesized authentic NOS species derived from monoterpenes (NOS_{MT}) standards quantified the same NOS_{MT} species as in this study and observed very similar concentrations.[194] For example, for the MW295 isomers, they found a mean concentration of 12.3 ng m⁻³ in Guangzhou in the winter, with the full range of observed concentrations across four cities (Hong Kong, Guangzhou, Beijing, and Shanghai) of 1.2–39.3 ng m⁻³. This compares very well with our estimated mean concentration of 11.1 ng m⁻³ and range of 0.32–26.7 ng m⁻³. [194] This would suggest that the use of the camphorsulfonic acid proxy standard gives a reasonable calibration compared to the use of authentic standards.

Table 3.2: Pollutant mean, median (Med), standard deviation (SD) and maximum values across the summer and winter campaigns.

| | Summer | | | | Winter | | | |
|---|--------|------|------|-------|--------|------|------|------|
| | Mean | Med | SD | Max | Mean | Med | SD | Max |
| Temp ($^{\circ}$ C) | 30.4 | 30.0 | 2.86 | 36.5 | 18.3 | 17.9 | 4.19 | 29.2 |
| RH (%) | 77.6 | 78.8 | 10.6 | 97.0 | 40.6 | 42.0 | 14.7 | 80 |
| ws (m s^{-1}) | 5.95 | 4.88 | 3.93 | 17.8 | 1.91 | 1.6 | 1.03 | 4.6 |
| wd ($^{\circ}$) | 74.7 | 94.8 | 52.3 | — | 241 | 237 | 45.1 | — |
| PM_{2.5} ($\mu\text{g m}^{-3}$) | 29.8 | 29.0 | 14.5 | 73.0 | 27.5 | 25.0 | 14.1 | 99 |
| O₃ (ppbv) | 43.1 | 29.7 | 37.3 | 169 | 31.8 | 33.6 | 23.1 | 141 |
| NO (ppbv) | 5.37 | 1.01 | 9.37 | 58.9 | 12.1 | 2.20 | 22.6 | 139 |
| NO_x (ppbv) | 32.2 | 26.8 | 20.4 | 114.5 | 41.1 | 22.6 | 39.3 | 223 |
| NO₂ (ppbv) | 26.8 | 24.6 | 14.4 | 73.7 | 28.9 | 20.6 | 20.2 | 93.5 |
| SO₄²⁻ ($\mu\text{g m}^{-3}$) | 5.56 | 4.84 | 3.70 | 22.7 | 7.84 | 2.23 | 6.04 | 58.9 |
| NO₃ ($\mu\text{g m}^{-3}$) | 3.55 | 2.97 | 3.01 | 17.2 | 6.06 | 4.93 | 6.05 | 64.2 |
| C₂O₄ ($\mu\text{g m}^{-3}$) | 0.43 | 0.38 | 0.32 | 2.00 | 0.354 | 0.31 | 0.25 | 2.2 |
| SO₂ (ppbv) | — | — | — | — | 2.91 | 2.73 | 1.10 | 7.2 |

3.2.6 Gas-Phase Measurements

Additional gas-phase and meteorological measurements were collected alongside the filter samples at the site (Table 3.2) by staff at GIG. Data included the following nitrogen species: NO, NO₂, and NO_x measured by Chemiluminescence with a Thermo Scientific 42i-TL. Ozone was measured via ultraviolet with a Thermo Scientific 49i, and SO₂ was measured via pulsed fluorescence with a Thermo Scientific 43i-TLE. Finally, PM_{2.5} was measured by a continuous particulate monitor (BAM-1020, Met One instruments Inc.).

3.2.7 Ion Chromatography

Inorganic sulfate and nitrate were quantified using ion chromatography using a method outlined in Xu et al. in 2020 by Erin White and Stefan Swift.[281] An area of 6.9 cm² was cut from each filter and cut into small pieces and transferred to a 15 mL vial. Two milliliters of 18.2 MΩ · cm deionized water was added to each vial before being sonicated for 30 min. A Dionex ICS- 1100 with a DS6 heated conductivity cell and a Dionex AS-DV carousel with Chromeleon Data system software were used for data analysis. For anion mode, a Dionex AG14A 4

mm guard column was used with a Dionex AS14A 4 mm analytical column and a DRS Dionex ADRS 600 suppressor. The anion eluent was prepared using 1.698 g of Na_2CO_3 and 0.168 g of NaHCO_3 with 2 L of $>18.2 \text{ M}\Omega$ deionized water added 1 L at a time. After each 1 L addition, the eluent bottle was sonicated in degas mode for 30 min. The column was equilibrated at an oven temperature of $35 \text{ }^\circ\text{C}$ and a current of 45 mA. Anions were calibrated using 12-point calibration curves: 0.01, 0.05, 0.1, 0.25, 0.5, 1, 2.5, 5, 10, 25, 50, and 100 ppm. The autosampler delivered $350 \text{ }\mu\text{L}$ at $4 \text{ mL}/\text{min}$ to the instrument that used $100 \text{ }\mu\text{L}$ and was at a flow rate of $1 \text{ mL}/\text{min}$ for ion separation and detection.

3.3 Results and Discussion

Figure 3.1 shows the time series of the following measured pollutants: NO, NO_2 , O_3 , and $\text{PM}_{2.5}$ alongside particulate sulfate during the two sampling periods (summer on the left, winter on the right). Mean and maximum values are shown in Table 3.2 for both campaigns, along with additional aerosol anion data. The meteorological conditions between the two campaigns were quite different with a mean temperature ($\pm\text{sd}$) of $30.4 \pm 2.9 \text{ }^\circ\text{C}$ in the summer compared to $18.3 \pm 4.2 \text{ }^\circ\text{C}$ during the winter campaign. The mean relative humidity (RH) in summer ($77.6 \pm 10.6\%$) was roughly double that of the winter campaign ($40.6 \pm 14.7\%$). The mean wind speed was much lower during the winter campaign ($1.9 \pm 1.0 \text{ ms}^{-1}$) compared to that of the summer ($6.0 \pm 3.9 \text{ ms}^{-1}$).

Figure 3.2 shows the average diurnal profiles for temperature, RH, O_3 , NO, NO_2 , SO_2 , and $\text{PM}_{2.5}$. The mean ozone mixing ratios were higher in the summer ($43.1 \pm 37.3 \text{ ppbv}$) than the winter ($31.8 \pm 23.1 \text{ ppbv}$) with a strong diurnal variation peaking mid-afternoon. The mean NO concentration was around double in the winter campaign ($12.1 \pm 22.6 \text{ ppbv}$) compared to that of the summer ($5.4 \pm 9.4 \text{ ppbv}$).[103]

NO was also lower during the day in winter with an afternoon average of $\sim 1.5 \text{ ppb}$. During the winter, several periods of high NO concentrations were

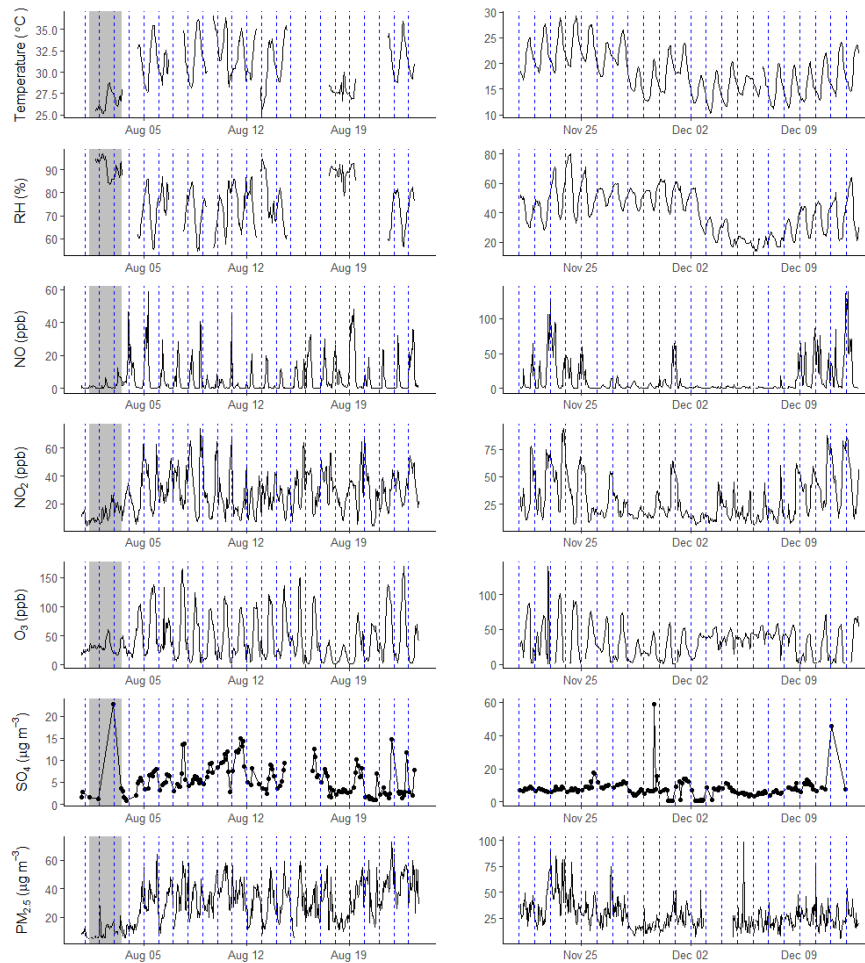


Figure 3.1: Time series of pollutants across the summer (left) and winter (right) campaigns. The highlighted section in the summer campaign indicates typhoon Wipha. The blue dotted lines indicate midnight of each day.

observed, as shown in Figure 3.1 (20–25 November, 30 November, and 9–12 December). The SO_2 mixing ratios were only measured in the winter campaign with an average of 2.9 ± 1.1 ppbv, with a morning peak around 07:00–08:00 am (Figure 3.3). Inorganic ions were measured via ion chromatography. Lower mean particulate SO_4^{2-} concentrations were observed in the summer ($5.6 \pm 3.7 \mu\text{g m}^{-3}$) compared to those in winter ($7.8 \pm 6.0 \mu\text{g m}^{-3}$), while the average particulate NO_3^- concentration during the winter campaign ($6.0 \pm 6.0 \mu\text{g m}^{-3}$) was double that of the summer campaign ($3.6 \pm 3.0 \mu\text{g m}^{-3}$). The mean $\text{PM}_{2.5}$ concentrations were similar across both campaigns, with neither campaign showing a strong diurnal variation.

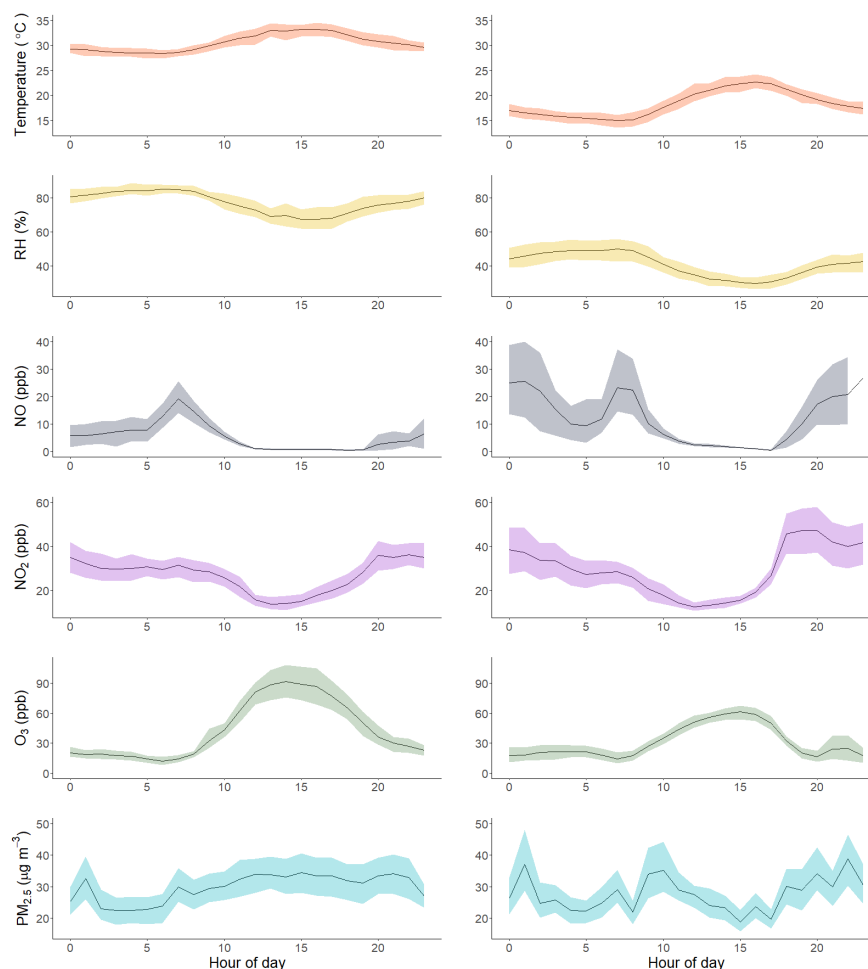


Figure 3.2: Diurnal variations of temperature ($^{\circ}\text{C}$), relative humidity (RH,%), NO (ppbv), NO_2 (ppbv), O_3 (ppbv) and $\text{PM}_{2.5}$ ($\mu\text{g m}^{-3}$) across summer (left) and winter (right) campaigns. The shaded area surrounding the black line is the 95% confidence interval.

3.3.1 Biogenic Organosulfates and Nitrooxyorganosulfates

3.3.1.1 Monoterpene Nitrooxy Organosulfates (NOS_{MT}).

The monoterpene derived NOS (NOS_{MT}) species include 26 $\text{C}_{9/10}$ species with five unique molecular formulas across both campaigns ($\text{C}_{10}\text{H}_{17}\text{NO}_7\text{S}$, $\text{C}_{10}\text{H}_{17}\text{NO}_8\text{S}$, $\text{C}_{10}\text{H}_{17}\text{NO}_9\text{S}$, $\text{C}_{10}\text{H}_{19}\text{NO}_9\text{S}$, and $\text{C}_9\text{H}_{15}\text{NO}_8\text{S}$) (Table 3.3). Species matching these formula have been shown to form in laboratory simulations from monoterpene photo-oxidation in the presence of NO and from dark NO_3 radical chemistry.[134] In this study, the total NOS_{MT} mean ($\pm\text{sd}$) concentration in the summer was 8.3

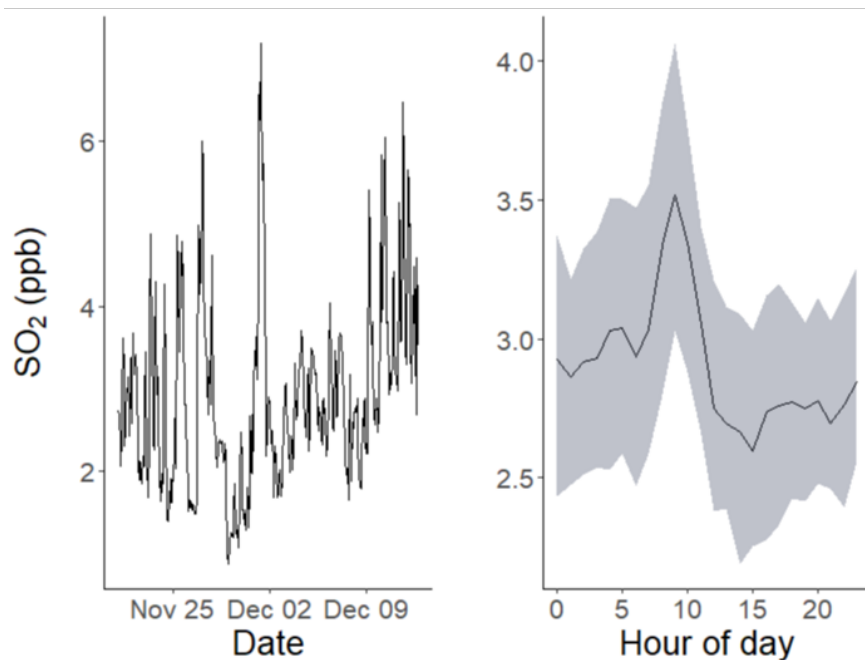


Figure 3.3: A- Time series of SO₂ during winter, B – Diurnal variation of SO₂ during winter with the shaded area around the black representing the 95% confidence interval.

$\pm 8 \text{ ng m}^{-3}$ and that in winter was $13.1 \pm 7.1 \text{ ng m}^{-3}$. The increase during the winter campaign may be due to higher NO_x concentrations, higher sulfate levels, or lower temperatures promoting condensation.[282] Higher summertime biogenic monoterpene concentrations have been modeled previously in the PRD.[283] Potential additional, non-biogenic sources of gas-phase emissions of monoterpenes in the winter include increased biomass burning or cooking.[44, 284–289] However, the lack of gas-phase observations of monoterpenes means it is not possible to draw conclusions currently. C₁₀H₁₇NO₇S was the dominant species across both campaigns, contributing $\sim 85\%$ of the NOS_{MT} mass on average, with summer and winter concentrations of 7.1 ± 7.3 and $11.1 \pm 6.5 \text{ ng m}^{-3}$, respectively.

These concentrations are comparable to concentrations observed in Shanghai (summer average: 5.71 ng m^{-3} ; winter average: 4.22 ng m^{-3}) [184] and summertime in Beijing (12 ng m^{-3}) [126] with C₁₀H₁₇NO₇S again identified as the most dominant NOS_{MT} across both studies.

These concentrations are also similar to those quantified by authentic standards

across four Chinese megacities (Hong Kong, 5.61 ng m^{-3} ; Guangzhou, 12.32 ng m^{-3} ; Shanghai, 16.51 ng m^{-3} ; Beijing, 13.15 ng m^{-3}).[194] He et al. in 2014 also observed higher wintertime NOS_{MT} concentrations at a regional background site in the PRD, although the reported $\text{C}_{10}\text{H}_{17}\text{NO}_7\text{S}$ concentrations were much higher (52.4 and 151 ng m^{-3} for summer and winter, respectively).[270]

Figures A and B of Figure 3.4 show the mean concentration of the sum of NOS_{MT} species during each filter collection time across the summer and winter campaigns, respectively. Several of the tracers were only identified in a small number of samples, and only tracers identified in more than 40% of the samples were included in the diurnal variations and carried forward for correlations. A strong diurnal variation is seen during both campaigns, peaking at night, with a minimum during the afternoon. A more pronounced increase in concentrations is observed in the 17:00–19:00 filter during the winter compared to that in the summer, likely due to the earlier sunset of 17:45 compared to 19:00 in the temperatures associated with lower tracer concentrations in the summer. This nighttime enhancement was also seen previously in Beijing and Shanghai.[126, 184] Although monoterpenes were not measured as part of this study, nighttime enhancements of monoterpenes have been observed previously in Beijing.[126] In contrast, He et al. in 2014 observed that $\text{C}_{10}\text{H}_{17}\text{NO}_7\text{S}$ in the background PRD peaked during the day, with daytime concentrations on average ~ 3 times higher than those at night.[270]

Surratt et al. in 2008 outlined both a daytime and nighttime route to the formation of the dominant NOS_{MT} ($\text{C}_{10}\text{H}_{17}\text{NO}_7\text{S}$).[134] The nighttime formation pathway proceeds via NO_3 radical oxidation, while the daytime formation route predominantly proceeds via hydroxyl radical oxidation followed by a reaction of the peroxy radical with NO . NOS_{MT} can also be formed during the day and night through monoterpene ozonolysis.[2] NOS_{MT} concentrations increased strongly with increasing SO_4^{2-} concentrations in summer night-time (Figure 3.5), but limited correlations were observed during the day and in the winter. This suggests that, during the summer, nighttime SO_4^{2-} is a limiting reagent, but other periods are

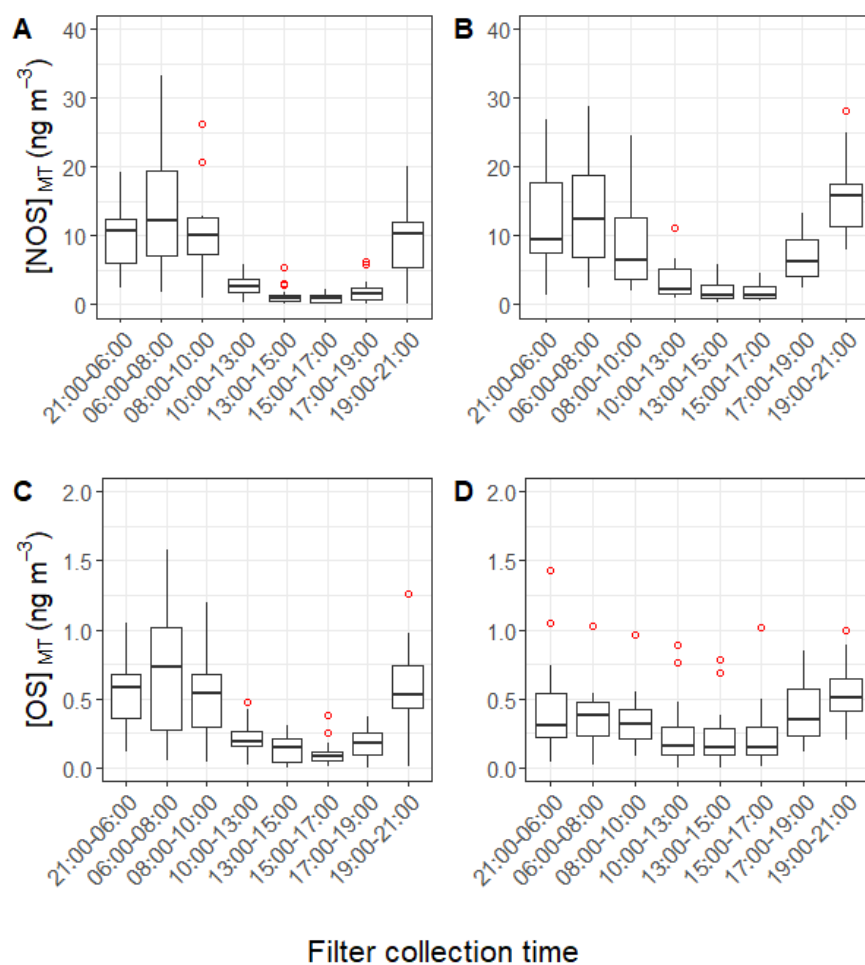


Figure 3.4: Diurnal variations of (A) NOS_{MT} during summer, (B) NOS_{MT} during winter, (C) OS_{MT} during summer, and (D) OS_{MT} during winter. The lower and upper parts of the box represent the 25th and 75th percentiles, with the upper and lower lines extending no further than $1.5 \times$ the interquartile range of the highest and lowest values within the line, respectively. Any data points outside of this range are shown as red circles.

VOC oxidation limited. The maximum observed NOS_{MT} concentrations during the summer and winter were 58.7 and 28.3 ng m^{-3} , respectively, both of which were observed during the 06:00–08:00 filter collection. The diurnal variation of monoterpenes measured in a previous study indicates higher monoterpene concentrations at night in Guangzhou, while daytime concentrations were roughly half the nighttime concentrations.[290] As such, the lower daytime NOS_{MT} concentrations could be linked to the monoterpene emission profile, decomposition via photolysis, or further OH oxidation of the NOS species.[291]

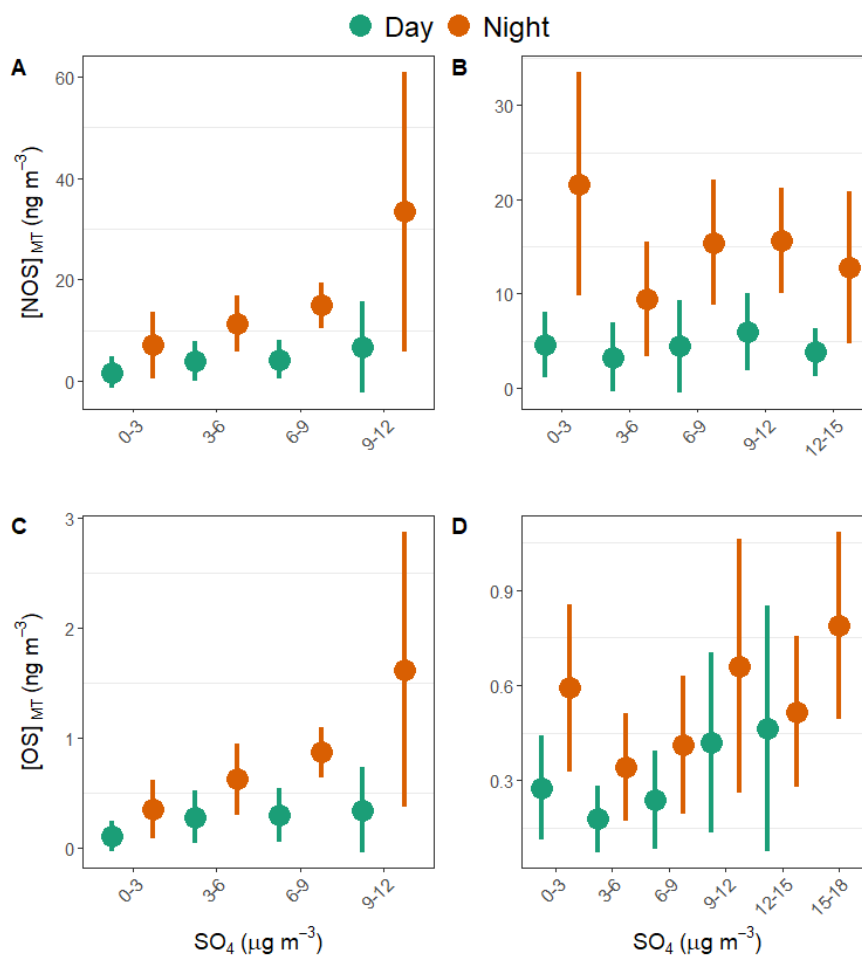


Figure 3.5: Correlation between NOS_{MT} and binned SO_4^{2-} concentrations during summer (A) and winter (B). Correlation between OS_{MT} and binned SO_4^{2-} concentrations during summer (C), and winter (D). The dots represent the mean tracer concentrations for the binned sulfate concentrations, with the lines representing \pm standard deviation.

NOS_{MT} concentrations showed generally decreased concentrations with increasing temperatures throughout the day across both campaigns (Figure 3.6), although the trend is not strong. Under higher temperatures, increased photolysis is expected, leading to higher OH radical concentrations [96] as well as photolysis of NOS_{MT} species. Therefore, under higher temperatures during the day, an enhanced degradation of the NOS_{MT} markers is expected. Under higher temperatures, NOS_{MT} species will be more volatile and thus their equilibrium partitioning may shift toward the gas phase. In contrast, at night, higher temperatures lead to increased NOS_{MT} concentrations, potentially as a result of higher monoterpene emissions.[292]

No conclusive direct correlation between NOS_{MT} concentrations and NO₂ was observed across either campaign, with $R^2 < 0.10$ both during the day and at night, although higher NOS_{MT} concentrations were generally observed with elevated NO₂ levels in both seasons within reasonable uncertainties, suggesting that formation via NO₃ initiated oxidation is important (Figure 3.7).

On the basis of previous observations in Beijing, NO₃ initiated oxidation can happen both at night and during the day as a result of very low NO mixing ratios.[104] Only 2 ppt of NO₃ accounted for 40% of isoprene nitrate production in the late afternoon. However, the relative role of OH versus NO₃ oxidation on the production of daytime monoterpene nitrates is unknown.

The campaign average steady state NO₃ concentration diurnal profile was estimated using Equation 3.1, with $k_1 = 1.4 \times 10^{-13} \exp(-2470/T)$ and $k_5 = 1.8 \times 10^{-11} \exp(110/T)$ [96] and is shown in Figure 3.8. J_{NO₃} values were estimated using the TUV model based on 1 day from the middle of each campaign.[292]

$$(\text{NO}_3) = \frac{k_1[\text{O}_3][\text{NO}_2]}{J_3 + J_4 + k_5[\text{NO}]} \quad (3.1)$$

During the summer campaign, the calculated NO₃ concentrations increased slightly throughout the morning and afternoon to ~3 pptv, before a sharp increase

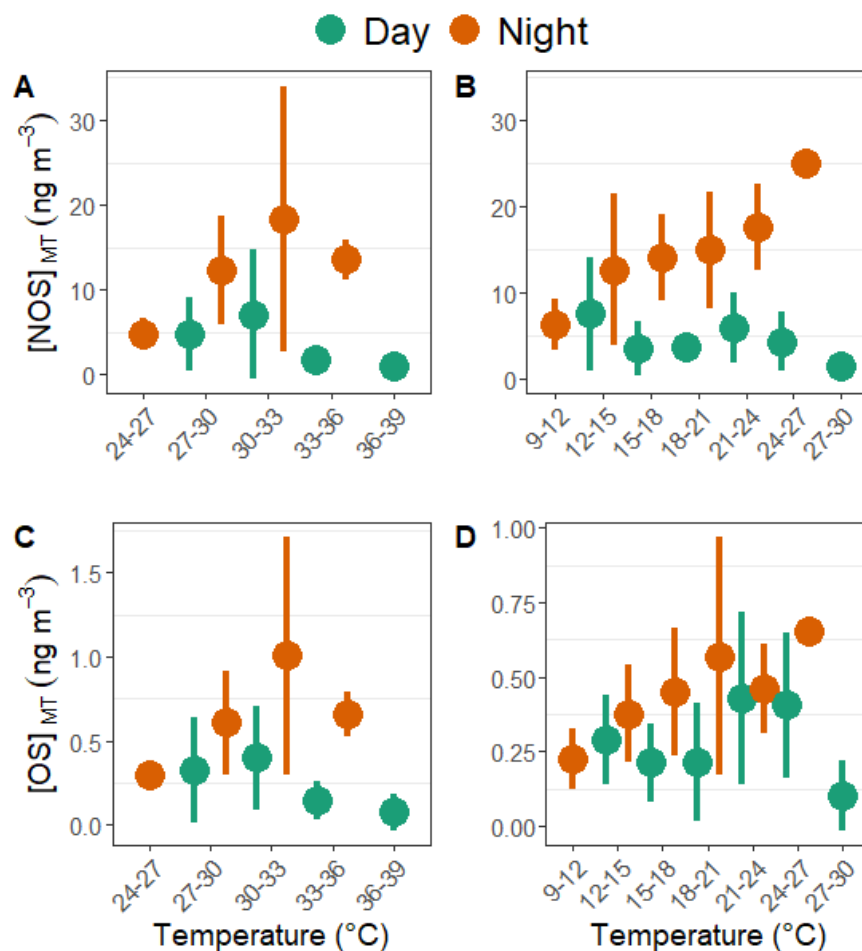


Figure 3.6: Binned correlation plots between markers and temperature: (A) NOS_{MT} during summer, (B) NOS_{MT} during winter, (C) OS_{MT} during summer, and (D) OS_{MT} during winter. The points represent the mean concentration \pm SD within each temperature range bin.

during the late afternoon into the evening reaching ~ 20 pptv, before a minimum around 08:00 of ~ 0.1 pptv. The winter diurnal variation shows two peaks in NO₃ concentrations; the first peak around 04:00 at ~ 2 pptv before a morning minimum and then another peak around 17:00, ~ 5 pptv in line with ozone concentrations. The average diurnal variation of the NOS_{MT} species, shown in Figure 3.4, is consistent with the calculated average NO₃ concentration profiles. However, no direct correlation was observed between the individual NOS_{MT} concentrations and concurrent NO₃ concentrations ($R^2 < 0.2$), likely due to the multigenerational and heterogeneous pathways of these tracers. Further work is needed to understand

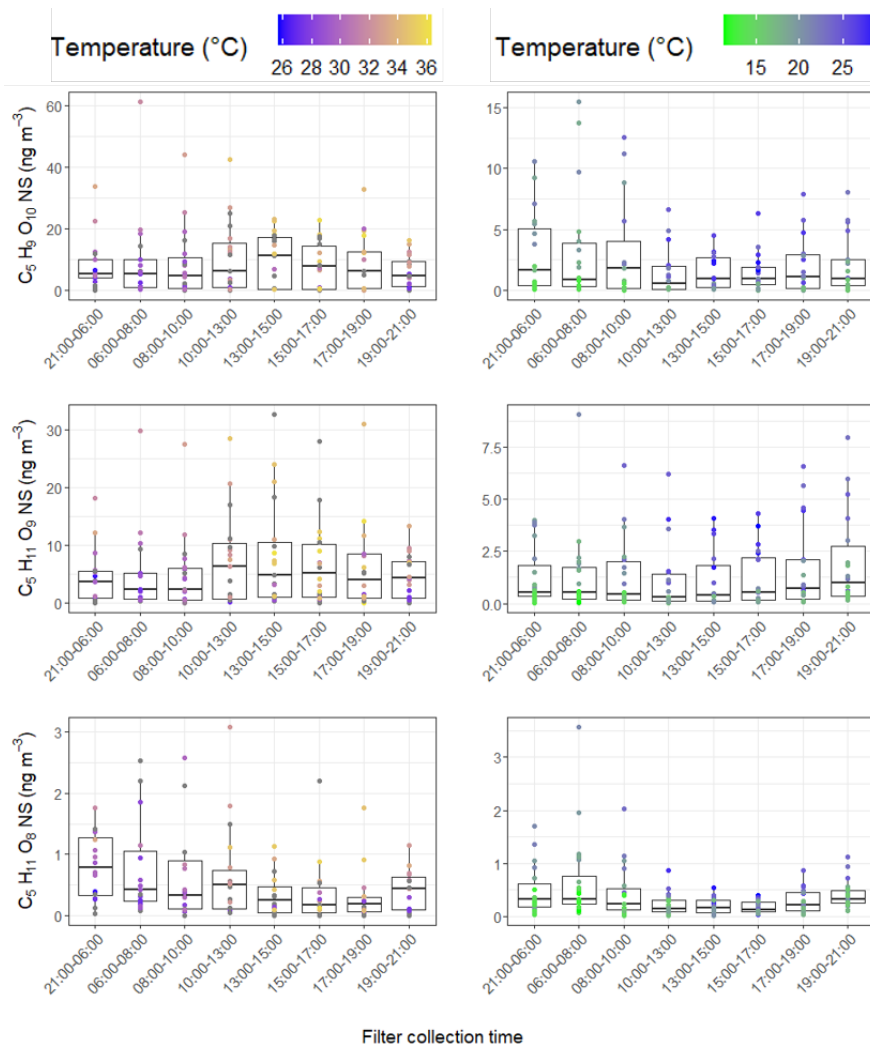


Figure 3.7: Diurnal variations of three mononitrated NOSi species across (A, C, and E) the summer (left) and (B, D, and F) the winter (right). Data points were then colored by the average temperature over the filter sampling time period. Where temperature measurements were not available, the data points are in gray.

the factors controlling NOS_{MT} in polluted areas during the day.

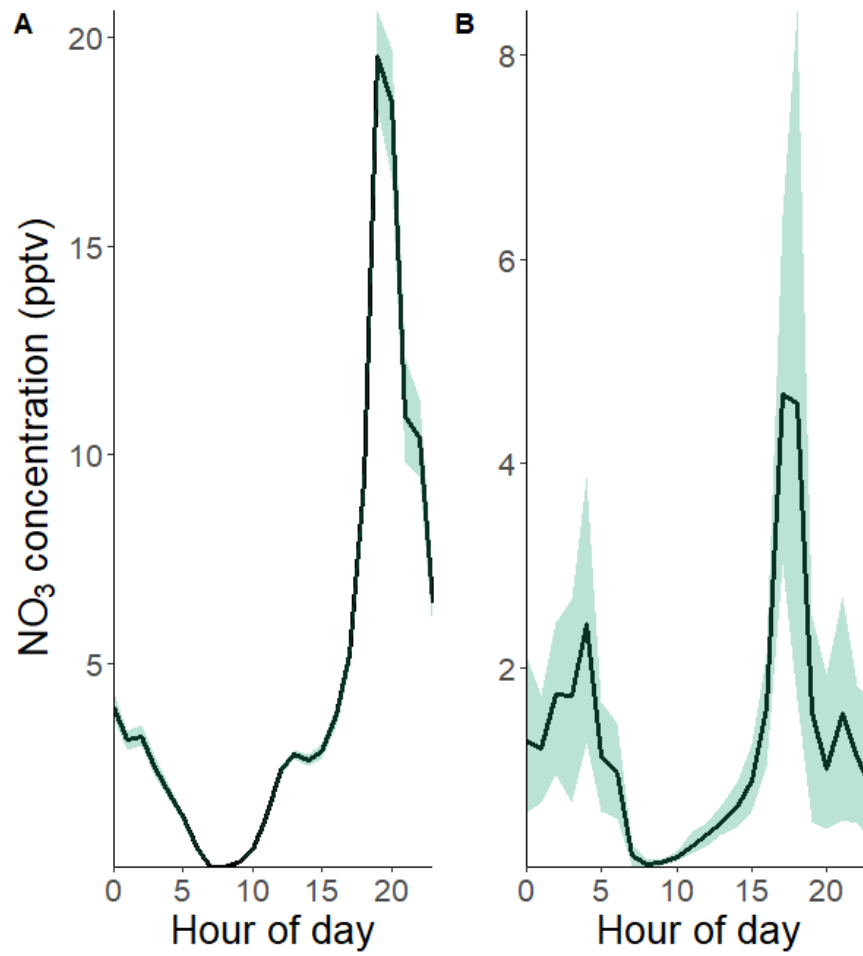


Figure 3.8: Diurnal variations of the steady state approximations of NO_3 concentrations during summer (A) and winter (B).

Table 3.3: Molecular formulae, retention times and time weighted means (ng m^{-3}) of nitrooxy organosulfates (NOS) and organosulfates (OS) from monoterpenes (MT) and isoprene (i) observed across summer and winter campaigns in Guangzhou. OSi species in bold had R correlation coefficients of less than 0.6 towards 2-MT-OS or 2-MG-OS and were therefore not used in the analysis of OSi formation. Isoprene OS is the sum of all potential isoprene OS species quantified in this study, while OSi is the sum of all isoprene OS species which had an R of greater than 0.6 towards either 2-Mt-OS or 2-MG-OS. Total BSOA is the sum of all quantified markers in this study.

| | | Conc. (ng m^{-3}) | | Retention time (min) |
|-----------------------|--|------------------------------|--------|--|
| | Formula | Summer | Winter | |
| NOS _{MT} | $\text{C}_{10}\text{H}_{17}\text{NO}_7\text{S}$ | 7.15 | 11.11 | 9.40, 10.50, 11.27, 11.64, 11.97, 12.37, 13.10, 13.76 |
| | $\text{C}_{10}\text{H}_{17}\text{NO}_8\text{S}$ | 0.48 | 0.62 | 4.77, 4.98, 5.55, 5.98, 6.40, 6.97, 7.18, 8.39 |
| | $\text{C}_{10}\text{H}_{17}\text{NO}_9\text{S}$ | 0.31 | 0.42 | 3.84, 6.61, 8.50, 9.03, 10.47, 13.27, 17.55 |
| | $\text{C}_{10}\text{H}_{19}\text{NO}_9\text{S}$ | 0.04 | 0.05 | 5.55 |
| | $\text{C}_9\text{H}_{15}\text{NO}_8\text{S}$ | 0.37 | 0.91 | 3.41, 5.98 |
| NOS _{MT} sum | | 8.34 | 13.10 | |
| OS _{MT} | $\text{C}_{10}\text{H}_{16}\text{O}_5\text{S}$ | 0.46 | 0.83 | 2.88, 3.84, 4.87, 5.66, 7.18, 7.43, 8.39, 9.38, 10.51, 11.29, 11.75, 12.8, 13.76 |
| | $\text{C}_{10}\text{H}_{16}\text{O}_6\text{S}$ | 0.05 | 0.08 | 9.07, 10.47 |
| | $\text{C}_{10}\text{H}_{16}\text{O}_7\text{S}$ | 0.09 | 0.65 | 2.74, 3.7, 7.04, 12.06 |
| | $\text{C}_{10}\text{H}_{18}\text{O}_5\text{S}$ | 0.33 | 0.26 | 2.89, 3.37, 6.86 |
| | $\text{C}_{10}\text{H}_{18}\text{O}_6\text{S}$ | 0.16 | 0.17 | 3.41 |
| | $\text{C}_{10}\text{H}_{18}\text{O}_7\text{S}$ | 0.07 | 0.07 | 6.08, 7.43 |
| | $\text{C}_{10}\text{H}_{18}\text{O}_8\text{S}$ | 0.04 | 0.07 | 9.38, 10.51, 11.29, 11.75, 11.99, 12.38, 13.76 |
| | $\text{C}_9\text{H}_{16}\text{O}_6\text{S}$ | 0.90 | 0.74 | 2.86, 3.44, 6.90, 7.37, 7.74, 8.84 |
| | $\text{C}_9\text{H}_{16}\text{O}_7\text{S}$ | 0.32 | 2.72 | 1.72, 2.85, 3.41, 4.52, 6.68, 6.97 |
| OS _{MT} sum | | 2.44 | 5.60 | |
| NOS _i | $\text{C}_5\text{H}_{10}\text{O}_{11}\text{N}_2\text{S}$ | 9.65 | 6.96 | 1.36, 1.68, 1.92, 2.95, 3.59 |
| | $\text{C}_5\text{H}_9\text{O}_{10}\text{NS}$ | 8.17 | 2.50 | 0.94 |
| | $\text{C}_5\text{H}_{11}\text{O}_9\text{NS}$ | 5.21 | 1.40 | 0.86 |

| | | Conc. (ng m ⁻³) | | |
|----------|--|-----------------------------|--------|----------------------|
| Formula | | Summer | Winter | Retention time (min) |
| | C ₅ H ₁₁ O ₈ NS | 0.61 | 0.40 | 1.09 |
| | C ₅ H ₉ O ₁₃ N ₃ S | 0.05 | 0.01 | 7.86,8.22,8.4 |
| NOSi sum | | 23.68 | 11.27 | |
| OSi | C ₅ H ₁₂ O ₇ S | 57.42 | 4.79 | 0.71 |
| | C ₂ H ₄ O ₆ S | 23.95 | 11.71 | 0.73 |
| | C₈H₁₄O₆S | 13.47 | 10.94 | 1.48 |
| | C ₃ H ₆ O ₅ S | 12.20 | 6.74 | 0.73 |
| | C ₄ H ₈ O ₇ S | 11.84 | 5.71 | 0.73 |
| | C ₅ H ₈ O ₇ S | 11.76 | 5.68 | 0.73 |
| | C ₅ H ₁₀ O ₇ S | 11.44 | 5.02 | 0.73 |
| | C ₅ H ₁₀ O ₆ S | 11.24 | 5.52 | 0.79 |
| | C ₄ H ₈ O ₆ S | 10.85 | 5.41 | 0.74 |
| | C₆H₁₀O₇S | 9.04 | 8.60 | 0.74 |
| | C₅H₁₀O₅S | 8.00 | 19.53 | 0.93 |
| | C ₈ H ₁₄ O ₇ S | 6.96 | 1.90 | 0.74 |
| | C₈H₁₂O₇S | 5.79 | 2.52 | 0.74 |
| | C ₃ H ₆ O ₆ S | 5.61 | 5.08 | 0.73 |
| | C₂H₆O₅S | 5.13 | 9.26 | 0.73 |
| | C ₅ H ₁₀ O ₈ S | 4.48 | 1.11 | 0.73 |
| | C ₂ H ₄ O ₅ S | 4.28 | 3.10 | 0.73 |
| | C₅H₈O₅S | 3.91 | 1.89 | 0.85 |
| | C₄H₈O₅S | 3.36 | 3.73 | 0.75 |
| | C₆H₁₂O₇S | 3.28 | 2.44 | 0.83 |
| | C ₈ H ₁₄ O ₈ S | 2.62 | 1.97 | 0.74 |
| | C ₃ H ₆ O ₇ S | 2.01 | 2.36 | 0.75 |
| | C ₅ H ₁₂ O ₆ S | 1.67 | 1.04 | 0.74 |
| | C ₅ H ₈ O ₉ S | 1.46 | 0.60 | 0.64 |
| | C₄H₆O₆S | 1.41 | 2.66 | 0.74 |
| | C ₃ H ₈ O ₆ S | 1.31 | 1.26 | 0.75 |
| | C₇H₁₀O₆S | 0.87 | 0.89 | 0.74 |
| | C ₈ H ₁₄ O ₁₀ S | 0.68 | 0.46 | 0.73 |
| | C₈H₁₀O₄S | 0.01 | 0.30 | 0.78 |

| Formula | Conc. (ng m ⁻³) | | Retention time (min) |
|-------------|-----------------------------|--------|----------------------|
| | Summer | Winter | |
| Isoprene OS | 236.07 | 132.20 | |
| OSi | 181.79 | 69.45 | |
| Total BSOA | 216.25 | 99.42 | |

3.3.1.2 Monoterpene Organosulfates (OS_{MT})

The identified monoterpene derived OSs (OS_{MT}) included 44 C_{9/10} species during the summer and winter campaigns, as shown in Table 3.3. These OS_{MT} have been shown to be produced from either photooxidation or nitrate radical oxidation of monoterpene VOCs, [134, 260] followed by reactive uptake or sulfate radical reaction.[262] Total OS_{MT} concentrations were roughly double during the winter (5.6 ± 0.8 ng m⁻³) compared to those in the summer (2.4 ± 0.8 ng m⁻³), similar to results seen in other areas in China.[126, 184]

C₉H₁₆O₆S was the most abundant OS_{MT} species during the summer with an average concentration of 0.9 ± 0.4 ng m⁻³, with similar concentrations observed previously in Shanghai (1.17 ng m⁻³).[184] C₁₀H₁₆O₅S was the second most abundant OS_{MT} species during the summer (0.46 ± 0.2 ng m⁻³) and was previously identified in Denmark, with concentrations of 0.8 and 0.6 ng m⁻³ observed at urban and semirural sites, respectively.[240] The highest OS_{MT} concentration observed across either campaign was C₉H₁₆O₇S during the winter, with a time averaged mean concentration of 2.72 ± 0.2 ng m⁻³, similar to concentrations (2.5 ± 2.3 ng m⁻³) observed at an urban site in Copenhagen, Denmark during the summer.[240] C₉H₁₆O₇S showed the most prominent winter enhancement, with winter concentrations ~ 8 times higher than those observed in the summer.

As for the NOS_{MT}, many of the OS_{MT} species were only identified in a small number of the samples, and only tracers that were identified in at least 40% of the samples were used for analysis. Total OS_{MT} species identified showed nighttime

enhancement with a minima during the afternoon, as shown in Figure 3.4C,D. This nighttime peak of OS_{MT} species is likely linked to the nighttime enhancements of precursor monoterpene concentrations.[290] Previous laboratory studies of monoterpenes with NO₃ radicals have also shown the formation of OS_{MT} with the same molecular formulas as measured here.[134] Interestingly, none of the OS_{MT} species showed a significant correlation ($R^2 < 0.10$) toward SO₄²⁻ across either campaign, although the highest OS_{MT} concentrations did generally occur under the highest SO₄²⁻ concentrations (Figure 3.5).

SO₂ was measured during the winter campaign, but again no significant correlation ($R^2 < 0.1$) was observed toward the OS_{MT} tracers. Chamber studies have shown that, for the reactive uptake of monoterpene derived epoxides to acidic sulfate aerosol, extreme acidity levels typically not observed in ambient environments are required and as such is not thought to be a major route to OS_{MT} formation.[145] Much like the NOS_{MT} species, OS_{MT} showed no direct correlation toward NO₂ concentrations at any time of day ($R^2 < 0.15$), although higher daytime OS_{MT} concentrations were associated with higher NO₂ concentrations during both campaigns. Another potential route of formation could be the degradation of nitrates or NOS_{MT} species to OS_{MT} species through hydrolysis.[247, 264] This is further evidenced by the strong correlation between NOS_{MT} and OS_{MT} concentrations (Figure 3.9) during the summer campaign ($R^2 = 0.87$), while a weaker correlation was observed in the winter ($R^2 = 0.32$), although no dependence on RH was observed in either campaign. Further work is needed to determine the hydrolysis pathways of these NOS_{MT} species leading to OS_{MT} in aqueous particles.

3.3.1.3 Isoprene Nitroxy Organosulfates (NOSi)

Eleven isoprene nitroxy organosulfate (NOSi) tracers were identified in the samples across the two campaigns, including mononitrated (C₅H₉O₁₀NS, C₅H₁₁O₉NS, C₅H₁₁O₈NS), dinitrated (C₅H₁₀O₁₁N₂S), and trinitrated (C₅H₉O₁₃N₃S) species. Unlike the NOS_{MT} species, NOSi concentrations were roughly double during the

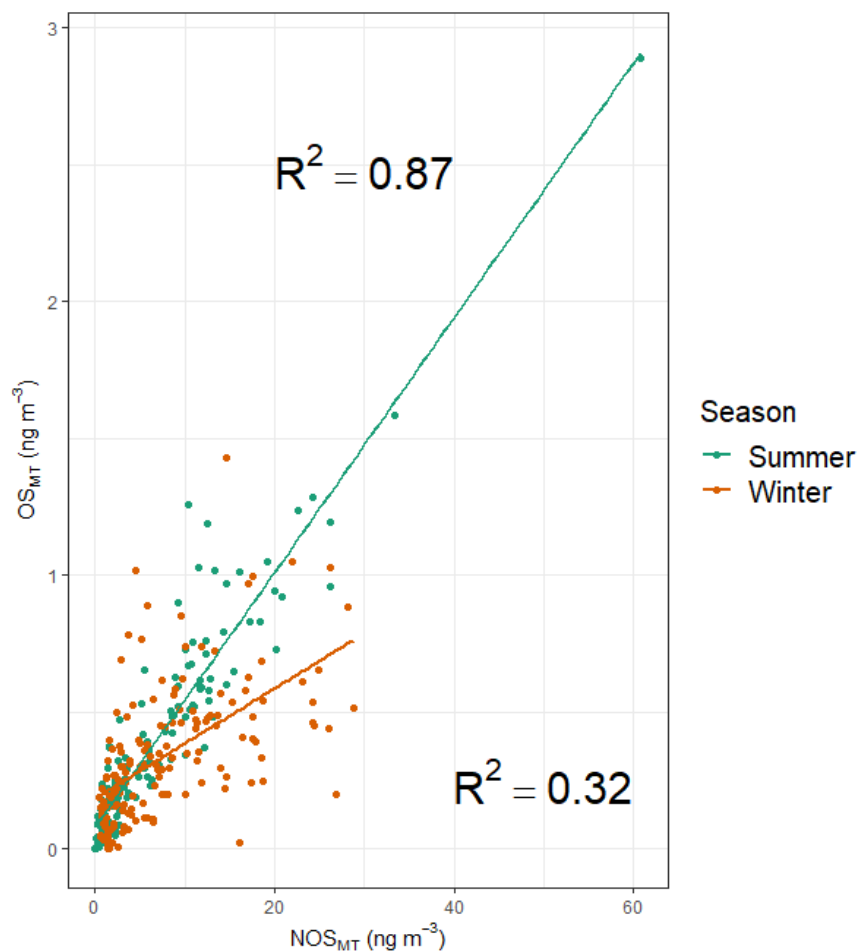


Figure 3.9: Correlation between OS_{MT} and NOS_{MT} concentrations coloured by season.

summer ($23.7 \pm 19.7 \text{ ng m}^{-3}$) than those in the winter ($11.3 \pm 10.2 \text{ ng m}^{-3}$), likely due to higher isoprene emissions. Three mononitrated species have been observed in ambient samples previously in Shanghai [184] and Beijing.[104, 125, 126, 184] The most abundant mono-NOSi across both campaigns was $C_5H_9O_{10}NS$, with average concentrations of 8.2 ± 9.8 and $2.5 \pm 3.0 \text{ ng m}^{-3}$ across the summer and winter campaigns, respectively. This is consistent with previous summertime measurements in Beijing in 2015 (9.17 ng m^{-3}) [293] and Shanghai, also for summer 2015 (2.14 ng m^{-3}) and 2019 (7.39 ng m^{-3}).[184] Interestingly Wang et al. in 2021 did not identify $C_5H_9O_{10}NS$ during the winter samples collected in Shanghai during 2016 and 2019. $C_5H_9O_{10}NS$ was first observed by Nestorowisz

et al. in 2018 via smog chamber experiments and is suggested to form from the photo-oxidation of isoprene in the presence of NO.^[149] More recently, it has been suggested that it could be produced from the heterogeneous sulfate reaction with isoprene hydroxy- α -lactone species formed from the oxidation of isoprene nitroxy aldehyde by NO₃ or OH radicals.^[109, 244] The average diurnal variation of C₅H₉O₁₀NS observed during the summer is almost flat, with a slight uptick during the afternoon, in line with expected peak isoprene emissions, while in the winter, the diurnal variation showed enhancement during the night and early morning (Figure 3.7 a,b). The diurnal variations also highlight the temperature dependence's of the concentrations, with the points colored by temperature, with overlapping scales. During both campaigns, lower temperatures are associated with lower tracer concentrations. Lower isoprene concentrations are linked to lower temperatures, with this variation in isoprene emissions likely the driver for the limited diurnal variation. Strong correlations ($R^2 = 0.61$) toward inorganic sulfate were observed during the day during the summer campaign but no correlation occurred at night ($R^2 = 0.16$), while during the winter campaign, a weaker correlation was seen during the day ($R^2 = 0.26$) and similar correlation during the night ($R^2 = 0.18$). C₅H₉O₁₀NS showed no direct correlation toward NO or NO₂ across the two campaigns ($R^2 < 0.1$). Overall, this suggests that particulate sulfate concentrations play a role in controlling in the formation of C₅H₉O₁₀NS, especially during the summer.

C₅H₁₁O₉NS was the second most abundant of the mono-NOSi tracers, with summer and winter concentrations of 5.2 ± 7.0 and 1.4 ± 1.8 ng m⁻³, compared to Beijing during the summer at 12.6 ng m⁻³ ^[104, 125] and Shanghai at 6.82 and 0.24 ng m⁻³ during the summer and winter, respectively.^[184] Hamilton et al. in 2021 proposed that this species is formed from the acid catalyzed heterogeneous uptake of isoprene nitroxy hydroxyepoxide via the initial NO₃ oxidation of isoprene. NO₃ oxidation is thought to be competitive with OH radicals in the formation of isoprene nitrates in Beijing during the afternoons as a result of low NO concentrations, similar to those observed in Guangzhou.

The average diurnal profiles of $C_5H_{11}O_9NS$ during the summer and winter are shown in Figure 3.7 C,D, respectively. During the summer, a slight increase in concentrations during the afternoon is observed, while during the winter, a slight increase is observed during the evening. No correlation was observed toward NO or NO_2 throughout either campaign, but a strong correlation toward particulate SO_4^{2-} ($R^2 = 0.62$) was observed in the summer daytime samples, compared to $R^2 = 0.22$ during the winter daytime.

In contrast to the other mono-NOSi species, $C_5H_{11}O_8NS$ showed similar concentrations during the summer and winter campaigns, with concentrations of 0.61 ± 0.6 and $0.4 \pm 0.4 \text{ ng m}^{-3}$, respectively. $C_5H_{11}O_8NS$ showed the clearest nighttime enhancement across both campaigns, as shown in Figure 3.7 E,F. $C_5H_{11}O_8NS$ was first identified by Surratt et al. in 2008 in chamber experiments and previously identified in Beijing during the summer with a lower mean concentration of 0.11 ng m^{-3} . [125] No studies to our knowledge have proposed a formation route for this species, with the species being identified in both isoprene/ H_2O_2 /NO/acidic seed and isoprene/HONO/neutral seed experiments. Unlike the other mono-NOSi species, $C_5H_{11}O_8NS$ showed a weak correlation toward sulfate, with the highest correlation observed during the summer daytimes ($R^2 = 0.26$). $C_5H_{11}O_8NS$ showed a limited direct correlation toward either NO or NO_2 mixing ratios. However, when the concentrations of $C_5H_{11}O_8NS$, across both campaigns were plotted against binned NO_2 (10 ppb bins size) and NO (5 ppb bin size), the average concentrations increased under more polluted conditions, as shown in Figure 3.10.

The dinitrate NOSi species ($C_5H_{10}O_{11}N_2S$) were identified across the summer ($9.7 \pm 6.3 \text{ ng m}^{-3}$) and winter ($7.0 \pm 6.5 \text{ ng m}^{-3}$) campaigns, with four isomers identified in the summer compared to five during the winter. The dominant isomer in terms of concentration eluted at 1.92 min and accounted for 76% and 85% of the summer and winter total $C_5H_{10}O_{11}N_2S$ concentrations, respectively. Figure 3.11 shows the diurnal variations of the isomers, which were identified in at least one filter sample per collection period. The isomers generally show a clear nighttime enhancement, with a minimum during the afternoon, suggesting that

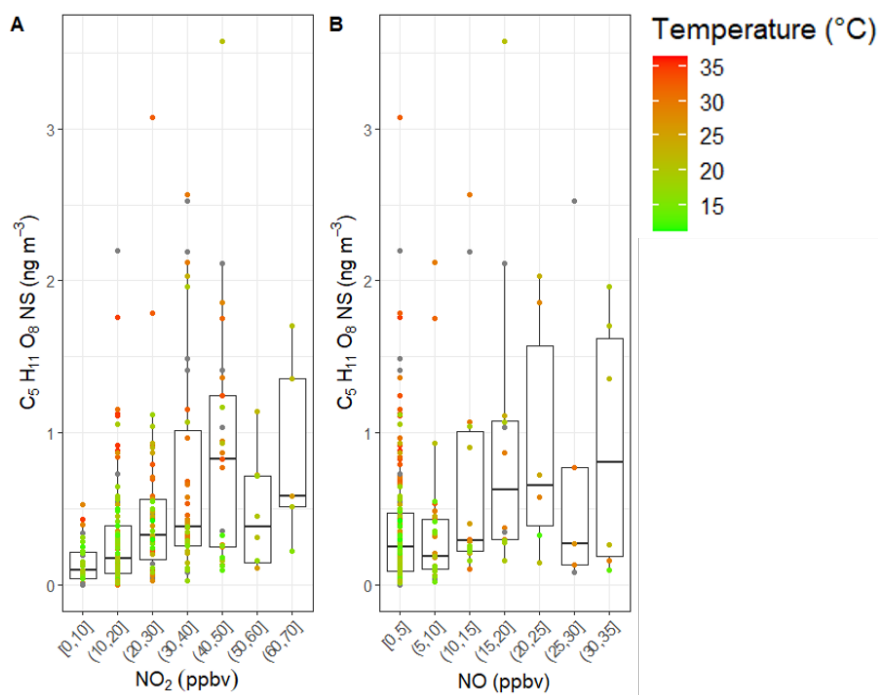


Figure 3.10: $C_5H_{11}O_8NS$ vs binned NO_x concentrations across both campaigns: (A) NO_2 and (B) NO . NO_2 concentrations were filtered to below 70 ppbv due to a limited number of data points. Data points were then colored by the average temperature over the filter sampling time period. Where temperature measurements were not available, the data points are in gray.

nighttime formation is the dominant route. High variability in concentrations of the dinitrate $NOSi$ were observed, most likely due to isoprene emission.

For the winter samples in Figure 3.11B,D, there is a clear temperature dependence in the concentrations observed. $C_5H_{10}O_{11}N_2S$ was first identified by Surratt et al., in 2008 via photo-oxidation in the presence of NO_x or nighttime NO_3 oxidation. $C_5H_{10}O_{11}N_2S$ was previously identified in Beijing, where four isomers were identified, with a strong nighttime enhancement and an average concentration of 2.6 ng m^{-3} .^[104, 125] Two dark NO_3 radical formation pathways have been proposed for this dinitrated species. Ng et al. in 2008 suggested formation via an isoprene hydroxynitrate from two subsequent NO_3 attacks, followed by reaction with sulfate.^[152] Hamilton et al. in 2021 proposed a different route via heterogeneous uptake onto sulfate of a dinitrated epoxide species formed via two subsequent NO_3 radical additions. A daytime formation route has also

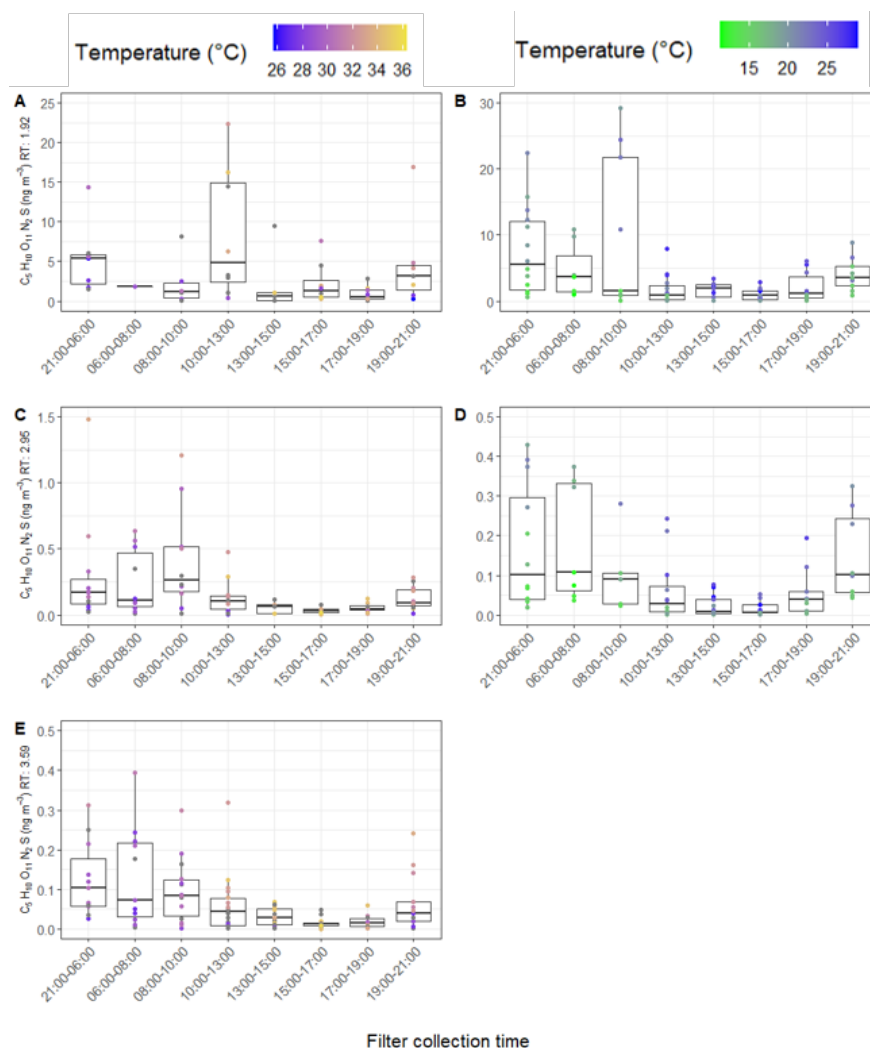


Figure 3.11: Diurnal variations of di-nitrated NOSi species across summer (left) and winter (right), coloured by temperature.

been proposed via the photo-oxidation of isoprene in the presence of NO.[109] Figure 3.12 shows the concentrations of the two dominant $C_5H_{10}O_{11}N_2S$ isomers against binned NO_2 concentrations during the summer (left) and winter (right) and show general increases in concentration with increasing NO_2 levels.

No correlation with NO or NO_3 concentrations was observed during either campaign. The lack of correlation toward NO_3 is likely due to the comparatively long lifetimes of the NOS species at night compared to NO_3 with NO_3 concentrations quickly dropping throughout the night during both campaigns. The $C_5H_{10}O_{11}N_2S$ markers also show high concentrations during the morning sample,

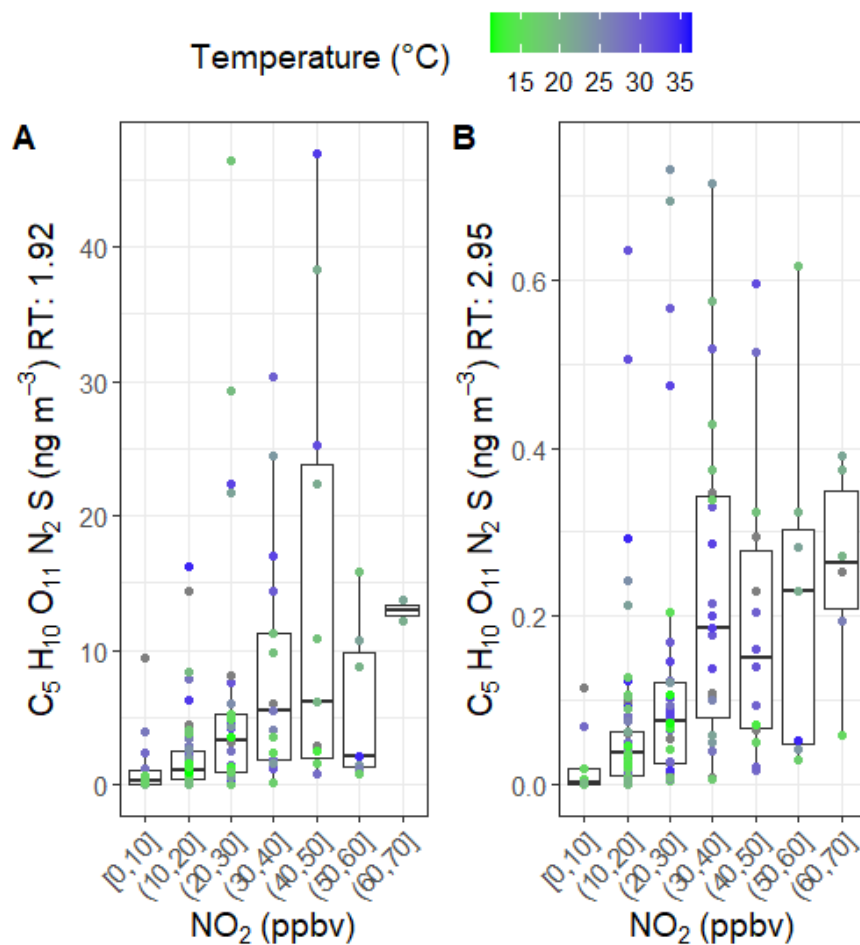


Figure 3.12: $C_5H_{10}O_{11}N_2S$ isomers A-1.92 min, B – 2.95 min concentrations correlated to NO_2 during across both campaigns.

under low NO_3 concentrations, likely due to nonlocal sources or boundary layer conditions. $C_5H_{10}O_{11}N_2S$ unlike the mononitrated species showed no correlation toward SO_4^{2-} during either campaign ($R^2 < 0.10$), suggesting that SO_4^{2-} is not a limiting reagent in the formation of this dinitrate, which has been observed previously in Beijing.[104] Overall, this suggests that $C_5H_{10}O_{11}N_2S$ is limited by the availability of NO_3 radicals rather than particulate sulfate concentrations, but further work is needed to understand the formation routes in the real atmosphere.

3.3.1.4 Isoprene Organosulfates (OSi)

Thirty-one OSi tracers were identified across the summer and winter (Table 3.3), while two OSi species were exclusively observed in the summer ($C_5H_{12}O_8S$ and $C_8H_{10}O_4S$) but were only minor components of the total summertime OSi concentrations (0.16%) and so were not considered further to allow for a direct comparison between the two seasons. Figure 3.13 and Figure 3.14 show correlation plots (corPlot, Openair, R package) containing the OSi tracers from the summer and winter, respectively. The plots highlight the strong correlations between the species. The number represents the Pearson coefficient (R) between the two species, i.e., 60 is an R of 0.6. More elongated circles represent higher correlations either positive (to the right) or negative (to the left), while darker red circles represent higher positive correlations and lighter green/blue circles represent stronger negative correlations.

In both campaigns, there are several tracers that have weaker correlations toward the rest of the tracers, which is more pronounced during the winter campaign, with $C_5H_{10}O_5S$ and $C_4H_6O_6S$ showing anticorrelations, suggesting a mixed biogenic/anthropogenic source. The two most well-studied isoprene tracers are $C_5H_{12}O_7S$ and $C_4H_8O_7S$. For quality control, OSi tracers that did not show a moderate ($R > 0.60$, as shown in Figure 3.13 and Figure 3.14) correlation toward at least one of these tracers in either campaign were removed from the data set. This was done to improve the confidence that these tracers are from isoprene chemistry rather than other sources. Eighteen OSi tracers were therefore used in the analysis across both campaigns and going forward known collectively as OSi.

The most abundant tracer during the summer campaign was $C_5H_{12}O_7S$ (2-methyl tetrol organosulfate, 2-MT-OS) with an average concentration of $57.4 \pm 90.4 \text{ ng m}^{-3}$ accounting for 32% of the total OSi. Much lower concentrations of 2-MT-OS were seen during the winter campaign, with an average concentration of $4.8 \pm 7.1 \text{ ng m}^{-3}$ and a lower contribution (6.9%) to the total OSi concentration. 2-MT-OS is one of the most common isoprene tracers and has been identified

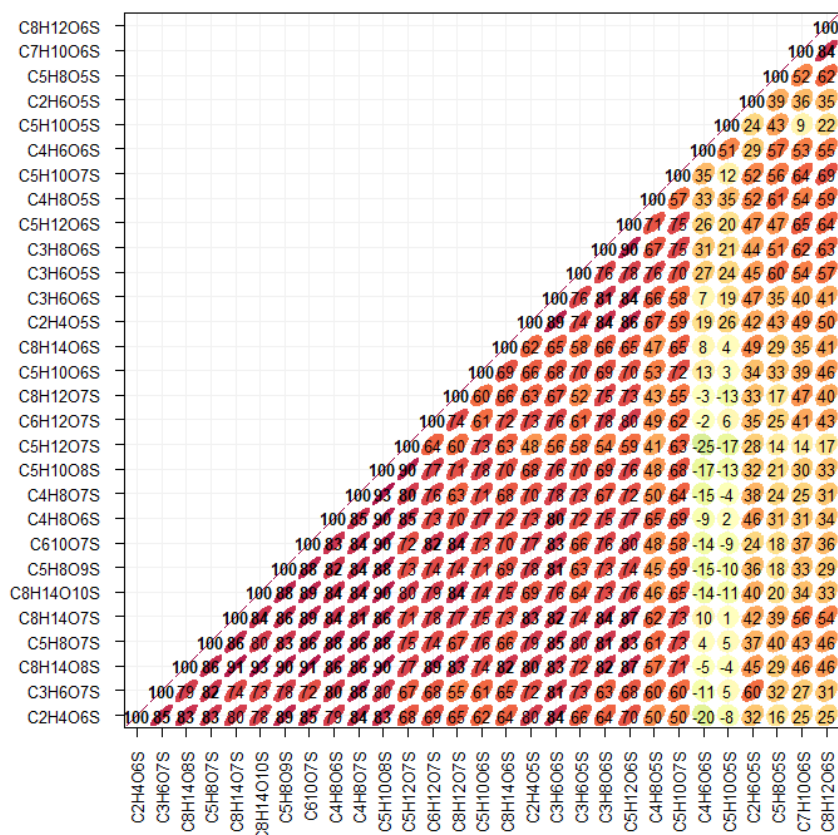


Figure 3.14: Correlation plot (CorPlot, Openair R package) between OSi species during the winter campaign.

concentrations could be influenced by high average temperatures during both campaigns (summer, 30.4 °C; winter, 18 °C) due to the rapid thermolysis of peroxyacetyl (PMA), the precursor to methacryloylperoxynitrate (MPAN) above 20 °C.[294] During the summer, the average 2-MT-OS/2-MG-OS ratio was 7.6, with a maximum of 49.2, which occurred under low NO conditions for an urban area (ca. 0.48 ppb). Mean NO concentrations were roughly double during the winter (12.1 ppb) compared to those in the summer (5.37 ppb). The average 2-MT-OS/2-MG-OS ratio observed in summer was very similar to previous observations in Shanghai (6.8–7.8).[184] The largest observed 2-MT-OS/2-MG-OS ratios are in line with those seen in the southeastern United States (33.8).[35]

During the winter, the average 2-MT-OS/2-MG-OS ratio was 0.73 (range 0.01–3.8). The lowest 2-MT-OS/2-MG-OS ratios occurred during the lowest NO concentrations, likely due to the extremely low afternoon NO concentrations and long sampling periods and were similar to those observed in summertime Beijing (0.55), suggesting that wintertime oxidation conditions in Guangzhou are similar to those during summer in Beijing.[125] Newland et al. in 2021 showed that up to 30% of isoprene derived peroxy radicals (ISOPROO) from OH oxidation can react with HO₂ rather than NO during the afternoon in Beijing when NO concentrations drop to less than 1 ppb.

Strong correlations were observed between the majority of tracers identified as OSi ($R = 0.50\text{--}0.97$), as shown in Figure 3.13 and Figure 3.14, indicating similar formation pathways or losses. The OSi tracers concentrations were summed to allow for an investigation of what influences OSi formation in Guangzhou. Total OSi concentrations showed moderate correlations toward particulate sulfate across both campaigns as shown in Figure 3.15 (summer, $R^2 = 0.55$; winter, $R^2 = 0.40$).

Interestingly, the gradients of the best fits during the summer and winter are very different, with the summer gradient ~ 6.7 times higher than that of the winter. During the summer, every additional $1 \mu\text{g m}^{-3}$ of sulfate available increases the OSi concentrations by $\sim 52 \text{ ng m}^{-3}$ but only 7.7 ng m^{-3} in the winter. Bryant et al. in 2020 showed a stronger correlation between OSi species with the product of ozone (as a proxy for photochemistry) and particulate sulfate in Beijing, highlighting the role of both local photochemistry and particulate sulfate in OSi formation. However, in Guangzhou, the correlation of total OSi concentrations toward $[\text{O}_3][\text{SO}_4^{2-}]$ were lower (summer $R^2 = 0.32$ and winter $R^2 = 0.20$) than the correlations toward sulfate (Figure 3.15). The correlation of $[\text{O}_3][\text{SO}_4^{2-}]$ is likely to be weaker at longer photochemical ages when the O₃ concentration is not directly related to the photochemical formation of the OSi local to the observation site. During the summer, the highest total OSi concentrations occurred under the lowest NO concentrations (0–5 ppb, Figure 3.15), highlighting the importance of “low-NO” oxidation routes for isoprene emissions during the summer.

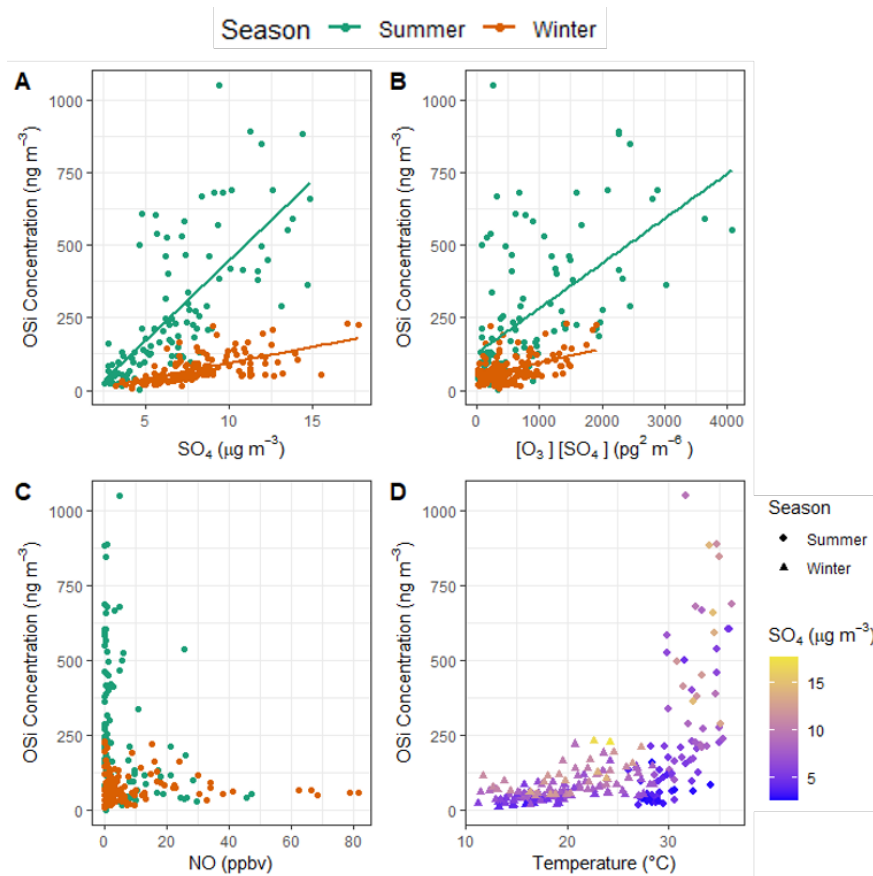


Figure 3.15: A – Correlation between OSi concentrations and particulate sulfate, coloured by season. B – Correlation between OSi and the product of [O₃][SO₄²⁻], coloured by season. C- Correlation between OSi concentration and NO, coloured by season. D- Correlation between OSi and temperature across both campaigns, coloured by SO₄²⁻ concentrations, with the shape indicating the campaign.

The OSi tracers showed strong seasonality in comparison to the other tracer groups, with average summer and winter concentrations of 181.8 (1.84–1049.8 ng m⁻³) and 69.5 ng m⁻³ (7.8–229.4 ng m⁻³), respectively. This large difference in concentrations is likely due to both changes in isoprene emissions, [283] and solar irradiance and has been observed at other locations.[184, 270]

OSi concentrations greatly increased with temperature above 30 °C, as shown in Figure 3.15. This type of temperature dependence has been seen for isoprene emissions previously.[292, 295] Overall, this suggests that increased OSi concentrations are driven by primary isoprene emissions as well as the availability of sulfate for uptake into the particle phase.

3.3.2 Conclusion

PM_{2.5} filter collection was conducted to investigate the formation processes of organosulfates (OSs) and nitrooxy-organosulfates (NOSs) across a summer and winter campaign in Guangzhou, a southern Chinese megacity, influenced by high biogenic and anthropogenic emissions. Targeted analysis of OSs and NOSs from isoprene and monoterpenes was undertaken, with tracers quantified using both authentic and proxy standards. Quantified biogenic OS and NOS concentrations averaged 216.3 ng m⁻³ and 99.4 ng m⁻³ during summer and winter respectively, with OSi contributing 84 % and 70 %. The majority of OS_{MT} and NOS_{MT} species showed strong nocturnal enhancements, owing to increased precursor emissions and/or NO₃ oxidation chemistry. OS_{MT} showed limited correlation to potential reactants, but showed a strong correlation towards NOS_{MT} species, especially during summer, suggesting a potential NOS_{MT} to OS_{MT} degradation route. Several NOSi species were identified, with mixed formation routes via both day-time OH and ozone initiated photo-oxidation and nocturnal NO₃ oxidation. Several of the mono-nitrated species showed moderate correlations to particulate sulfate ($R^2 = 0.61$), while the di-nitrated species were poorly correlated ($R^2 < 0.1$). 2-MT-OS was the most abundant isoprene tracer during the summer campaign, with an average concentration of 57.4 ng m⁻³, 32 % of the total OSi. 2-MT-OS:2-MG-OS ratios during summer (7.6) compared to winter (0.73), suggests that low-NO formation pathways were dominant in summer, as seen in Beijing previously. OSi species showed a strong temperature dependence, with concentrations increasing sharply with temperatures above 30 °C, likely due to increased precursor isoprene emissions. OSi showed a direct relationship towards particulate sulfate, especially during the summer, and highlights the extensive heterogeneous chemistry occurring. Future studies should focus on increasing the time resolution of observations of OS/NOS, taken alongside detailed speciated VOC measurements and NO₃ radical measurements, to allow for more detailed diurnal variations to be studied as well as improving our ability to accurately

quantify tracers through synthesis of standards or new quantification techniques.

Chapter 4

Biogenic and anthropogenic sources of isoprene and monoterpenes and their secondary organic aerosol in Delhi, India

4.1 Introduction

India is undergoing rapid urbanization and industrialisation, with an ever-growing population. Delhi, India's capital, is estimated to have a population of over 20 million (2011) inhabitants, up from around 1.3 million in 1950.[296] According to the WHO in 2018, India was home to 9 out of the top 10 most polluted cities in the world in terms of annual mean $\text{PM}_{2.5}$ concentrations.[20] In Delhi, the population-weighted mean $\text{PM}_{2.5}$ (particulate matter less than 2.5 micrometres in diameter) was estimated to be 209 (range: 120 – 339.5) $\mu\text{g m}^{-3}$ in 2017, well above the WHO annual mean guidelines of 5 $\mu\text{g m}^{-3}$, and still well above India's own standard of 40 $\mu\text{g m}^{-3}$. [297] Air pollution is estimated to cause over 1 million deaths per year in India alone.[21] It was estimated that in 2017 the average number of premature deaths due to air pollution in Delhi was over 12000, with the majority attributed to PM exposure. [297]

Numerous studies have investigated $\text{PM}_{2.5}$ concentrations, characteristics and meteorological effects in Delhi.[298–303], but limited individual molecular level analysis of aerosol particles has been undertaken [299, 302, 304–307]. The key sources of $\text{PM}_{2.5}$ identified are secondary aerosol, fossil fuel combustion, municipal waste and biomass burning. [288, 299, 308, 309] Previous studies have shown that alongside extremely high emissions of pollutants, regional sources and meteorology in particular play an important role in high pollution events in Delhi. [310–313]

Secondary species have been shown to be significant contributors to PM_1 and $\text{PM}_{2.5}$ mass in Delhi, with organics contributing 40-70 % of PM_1 mass.[308, 314–316] Kirillova et al., 2014 analysed the sources of water-soluble organic carbon (WSOC) in Delhi, using radiocarbon measurements constraints.[257] The study showed that 79% of WSOC was classified as non-fossil carbon, attributed to biogenic/biomass burning sources in urban Delhi, similar to other studies from India.[256, 258] Previous studies in cities across Asia, Europe and North America have also shown a high contribution from non-fossil sources to ambient $\text{PM}_{2.5}$ concentrations. [317–320] The sources of this modern carbon in urban areas are

poorly understood, although biomass burning is a key component.[206, 303, 321, 322] Recently in Delhi, solid-fuel combustion sources such as cow dung cake or municipal solid waste have been shown to release over 1000 different organic components into the aerosol phase at emission.[288] Alongside biomass burning, another potential source of this non-fossil aerosol is biogenic secondary organic aerosol (BSOA), formed via the oxidation of biogenic volatile organic compounds (BVOCs) and subsequent gas-particle phase transfer. [1, 323]

This study aims to improve our understanding of the sources of isoprene and monoterpene SOA markers and formation pathways in extremely polluted urban areas. Biogenic VOC emissions were observed to correlate strongly to anthropogenic markers, suggesting anthropogenic sources of these VOCs. OSi species showed strong seasonality and strong correlations to particulate sulfate. NOS species showed strong nocturnal enhancements, likely due to nitrate radical chemistry. This study is the first molecular level particle phase analysis of OS and NOS markers from isoprene and monoterpenes in Delhi. Offline PM_{2.5} filter samples were collected across two campaigns in central Delhi, alongside a suite of atmospheric pollutant measurements. Filters were analysed using ultra-high performance liquid chromatography tandem mass spectrometry and isoprene and monoterpene OS/NOS markers quantified using both authentic and proxy standards.

4.2 Experimental

4.2.1 Filter collection and site information

PM_{2.5} filter samples were collected as part of the air pollution and human health (APHH)-India campaign, at the Indira Gandhi Delhi Technical University for Women in New Delhi, India, (28°39'55" N 77°13'56" E) by Stefan Swift. The site is situated inside the third ring road which caters to huge amounts of traffic, with a major road to the east, between the site and the Yamuna river. Two

train stations are located to the south and south west of the site, and there are several green spaces locally in all directions. Filters were collected during two field campaigns in 2018. The first campaign was during the pre-monsoon period, with 35 filters were collected between 28/05/2018 and 05/06/2018. The second campaign during the post-monsoon period, 108 filters were collected between 09/10/2018 and 6/11/2018. Quartz filters (Whatman QMA, 10" by 8") were pre-baked at 550 °C for 5 hours and wrapped in foil before use. Samples were collected using an HiVol sampler (Ecotech 3000, Victoria Australia) with selective PM_{2.5} inlet at a flow rate of 1.33 m³ min⁻¹. Once collected, filters were stored in foil at -20°C before, during and after transport for UK based analysis.

4.2.2 Filter extraction

Using a standard square filter cutter, a section of filter was taken with an area of 30.25 cm² which was then cut into roughly 1 cm² pieces and placed in a 20 mL glass vial. Next, 8 mL of LC-MS grade MeOH (Optima, Fisher Chemical, USA) was added to the sample and sonicated for 45 min. Ice packs were used to keep the bath temperature below room temperature, with the water swapped mid-way through. Using a 5 mL plastic syringe, the MeOH extract was then pushed through a 0.22 μm filter (Millipore) into another sample vial. An additional 2 mL (2 x 1 mL) of MeOH was added to the filter sample, and then extracted through the filter to give a combined extract ~ 10mL. This extract was then reduced to dryness using a Genevac solvent evaporator under vacuum. The dry sample was then reconstituted in 50:50 MeOH:H₂O (Optima, Fisher Chemical, USA) for analysis. Extraction efficiencies of 2-MG-OS and camphorsulfonic acid were determined using authentic standards spiked onto a pre-baked clean filter and recoveries were calculated to be 71 % and 99 % respectively.

4.2.2.1 Ultra-high performance liquid chromatography tandem mass spectrometry (UHPLC-MS²)

The extracted fractions of the filter samples were analysed using an Ultimate 3000 UHPLC (Thermo Scientific, USA) coupled to a Q Exactive Orbitrap MS (Thermo Fisher Scientific, USA) using data dependent tandem mass spectrometry (ddMS²) with heated electrospray ionization source (HESI). The UHPLC method uses a reversed-phase 5 μm , 4.6 mm \times 100 mm, polar end capped Accucore column (Thermo Scientific, UK) held at 40 °C. The mobile phase consisted of water (A) and methanol (B) both with 0.1 % (v/v) of formic acid (98 % purity, Acros Organics). Gradient elution was used, starting at 90 % (A) with a 1-minute post-injection hold, decreasing to 10 % (A) at 26 minutes, returning to the starting mobile phase conditions at 28 minutes, followed by a 2-minute hold allowing the re-equilibration of the column. The flow rate was set to 0.3 mL min⁻¹. A sample injection volume of 4 μL was used. The capillary and auxiliary gas heater temperatures were set to 320 °C, with a sheath gas flow rate of 45 (arb.) and an auxiliary gas flow rate of 20 (arb.). Spectra were acquired in the negative ionization mode with a scan range of mass-to-charge (m/z) 50 to 750. Tandem mass spectrometry was performed using higher-energy collision dissociation with a stepped normalized collision energy of 10,45,60. The isolation window was set to m/z 2.0 with a loop count of 10, selecting the 10 most abundant species for fragmentation in each scan.

A mass spectral library was built using the compound database function in Tracefinder 4.1 General Quan software (Thermo Fisher Scientific, USA). To build the library, compounds from previous studies [134, 149, 152, 235, 263, 279] were searched for in an afternoon and a night-time filter sample extract analysis using the Xcalibur software. Data processing was conducted as described in 3.2.4.

4.2.3 Quantification and uncertainties

Quantification of markers and associated matrix effects were conducted as outlined in section 3.2.5. Table 4.1 shows the ratios across 5 ambient samples collected

Table 4.1: Matrix effect analysis results from 5 filter samples on three different organosulfate standards (CAM-OS – Camphorsulfonic acid, MG-OS – 2-methyl glyceric acid organosulfate, MT-OS – 2-methyl tetrol organosulfate). Alongside PM_{2.5} and SO₄²⁻ concentrations. The values in bold are the average ratios between a clean matrix and an ambient sample matrix.

| Start date | Time of day | Conc. ($\mu\text{g m}^{-3}$) | | CAM -OS | MG -OS | MT -OS |
|------------|-------------|--------------------------------|-------------------------------|---------------------------|---------------------------|---------------------------|
| | | PM _{2.5} | SO ₄ ²⁻ | | | |
| 16-Oct | 13:30–14:30 | NA | 18.2 | 0.67 | 0.49 | 0.21 |
| 18-Oct | 09:90–10:00 | NA | 25 | 0.60 | 0.58 | 0.23 |
| 18-Oct | 19:00–09:30 | 120.2 | 11 | 0.69 | 0.10 | 0.16 |
| 30-May | 17:30–08:00 | 134 | 12.8 | 0.84 | 0.22 | 0.06 |
| 04-June | 08:30–11:30 | 124.7 | 19.7 | 1.01 | 0.59 | 0.16 |
| Average | | | | 0.76 ± 0.16 | 0.40 ± 0.23 | 0.17 ± 0.06 |

during both campaigns, which represent a mixture of high and low PM_{2.5} concentrations across different times of day. 2-MT-OS and 2-MG-OS showed significant matrix effects, with average \pm SD matrix ratios of 0.17 ± 0.06 and 0.40 ± 0.23 , suggesting 83% and 60% suppressions in signal response. Camphorsulfonic acid exhibited a much smaller matrix suppression, with an average of 0.76 ± 0.16 suggesting a 24 % suppression, in line with those calculated in Guangzhou (Chapter 3). The suppression is likely due to the large numbers of co-eluting inorganic and organic species, reducing the ionisation efficiency of the marker compounds. Matrix correction factors were applied alongside calibrations to different compound classes and for compounds eluting at different times. Overall uncertainties associated with calibrations, proxy standards and matrix effects were estimated. The uncertainties associated with 2-MG-OS and 2-MT-OS were calculated to be 58.9 % and 37.6 % respectively, mainly due to the large uncertainties in the matrix correction factors. Isoprene SOA markers quantified by the average of 2-MT-OS and 2-MG-OS calibrations have an associated uncertainty of 69.9 %. For monoterpene SOA species which were quantified by camphorsulfonic acid, the associated uncertainty is estimated to be 24.8 %.

4.2.4 Supplementary measurements

A suite of complementary measurements (Table 4.2) were made alongside the filter collection including VOCs, o-VOCs, NO_x, CO, SO₂, photolysis rates and measurements of PM₁ non-refractory aerosol chemical components with a high resolution Aerosol Mass Spectrometer (HR-AMS). Detailed instrument descriptions can be found in Nelson et al., 2021.[324] Briefly, VOCs and o-VOCs were measured via two gas-chromatography (GC) instruments and a proton transfer reaction time-of-flight mass spectrometer with quadrupole ion guide (PTR-QiTOF). NO_x was measured via a dual channel chemiluminescence analyser with fitted with a blue light converter for NO₂ (Air Quality Designs Inc., Colorado) alongside CO which was measured with a resonance fluorescent instrument (Model AI5002, Aerolaser GmbH, Germany). O₃ was measured using an ozone analyser (49i, Thermo Scientific). SO₂ was measured using a 43i SO₂ analyser (Thermo scientific). High-resolution aerosol mass spectrometry measurements were conducted as outlined in Cash et al., 2021.[325] Ion chromatography measurements were conducted by Stefan Swift with the experimental approach outlined by Xu et al., 2020 as part of an intercomparison study. Briefly, filter cuttings were taken from the filter and extracted ultrasonically for 30 mins in 10 mL of ultrapure water and then filtered before analysis.[281]

Meteorology data was downloaded from the NOAA Integrated Surface Database via the Worldmet R package for the Indira Gandhi International Airport (code: 421810-99999).[326] The planetary boundary layer height (PBLH) was obtained from the ERA5 (ECMWF ReAnalysis 5) data product at 0.25 °resolution in 1-hour time steps at the position Lat 28.625°, Lon 77.25°. The data for both campaigns was then selected between the start time of the first filter of that campaign, and the end time of the last filter of the same campaign.

Table 4.2: Average pollutant and meteorological values across the pre- and post-monsoon campaigns.

| Pollutant | Pre-Monsoon | | | | Post-Monsoon | | | |
|---|-------------|--------|-------|-------|--------------|-------|------|------|
| | Mean | Med | SD | Max | Mean | Med | SD | Max |
| NO (ppbv) | 17.8 | 1.65 | 66.1 | 474 | 176 | 71.8 | 223 | 871 |
| NO ₂ (ppbv) | 30.8 | 25 | 17.9 | 109 | 41.7 | 38.1 | 21.1 | 169 |
| NOX (ppbv) | 48.7 | 27.2 | 77.3 | 548 | 218 | 123 | 221 | 900 |
| SO ₂ (ppbv) | 5.29 | 3.55 | 15.8 | 431 | 5.41 | 4.72 | 3.95 | 69.6 |
| O ₃ (ppbv) | 50.8 | 46.8 | 30.6 | 182 | 22.4 | 5.91 | 29.4 | 285 |
| PM _{2.5} (µg m ⁻³) | 141 | 125 | 66.2 | 672 | 182 | 170 | 93.9 | 695 |
| Inorg SO ₄ (µg m ⁻³) | 16.9 | 17.7 | 4.56 | 26.7 | 16.5 | 16.2 | 3.38 | 26.4 |
| Org SO ₄ (µg m ⁻³) | 7.5 | 7.3 | 1.78 | 13.2 | 5.55 | 5.16 | 2.68 | 14.2 |
| Organics (µg m ⁻³) | 19.8 | 15.8 | 13.7 | 114 | 48.7 | 37.8 | 35.4 | 221 |
| Nitrate (µg m ⁻³) | 1.58 | 1.13 | 1.36 | 8.01 | 5.83 | 4.68 | 4.18 | 28.8 |
| PBLH (m) | 891 | 508 | 879 | 4064 | 412 | 84.9 | 601 | 2722 |
| ws (m s ⁻¹) | 3.81 | 4.1 | 1.44 | 8.23 | 1.71 | 1.8 | 1.33 | 5.4 |
| Temp (° C) | 35.8 | 35.5 | 4.53 | 46.5 | 24.7 | 24.5 | 4.56 | 35 |
| RH (%) | 39.4 | 39.3 | 13.6 | 70.6 | 57.3 | 58.1 | 16.6 | 90.1 |
| Isoprene (ppbv) | 1.22 | 0.51 | 1.28 | 4.62 | 0.93 | 0.79 | 0.65 | 6.67 |
| limonene (ppbv) | 0.0095 | 0.0065 | 0.017 | 0.19 | 0.42 | 0.19 | 0.51 | 2.12 |
| α-pinene (ppbv) | 0.034 | 0.034 | 0.011 | 0.078 | 0.1 | 0.052 | 0.11 | 0.56 |

4.2.5 Radical Modelling

For both the pre-monsoon and post-monsoon campaigns, concentrations of OH and NO₃ radicals were modelled by Beth Nelson using a zero-dimensional chemical box model, incorporating a subset of the Master Chemical Mechanism (MCM v3.3.1)[243] into the AtChem2 modelling toolkit.[327] The MCM describes the detailed atmospheric chemical degradation of 143 VOCs, though 17,500 reactions of 6900 species. The model was constrained to 86 unique VOCs, NOX, CO, SO₂, O₃, and HONO, along with 34 observationally derived photolysis rates, temperature, pressure, and relative humidity (RH).

The post-monsoon campaign was also constrained to total aerosol surface area. Measurements were averaged or interpolated to 15 min data. For measured species not described in the MCM, surrogate species were selected based on their structural similarity to the species of interest. A fixed deposition rate of $1.2 \times 10^{-5} \text{ s}^{-1}$ was applied model-generated species, giving them an approximate lifetime of 24 h.

4.3 Results

4.3.1 Meteorology

The time series and diurnal variations for temperature, PBLH and RH are shown in Figures 4.1 and 4.2 respectively. For the pre-monsoon campaign, the average air temperature was (35.8 ± 4.5) °C compared to (24.7 ± 4.6) °C in the post-monsoon campaign. The pre-monsoon campaign also showed higher average wind speeds, with an average of (3.8 ± 1.4) m s⁻¹, compared to (1.7 ± 1.3) m s⁻¹ in the post-monsoon campaign. The average RH of the pre- and post-monsoon were (39.4 ± 13.6) % and (57.3 ± 16.6) % respectively, both showing similar diurnals with a minimum around mid-morning and nocturnal maximum. The PBLH shows a similar diurnal between the two campaigns. With the nocturnal boundary layer breaking down around 06:00-07:00 h with a midday peak, before re-establishing the nocturnal boundary layer around 19:00 h. It should be noted that the pre-monsoon PBLH has an average maximum of ~2400 m compared to post-monsoon ~1700 m and a minimum of 270 m compared to 52 m. The ventilation coefficient ($VC = \text{wind speed} \times \text{PBLH}$) has been used previously to identify periods of adverse meteorological conditions and gives an idea of how stagnant atmospheric conditions are and the general role of the atmosphere in the dilution of species. The VC was on average 4.5 times higher during the pre-monsoon campaign compared to the post-monsoon campaign, in line with previous studies.[314] The very low nocturnal boundary layer in the post monsoon campaign, along with a low VC, likely traps any nocturnal emissions and their reaction products close to the surface, allowing for a build-up of concentrations.

4.3.2 Particle phase observations

The mean ($\pm \sigma$) PM_{2.5} concentration (Table 4.2) during the pre-monsoon campaign was 141 ± 31 μg m⁻³ with a maximum concentration of 672 μg m⁻³ on the 01/6/2018 at 21:00 (Figure 4.3). The diurnal (Figure 4.4) shows concentrations generally

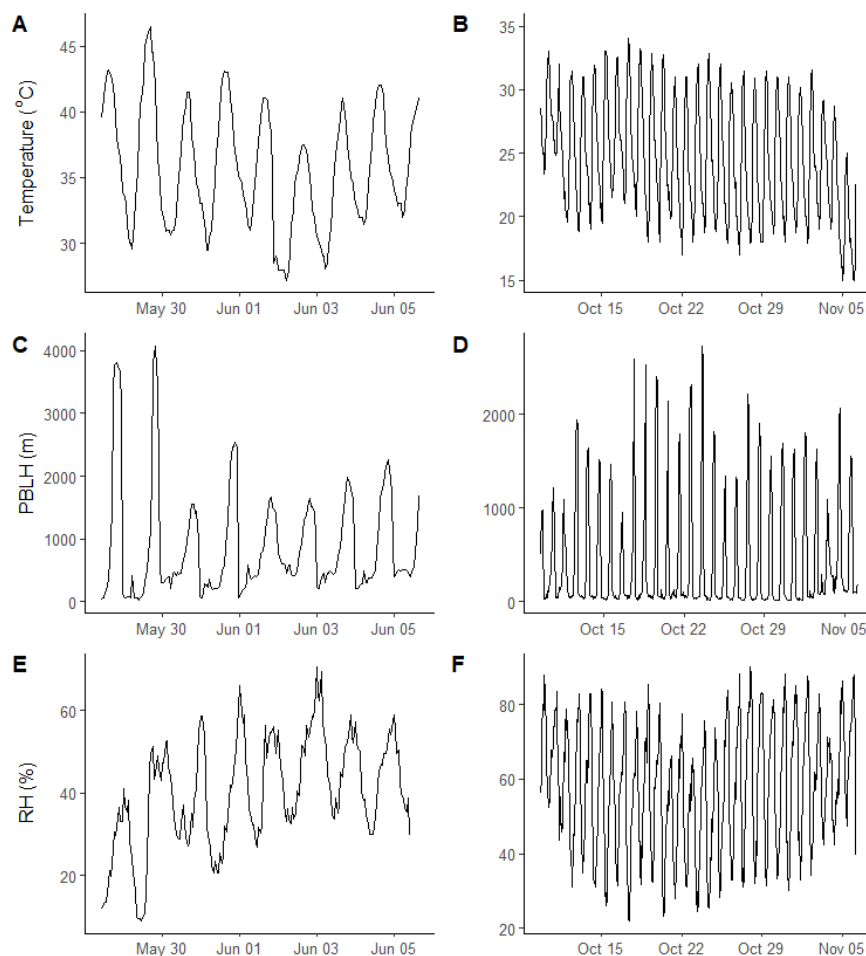


Figure 4.1: Time series variations of measured temperature, planetary boundary layer height (PBLH) and relative humidity (RH) across pre- (left) and post- (right) monsoon.

flat throughout the day, with a spike around 21:00, before dropping throughout the night to a minimum at 02:00. During the post-monsoon campaign, the average $\text{PM}_{2.5}$ concentration was higher at $182 \pm 94 \mu\text{g m}^{-3}$, with a maximum concentration of $695 \mu\text{g m}^{-3}$ (Figure 4.3). The diurnal shows a mid-afternoon minimum with high morning and night concentrations. HR-AMS was used to measure the PM_1 sulfate and total organics. Campaign averaged total organic concentrations were approximately double in the post-monsoon ($48.7 \pm 35.4 \mu\text{g m}^{-3}$) compared to the pre-monsoon ($19.8 \pm 13.7 \mu\text{g m}^{-3}$). Organic sulfate averaged $7.5 \pm 1.8 \mu\text{g m}^{-3}$ during the pre-monsoon campaign, with slightly lower average concentrations observed in the post-monsoon: $5.6 \pm 2.7 \mu\text{g m}^{-3}$.

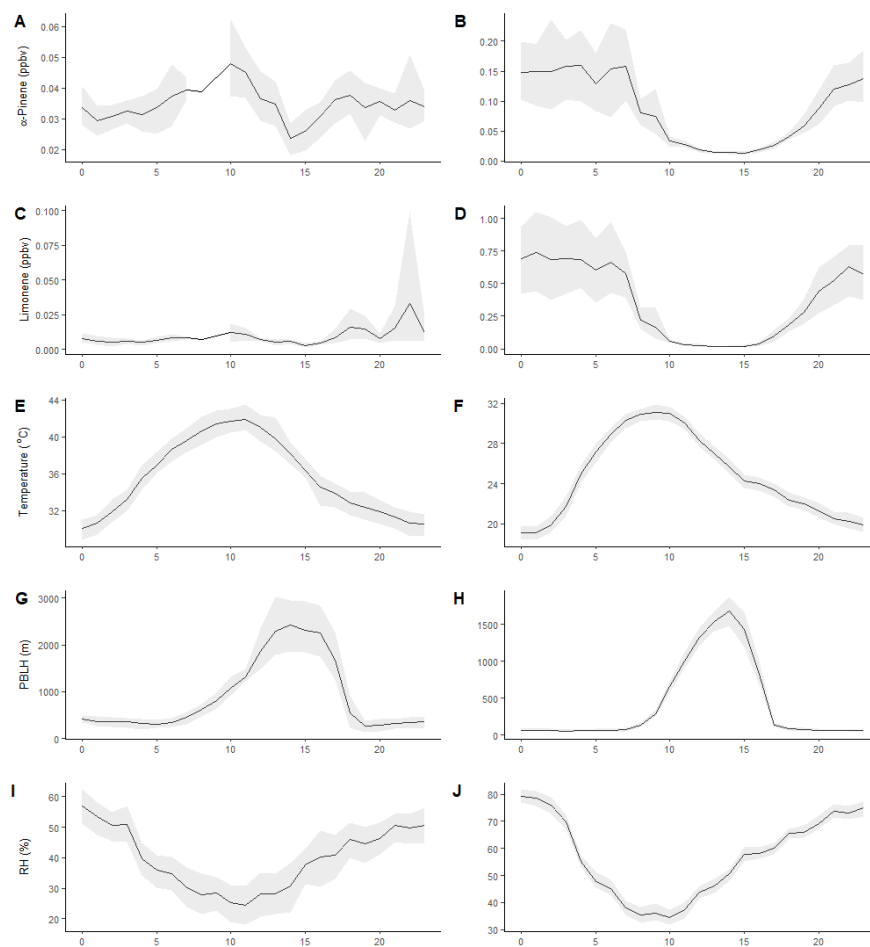


Figure 4.2: Diurnal variations of measured monoterpene VOC's, temperature, planetary boundary layer height (PBLH) and relative humidity (RH) across pre- (left) and post- (right) monsoon.

4.3.3 Gas phase observations

The measurement site was heavily polluted in terms of gas and particulate pollutants. Time series of the observed mixing ratios (ppbv) of NO, NO₂ and O₃ are shown in Figure 4.3, for the pre (left) and post (left) monsoon campaigns. The campaign averaged diurnal profiles are shown in Figure 4.4 and the mean, median and maximum mixing ratios are given in Table 4.2. It should be noted that only 1 week of data was available for the pre-monsoon period. During the post monsoon campaign, extremely high mixing ratios of NO were observed with a campaign maximum mixing ratio of 780 ppbv.

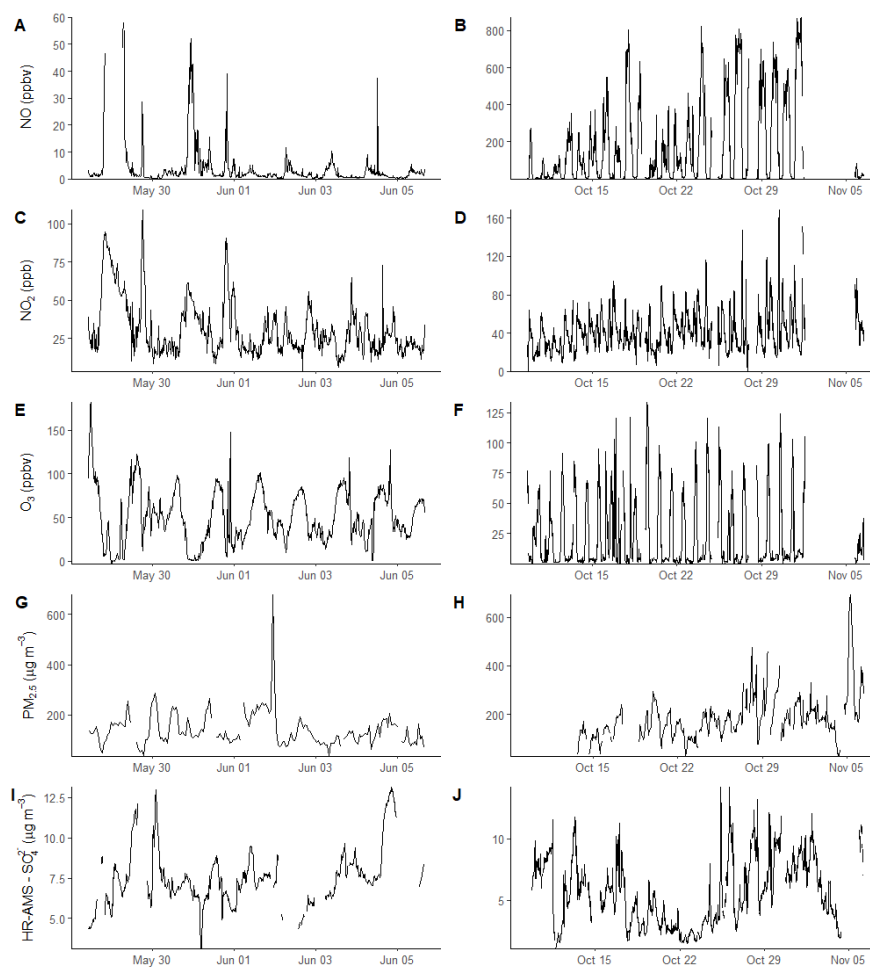


Figure 4.3: Time series of pollutants across the pre- (A,C,E,G,I) and post – monsoon (B,D,F,H,J) campaigns. NO concentrations were filters to below 60 ppbv, due to a large enhancement in concentrations at the start of the campaign. The full time series is shown in figure 4.5. NO, NO₂, O₃ and HR-AMS – SO₄²⁻ were averaged to 15 minutes. PM_{2.5} was measured hourly.

During the early part of the pre-monsoon campaign, a large enhancement in NO was observed with mixing ratios around 400 ppbv (Figure 4.5), followed by lower concentrations throughout the rest of the campaign. The campaign-average NO diurnal profile shows high NO mixing ratios at night (pre-: ~ 50 ppbv, post-: ~ 300 ppbv), with low afternoon mixing ratios < 2 ppbv due to ozone titration. Ozone showed a strong diurnal variation across both campaigns, with average afternoon mixing ratios ~ 75 ppbv with pre- and post-monsoon maximums of 182.2 ppbv and 134 ppbv respectively.

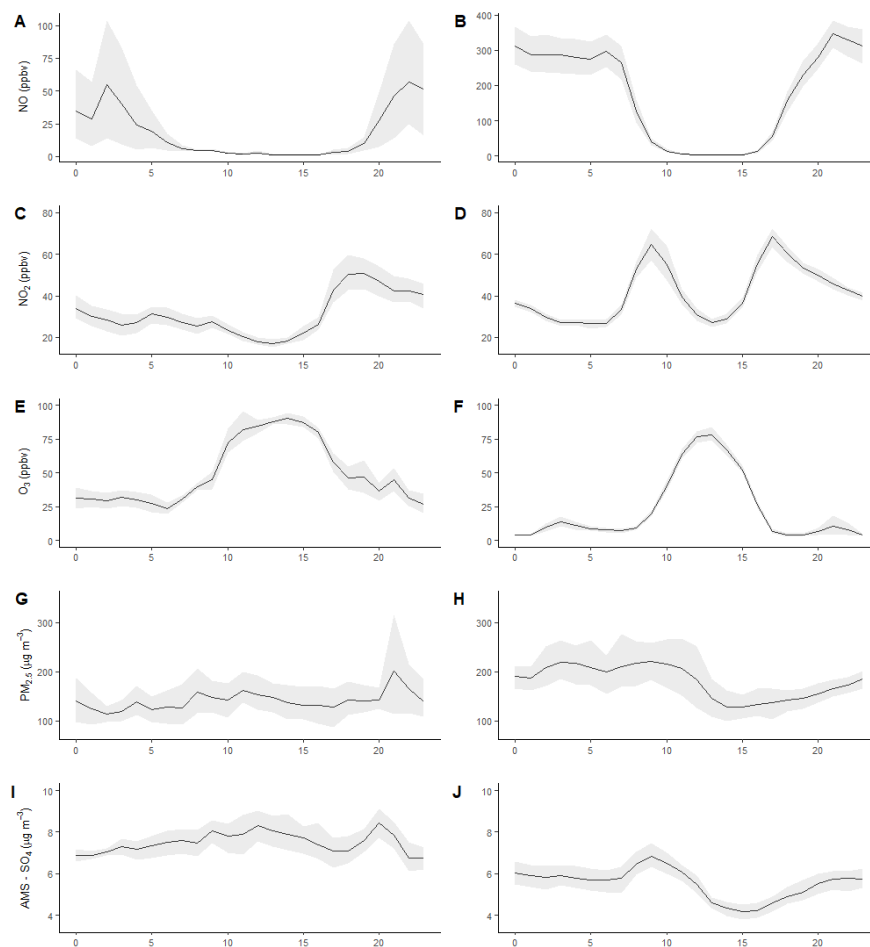


Figure 4.4: Diurnal variations of pollutants during pre- (left) and post- (right) monsoon.

To investigate the oxidation conditions in Delhi, the NO_3 and OH radical concentrations were modelled as discussed in section 3.2.5 with the time series and diurnal variations of the predicted concentrations of OH and NO_3 shown in Figure 4.6. The predicted OH concentrations across both campaigns peak around midday, in line with peak photolysis. During the post-monsoon the modelled OH concentrations drop throughout the campaign, from 8×10^6 molecules $\text{cm}^{-3} \text{ s}^{-1}$ on the 13th of October with the lowest peak OH concentrations $\sim 5 \times 10^6$ molecules $\text{cm}^{-3} \text{ s}^{-1}$ predicted on the 26th October. This drop likely reflects a seasonal change, with lower formation of OH. Predicted NO_3 concentrations show distinct diurnal profiles across the pre- and post-monsoon. During the pre-monsoon NO_3

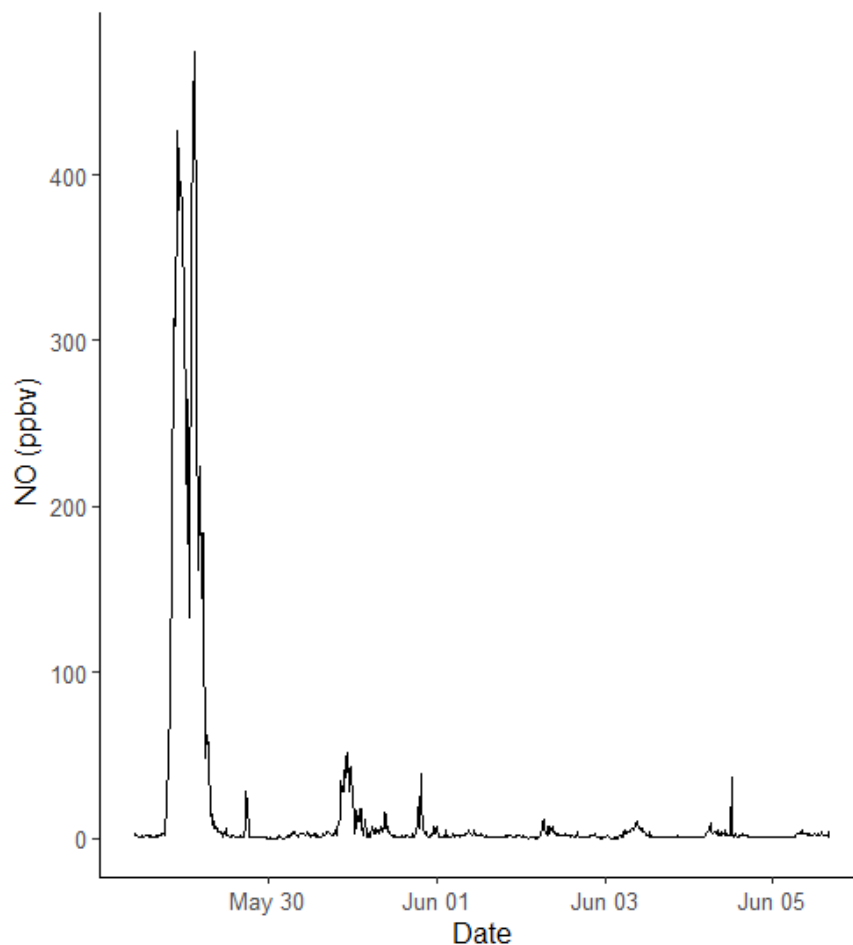


Figure 4.5: Full time series of NO concentrations during the pre-monsoon campaign.

concentrations show an early morning minimum before concentrations increase steadily throughout the day to a maximum around 18:00 then decrease before another nocturnal peak, before the early morning minimum. The diurnal variation of NO_3 concentrations during the post-monsoon is like that of the OH radicals, peaking around midday. The peak post-monsoon NO_3 concentrations are similar to those at the same time during the pre-monsoon $\sim 3 \times 10^7$ molecules $\text{cm}^{-3} \text{s}^{-1}$, while the lack of nocturnal NO_3 is likely due to the extremely high NO concentrations. The high NO concentrations titrated O_3 leading to limited NO_3 formation, but also reacted rapidly with the limited amount of NO_3 that is produced (Figure 4.4).

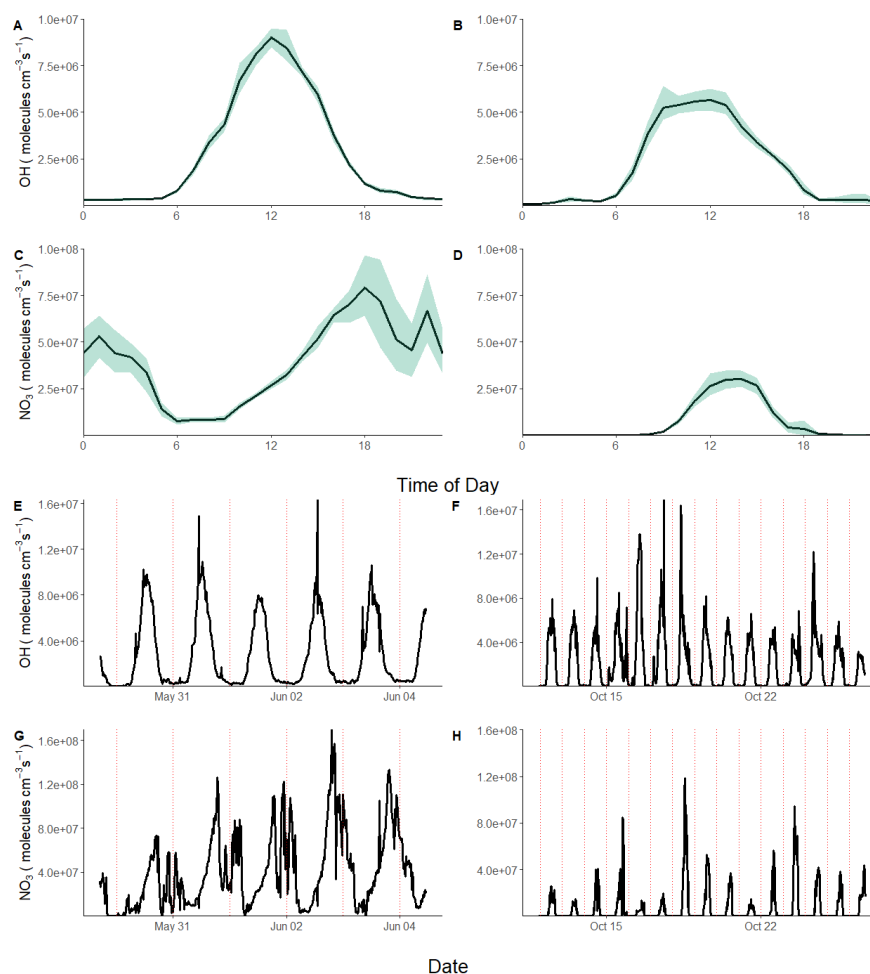


Figure 4.6: Diurnal variations (A-D) and time series (E-H) of modelled OH and NO₃ concentrations across the pre- (A,C,E,G) and post-monsoon (B,D,F,H). The band represents the 95 % confidence interval. The red line represents midnight (00:00) at each day.

4.3.4 Isoprene and monoterpene measurements

Isoprene was measured hourly via gas-chromatography with flame-ionisation-detection (GC-FID) across the two campaigns, with the time series shown in Figure 4.7. Figure 4.8 shows the average diurnal profiles of isoprene during pre-monsoon (B) and post-monsoon (D). The mean isoprene mixing ratios were 1.22 ± 1.28 ppbv and 0.93 ± 0.65 ppbv, with maximum isoprene mixing ratios of 4.6 ppbv and 6.6 ppbv observed across the pre- and post-monsoon, respectively. This is in the same range as measured in Beijing (winter mean: 1.21 ppbv, summer mean: 0.56 ppbv)[328] and the SEUS (mean diurnal 2-6 ppb)[38]. The diurnals highlight

a rapid increase of isoprene around 05:00, reaching a peak around or after midday, before a nocturnal minimum. Figure 4.8 indicates that average daytime peak isoprene mixing ratios during the pre-monsoon campaign were roughly double that of the post-monsoon campaign.

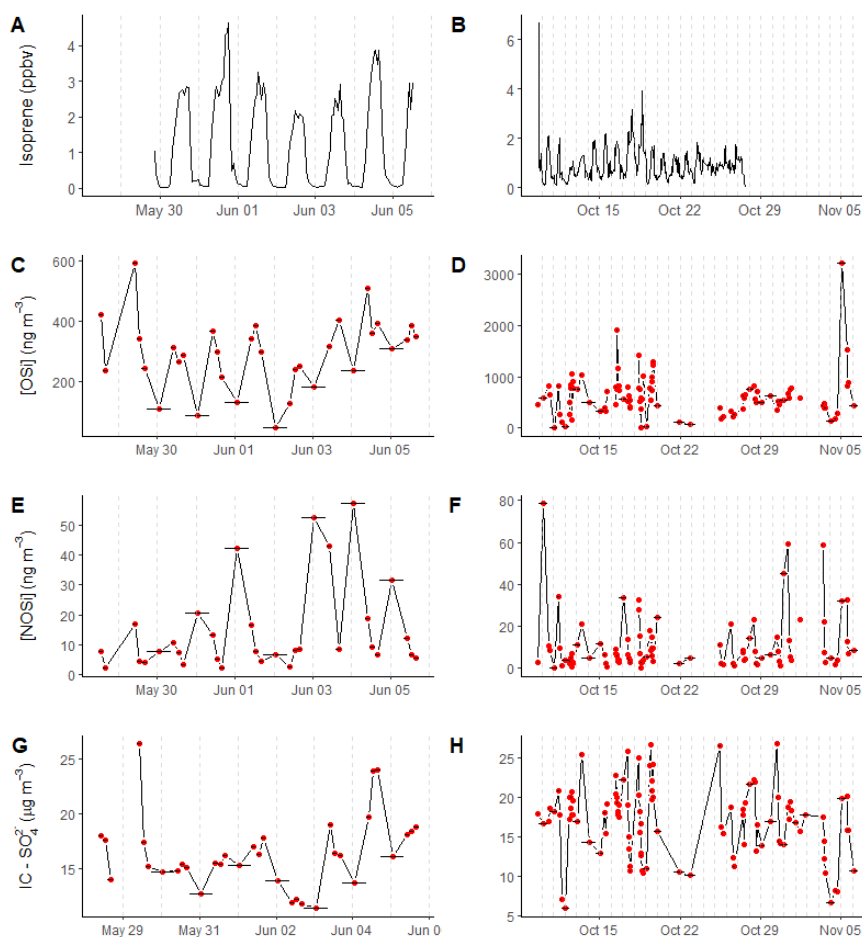


Figure 4.7: Time series across the pre- (left) and post-monsoon (right) campaigns of Isoprene (A,B), total quantified potential OSi marker concentrations (C, D), total quantified potential NOSi marker concentrations (E, F) and inorganic sulfate concentrations (G,H). The horizontal lines represent the length of time the filter sample was collected for.

In contrast, average nocturnal mixing ratios of isoprene were 5 times higher in the post monsoon compared to the pre-monsoon (0.65 ppbv versus 0.13 ppbv). The night-time values were substantially higher than measured previously in Beijing (<50 pptv)[125], but lower than observed in the SE-US (1-2ppbv)[38]. The

time series for the pre-monsoon highlights relatively consistent biogenic emissions of isoprene. In the post-monsoon campaign, isoprene mixing ratios show a strong biogenic diurnal profile at the start of the campaign. However, towards the end of the post monsoon measurement period, the isoprene mixing ratios become less variable with a high mixing ratio maintained overnight. The ambient temperature decreased throughout the post monsoon campaign as the season changed to winter (Figure 4.1).

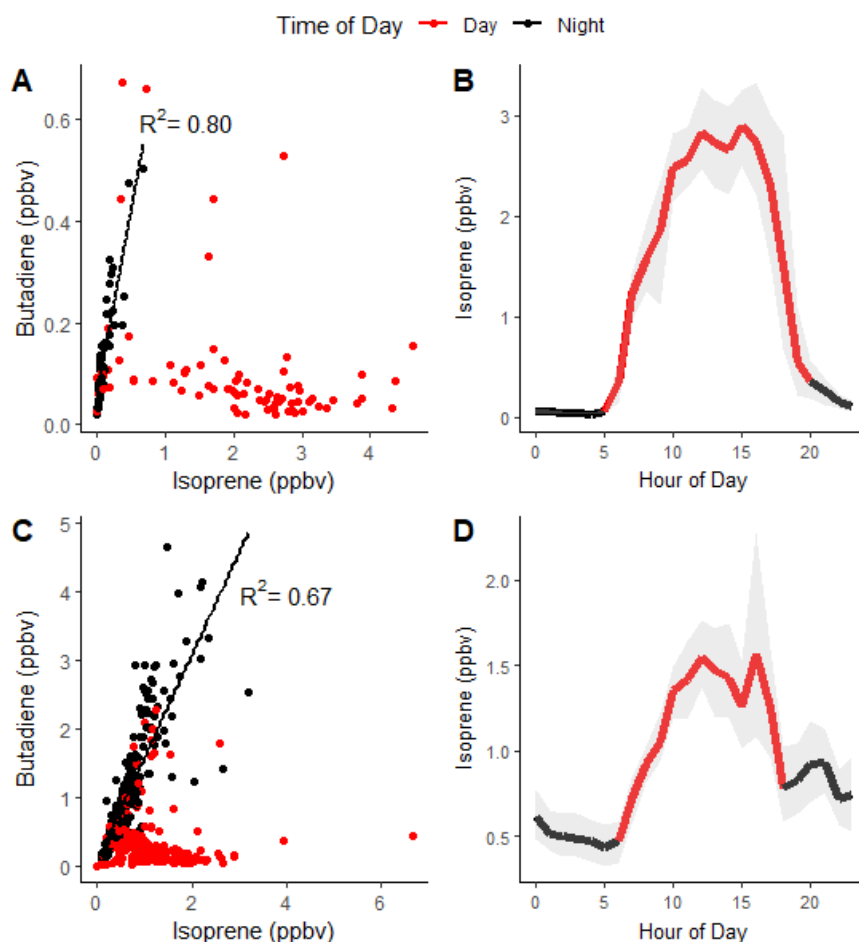


Figure 4.8: Correlations between isoprene and butadiene and diurnal variations of isoprene across pre- (A, B) and post-monsoon (C, D) campaigns. The plots are coloured by the time of day to highlight the dual biogenic/anthropogenic sources of isoprene.

A recent study in Delhi across post-monsoon, summer and winter campaigns found that at vegetative sites biogenic isoprene contributed on average 92 - 96 %

to the total isoprene, while at traffic dominated sites only 30 - 39 % of isoprene was biogenic.[151] To gain some understanding of the sources of isoprene at our site in Delhi, the observed concentrations of isoprene were correlated to butadiene, which is an anthropogenic combustion tracer from petrol vehicles with a similar atmospheric lifetime (Figure 4.8) The isoprene concentrations were split between night and day (pre-monsoon; night: 19:00 – 05:00 h, day 05:00 – 19:00 h, post-monsoon; night: 17:00 - 06:00 h, day: 06:00 - 17:00 h), based on the observed isoprene diurnals as shown in Figure 4.8. Isoprene correlated strongly with butadiene during the night across both campaigns (pre-monsoon: $R^2= 0.80$, post-monsoon: $R^2= 0.67$), but no correlation was observed during the day ($R^2 < 0.1$).

This suggests that daytime isoprene is pre-dominantly from biogenic sources, although a small amount will be from anthropogenic sources and that nocturnal isoprene is emitted from anthropogenic sources. Alternatively, this could indicate that night-time concentrations are affected more by boundary layer dynamics, affecting all compounds similarly. Biogenic emissions of isoprene are also not expected because they tend to be driven by light. The high night-time levels towards the end of October are most likely a result of the formation of a very low boundary layer trapping emissions near the surface and although increased biomass burning may also be a factor. Therefore, during the post monsoon campaign a significant amount of isoprene oxidation products and iSOA will have an anthropogenic source.

The time series of two monoterpenes, limonene and α -pinene, are shown in Figure 4.9. The α -pinene mixing ratio averaged (0.034 ± 0.011) ppbv during the pre-monsoon campaign and (0.10 ± 0.11) ppbv during the post monsoon period. A strong diurnal variation was observed in the post-monsoon, peaking during the night (Figure 4.2). Limonene averaged (0.01 ± 0.02) ppbv and (0.42 ± 0.51) ppbv across the pre- and post-monsoon campaigns, respectively. The large increase during the post-monsoon is likely due to stagnant conditions and a very low boundary layer. The pre-monsoon measurements show three large

spikes in mixing ratio at the beginning of the campaign. In contrast, during the post-monsoon, a clearer diurnal variation is observed. During the post-monsoon campaign, both monoterpenes show nocturnal enhancements. A further 10 monoterpenes were measured concurrently using comprehensive two-dimensional gas chromatography.[288, 324] In all cases, the post monsoon period had higher mean mixing ratios, with large nocturnal enhancements in mixing ratios.

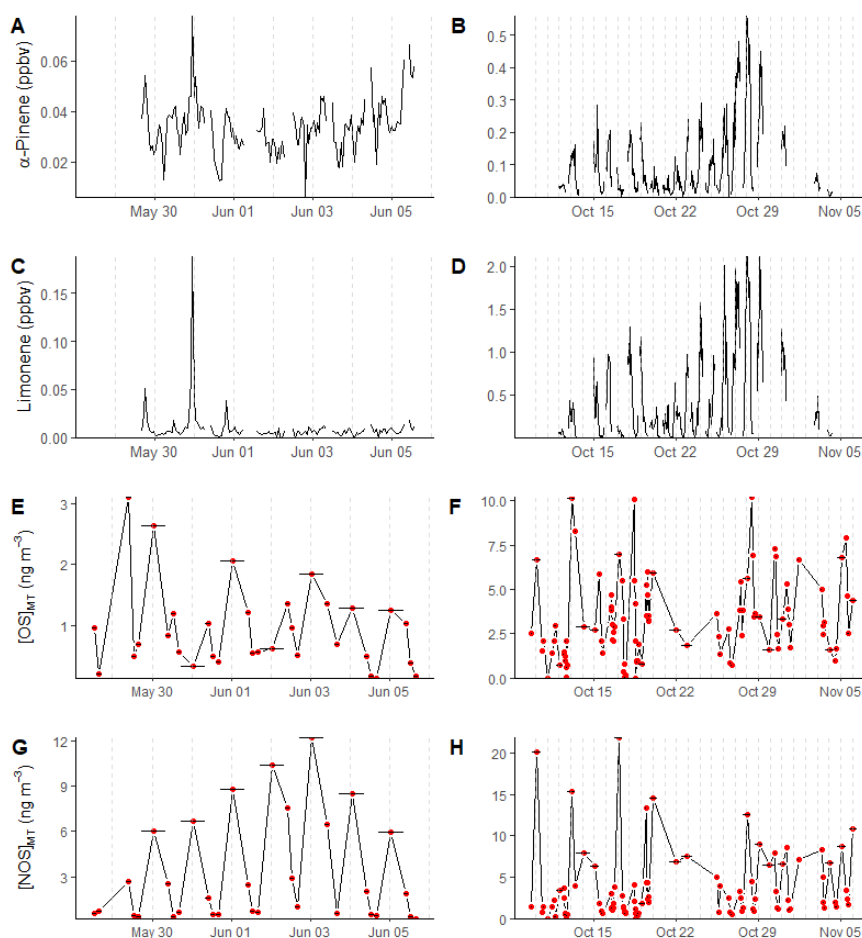


Figure 4.9: Time series across the pre- (left) and post-monsoon (right) campaigns of α -pinene (A,B),limonene (C,D), total quantified potential OSMT marker concentrations (E, F), and total quantified potential NOSMT marker concentrations (G, H).

α -pinene and limonene correlated moderately with CO during the day (α -pinene; $R^2 = 0.82$, limonene; $R^2 = 0.90$) and night (α -pinene; $R^2 = 0.49$, limonene; $R^2 = 0.56$) during the post-monsoon as shown in Figure 4.10, suggesting anthro-

pogenic sources.

Further analysis of the PTR-Qi-TOF measurements estimates that (during post-monsoon) 60% of the monoterpene concentrations observed at the site originated from traffic related sources.[325] Other potentially important anthropogenic monoterpene sources include biomass burning, cooking and the use of personal care/volatile chemical products.[284, 289, 329, 330]

The shallow nocturnal boundary layers across both campaigns (Figure 4.1) leads to relatively high concentrations of total monoterpenes, with a maximum mixing ratio of 6 ppb observed during the post-monsoon. [309] In addition, some extremely reactive monoterpenes, including α -phellandrene and δ -terpinene, were observed with maximum mixing ratios of 350 pptv and 140 pptv respectively.[309] The zero-dimensional box modelling predicts very low levels of OH and NO₃ radicals at night. The extremely high NO mixing ratios have quenched the nocturnal chemistry, removing ozone and thus the NO₃ formation pathway, as well as increasing the loss rate of NO₃ via reaction. After sunrise, the expanding boundary layer and increase in OH concentrations, cause a rapid decrease in the monoterpene mixing ratio.

4.4 Secondary organic aerosol formation

At the measured concentrations, monoterpenes and isoprene are an important source of ozone and OH reactivity at this site.[324] The oxidised products will also be a key source of SOA production. The UHPLC-MS² analysis identified and quantified 75 potential markers for OS and NOS formed from the oxidation of isoprene and monoterpenes.

4.4.1 Isoprene SOA

A total of 21 potential OSi C₂₋₅ markers were quantified in the ambient samples which have been previously identified in chamber studies [134, 173, 234, 235] and other ambient studies[34, 35, 125, 126, 180, 191, 194, 250] It should be

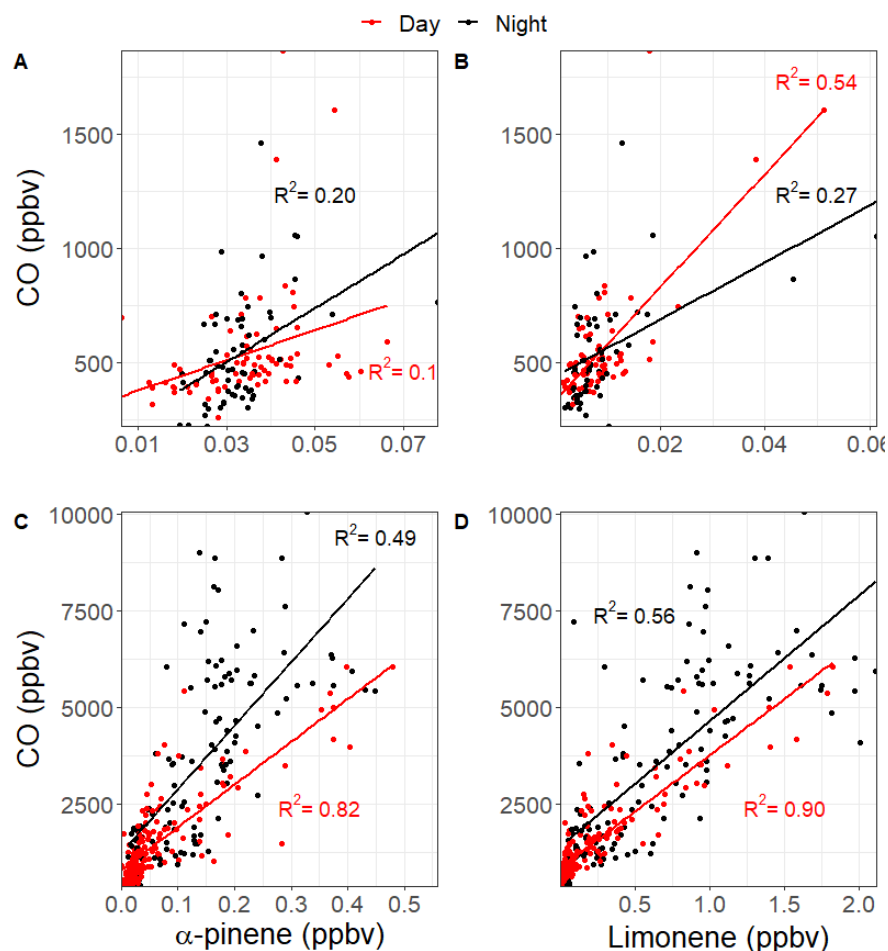


Figure 4.10: Correlation between measured monoterpenes and CO across the pre-monsoon (A,B) and post-monsoon (bottom).

noted that several of the smaller ($C_{2/3}$) OSi tracers likely form from glyoxal, methylglyoxal and hydroxyacetone as well as isoprene, and as such present a potential non-isoprene source of OSi. [331, 332]

Figure 4.7 shows the time series of total OSi concentrations observed across pre- (left) and post-(right)monsoon campaigns. Total OSi time averaged concentrations were ~ 2.3 times higher during the post-monsoon ($\sim 556.6 \pm 422.5$ ng m^{-3}) campaign than the pre-monsoon campaign ($\sim 237.8 \pm 118.4$ ng m^{-3}) as shown in Table 4.3. These concentrations are similar to those observed in Beijing during summer 2017 (237.1 ng m^{-3})[125], but higher than those observed in Shanghai in 2018 (40.4 ng m^{-3}) and 2019 (34.3 ng m^{-3})[194].

Table 4.3: Molecular formulae, retention times and time weighted mean \pm SD (ng m^{-3}) of nitrooxy oganosulfates (NOS) and organosulfates (OS) from monoterpenes (MT) and isoprene (i) observed across pre and post-monsoon campaigns in Delhi.

| | | Conc. (ng m^{-3}) | | Retention time (min) |
|---|--|------------------------------|--------------------|----------------------|
| | Formula | Pre- | Post- | |
| OSi | $\text{C}_5\text{H}_{12}\text{O}_7\text{S}$ | 38.79 ± 30.19 | 17.91 ± 19.87 | 0.71 |
| | $\text{C}_5\text{H}_{10}\text{O}_5\text{S}$ | 26.16 ± 23.30 | 53.63 ± 131.19 | 0.93 |
| | $\text{C}_2\text{H}_4\text{O}_6\text{S}$ | 21.35 ± 18.27 | 84.65 ± 82.79 | 0.73 |
| | $\text{C}_5\text{H}_{10}\text{O}_6\text{S}$ | 19.80 ± 13.78 | 45.87 ± 29.47 | 0.79 |
| | $\text{C}_4\text{H}_8\text{O}_7\text{S}$ | 19.70 ± 12.48 | 47.96 ± 39.01 | 0.73 |
| | $\text{C}_3\text{H}_6\text{O}_5\text{S}$ | 19.50 ± 12.47 | 35.27 ± 40.15 | 0.73 |
| | $\text{C}_5\text{H}_8\text{O}_7\text{S}$ | 18.76 ± 11.01 | 38.75 ± 25.34 | 0.73 |
| | $\text{C}_4\text{H}_8\text{O}_6\text{S}$ | 16.57 ± 9.77 | 45.48 ± 37.46 | 0.74 |
| | $\text{C}_5\text{H}_{10}\text{O}_7\text{S}$ | 11.82 ± 7.04 | 25.89 ± 18.06 | 0.73 |
| | $\text{C}_3\text{H}_6\text{O}_6\text{S}$ | 6.64 ± 5.00 | 38.06 ± 40.30 | 0.73 |
| | $\text{C}_4\text{H}_8\text{O}_5\text{S}$ | 6.46 ± 4.08 | 22.44 ± 21.39 | 0.75 |
| | $\text{C}_5\text{H}_{10}\text{O}_8\text{S}$ | 6.25 ± 5.07 | 7.00 ± 5.54 | 0.73 |
| | $\text{C}_2\text{H}_4\text{O}_5\text{S}$ | 5.33 ± 3.37 | 15.92 ± 13.79 | 0.73 |
| | $\text{C}_2\text{H}_6\text{O}_5\text{S}$ | 5.23 ± 6.36 | 24.99 ± 20.38 | 0.73 |
| | $\text{C}_5\text{H}_8\text{O}_5\text{S}$ | 5.16 ± 2.57 | 7.87 ± 7.93 | 0.85 |
| | $\text{C}_3\text{H}_6\text{O}_7\text{S}$ | 3.54 ± 3.49 | 14.78 ± 11.50 | 0.75 |
| | $\text{C}_5\text{H}_{12}\text{O}_6\text{S}$ | 2.01 ± 1.23 | 6.53 ± 4.32 | 0.74 |
| | $\text{C}_3\text{H}_8\text{O}_6\text{S}$ | 1.90 ± 1.08 | 12.25 ± 10.82 | 0.75 |
| | $\text{C}_5\text{H}_8\text{O}_9\text{S}$ | 1.20 ± 1.04 | 2.12 ± 1.85 | 0.64 |
| | $\text{C}_5\text{H}_8\text{O}_9\text{S}$ | 1.10 ± 0.76 | 8.61 ± 15.65 | 0.74 |
| $\text{C}_5\text{H}_{12}\text{O}_8\text{S}$ | 0.55 ± 0.43 | 0.65 ± 0.61 | 0.75 | |
| OSi sum | | 237.83 | 556.64 | |
| NOSi | $\text{C}_5\text{H}_{10}\text{O}_{11}\text{N}_2\text{S}$ | 18.65 ± 8.77 | 11.63 ± 8.09 | 1.39,1.92,2.85,3.4 |
| | $\text{C}_5\text{H}_{11}\text{O}_9\text{NS}$ | 8.55 ± 5.71 | 5.93 ± 5.06 | 0.86 |
| | $\text{C}_5\text{H}_9\text{O}_{10}\text{NS}$ | 3.91 ± 3.46 | 1.42 ± 1.31 | 0.94 |
| | $\text{C}_5\text{H}_{11}\text{O}_8\text{NS}$ | 1.52 ± 0.84 | 1.17 ± 1.20 | 1.09 |
| | $\text{C}_5\text{H}_9\text{O}_{13}\text{N}_3\text{S}$ | 0.002 ± 0.001 | 0.011 ± 0.009 | 6.67,7.89,8.06 |

| | | Conc. (ng m ⁻³) | | Retention time (min) |
|-----------------------|---|-----------------------------|--------------|---|
| Formula | | Pre- | Post- | |
| NOSi sum | | 32.63 | 20.15 | |
| OS _{MT} | C ₉ H ₁₆ O ₆ S | 1.10 ± 0.61 | 1.67 ± 0.88 | 6.67, 7.14, 7.5, 8.3 |
| | C ₁₀ H ₁₈ O ₅ S | 0.56 ± 0.63 | 0.10 ± 0.12 | 3.39 |
| | C ₁₀ H ₁₆ O ₅ S | 0.28 ± 0.13 | 0.77 ± 0.06 | 4.91, 7.0, 9.08, 10.9, 11.33, 11.97, 13.26 |
| | C ₁₀ H ₂₀ O ₇ S | 0.25 ± 0.21 | 0.27 ± 0.21 | 4.19 |
| | C ₁₀ H ₁₆ O ₇ S | 0.23 ± 0.15 | 0.21 ± 0.13 | 3.61, 11.68 |
| | C ₉ H ₁₆ O ₇ S | 0.16 ± 0.17 | 0.22 ± 0.19 | 4.39, 6.77 |
| | C ₁₀ H ₁₈ O ₆ S | 0.15 ± 0.10 | NA ± NA | 10.27 |
| | C ₉ H ₁₄ O ₆ S | 0.15 ± 1.10 | 0.25 ± 0.14 | 3.5, 5.81 |
| | C ₁₀ H ₁₆ O ₆ S | 0.10 ± 0.06 | 0.06 ± 0.03 | 9.33 |
| | C ₁₀ H ₁₈ O ₈ S | 0.02 ± 0.01 | 0.04 ± 0.24 | 7.24 |
| | C ₈ H ₁₄ O ₇ S | 0.04 ± 0.03 | 0.10 ± 0.15 | 4.46 |
| | OS _{MT} sum | | 3.05 | 3.68 |
| NOS _{MT} | C ₁₀ H ₁₇ NO ₇ S | 5.96 ± 3.33 | 13.36 ± 4.98 | 9.1, 10.16, 10.67, 10.92, 11.07, 11.36, 11.57, 12.01, 13.28 |
| | C ₉ H ₁₅ NO ₈ S | 1.12 ± 0.51 | 2.79 ± 1.14 | 3.5, 5.81 |
| | C ₁₀ H ₁₇ NO ₉ S | 0.47 ± 0.19 | 1.15 ± 0.29 | 3.93, 5.34, 6.39, 7.89, 9.26, 10.11, 17.94 |
| | C ₉ H ₁₅ NO ₉ S | 0.022 ± 0.004 | 0.22 ± 0.14 | 2.69, 3.46 |
| | C ₁₀ H ₁₇ NO ₈ S | 0.01 ± 0.01 | 0.07 ± 0.04 | 5.77 |
| NOS _{MT} sum | | 7.59 | 17.59 | |

OSi species have been shown to form via the gas-phase photo-oxidation of isoprene, with the reactive uptake of the oxidised species into to particulate phase via sulfate.[127, 130] Recently, a heterogeneous photo-oxidation pathway from 2-MT-OS (C₅H₁₂O₇S) to several OSi species was proposed, including C₅H₁₀O₇S, C₅H₈O₇S, C₅H₁₂O₈S, C₅H₁₀O₈S and C₄H₈O₇S.[137]

2-MT-OS showed moderate correlations (pre-monsoon : R² = 0.52-0.72, post-monsoon: R² = 0.14-0.35) with these OSi tracers but were lower than observed in Beijing summer (R² = 0.83-0.92).[125] The correlations could suggest that this is

a viable formation route in pre-monsoon Delhi, but less viable in post-monsoon. However, the correlations could also be driven by the common pathways between the OSi species, with the reactive uptake of gas phase intermediates via sulfate.

Figure 4.11 shows the binned OSi concentrations for each filter collection time across the pre- and post-monsoon campaigns to create a partial diurnal profile. During the pre-monsoon, the daily variation in OSi concentrations was much clearer, with day-time maxima and nocturnal minima, which are in line with daily peak isoprene (Figure 4.7) and OH radical concentrations (Figure 4.6). The highest observed OSi concentrations during the pre-monsoon were $\sim 600 \text{ ng m}^{-3}$, which occurred at the start of the campaign. High isoprene concentrations may have been the cause, but unfortunately isoprene measurements were not available during this period to confirm. However, high OSi concentrations also occurred when particulate inorganic sulfate concentrations were at their largest, with sulfate measured via the HR-AMS was also high during this period. During the post-monsoon, although a similar diurnal pattern was observed, the variation was less clear, with higher OSi concentrations observed at the start and end of the campaign (Figure 4.7). The low OSi concentrations during the middle of the campaign, coincide with lower isoprene concentrations, as the temperatures decreased moving towards winter, while sulfate concentrations were still high.

The sum of OSi species across all filters sampled showed a moderate correlation with particulate sulfate across both campaigns (pre-monsoon, R^2 : 0.55, post-monsoon, R^2 : 0.28). The pre-monsoon correlation was similar to those observed in Beijing, Guangzhou and the SE-US[34, 125, 191, 250] while the post-monsoon was significantly weaker. However, a clear relationship between OSi tracers and inorganic sulfate can be seen in Figure 4.11 across both campaigns, where the highest OSi concentrations occurred under the highest binned SO_4^{2-} concentrations. During the post-monsoon campaign, OSi concentrations levelled off at high sulfate concentrations. During the pre-monsoon this levelling off is not observed, likely due to the lower numbers of filters collected and analysed. The high concentrations of aerosol phase pollutants measured by the HR-AMS (Table

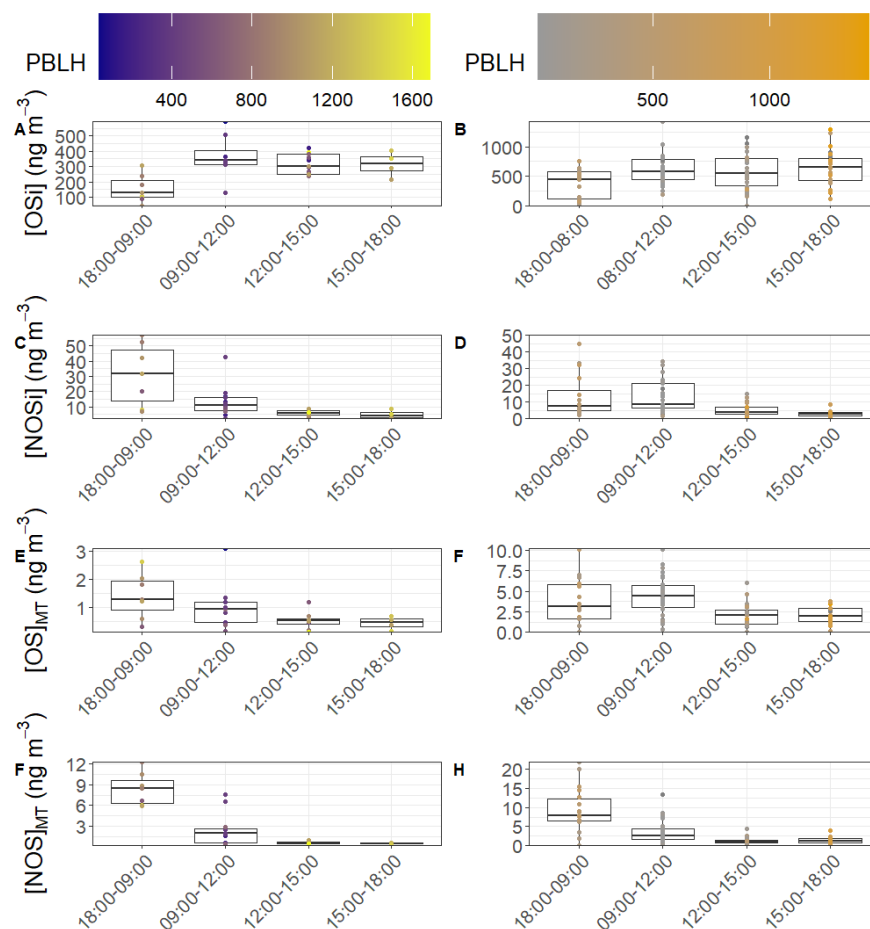


Figure 4.11: Diurnal variations of quantified BSOA classes (OSi , $NOSi$, OS_{MT} , NOS_{MT}) across the pre- (left) and post-monsoon (right) campaigns. The lower and upper part of the box representing the 25th and 75th percentiles, with the upper and lower lines extending no further than 1.5 times the interquartile range of the highest and lowest values within the hinge respectively. All data points used for the boxplots are also plotted, coloured by the average PBLH for the filter collection period.

4.2) during the post-monsoon (48.7 ± 35.4) $\mu\text{g m}^{-3}$ compared to the pre-monsoon (19.8 ± 13.7) $\mu\text{g m}^{-3}$, indicate the reactive uptake of the gaseous OSi intermediates to the aerosol phase may be limited due to extensive organic coatings on the sulfate aerosol. Multiple studies have now shown that organic coatings on sulfate aerosol can limit the reactive uptake of IEPOX, suggesting the pre-monsoon is volume limited but the post-monsoon is diffusion limited.[129, 138, 333]

Ten $NOSi$ tracers were screened for across the two campaigns, with eight identi-

fied in the pre-monsoon and 10 in the post-monsoon. These tracers included, mono-nitrated ($C_5H_9O_{10}NS$, $C_5H_{11}O_9NS$, $C_5H_{11}O_8NS$), di-nitrated ($C_5H_{10}O_{11}N_2S$), and tri-nitrated ($C_5H_9O_{13}N_3S$) species. These tracers have been identified previously in China [104, 125, 126, 194, 250], with night-time nitrate radical chemistry thought to be the dominant pathway. Unlike the OSi tracers, total NOSi concentrations were on average higher during the pre-monsoon (32.6 ± 19.9) $ng\ m^{-3}$ compared to the post-monsoon (20.2 ± 13.3) $ng\ m^{-3}$, likely due to larger isoprene and NO_3 concentrations. The NOSi time series and diurnal shown in Figure 4.7 highlight the strong nocturnal enhancements in concentrations during the pre-monsoon. During the post-monsoon, although NOSi concentrations were higher during the night than during the afternoon, the average concentration observed during the morning sample (09:00-12:00 h) is higher than at night. These high morning concentrations could be due to low boundary layer conditions, concentrating the markers. However, nitrate radical oxidation is also likely occurring due to nitrate radical formation throughout the morning (Figure 4.6) and moderate isoprene concentrations (Figure 4.8). A large spike in NOSi concentrations is also observed at the start of the post-monsoon campaign, which was not observed for the OSi tracers, this coincides with lower modelled NO_3 concentrations, but also lower NO concentrations than the rest of the post-monsoon campaign, which could be limiting the reaction of peroxy radicals and NO, allowing for more nitrate formation.

The nocturnal peak in NO_3 concentrations is only predicted during the pre-monsoon period, with a late afternoon peak predicted in the post-monsoon as discussed in section 4.3.2. For the pre-monsoon, this coincides with peak NOSi concentrations, but not for the post-monsoon. During the pre-monsoon it is likely these NOSi tracers are being formed throughout the afternoon and into the evening during peak isoprene and then peak NO_3 concentrations, leading to high nocturnal concentrations. During the post-monsoon however peak NO_3 concentrations coincide with peak isoprene concentrations, but this does not translate into high NOSi concentrations during the afternoon. This suggests that either isoprene is

reacting more quickly with OH, or that the intermediate species being formed from isoprene + NO₃ or the tracers themselves are being photolyzed.[334] It is only into the evening, when the NO₃ pathway is more competitive with OH that these markers can form, but not under peak isoprene concentrations, which may also explain the lower post-monsoon NOSi concentrations. The NOSi species did not correlate towards particulate sulfate ($R^2 < 0.2$) across either campaign, suggesting unlike the OSi species that uptake onto sulfate is not the limiting step in NOSi formation.

4.4.2 Monoterpene secondary organic aerosol

Twenty-three monoterpene-derived organosulfate (OS_{MT}) species, which have been seen previously in chamber[134] and ambient studies[126, 185, 194], were identified across the pre- and post-monsoon campaigns. It should be noted that recently OS_{MT} artefacts has been shown to form when filters have been sampled without a denuder.[267] However, the strong diurnal variations of the OS_{MT} species, and lack of correlation with SO₂ suggest this process is unlikely to have contributed significantly to the OS_{MT} measured in this study. Post-monsoon concentrations were slightly higher (3.96 ± 1.6) ng m⁻³ than during the pre-monsoon (3.05 ± 1.3) ng m⁻³, with C₉H₁₆O₆S (RT 7.5 min) the dominant species across both campaigns, contributing on average 29 % of the OS_{MT} mass. It should be noted that the majority of the OS_{MT} were not identified in every sample, and as such only tracers which were identified in at least 40 % of the samples were summed for further investigation. Total OS_{MT} showed a strong diurnal across both campaigns, peaking at night, with an afternoon minimum (Figure 4.9).

During the pre-monsoon campaign, the highest OS_{MT} concentrations were observed during a day-time sample, coinciding with peak sulfate and NO concentrations like the OSi tracers. Both limonene and α -pinene also show peaks during this filter sampling period. Spikes in limonene and α -pinene concentrations were also observed on the 31st May, but OS_{MT} concentrations were much lower, likely

due to the lower sulfate concentrations. During the post-monsoon campaign, a less defined diurnal is observable from the time series (Figure 4.9), but the diurnal plot (Figure 4.11) highlights the nocturnal enhancements. Like the NOSi markers, higher OS_{MT} concentrations were observed during the early morning sample, likely due to a lower PBLH concentrating the markers and oxidation after sunrise. The night-time formation of the OS_{MT} species is in line with observations in Guangzhou[250], and with the diurnal variations of α -pinene and limonene, which peak at night. Previous laboratory studies investigating reactions of monoterpenes with NO₃ radicals have also shown formation of OS_{MT} with the same molecular formulae as measured here.[134]

OS_{MT} concentrations observed in Delhi are much lower than those of the OSi, similar to other studies. [35, 126, 194] Considering the high concentrations of extremely reactive α -pinene and limonene observed during the post-monsoon period, higher OS_{MT} concentrations might be expected. One possible reason for the low OS_{MT} is the inability of OS_{MT} intermediates to undergo reactive uptake into the aerosol phase under atmospherically relevant acidity conditions, with chamber studies suggesting extremely acidic conditions are needed for uptake to occur. [145] Delhi is characterised by large concentrations of free ammonia and alkaline dust, and previous studies have highlighted that it has less acidic aerosol (pH 5.7 – 6.7)[335] across the year than Beijing (pH 3.8 – 4.5)[336] and the SEUS (pH 1.6 – 1.9)[191].

Unlike the OS_{MT} species, the NOS_{MT} species (C₁₀H₁₇NO₇S, C₉H₁₅NO₈S, C₁₀H₁₇NO₉S, C₉H₁₅NO₉S, C₁₀H₁₇NO₈S) showed strong seasonality, with pre- and post-monsoon concentrations of (7.6 ± 3.8) ng m⁻³ and (17.6 ± 6.1) ng m⁻³ respectively. This is opposite to the quantified NOSi species, which showed higher pre-monsoon concentrations. This is likely due to higher post-monsoon concentrations of monoterpenes. Like the NOSi species, the NOS_{MT} species mainly arise from monoterpene photooxidation in the presence of NO_x or night-time NO₃ chemistry. [134] Of the NOS_{MT} species, C₁₀H₁₇NO₇S was the most abundant, contributing on average 79 % and 76 % of the NOS_{MT} concentrations across

Table 4.4: Comparison of C₁₀H₁₇NO₇S concentrations across different locations. Locations and concentrations in bold were quantified by authentic standards.

| Location | C ₁₀ H ₁₇ NO ₇ S (ng m ⁻³) | Reference |
|--------------------|---|--------------|
| Delhi Pre-monsoon | 5.96 | This study |
| Delhi Post-monsoon | 13.36 | This study |
| Guangzhou summer | 7.15 | [250] |
| Guangzhou winter | 11.11 | [250] |
| Shanghai 15/16 | 6.21 | [184] |
| Shanghai 16/17 | 5.55 | [184] |
| Beijing | 12 | [126] |
| Atlanta | 9 | [35] |
| Hong Kong | 5.61 | [337] |
| Guangzhou | 12.32 | [337] |
| Shanghai | 16.51 | [337] |
| Beijing | 13.15 | [337] |

the pre- and post-monsoon respectively. Previous studies have also highlighted C₁₀H₁₇NO₇S to be the dominant monoterpene derived sulfate containing tracer. [126] In the post-monsoon nine C₁₀H₁₇NO₇S isomers were observed and seven in the pre-monsoon. The summed C₁₀H₁₇NO₇S concentrations during the pre- (5.96 ± 3.33) ng m⁻³ and post-monsoon (13.36 ± 4.98) ng m⁻³, are similar to those observed in other locations as shown in Table 4.4. These concentrations are also similar to those quantified by authentic standards across four Chinese megacities.[337]

Like the OS_{MT} species, some NOS_{MT} species were not identified in many of the filter samples, and as such only tracers which were observed in more than 40 % of the samples were summed for further analysis. The NOS_{MT} pre-monsoon time series (Figure 4.9) shows a similar temporal profile to the NOS_i species, with lower concentrations during the enhancement in NO concentrations (Figure 4.4) at the start of the campaign. NOS_{MT} showed strong diurnal variations across both campaigns (Figure 4.9), peaking at night with lower concentrations during the afternoon, as seen previously. [126, 250] Like the NOS_i species, the NOS_{MT} are likely forming from NO₃ radical chemistry. The NOS_{MT} species showed limited correlation towards particulate sulfate (R² < 0.1.).

4.4.3 Contributions of total quantified SOA (qSOA) to particulate mass

Particulate concentrations in Delhi are among the highest observed across the world, with concentrations of over $600 \mu\text{g m}^{-3}$ being observed during this study. Total quantified SOA (qBSOA) which includes all OSi, NOSi, OS_{MT}, and NOS_{MT} tracers quantified was calculated to give an understanding of the contributions these species make to particulate mass in Delhi. The estimated contribution of qBSOA to the observed total particulate mass determined here should be taken as a lower limit due to the markers identified only being sulfate containing species and likely comprise only a small fraction of the BSOA mass. During the pre-monsoon campaign, qBSOA contributed on average $0.24 \pm 0.11\%$ to the PM_{2.5}, but up to 0.46% on certain days. The highest relative contribution during the pre-monsoon occurred during some of the lowest PM_{2.5} concentrations ($86.2 \mu\text{g m}^{-3}$), but moderate qBSOA concentrations (400 ng m^{-3}). During the post-monsoon qBSOA contributed on average $0.31 \pm 0.19 \%$ to PM_{2.5}, but up to 0.94% on certain days. Total oxidised organic aerosol (OOA) in PM₁ was derived from the HR-AMS measurements during the pre- and post-monsoon campaigns, with averages of $19.8 \pm 13.7 \mu\text{g m}^{-3}$ and $48.7 \pm 35.4 \mu\text{g m}^{-3}$ respectively. qBSOA contributed on average $2.0 \pm 0.9 \%$ and $1.8 \pm 1.4 \%$ to the total OOA but up to a maximum of 4.2 % and 6.6 % during the pre- and post-monsoon, respectively. This is under the assumption that all OS and NOS species fragment in the ion source of the HR-AMS lose sulfate and nitrate groups. This is similar to the contributions made by OSi markers in Beijing to total OOA (2.2 %).[125]

Previous studies (employing aerosol chemical speciation monitors) have reported much higher contributions of total OSi species in the SEUS. On average total summed iSOA tracers accounted for 9.4 % of measured OA at Look Rock, downwind of Maryville and Knoxville, but up to a maximum of 28.1 %.[34] This is much less than measured at a rural site at Yorkville, Georgia with just low-NO iSOA tracers accounting for between 12-19 % of total OA. [130].

Sulfate was also measured in the PM₁ size range by HR-AMS, with pre- and post-monsoon mean concentrations of $7.5 \pm 1.78 \mu\text{g m}^{-3}$ and $5.55 \pm 2.68 \mu\text{g m}^{-3}$. To estimate the contribution that qSOA sulfate containing species make to total sulfate, the quantified mass of sulfate contained within each marker was calculated based on the fraction of sulfate to each marker molecular mass. For example, 2-MT-OS has an accurate mass of m/z 216.21, meaning the fraction of 2-MT-OS mass associated with sulfate is ~ 0.44 . During the pre-monsoon campaign the BSOA sulfate accounted for on average 2.2 % to the total PM₁ sulfate, but up to 4.8 % on certain days. qSOA contributed considerably more to the sulfate in the post-monsoon campaign, with an average of 6.1 ± 4.5 % with a maximum of 18.7 %. This finding has implications for the need to consider the sources of sulfate when calculating aerosol pH. Overall, this highlights that BSOA can make significant contributions to particulates, even in extremely polluted environments such as Delhi. It should be noted that this is just a subset of potentially many more BSOA markers and only focusses on sulfate containing species.

4.5 Conclusion

Isoprene and monoterpene-derived OS and NOS species were quantified during pre- and post-monsoon periods in the Indian megacity of Delhi. An extensive dataset of supplementary measurements was obtained alongside the filter samples, including isoprene and individual monoterpenes. Isoprene and monoterpene concentrations were found to be highly influenced by anthropogenic sources, with strong correlations to anthropogenic tracers at night across both campaigns. Stagnant conditions lead to the concentrating of pollutants especially during the post-monsoon. Extremely high concentrations of NO during the post-monsoon quenched night-time reactivity, leading to high concentrations of nocturnal VOCs. Due to the extremely high NO concentrations, predicted NO₃ radical concentrations were extremely low at night, with the diurnal variation more in line with OH radicals during the post-monsoon period.

OSi markers were observed in higher concentrations during the post-monsoon ($556.6 \pm 422.5 \text{ ng m}^{-3}$) compared to the pre-monsoon campaign ($237.8 \pm 118.4 \text{ ng m}^{-3}$). OSi markers showed a moderate association with inorganic sulfate across both campaigns. However, concentrations levelled off at high sulfate concentrations during the post-monsoon which is consistent with organic coatings limiting uptake of isoprene epoxides. NOSi species showed nocturnal enhancements across both campaigns, while the highest average concentrations were observed in the morning samples of the post-monsoon campaign. The high morning concentrations are likely due to morning oxidation of VOCs via NO_3 radicals which are formed throughout the morning. OS_{MT} and NOS_{MT} markers were observed to have nocturnal enhancements in concentrations, in-line with their precursors. NOS_{MT} markers were observed in similar concentrations to those of other megacities. Overall, the total marker concentrations contributed on average ($0.24 \pm 0.11 \%$) and ($0.31 \pm 0.19 \%$) to the total $\text{PM}_{2.5}$ up during the pre- and post-monsoon campaigns respectively. Considering high OA concentrations were observed across the two campaigns, the total markers contributed up to a maximum of 4.2 % and 6.6 % across the pre- and post-monsoon respectively. Overall, this work highlights that even small numbers of isoprene and monoterpene derived SOA markers can make significant contributions to OA mass even in highly polluted megacities.

Chapter 5

Overcoming the lack of authentic standards for the quantification of biogenic secondary organic aerosol markers

5.1 Introduction

PM_{2.5} (particulate matter less than 2.5 μm in diameter) is considered to be the most dangerous form of air pollution to human health and is a complex mixture of different compounds from a range of natural and anthropogenic sources.[1] Secondary organic aerosol (SOA) makes up a significant portion of PM_{2.5} [208, 209] and consists of thousands of individual compounds, comprised of multiple chemical functionalities from a variety of sources.[1] A key subset of SOA is biogenic SOA (BSOA), which can be formed during the oxidation of biogenic volatile organic compounds (BVOCs) emitted from plants.[134, 135, 239, 252, 260, 261] In less polluted regions BSOA can represent between 23 – 50 % of organic aerosol mass [33, 34, 123, 191, 215], and has been shown to contribute significantly even in urban areas [213, 214]. One of the challenges when analysing SOA is the number of pathways and subsequent products that can be formed, with one precursor having the potential to create 100's of different compounds.[106, 179, 221] High resolution mass spectrometry (HRMS) with electrospray ionisation (ESI) sources have become an extremely versatile technique for improving our understanding of complex environmental samples.[58] ESI is a soft ionisation technique allowing for the molecular identification of thousands of individual species.[180, 338] However a species ability to be ionised is highly structurally specific [339], meaning the relative contribution of sample is hard to determine. Many previous studies have used direct injection techniques, without prior separation by liquid chromatography.[178, 340–342] Direct injection allows for the identification of 1000's of different molecular formulas within one sample. However, due to a lack of isomer identification, quantification of individual compounds is not possible. Most studies use data visualisation techniques such as van krevelen and kendrick mass diagrams, and other chemical metrics such as average O:C and H:C ratios to draw conclusions about the aerosol composition, ageing and source composition.[177–179, 219, 251, 338, 343, 344]

However, these chemical metrics are based on signal response, not quantified

concentrations, and as such assume all species ionise with equal efficiency. While semi-quantitative information can be obtained for samples of similar chemical speciation, ionisation efficiencies can vastly differ resulting in data bias and misinterpretation as shown by Pereira et al., 2021 and references therein.[345] Targeted analysis and quantification using authentic standards overcomes these issues. However, due to the sheer number of compounds present in SOA and inherent lack of authentic standards, proxy standards are routinely used where equivalent analyte ionisation efficiencies are assumed.[125, 191, 250] However, the use of proxy standards still assumes all species in one functionality group or retention time have the same ionisation efficiency.

Ideally, all species would have their own authentic standard for quantification, and recently groups have started to synthesise compounds such as organosulfates from isoprene and monoterpenes [185, 192, 193, 195], nitrooxy organosulfates from monoterpenes [194, 337] and organic acids from a range of monoterpenes [190, 346–348]. Kenseth et al., 2020 recently synthesised 6 α -pinene derived carboxylic and dimer ester species and found large differences between their ESI efficiencies. The measured relative ionisation efficiencies (RIE) relative to *cis*-pinonic acid ranged from 0.46 to 35.65. The large differences in ionisation efficiencies observed by this study highlight the need to consider these differences in the quantification of species with similar functionalities and retention time windows. However, two issues arise with this approach; firstly, the time and expenses to synthesise different BSOA standards limits the work to larger labs with synthesis facilities, and secondly the number of BSOA standards that would need to be synthesised for the hundreds of identified compounds makes this approach impractical.

A species' ability to ionise in the ESI source, both in the negative and positive modes, is highly dependent on its functionality and structure as well as the ionisation conditions.[339, 349, 350] This has led to the development of models that are capable of predicting how well a compound can ionise based on structural descriptors or properties relative to a standard compound.[197, 349–351] The RIE, i.e how well a compound ionises in comparison to a reference compound, is

calculated as shown in Equation 5.1, where $\text{LogRIE}(C_1, C_2)$ is the log value of the ratio of the gradients for compounds C_1 and C_2 across a concentration-response curve.[197, 349]

$$\text{logRIE}(C_1, C_2) = \log \left(\frac{\text{slope}([C_1 - H]^{-1})}{\text{slope}([C_2 - H]^{-1})} \right) \quad (5.1)$$

This type of RIE scale has been used to investigate the structural or chemical features which affect a species' ability to ionise in the ESI. Early studies focussed on measured or calculated physical properties such as logP or pKa.[352–356] Recent studies have focussed on using computationally calculated molecular fingerprints or structural descriptors to assess and predict a species RIE.[197, 351] Mayhew et al., 2020 measured RIE's of 51 carboxylic acids which combined with structural fingerprints were used to develop a Bayesian ridge regression model. The model showed R^2 and RMSE values in line with comparable studies, without the need to measure or predict physical properties of compounds. Liigand et al., 2020 recently developed a predictive machine learning model, which can predict the RIE's of species relative to benzoic acid based on their structure, both in the positive and negative ionisation modes across a range of solvent compositions. Their model used data collected over a decade and contains RIE measurements of 3139 and 1286 compound-solvent combinations in the positive and negative modes respectively. Previously, to our knowledge only one study has predicted RIE factors for BSOA species.[357] Zhang et al., 2015 estimated the RIE's of a range of α -pinene derived organic acids based on a linear model developed by Krueve et al.,2014.[350] The predicted RIE's ranged from 0.54 – 51.64, with dimer species such as $C_{16}H_{26}O_6$ having the largest predicted RIE values, in-line with the observations in Kenseth et al., 2020.

In this study we aim to establish an RIE model and apply it to improving our ability to reliably quantify biogenic organic acids present in BSOA. RIE measurements of 89 authentic organic compounds relative to *cis*pinonic acid were

conducted in negative ionisation mode. These measurements were then coupled to easily obtained chemical descriptors of molecular structure from ChemDes [358] as well as pKa and logP values and a random forest model was developed for the prediction of BSOA RIE factors. Using this model, RIE factors were then predicted for previously identified BSOA markers which were used to correct concentrations calculated from a proxy *cis*-pinonic acid calibration in ambient samples collected in summertime Beijing. Overall, this study is the first to apply a method for the prediction of BSOA ESI response factors based on RIE measurements, and as such provides a basis for future studies to establish more reliable quantification methods.

5.2 Experimental

5.2.1 Instrument and data analysis

Samples were analysed using an Ultimate 3000 UHPLC (Thermo Scientific, USA) coupled to a Q Exactive Orbitrap MS (Thermo Fisher Scientific, USA) using data dependent tandem mass spectrometry (ddMS²) with heated electrospray ionization source (HESI). The UPLC method uses a reverse phase, 2.6 μm , 100 x 2.1 mm, Accucore column (Thermo Scientific, UK), held at 40 °C. The mobile phase consisted of water (A) and methanol (B) both Optima grade (Thermo Fisher Scientific) with 0.1% (v/v) of formic acid (98% purity, Acros Organics). The injection volume was 4 μL . The solvent gradient was held for one minute at 90:10 H₂O:MeOH, then changed linearly to 10:90 over 24 minutes, returning to 90:10 over 2 minutes and then held for 2 minutes, with a flow rate of 300 $\mu\text{l min}^{-1}$. The MS was operated in negative mode, using full scan data dependant MS². The scan range was set between 50 - 750 m/z, with a mass resolution of 120,000. The capillary and auxiliary gas temperatures were 320 °C. The number of most abundant precursors for MS² fragmentation was set to 10. Data was analysed using TraceFinder 4.1 General Quan software (Thermo Fisher Scientific) using

a targeted compound library of both standards and BSOA species, with a mass accuracy of 3 ppm for marker identification.

5.2.2 Commercially available standards

RIE measurements of 89 authentic standards relative to *cis*-pinonic acid were conducted, as shown in Table 5.1. All standards were of high purity (> 95 %) to reduce the effect of purity on measured RIE values. The standards were prepared in mixtures, in 50:50 methanol:water, where no compound had the same RT to reduce matrix effects which would affect the measured RIE. The mixtures were prepared across a 7-point concentration gradient (5, 2.5, 1, 0.5, 0.25, 0.125, 0.0625 ppm, $R^2 > 0.95$), with 3 replicate measurements per concentration. However, some compounds reached limit of detection before the lowest concentration. A 9-point *cis*-pinonic acid calibration was run alongside the ambient PM_{2.5} samples which was used for quantification ($R^2 > 0.99$). 35 compounds were common between this study and that conducted in Mayhew et al., 2020 on the same mass spectrometer but via direct infusion. The 35 compounds showed a high correlation ($R^2 = 0.83$) across the two methods, with an average difference in the measured logRIE’s of 0.24 ± 0.42 , highlighting the reliability of these measurements. The errors in the measured logRIE values were small, on average 3.6 % across the 89 standards based on the standard error of the calibration slopes.

Table 5.1: Measured ($\log\text{RIE}_M$) and predicted ($\log\text{RIE}_P$) logRIE values for the 89 standards used for the development of the random forest model. Predicted logRIE values have an error range of ± 0.59 . Alongside their molecular formulas, retention times (RT) and the dominant functionality.

| Compound | Formula | RT | Functionality | $\log\text{RIE}_M$ | $\log\text{RIE}_P$ |
|----------------------------|--|-------|---------------|--------------------|--------------------|
| 2,6 dimethyl-4-nitrophenol | $\text{C}_8\text{H}_9\text{NO}_3$ | 12.71 | -OH | 1.75 | 0.33 |
| 4-nitro-1-naphthol | $\text{C}_{10}\text{H}_7\text{NO}_3$ | 14.99 | -OH | 1.75 | 1.17 |
| 2-methyl-4-nitrophenol | $\text{C}_7\text{H}_7\text{NO}_3$ | 10.42 | -OH | 1.72 | 1.39 |
| Isoborneolacetic acid | $\text{C}_{13}\text{H}_{22}\text{O}_3$ | 14.87 | -OOH | 1.62 | 0.81 |
| 2-fluro nitrophenol | $\text{C}_6\text{H}_4\text{FNO}_3$ | 7.16 | -OH | 1.6 | 1.22 |

| Compound | Formula | RT | Functionality | logRIEM | logRIEP |
|----------------------------------|---|-------|---------------|---------|---------|
| 3-methyl-4-nitrophenol | C ₇ H ₇ NO ₃ | 9.3 | -OH | 1.57 | 1.43 |
| Sebacic acid | C ₁₀ H ₁₈ O ₄ | 13.14 | -OOH | 1.46 | 1.15 |
| 4-nitrocatechol | C ₆ H ₅ NO ₄ | 4.76 | -OH | 1.36 | 1.03 |
| 4-nitrobenzene-1,3-diol | C ₆ H ₅ NO ₄ | 6.73 | -OH | 1.34 | 0.31 |
| Azelaic acid | C ₉ H ₁₆ O ₄ | 10.51 | -OH | 1.33 | 1.25 |
| 2-methyl-5-nitrophenol | C ₇ H ₇ NO ₃ | 11 | -OH | 1.33 | 1.34 |
| 2-methyl-3-nitrophenol | C ₇ H ₇ NO ₃ | 9.77 | -OH | 1.31 | 1.08 |
| 2,4-dinitrophenol | C ₆ H ₄ N ₂ O ₅ | 7.42 | -OH | 1.3 | 0.4 |
| Suberic acid | C ₈ H ₁₄ O ₄ | 7.56 | -OH | 1.29 | 0.94 |
| 4-hydroxybenzaldehyde | C ₇ H ₆ O ₂ | 4.2 | -CHO/-OH | 1.26 | 0.39 |
| 3-nitrophenol | C ₆ H ₅ NO ₃ | 9.89 | -OH | 1.23 | 1.12 |
| 4-methyl-3-nitrophenol | C ₇ H ₇ NO ₃ | 9.89 | -OH | 1.23 | 1.34 |
| Camphoric acid | C ₁₀ H ₁₆ O ₄ | 9.04 | -OOH | 1.2 | 0.9 |
| 2-Hydroxyhexanoic acid | C ₆ H ₁₂ O ₃ | 5.68 | -OOH | 1.14 | 0.32 |
| 3,3-dimethyl glutaric acid | C ₉ H ₁₆ O ₄ | 4.43 | -OOH | 1.13 | 0.65 |
| p-coumaric acid | C ₉ H ₈ O ₃ | 6.4 | -OOH | 1.13 | 0.8 |
| 2,3-naphthalenedicarboxylic acid | C ₁₂ H ₆ O ₃ | 10.68 | -CO | 1.03 | 0.75 |
| 2-hydroxy-3-methylbutyric acid | C ₅ H ₁₀ O ₃ | 2.39 | -OOH | 1.01 | -0.07 |
| Pimelic acid | C ₇ H ₁₂ O ₄ | 4.63 | -OOH | 0.92 | 0.8 |
| Isophthalic acid | C ₈ H ₆ O ₄ | 6.24 | -OOH | 0.92 | 0.62 |
| Citraconic acid | C ₅ H ₆ O ₄ | 1.17 | -OOH | 0.91 | 0.34 |
| 2,5-dihydroxybenzoic acid | C ₇ H ₆ O ₄ | 2.91 | -OOH | 0.91 | 0.42 |
| 2-Methoxy-4-nitrophenol | C ₇ H ₇ NO ₄ | 7.61 | -OH | 0.91 | 0.19 |
| Cholic acid | C ₂₄ H ₄₀ O ₅ | 20.4 | -OOH | 0.91 | 0.88 |
| Diphenolic acid | C ₁₇ H ₁₈ O ₄ | 11.52 | -OOH | 0.87 | 0.91 |
| 1,2,4-Butanetricarboxylic acid | C ₇ H ₁₀ O ₆ | 1.23 | -OOH | 0.8 | 0.45 |
| 3,4-Dihydroxy benzoic acid | C ₇ H ₆ O ₄ | 1.82 | -OOH | 0.77 | 0.58 |
| Sinapic acid | C ₁₁ H ₁₂ O ₅ | 7.85 | -OOH | 0.76 | 0.52 |
| Adipic acid | C ₆ H ₁₀ O ₄ | 2.33 | -OOH | 0.75 | 0.69 |
| Levulinic acid | C ₅ H ₈ O ₃ | 1.22 | -OOH | 0.72 | -0.58 |
| Hippuric acid | C ₉ H ₉ NO ₃ | 3.57 | -OOH | 0.63 | 0.82 |
| 3-methyl adipic acid | C ₇ H ₁₂ O ₄ | 4.54 | -OOH | 0.62 | 0.8 |

| Compound | Formula | RT | Functionality | logRIEM | logRIEP |
|---|--|-------|---------------|---------|---------|
| Succinic acid | C ₄ H ₆ O ₄ | 0.97 | -OOH | 0.6 | 0.5 |
| 3-nitrobenzoic acid | C ₇ H ₅ NO ₄ | 7.53 | -OOH | 0.59 | 0.79 |
| 1,4-cyclohexanedicarboxylic acid | C ₈ H ₁₂ O ₄ | 5.83 | -OOH | 0.58 | 0.88 |
| Glutaric acid | C ₅ H ₈ O ₄ | 1.31 | -OOH | 0.57 | 0.75 |
| 4-methyl-catechol | C ₇ H ₈ O ₂ | 4.65 | -OH | 0.56 | 0.44 |
| 4-hydroxy benzoic acid | C ₇ H ₆ O ₃ | 3.38 | -OOH | 0.5 | 0.62 |
| 2-Methylsuccinic acid | C ₅ H ₈ O ₄ | 1.76 | -OOH | 0.49 | 0.55 |
| 3-hydroxy benzoic acid | C ₇ H ₆ O ₃ | 4.42 | -OOH | 0.41 | 0.42 |
| Itaconic acid | C ₅ H ₆ O ₄ | 1.48 | -OOH | 0.39 | 0.55 |
| Malic acid | C ₄ H ₆ O ₅ | 0.72 | -OOH | 0.3 | -0.2 |
| Citric acid | C ₆ H ₈ O ₇ | 0.93 | -OOH | 0.28 | 0.45 |
| Mandelic acid | C ₈ H ₈ O ₃ | 3.33 | -OOH | 0.27 | 0.55 |
| Maleic acid | C ₄ H ₄ O ₄ | 0.75 | -OOH | 0.26 | 0.47 |
| trans,trans,1,3-butadiene-1,4-dicarboxylic acid | C ₆ H ₆ O ₄ | 2.11 | -OOH | 0.19 | 0.63 |
| DL-tartaric acid | C ₄ H ₆ O ₆ | 0.72 | -OOH | 0.15 | -0.25 |
| Shikimic acid | C ₇ H ₁₀ O ₅ | 0.74 | -OOH | 0.1 | 0.29 |
| O-toluic acid | C ₈ H ₈ O ₂ | 10.74 | -OOH | 0.1 | -0.62 |
| Vanillin | C ₈ H ₈ O ₃ | 5.55 | -CHO/-OH | 0.09 | 0.05 |
| 4-nitrocinnamic acid | C ₉ H ₇ NO ₄ | 10.97 | -OOH | 0.03 | 0 |
| Nonanoic acid | C ₉ H ₁₈ O ₂ | 19.46 | -OOH | -0.11 | -0.32 |
| Dodecanoic acid | C ₁₂ H ₂₄ O ₂ | 23.62 | -OOH | -0.14 | -0.51 |
| Benzoic acid | C ₇ H ₆ O ₂ | 7.93 | -OOH | -0.19 | -0.7 |
| Methylmalonic acid | C ₄ H ₆ O ₄ | 1.05 | -OOH | -0.21 | -0.89 |
| Vallinic acid | C ₈ H ₈ O ₄ | 4.34 | -OOH | -0.25 | 1.02 |
| 2-nitro-1-naphthol | C ₁₀ H ₇ NO ₃ | 18.83 | -OH | -0.34 | -0.48 |
| m-toluic acid | C ₈ H ₈ O ₂ | 11.42 | -OOH | -0.38 | -0.47 |
| 2-nitroresorcinol | C ₆ H ₅ NO ₄ | 5.41 | -OH | -0.4 | -0.49 |
| Valeric acid | C ₅ H ₁₀ O ₂ | 2.31 | -OOH | -0.46 | -1.1 |
| p-toluic acid | C ₈ H ₈ O ₂ | 11.45 | -OOH | -0.47 | -0.95 |
| 2-nitrobenzoic acid | C ₇ H ₅ NO ₄ | 2.94 | -OOH | -0.49 | 0.15 |
| 2-nitrophenol | C ₆ H ₅ NO ₃ | 10.84 | -OH | -0.54 | -0.6 |
| pyruvic acid | C ₃ H ₄ O ₃ | 0.78 | -OOH | -0.57 | -1.6 |

| Compound | Formula | RT | Functionality | logRIEM | logRIEP |
|----------------------------|--|-------|---------------|---------|---------|
| 4-methoxy-benzoic acid | C ₈ H ₈ O ₃ | 9.09 | -OOH | -0.57 | -0.02 |
| 5-methyl-2-nitrophenol | C ₇ H ₇ NO ₃ | 12.92 | -OH | -0.59 | -0.01 |
| DL-isoleucine | C ₆ H ₁₃ NO ₂ | 0.99 | -OOH | -0.64 | -0.49 |
| Trans-cinnamic acid | C ₉ H ₈ O ₂ | 11.76 | -OOH | -0.67 | -0.5 |
| Malonic acid | C ₃ H ₄ O ₄ | 0.76 | -OOH | -0.7 | -0.54 |
| 4-methyl-2-nitrophenol | C ₇ H ₇ NO ₃ | 12.86 | -OH | -0.75 | 0.03 |
| 2-methyl-6-nitrophenol | C ₇ H ₇ NO ₃ | 14.54 | -OH | -0.75 | -0.58 |
| 4-methoxy-2-nitrophenol | C ₇ H ₇ NO ₄ | 11.75 | -OH | -0.76 | -0.47 |
| 4-Phenylbutyric acid | C ₁₀ H ₁₂ O ₂ | 13.37 | -OOH | -0.77 | -0.65 |
| Acetoxyacetic acid | C ₄ H ₆ O ₄ | 1.17 | -OOH | -0.78 | -0.05 |
| Ketopinic acid | C ₁₀ H ₁₄ O ₃ | 8.66 | -OOH | -0.85 | -0.38 |
| 3,4-di-methyl-benzoic acid | C ₉ H ₁₀ O ₂ | 14.14 | -OOH | -1.03 | -0.67 |
| Furoic acid | C ₅ H ₄ O ₃ | 3.21 | -OOH | -1.23 | -0.93 |
| 4-hydroxycinnamic acid | C ₉ H ₈ O ₃ | 6.38 | -OOH | -1.29 | -0.48 |
| Aconitic acid | C ₆ H ₆ O ₆ | 1 | -OOH | -1.39 | 0.49 |
| Crotonic acid | C ₄ H ₆ O ₂ | 1.05 | -OOH | -1.76 | -1.92 |
| Sorbic acid | C ₆ H ₈ O ₂ | 7.88 | -OOH | -1.8 | -0.96 |
| Phenyl acetic acid | C ₈ H ₈ O ₂ | 4.96 | -OOH | -2.09 | -0.7 |
| Butyric acid | C ₄ H ₈ O ₂ | 3.16 | -OOH | -2.34 | -1.33 |
| 3,3-dimethyl acrylic acid | C ₅ H ₈ O ₂ | 5.04 | -OOH | -2.84 | -1.38 |

5.2.3 Chamber samples

To identify the retention time of BSOA tracers from specific precursors, BSOA was generated from α -pinene, limonene and β -caryophyllene using an aerosol flow reactor as outlined in Table 1 of Pereira et al., 2019.[359] The generated BSOA was collected using an electrical low-pressure impactor onto foil-lined impactor plates and dissolved in 50:50 methanol: water (optima, LC-MS grade, Fisher Scientific, UK). Individual α -pinene markers were isolated and collected based on their retention times from generated BSOA mass using a HPLC- ion-trap mass spectrometer coupled to an automated fraction collector, using the method in Finessi et al., 2014.[360]

5.2.4 Ambient Samples: collection and extraction

Ambient PM_{2.5} samples were collected in summer 2017 (24/05/2017 – 30/05/2017) at the Institute of Atmospheric Physics (IAP) in Beijing, China. This sampling was part of the Sources and Emissions of Air Pollutants in Beijing (AIRPOLL-Beijing) project, as part of the wider Atmospheric Pollution and Human Health in a Chinese Megacity (APHH-Beijing) programme.[220] The samples were collected using a HiVol sampler at a flow rate of 1.33 m³ min⁻¹. The samples were then stored at -20 °C before use. A 38.44 cm² cutting was taken from the filter and cut into roughly 1 cm² pieces. 8 mL of MeOH (Optima LC-MS grade) was then added to the filter pieces and sonicated for 45 mins under ice. The extract was then removed and filtered through a 0.22 μm syringe filter (Millipore) into a new vial. 2 mL (2 * 1mL) of MeOH was then added to the filter pieces and extracted through the 0.22 μm filter and combined with the rest of the extract. The combined extract was then reduced to dryness using a solvent evaporator, before being reconstituted in 50: 50 MeOH:H₂O. Triplicate recovery tests showed an almost complete recovery of *cis*-pinonic acid (99 ± 15.6 %) from the filter.

5.3 Results and Discussion

5.3.1 Development of a RIE predictive model

Authentic standards were analysed for model development alongside *cis*-pinonic acid within mixtures for RIE calculation and to allow correction for inter-day variability in instrument sensitivity. All standards contained a carboxylic acid or alcohol functional group but spanned a wide range of structures and other functionalities. The species eluted across a wide range of retention times, from highly polar species such as malic acid eluting within the first minute, to non-polar species such as dodecanoic acid eluting at the end of the elution gradient. The gradient of calibration curves of the 89 standards were determined using linear regression. The calculated logRIE values of the species, given in Table 5.1 ranged

from -2.84 to 1.75, covering four orders of magnitude.

Several basic parameters were correlated toward the measured logRIE including mass, RT, number of carbon and oxygen atoms as well as the O:C and H:C ratios, however no correlation was observed. On average, the lowest RIE values were observed for species eluting before 6 minutes, and after 15 minutes, with the highest eluting between 9 and 12 minutes. Matrix effects were investigated using the same method as in Bryant et al., 2021 using *cis*-pinonic acid to determine if signal suppression was occurring due to the highly complex nature of the samples. However, no significant matrix effect was observed for *cis*-pinonic acid, but further work is required for a range of different acid species. These measured logRIE values were then combined with over 3000 predicted chemical structural descriptors from ChemDes from Chemopy, CDK, RDKit, Pybel and PaDEL packages.[358]

Several data cleaning steps were undertaken before model development. Firstly, non-numeric descriptors and descriptors containing only one value were removed resulting in 1766 descriptors. Finally, descriptors with a pairwise correlation greater than $R^2 = 0.8$ were removed, in-line with previous studies [197] resulting in 224 descriptors using the "findCorrelation" function from the Caret R package [361]. The remaining descriptors were then correlated to the logRIE values of the standards, and those with an R greater than 0.3 were selected (Table 5.2). Two descriptors were removed ("fr_nitro_ arom_nonortho" and "fr_phenol"), due to their lack of applicability to functionalities of the BSOA. pKa and logP were also predicted using ChemDraw Prime 18.1 software, based on previous studies highlighting their importance to the ionisation efficiencies of compounds. The pKa showed a moderate R correlation of 0.32 towards logRIE, but limited correlations were observed for logP ($R < 0.1$), however a more accurate model was obtained with the inclusion of logP. The predicted pKa and logP values were combined with the remaining descriptors, giving 18 descriptors for model development. Several predictive models were developed using the Caret R package including random forest, Bayesian ridge regression and linear regression, with regularised random forest (RRF) being the best performing based on the lowest RMSE. The number

of trees used in the random forest was optimised to 100 trees, and *mtry* (the number of variables available for splitting at each tree node) was optimised to 10.

Due to the small dataset size, leave one out cross validation (LOOCV) was used to test the predictive capabilities of the model. LOOCV uses each compound in the data set once as a test set, with the other $n-1$ compounds as the training set. Figure 5.1 shows the correlation between the measured and predicted logRIE values for the 89 readily available standards. The optimised model shows similar accuracy and linearity to previous studies [197, 349–351, 362, 363], with an R^2 of 0.66 and RMSE of 0.59. The RMSE error means that if compound A is predicted to have an RIE 10 times higher ($\log\text{RIE} = 1$) than *cis*-pinonic acid ($\log\text{RIE} = 0$), the actual RIE would be in the range 2.6 – 38.9 ($\log\text{RIE} = 1.0 \pm 0.59$). Overall, the model performed similarly to previous studies, although performed poorly for compounds with logRIE's less than -1, as seen previously likely due to the lack of observations.[197, 351] Further work is needed to increase the RIE measurements for more accurate model development.

Liigand et al., 2020 has extensively developed this machine learning quantitative ESI-LC-MS approach, using to date, the largest compiled dataset of RIE measurements. This is a complex dataset, spanning an array of different solvent compositions, ionisation modes and instruments, for compound quantification. The model presented here is the first to predict BSOA RIE factors based off RIE measurements of authentic standards. The model was built for the purpose of quantifying BSOA compounds in a set solvent mixture, and only on one instrument, meaning the dataset could be less complex. This study therefore highlights a method for quantification of SOA species without authentic standards, without the need of large datasets which take a long time to accumulate, using commercially available, low-cost standards. This method also negates the need to perform numerous standard calibrations for component quantification, leading to faster throughput of samples. However, more authentic BSOA standards are needed to further develop the model and compared predicted and measured RIE values. Furthermore, Liigand et al., 2020 shows that these models can be transferred

Table 5.2: Contains descriptors obtained from Chemdes which had a R correlation greater than 0.3 to the logRIE values of the standards in Table 5.1. Package from which the descriptor as obtained and the description of the descriptor.

| Descriptor | R | Package | Description |
|-------------------|----------|----------------|--|
| ATSm5 | 0.46 | Chemopy | Broto-Moreau autocorrelation of a topological structure-lag5/weighted by atomic masses |
| ZMIC5 | 0.43 | PaDEL | Z-modified information content index (neighbourhood symmetry of 5-order) |
| EstateVSA1 | 0.43 | Chemopy | MOE-type descriptors using Estate indices and surface area contributions |
| SpMAD_Dzp | 0.42 | PaDEL | Spectral mean absolute deviation from Barysz matrix / weighted by polarizabilities |
| PEOE_VSA13 | 0.41 | RDKit | MOE Charge VSA Descriptor 13 ($0.25 \leq x < 0.30$) |
| AATS6s | 0.39 | PaDEL | averaged moreau-broto autocorrelation of lag 6 weighted by intrinsic state |
| AATS7i | 0.37 | PaDEL | Average Broto-Moreau autocorrelation - lag 7 / weighted by first ionization potential |
| MLFER_A | 0.37 | PaDEL | Overall or summation solute hydrogen bond acidity |
| MATS1p | 0.37 | PaDEL | moran coefficient of lag 1 weighted by polarizability |
| AATS6e | 0.36 | PaDEL | Average Broto-Moreau autocorrelation - lag 6 / weighted by Sanderson electronegativities |
| MLFER_S | 0.36 | PaDEL | combined dipolarity/polarizability |
| JGI4 | 0.35 | PaDEL | Mean topological charge index of order 4 |
| EState_VSA10 | 0.35 | RDKit | MOE-type descriptors using EState indices and surface area contributions |
| MATSm6 | 0.33 | Chemopy | Moran autocorrelation-lag6/weighted by atomic masses |
| AATS6v | 0.31 | PaDEL | Average Broto-Moreau autocorrelation - lag 6 / weighted by van der Waals volumes |
| PEOE_VSA2 | 0.31 | RDKit | MOE Charge VSA Descriptor 2 ($-0.30 \leq x < -0.25$) |

between instruments, while each instrument and method would produce a specific RIE value for a compound, specific compounds have been shown to be effective at moving the model across instruments. This suggests an aerosol community model could be developed but more work is needed. An open-source database which has now been developed by the Krueve group allows for large amounts of RIE measurements to be compiled across instruments and laboratories.[339] This would allow for a generalised RIE model to be produced for standardised RIE factors of SOA species based on a set of defined authentic standards. Further work is needed to implement a generalised SOA RIE model for the aerosol community.

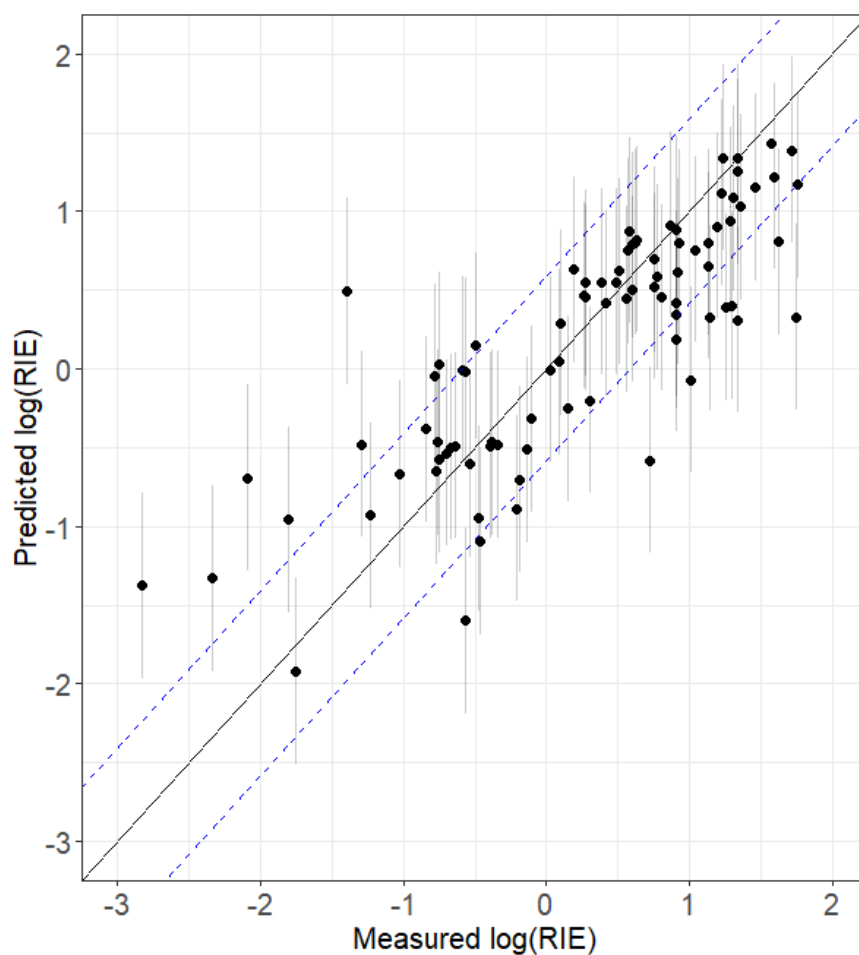


Figure 5.1: Comparison between measured logRIE and predicted logRIE produced by a linear model. The solid black line is 1:1 i.e would represent perfect predictions of the measured values. The blue dotted lines represent $2 \times \text{RMSE}$ from the 1:1 line. The grey vertical lines represent predicted logRIE $\pm \text{RMSE}$.

5.3.2 Predicted BSOA RIE factors

Several previous studies have investigated the formation of organic acids derived from α -pinene, limonene and β -caryophyllene.[190, 260, 357, 364–366] Table 5.3 contains the SMILES formulas of 87 organic acid structures across 60 unique molecular formulae previously proposed in these studies. One of the main challenges of the quantification approach used in this study is the need for structure elucidation. Where multiple isomeric species are present, tandem mass spectrometry data is essential to elucidate chemical structure although similar precursor spectra may still be obtained. The chemical descriptors for these structures were obtained from chemDes and using the optimised model described previously and the logRIE values were predicted. The predicted RIE's ranged from 0.27 to 13.5, with an average of (4.2 ± 3.9) (mean \pm SD). These values are of similar magnitude to those measured by Kenseth et al., 2020 and proposed by Wang et al., 2015. The α -pinene and β -caryophyllene markers had similar average RIE values of (5.2 ± 4.0) and (5.6 ± 4.5) respectively, while limonene markers had an average of (2.4 ± 2.3) .

It should be noted that multiple isomers are likely for most of the markers, however only selected isomers which had previously proposed structures were used in this study. For example, 10 isomeric structures of Lim_199 ($C_{10}H_{16}O_4$) were proposed by Hammes et al., 2019. The average RIE of these 10 structures was (1.4 ± 1.7) , with a range of 0.49 - 4.80, highlighting the importance of structure confirmation for quantification. The highest predicted RIE for the α -pinene markers was 12.7 for Pinene_353a ($C_{19}H_{30}O_6$) and, Pinene_353b ($C_{20}H_{34}O_5$), both of which are dimer species. This is in-line with high RIE values measured via authentic standards of 35.6 and 21.1 for Pinene 353a and 353b respectively by Kenseth et al., 2020. Measured and predicted RIE values were not expected to be the same due to the method specific nature of the values as discussed earlier, but the RIE values are in-line with one another.

The species in Table 5.3 were then targeted in the SOA samples generated from

α -pinene, limonene and β -caryophyllene precursors. The majority of the α -pinene marker structures were confirmed via comparison to either authentic standards [359] or matching product ion mass spectra with previous studies.[190, 357] Comparatively less MS² data was available for the limonene markers, with far more isomers identified and structures proposed. Several markers were authenticated via matching MS² peaks to Witkowski et al., 2019. For the β -caryophyllene markers, only one species (β -caryophyllinic acid) was authenticated via MS². Several of the β -caryophyllene markers identified in the chamber samples only had one previously proposed structure, as such markers with only one isomer were assumed to be the same structure. 25 markers were added into a targeted database containing accurate masses and retention times for targeted identification in the ambient samples.

Table 5.3: Compound tag and reference predicted RIE factors and SMILE formulas for the structures of the previously proposed BSOA markers. Based on the RMSE uncertainty of 0.59, the predicted RIE values have an uncertainty range, as shown by the minimum and maximum RIE values. *Markers that have been structurally confirmed by comparison to an authentic standard or MS² data in the BSOA chamber samples.

| TAG | MF | RIE | SMILE | REF |
|--------------|--|-------------------|---|-------|
| *Pinene_169 | C ₉ H ₁₄ O ₃ | 0.33 (0.09–1.29) | CC1(C)C(CC=O)CC1C(O)=O | [357] |
| *Pinene_171a | C ₈ H ₁₂ O ₄ | 0.58 (0.15–2.27) | CC1(C)C(C(C)=O)CC1C(O)=O | [357] |
| *Pinene_171b | C ₈ H ₁₂ O ₄ | 2.24 (0.57–8.7) | CC1(OC(CC1CC(O)=O)=O)C | [357] |
| *Pinene_185a | C ₉ H ₁₄ O ₄ | 7.27 (1.87–28.26) | CC1(C)C(C(C)=O)CC1CC(O)=O | [357] |
| Pinene_185b | C ₁₀ H ₁₈ O ₃ | 12.06 (3.1–46.92) | CC1(C)C(C(C)O)CC1CC(O)=O | [190] |
| Pinene_189 | C ₈ H ₁₄ O ₅ | 3.41 (0.88–13.27) | CC(O)(C(CC(O)=O)CC(O)=O)C | [357] |
| *Pinene_197 | C ₁₀ H ₁₄ O ₄ | 0.61 (0.16–2.38) | CC1(C)C(C(C=O)=O)CC1CC(O)=O | [357] |
| *Pinene_199a | C ₁₀ H ₁₆ O ₄ | 5.69 (1.46–22.13) | CC1(C)C(C(CO)=O)CC1CC(O)=O | [357] |
| *Pinene_199b | C ₁₀ H ₁₆ O ₄ | 5.24 (1.35–20.38) | CC1(C(CC1CC(O)=O)C(C)=O)CO | [357] |
| *Pinene_213 | C ₁₀ H ₁₄ O ₅ | 4.06 (1.04–15.8) | OC(C(C1CC(CC(O)=O)C1(C)C)=O)=O | [357] |
| Pinene_231 | C ₁₀ H ₁₆ O ₆ | 4.77 (1.23–18.57) | CC(OC(C)(C(CC(O)=O)CC(O)=O)C)=O | [357] |
| Pinene_309 | C ₁₇ H ₂₆ O ₅ | 0.74 (0.19–2.88) | OC(C1CC(CC(OC2CC(CC=O)C2(C)C)=O)C1(C)C)=O | [357] |
| Pinene_313 | C ₁₆ H ₂₆ O ₆ | 5.82 (1.5–22.66) | OC(C1CC(CC(OC(C(C(C)O)C)CC=O)=O)C1(C)C)=O | [357] |
| Pinene_325 | C ₁₇ H ₂₆ O ₆ | 9.67 (2.49–37.64) | OC(C1CC(CC(OC2CC(C(O)=O)C2(C)C)=O)C1(C)C)=O | [357] |

| TAG | MF | RIE | SMILE | REF |
|-------------|--|--------------------|---|-------|
| Pinene_343a | C ₁₆ H ₂₄ O ₈ | 5.21 (1.34–20.28) | <chem>CC(OC1=O)(C(CC(OC(C)(C(CC(O)=O)CC(O)=O)C)=O)C1)C</chem> | [357] |
| Pinene_343b | C ₁₆ H ₂₄ O ₈ | 5.19 (1.33–20.2) | <chem>O=C(C1C(C(C(C(OC(C)(C(CC(O)=O)CC(O)=O)C)=O)C1(C)C)O</chem> | [190] |
| Pinene_351 | C ₂₀ H ₃₂ O ₅ | 0.79 (0.2–3.09) | <chem>CC(C1CC(CC(OC(C2CC(CC(O)=O)C2(C)C)C)=O)C1(C)C)=O</chem> | [190] |
| Pinene_353a | C ₁₉ H ₃₀ O ₆ | 12.69 (3.26–49.36) | <chem>OC(C1CC(CC(OC(C2CC(CC(O)=O)C2(C)C)C)=O)C1(C)C)=O</chem> | [190] |
| Pinene_353b | C ₂₀ H ₃₄ O ₅ | 12.72 (3.27–49.51) | <chem>C(C(O)C1C(C(C(C(OC(C2C(C(C(C(O)=O)C2(C)C)C)=O)C1(C)C</chem> | [190] |
| Pinene_357 | C ₁₇ H ₂₆ O ₈ | 1.72 (0.44–6.7) | <chem>OC(CC(CC(O)=O)C(C)(OC(C1CC(CC(O)=O)C1(C)C)=O)C)=O</chem> | [357] |
| *Pinene_367 | C ₁₉ H ₂₈ O ₇ | 8.58 (2.21–33.39) | <chem>OC(C1CC(CC(OC(C2CC(CC(O)=O)C2(C)C)=O)C1(C)C)=O</chem> | [357] |
| Bcary_171a | C ₈ H ₁₂ O ₄ | 4.56 (1.17–17.74) | <chem>CC1(C)CC(C(O)=O)C1C(O)=O</chem> | [366] |
| *Bcary_171b | C ₉ H ₁₆ O ₃ | 7.09 (1.82–27.59) | <chem>CC1(C)CC(C(O)=O)C1CCO</chem> | [366] |
| Bcary_183a | C ₁₀ H ₁₆ O ₃ | 0.44 (0.11–1.72) | <chem>CC1(C)CC(C(O)=O)C1CCC=O</chem> | [366] |
| Bcary_183b | C ₁₀ H ₁₆ O ₃ | 7.2 (1.85–28.02) | <chem>CC1(C)CC(C(CC(O)=O)=C)C1O</chem> | [366] |
| Bcary_185 | C ₉ H ₁₄ O ₄ | 6.59 (1.69–25.63) | <chem>CC1(C)CC(C(O)=O)C1CC(O)=O</chem> | [366] |
| *Bcary_197 | C ₁₁ H ₁₈ O ₃ | 0.54 (0.14–2.11) | <chem>CC1(C)CC(C(O)=O)C1CCC(C)=O</chem> | [366] |
| Bcary_199 | C ₁₀ H ₁₆ O ₄ | 11.09 (2.85–43.13) | <chem>CC1(C(CCC(O)=O)C(C(O)=O)C1)C</chem> | [366] |
| Bcary_225 | C ₁₂ H ₁₈ O ₄ | 11.44 (2.94–44.51) | <chem>CC1(C)CC(C(C(O)=O)=C)C1CCC(O)=O</chem> | [366] |
| *Bcary_237 | C ₁₄ H ₂₂ O ₃ | 0.45 (0.12–1.75) | <chem>CC1(C)CC(C(CCC=O)=C)C1CCC(O)=O</chem> | [366] |
| *Bcary_241 | C ₁₃ H ₂₂ O ₄ | 6.51 (1.67–25.34) | <chem>CC1(C)CC(C(CCC)=C)C1C(O)CC(O)=O</chem> | [366] |
| Bcary_251a | C ₁₄ H ₂₀ O ₄ | 0.67 (0.17–2.63) | <chem>CC1(C)CC2C1C=C(C(C)=O)OC2CCC(O)=O</chem> | [260] |
| *Bcary_251b | C ₁₅ H ₂₄ O ₅ | 0.6 (0.15–2.32) | <chem>CC1(C)CC(C(CCC(O)=O)=C)C1CCC(C)=O</chem> | [366] |
| Bcary_253a | C ₁₄ H ₂₂ O ₄ | 0.74 (0.19–2.86) | <chem>CC1(C)CC(C(CCC(O)=O)=O)C1CCC(C)=O</chem> | [366] |
| *Bcary_253b | C ₁₄ H ₂₂ O ₄ | 13.54 (3.48–52.69) | <chem>CC1(C)CC(C(CCC(O)=O)=C)C1CCC(O)=O</chem> | [366] |
| *Bcary_255a | C ₁₃ H ₂₀ O ₅ | 9.08 (2.33–35.31) | <chem>CC1(C)CC(C(CCC(O)=O)=O)C1CCC(O)=O</chem> | [366] |
| Bcary_255b | C ₁₄ H ₂₄ O ₄ | 10.12 (2.6–39.38) | <chem>CC1(C)CC(C(C(O)=O)=C)C1CCC(O)(O)C</chem> | [260] |
| Bcary_265 | C ₁₅ H ₂₂ O ₄ | 0.77 (0.2–3) | <chem>CC1(C)CC(C(CCC(O)=O)=C)C1CCC(C=O)=O</chem> | [260] |
| Bcary_267a | C ₁₄ H ₂₀ O ₅ | 0.75 (0.19–2.93) | <chem>CC1(C)CC(C(CCC(O)=O)=O)C1CCC(C=O)=O</chem> | [260] |
| Bcary_267b | C ₁₅ H ₂₄ O ₄ | 0.72 (0.18–2.79) | <chem>CC1(CC(C1C(O)CC(C)=O)C(CCC(O)=O)=C)C</chem> | [366] |
| Bcary_267c | C ₁₅ H ₂₄ O ₄ | 11.36 (2.92–44.18) | <chem>CC1(C)CC(C(CCC(O)=O)=C)C1CCC(CO)=O</chem> | [366] |
| Bcary_269a | C ₁₄ H ₂₂ O ₅ | 5.71 (1.47–22.22) | <chem>CC1(C)CC(C(CCC(O)=O)=O)C1CCC(CO)=O</chem> | [260] |
| Bcary_269b | C ₁₅ H ₂₆ O ₄ | 10.68 (2.74–41.54) | <chem>CC1(C)CC(C(CCC(O)=O)=C)C1CCC(O)(O)C</chem> | [260] |
| Bcary_271a | C ₁₄ H ₂₄ O ₅ | 8.83 (2.27–34.36) | <chem>CC1(C)CC(C(CCC(O)=O)=O)C1CCC(O)(O)C</chem> | [260] |
| Bcary_271b | C ₁₄ H ₂₄ O ₅ | 5.43 (1.4–21.14) | <chem>CC1(C)CC(C(CCC(O)=O)=O)C1C(O)CC(O)=O</chem> | [366] |
| Bcary_271c | C ₁₄ H ₂₄ O ₅ | 0.64 (0.16–2.49) | <chem>CC1(C)CC(C(CCC(O)=O)=O)C1CCC(OO)=O</chem> | [366] |
| Bcary_283 | C ₁₅ H ₂₄ O ₅ | 11.83 (3.04–46.04) | <chem>CC1(C)CC(C(CCC(O)=O)=C)C1CCC(C(O)O)=O</chem> | [260] |
| Bcary_285a | C ₁₄ H ₂₂ O ₆ | 0.85 (0.22–3.31) | <chem>CC1(CC(C1CCC(CO)=O)C(C(O)CC(O)=O)=O)C</chem> | [260] |
| Bcary_285b | C ₁₅ H ₂₆ O ₅ | 10.44 (2.68–40.62) | <chem>CC1(CC(C1CCC(O)(O)C)C(CCC(O)=O)=C)C</chem> | [260] |
| Bcary_287a | C ₁₄ H ₂₄ O ₆ | 8.4 (2.16–32.67) | <chem>CC1(C)CC(C(CCC(OO)O)=C)C1C(O)CC(O)=O</chem> | [366] |

| TAG | MF | RIE | SMILE | REF |
|------------|--|-------------------|--|-------|
| Bcary_287b | C ₁₄ H ₂₄ O ₆ | 0.86 (0.22–3.36) | CC1(CC(C1C(CC(OC)=O)O)C(C(O)CCO)=O)C | [366] |
| Lim_157a | C ₇ H ₁₀ O ₄ | 0.63 (0.16–2.43) | CC(CC(CCC(O)=O)=O)=O | [364] |
| Lim_157b | C ₇ H ₁₀ O ₄ | 2.64 (0.68–10.25) | O=CCC(CC(O)=O)C(C)=O | [364] |
| Lim_157c | C ₇ H ₁₀ O ₄ | 1.59 (0.41–6.18) | O=CC(C(C)=O)CCC(O)=O | [364] |
| Lim_157d | C ₇ H ₁₀ O ₄ | 0.69 (0.18–2.69) | CC(CCC(CC(O)=O)=O)=O | [364] |
| Lim_171a | C ₈ H ₁₂ O ₄ | 1.58 (0.41–6.16) | OC(CCC(C(C)=O)CC=O)=O | [364] |
| Lim_171b | C ₈ H ₁₂ O ₄ | 2.91 (0.75–11.33) | OC(C(C(CO)C(C)=C)=O)=O | [364] |
| *Lim_173a | C ₇ H ₁₀ O ₅ | 5 (1.28–19.44) | OC(CCC(CCC(O)=O)=O)=O | [364] |
| Lim_173b | C ₇ H ₁₀ O ₅ | 3.21 (0.82–12.48) | OC(CC(C(C)=O)CC(O)=O)=O | [364] |
| Lim_173c | C ₇ H ₁₀ O ₅ | 1.37 (0.35–5.32) | OC(C(C(CO)C(C)=O)=O)=O | [364] |
| *Lim_183 | C ₁₀ H ₁₆ O ₃ | 0.27 (0.07–1.04) | CC(CCC(C(C)=C)CC(O)=O)=O | [365] |
| *Lim_185a | C ₉ H ₁₄ O ₄ | 0.69 (0.18–2.68) | CC(CCC(CC(O)=O)C(C)=O)=O | [365] |
| *Lim_185b | C ₉ H ₁₄ O ₄ | 6.33 (1.63–24.63) | OC(CCC(C(C)=C)CC(O)=O)=O | [365] |
| *Lim_187a | C ₈ H ₁₂ O ₅ | 5.11 (1.31–19.87) | OC(CCC(C(C)=O)CC(O)=O)=O | [365] |
| *Lim_187b | C ₈ H ₁₂ O ₅ | 1.2 (0.31–4.69) | CC(C(C(C(C)=O)C(O)=O)O)=O | [365] |
| *Lim_187c | C ₈ H ₁₂ O ₅ | 0.71 (0.18–2.76) | OCCC(CC(C(O)=O)CC=O)=O | [365] |
| Lim_189 | C ₇ H ₁₀ O ₆ | 5.29 (1.36–20.59) | OC(CC(CCC(O)=O)C(O)=O)=O | [364] |
| Lim_199a | C ₁₀ H ₁₆ O ₄ | 0.68 (0.18–2.66) | CC(CCC(C(CO)=C)C(C=O)O)=O | [364] |
| Lim_199b | C ₁₀ H ₁₆ O ₄ | 0.64 (0.16–2.48) | CC(C(O)CC(C(C=O)O)C(C)=C)=O | [364] |
| Lim_199c | C ₁₀ H ₁₆ O ₄ | 0.62 (0.16–2.39) | OCC(CC(C(C(C)=C)CC=O)O)=O | [364] |
| Lim_199d | C ₁₀ H ₁₆ O ₄ | 0.64 (0.16–2.48) | CC(C(C(C(C(O)C=O)C(C)=C)O)=O | [364] |
| Lim_199e | C ₁₀ H ₁₆ O ₄ | 4.56 (1.17–17.75) | OCC(CCC(CC(O)=O)C(C)=C)=O | [364] |
| Lim_199f | C ₁₀ H ₁₆ O ₄ | 0.68 (0.18–2.66) | CC(CCC(C(CO)=C)C(O)C=O)=O | [364] |
| Lim_199g | C ₁₀ H ₁₆ O ₄ | 0.64 (0.16–2.48) | CC(C(O)CC(C(C=O)O)C(C)=C)=O | [364] |
| Lim_199h | C ₁₀ H ₁₆ O ₄ | 0.62 (0.16–2.39) | OCC(CC(C(C(C)=C)CC=O)O)=O | [364] |
| Lim_199i | C ₁₀ H ₁₆ O ₄ | 0.64 (0.16–2.48) | CC(C(C(C(C(O)C=O)C(C)=C)O)=O | [364] |
| Lim_199j | C ₁₀ H ₁₆ O ₄ | 3.35 (0.86–13.03) | CC(CCC(C(C)=C)C(O)C(O)=O)=O | [364] |
| Lim_201a | C ₉ H ₁₄ O ₅ | 2.12 (0.54–8.23) | CC(C(C(C(CO)=O)C(C)=O)O)=O | [364] |
| Lim_201b | C ₉ H ₁₄ O ₅ | 2.5 (0.64–9.74) | OCC(CCC(CC(O)=O)C(C)=O)=O | [364] |
| Lim_201c | C ₉ H ₁₄ O ₅ | 0.84 (0.21–3.25) | OCC(CC(C(C)=C)CCC(O)=O)=O | [364] |
| *Lim_203 | C ₈ H ₁₂ O ₆ | 5.31 (1.37–20.67) | OC(CC(CCCC(O)=O)C(O)=O)=O | [364] |
| Lim_213 | C ₁₀ H ₁₄ O ₅ | 4.64 (1.19–18.05) | OC(CC/C(C)=C(CC(O)=O)/C(C)=O)=O | [364] |
| Lim_215 | C ₁₀ H ₁₆ O ₅ | 0.48 (0.12–1.85) | CC(CCC(C(C)=C)C(C(O)=O)O)=O | [364] |
| *Lim_339a | C ₁₈ H ₂₈ O ₆ | 0.67 (0.17–2.6) | CC(CCC(C(OC(CC(CCC(C)=O)C(C)=O)O)O)C(C)=C)=O | [364] |
| Lim_339b | C ₁₈ H ₂₈ O ₆ | 0.73 (0.19–2.86) | O=CC(C(C)=C)CCC(CC(C)(CCC(CC(O)=O)C(C)=O)O)=O | [364] |
| Lim_367a | C ₁₉ H ₂₈ O ₇ | 8.41 (2.16–32.71) | OC(CCC(CC(OCC(CCC(CC(O)=O)C(C)=C)=O)=C)C(C)=C)=O | [365] |
| Lim_367b | C ₁₉ H ₂₈ O ₇ | 7.7 (1.98–29.95) | CC(C(CCC(OCC(CCC(CC(O)=O)C(C)=C)=O)=O)CC(O)=O)=C | [365] |

5.3.3 Quantification of BSOA in summertime Beijing

To investigate the impact of using these RIE factors on the quantification of BSOA markers in the real atmosphere, 26 markers including *cis*-pinonic acid were targeted in 25 ambient PM_{2.5} filter extracts collected in summertime Beijing, China in 2017 as part of the APHH campaign (see Shi et al., 2019 for more details). Of the 26 targeted markers, 18 were identified in at least one of the samples, while only 9 were identified in more than 40 % of the samples, and these will be used for further analysis. The markers were then quantified using a 9-point *cis*-pinonic acid calibration ($R^2 > 0.99$), with the time averaged concentrations shown in Table 5.4. The total average concentration of the markers was 146 ng m⁻³, with *cis*-pinonic acid contributing on average 6 % of the mass. Using this method, Lim_173 had the highest predicted concentration, with a mean concentration of 71.8 ng m⁻³, contributing 49 % of the mass. The marker concentrations were then corrected using the predicted RIE factors as shown in Figure 5.2.

The total marker concentration decreased to 51 ng m⁻³, a factor of 3 decrease compared to the quantification via *cis*-pinonic acid. The ionisation efficiency of *cis*-pinonic acid is low compared to many of the other BSOA compounds, most likely as a result of it having a single carboxylic acid and a carbonyl functionality. This highlights that using *cis*-pinonic acid as a proxy for quantification can lead to significant overestimations in marker concentrations. Using the RIE method, Lim_173 was still the most abundant marker, but only contributed 28.2 % (compared to 49 %) to the mass, while the contribution from *cis*-pinonic acid increased to 17.4 % from 6 %. This change in contributions could have important implications on conclusions from chamber and ambient studies. For example, Thomsen et al., 2021 identified and quantified organic acids formed from the oxidation of δ^3 -carene and α -pinene using proxy standards of *cis*-pinic acid, *cis*-pinonic acid and diaterpenylic acid acetate. They found large contributions of caric acid from δ^3 -carene oxidation and large contributions of dimer species from α -pinene oxidation. These large contributions however could be due to the

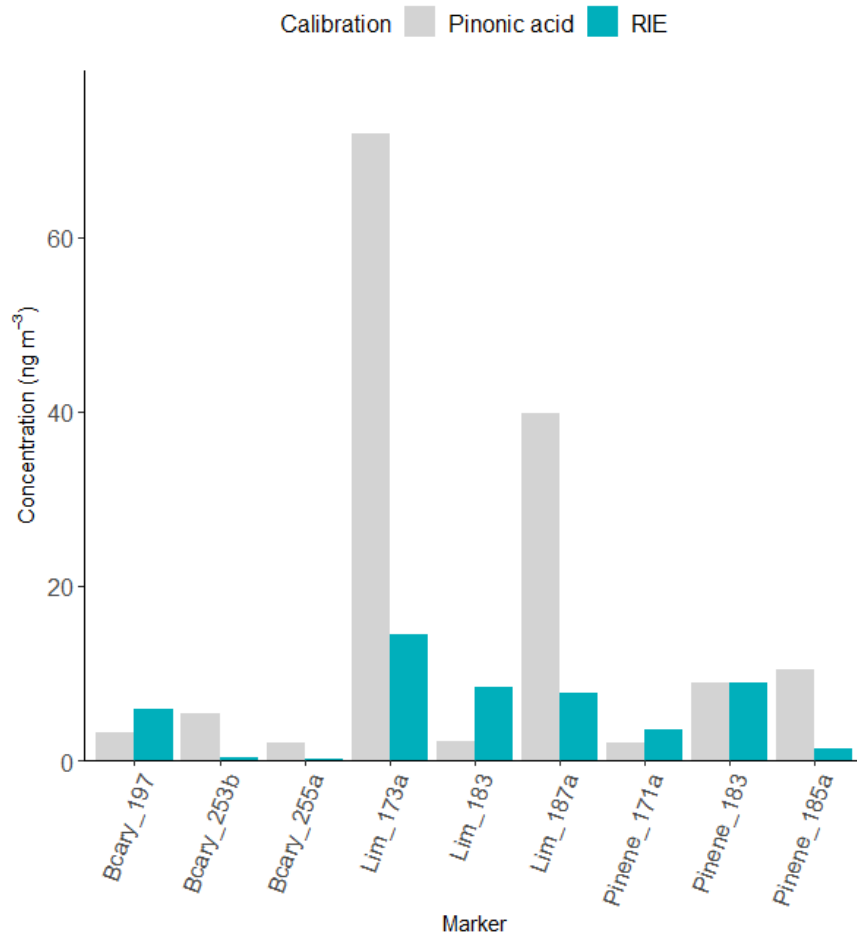


Figure 5.2: Concentration comparison for the 9 BSOA species identified in the ambient samples, quantified by *cis*-pinonic acid, and then “corrected” using the predicted RIE factors. The concentration of *cis*-pinonic acid stayed the same due to having an RIE factor of 1 ($\log\text{RIE} = 0$).

differing ionisation efficiencies of the markers and comparatively lower ionisation efficiencies of the proxy standards.

To investigate the use of generalised RIE factors for quantification, the concentrations were corrected using the average RIE predicted (4.2 ± 3.9) from all 89 structures previously identified in Table 5.3 and the precursor specific average RIE’s discussed in the previous section. Using the total RIE factor the total time averaged concentration decreased to 34.8 ng m^{-3} (from 145 ng m^{-3}), compared to 43.4 ng m^{-3} for the marker specific RIE correction. By using the precursor specific RIE averages, the total concentration decreased to 61.0 ng m^{-3} . Although these

Table 5.4: Comparison between marker concentrations quantified by a standard *cis*-pinonic acid calibration (PA) and corrected by the predicted RIE factors in Table 5.3.

| Tag | MF | Conc. (ng m ⁻³) | |
|-------------|--|-----------------------------|------|
| | | PA | RIE |
| Lim_173a | C ₇ H ₁₀ O ₅ | 71.9 | 14.4 |
| Lim_187a | C ₈ H ₁₂ O ₅ | 39.8 | 7.8 |
| Pinene_185a | C ₉ H ₁₄ O ₄ | 10.4 | 1.4 |
| Pinene_183 | C ₁₀ H ₁₆ O ₃ | 8.9 | 8.8 |
| Bcary_253b | C ₁₄ H ₂₂ O ₄ | 5.4 | 0.4 |
| Bcary_197 | C ₁₁ H ₁₈ O ₃ | 3.2 | 5.9 |
| Lim_183 | C ₁₀ H ₁₆ O ₃ | 2.3 | 8.4 |
| Pinene_171a | C ₈ H ₁₂ O ₄ | 2.1 | 3.6 |
| Bcary_255a | C ₁₃ H ₂₀ O ₅ | 2.0 | 0.2 |
| Total | | 146.0 | 51.0 |

differences are small in terms of mass change and within error of one another, this is only for 9 markers, where most non-targeted high resolution mass spectrometry aerosol studies identify thousands of unique molecular formulae.

High resolution MS studies of aerosol composition generally employ mass spectral data evaluation methods such as Van Krevelen diagrams, double bond equivalents, average oxidation states and average molecular formulas based on the number of detected molecular formulae.[177, 179, 180, 182] For example, Kundu et al., 2012 investigated the relative abundance of compounds with different O:C and H:C ratios and found a high abundance of high molecular weight functionalised aliphatic compounds. These relative abundances when corrected for by RIE factors could be drastically different to that proposed using the raw signal.

To investigate the effect of RIE factors on these evaluation methods, the hydrogen to carbon (H:C) and oxygen to carbon (O:C) ratios, DBE and average molecular formulas were standardised by number, proxy concentration (i.e. proportional to peak area) and RIE corrected concentrations as summarised in Table 5.5. First, the average O:C and H:C ratios were calculated for the 9 markers. O:C was calculated to be 0.43 based on the number of markers but increased to

Table 5.5: Comparison of average aerosol metrics weighted by the number of markers, *cis*-pinonic acid calibration derived concentrations and RIE corrected concentrations.

| Metric | Number | Calibrations | |
|------------|---------------------|--------------------------|--------------------------|
| | | <i>cis</i> -Pinonic acid | RIE |
| O:C | 0.43 | 0.61 | 0.48 |
| H:C | 1.55 | 1.48 | 1.53 |
| DBE | 3.22 | 3.05 | 3.01 |
| C | 10 | 8.1 | 8.84 |
| H | 15.6 | 12.1 | 13.65 |
| O | 4 | 4.7 | 4 |
| MF | $C_{10}H_{15.6}O_4$ | $C_{8.1}H_{12.1}O_{4.7}$ | $C_{8.8}H_{13.7}O_{4.0}$ |

0.61 when the average was weighted by the *cis*-pinonic acid derived concentrations and 0.48 when weighted by the RIE corrected concentrations. This is a significant difference considering relative small differences in O:C ratios between different grouped MF's based on mass ranges [367, 368] and different sources [39, 178, 340]. A significant shift in average molecular formulas was seen when using the number of unique formulas identified: $C_{10}H_{15.6}O_4$, weighted by *cis*-pinonic acid calibration concentrations: $C_{8.1}H_{12.1}O_{4.7}$ and weighted by the RIE corrected concentrations: $C_{8.8}H_{13.7}O_{4.0}$. Overall, this shows that even with a small number of markers, the average MF can change, moving from C_{10} species to C_8/C_9 depending on the weighting of the average. More work is needed to understand the impact of different RIEs when many hundreds of compounds are used to calculate these metrics.

5.4 Conclusion

This study has outlined a method for the semi-quantification of biogenic organic acid markers using ESI, attempting to overcome the lack of commercially available authentic standards. Based on a method developed by Liigand et al., 2020, a predictive random forest model was developed to predict the RIE's of BSOA

markers. RIE values for the BSOA markers ranged from 0.27–13.5, meaning that by using *cis*-pinonic acid as a calibrant, concentrations of individual BSOA components could be underpredicted by a factor of 3.7 or over predicted by 13.5. 9 organic acid BSOA markers including *cis*-pinonic acid were then quantified in 25 ambient Beijing PM_{2.5} samples. Time averaged quantified compound concentrations decreased from 146.0 ng m⁻³ to 51 ng m⁻³ when calibrating using a standard *cis*-pinonic acid calibration and then correcting using the predicted RIE factors. The effect of these factors was then investigated on aerosol evaluation methods, with differences in O:C ratios of 0.61 vs 0.48 for *cis*-pinonic acid and RIE corrected weighted average concentrations. Overall, this study highlights a need to account for the differences in ionisation efficiencies when analysing organic aerosol, due to the significant differences in calculated aerosol evaluation metrics, which could influence source contributions. Further work is needed to expand this method to include newly synthesised organic compounds relevant for BSOA analysis and to expand the range of functional groups and VOC precursors. Previous studies have suggested the applicability of transferring the predictive model between instruments, suggesting an open-source aerosol community model could be developed in the future.

Chapter 6

Formation of organic acids across three Asian Megacities

6.1 Introduction

Organic aerosol (OA) is strongly linked to adverse human and environmental health and is a key pollutant in terms of anthropogenically influenced climate change.[16, 21, 369] Secondary organic aerosol (SOA) contributes significant mass towards OA[1], but is an extremely complex mixture comprising of thousands of compounds, making molecular understanding and quantification difficult.[1, 180, 221] Biogenic volatile organic compounds (BVOCs) such as isoprene (C_5H_8), monoterpenes ($C_{10}H_{16}$) and sesquiterpenes ($C_{15}H_{24}$) are emitted in large quantities by vegetation into the atmosphere.[27, 370] In the atmosphere, these highly reactive species can be oxidised by OH and NO_3 radicals or ozone to form SOA containing a variety of functionalities.[97, 106, 119, 186] Isoprene is the dominant non-methane BVOC emitted to the atmosphere (50%), while monoterpenes and sesquiterpenes are estimated to contribute 15 % and 3 % respectively of total BVOC emissions.[27] However, many monoterpenes and sesquiterpenes are more reactive with OH and O_3 than isoprene.[97, 102], and have higher SOA mass yields due to their large carbon backbone.[119, 165, 371]

A substantial amount of work has also been dedicated to the formation of SOA from monoterpenes, mainly α -pinene and limonene as well as from sesquiterpenes such as β -caryophyllene. These studies have focussed on characterising SOA composition from the oxidation of these BVOCs in atmospheric simulation studies, identifying key products and formation routes.[41, 134, 165, 260, 273, 357, 365, 372, 373] Organic acids, carbonyls, alcohols, and peroxides have been identified from the oxidation of monoterpenes and sesquiterpenes in chamber simulations but less so in the ambient atmosphere.[41, 134, 165, 260, 273, 357, 365, 372, 373]

Key particulate phase functionalities identified in ambient samples include organic nitrates (ON), organosulfates (OS), nitrooxy organosulfates (NOS) which are heavily influenced by anthropogenic pollutants.[2, 35, 37, 38, 125, 153, 250] Numerous publications have focused on both qualitative and quantitative studies of monoterpene derived OS and NOS in the real atmosphere, however more limited

studies have focused on organic acids.[35, 177, 179, 184, 194, 250, 270, 373, 374]

Organic acids have been shown to form from both monoterpenes and sesquiterpenes through reaction with OH or ozonolysis and through heterogenous processes which are competing in the real atmosphere. These biogenic secondary organic aerosol (BSOA) acid species are formed both in rural clean environments and polluted environments. Numerous organic acid markers have been identified in chamber studies, for example, *cis*-pinonic acid from α -pinene, limononic acid from limonene and β -caryophyllinic acid from β -caryophyllene.[260, 357, 364–366] However, several obstacles need to be overcome in the quantification of biogenic organic acids.

Due to the extremely complex nature of OA, with thousands of distinct molecular formulas, organic acid markers need to be structurally confirmed either through comparison to an authentic standard[190] or generated BSOA from chamber studies[359]. For the accurate quantification of these markers, authentic standards are also needed, however a limited number of authentic organic acids are readily available, with the most readily available being *cis*-pinonic acid. The lack of authentic standards has led previous studies to synthesise individual authentic biogenic organic acids standards[190, 347, 373] or use proxy standards of similar structure and/or functionalities. Recently, Kenseth et al., 2020 synthesised 6 α -pinene derived organic acid markers and found large differences in their ionisation efficiencies in comparison to *cis*-pinonic acid, the most readily available proxy standard. This study highlighted the need to consider associated differences in ionisation efficiencies between BSOA acids, while being limited by the lack of authentic standards. Without large scale synthesis of numerous BSOA acid markers, and effective sharing of standards between labs, the lack of authentic standards limits quantitative ambient observations to only a few BSOA acid markers. Chapter 4 proposed a method of quantification using predicted relative ionisation efficiency (RIE) factors to correct concentrations based on the response curve of *cis*-pinonic acid. These RIE factors were predicted using a random forest model developed from RIE measurements of a range of readily available authentic

organic acids.

In this study we use an organic acid marker library developed in Chapter 4 to screen 800 extracted PM_{2.5} samples from three contrasting megacities (Beijing, Delhi and Guangzhou). BSOA acid markers were retention time matched to structurally confirmed markers in chamber generated BSOA samples, before being quantified using the RIE method outlined in Chapter 4. This study represents to our knowledge the largest ambient study of biogenic organic acid markers to date and provides insight into atmospheric concentrations across 6 sampling campaigns in 3 urban locations.

6.2 Experimental

6.2.1 Biogenic secondary organic aerosol generation

BSOA was generated via an aerosol flow reactor as discussed in chapter 4 section 4.3.2.[359] BSOA was generated from α -pinene, limonene and β -caryophyllene and known markers were identified in the samples for the development of a library.

6.2.2 Filter Sampling

Filter samples were collected using an Ecotech HiVol 3000 (Ecotech, Australia) high-volume air sampler with a selective PM_{2.5} inlet. Filters (Whatman QMA, 10" by 8") were baked at 500 °C for 5 h before use. After collection, samples were wrapped in foil, stored at -20 °C and then shipped to the laboratory for analysis.

6.2.2.1 Beijing

Samples were collected during winter (9th November – 9th December 2016, n = 124) and summer (18th May and 24th June 2017, n = 193) at the Institute of Atmospheric Physics (IAP) in Beijing, China. This sampling was part of Natural Environmental Research Council's (NERCs) Sources and Emissions of Air Pollutants in Beijing (AIRPOLL-Beijing) project, as part of the wider Atmospheric

Pollution and Human Health (APHH) in a Chinese Megacity programme. [220] Samples were collected at a height of 8 m on top of a building in the IAP complex. Samples were collected every 3 h during the day (between approximately 08:30 and 17:30 LT) and then one sample was collected overnight (between approximately 17:30 and 08:30 LT). Hourly samples were also taken on certain high-pollution days towards the end of the sampling period during summer. The site was located between the fourth and third north ring roads of Beijing in a residential area. To the south, north, and west ends there are roads about 150 m away. The Olympic forest park is several kilometres to the north.

6.2.2.2 Delhi

Samples were collected as part of the Delhi Flux campaign funded as part of NERCs APHH-India campaign, at the Indira Gandhi Delhi Technical University for Women in New Delhi, India. Aerosol samples were collected during a pre-monsoon campaign (28th May – 5th June, n = 35) and post-monsoon (9th October – 6th November, n= 108). Samples were collected every 3 h during the day (between approximately 08:30 and 17:30 LT) and then one sample was collected overnight (between approximately 17:30 and 08:30 LT). The site is situated inside the third ring road, with a major road to the east, between the site and the Yamuna river. Two train stations are located to the south and south west of the site, and there are several green spaces locally in all directions.

6.2.2.3 Guangzhou

Samples were collected as part of NERCs APHH-NITRO-PM project in Guangzhou, China at the Guangzhou Institute for Geochemistry (GIG). Samples were collected during summer (31st July – 23rd August 2019, n = 146) and winter (20th November – 12th December 2019, n = 168) campaigns. The sampling took place on top of a 12-story mixed use office and laboratory building. The site was surrounded by residential buildings, with a 6-lane road 500 m to the south and a forest park 4km to the north. Filter samples were collected 8 times a

day on most days; 06:00-08:00, 08:00-10:00, 10:00-13:00, 13:00-15:00, 15:00-17:00, 17:00-19:00, 19:00-21:00, 21:00-06:00 LT. On some days, lower resolution samples were collected due to extreme weather conditions, including Tropical Cyclone Wipha between 1st and 3rd August 2019.

6.2.3 Extractions

Using a standard square filter cutter, an aliquot of filter was taken, which was then cut into roughly 1 cm² pieces and stored in a 20 mL glass vial. The size of the filter aliquot was different for each location, Beijing: 38.44 cm², Delhi: 30.25 cm², Guangzhou: 47.61 cm². Next, 8 mL of LC-MS grade MeOH (Optima, Fisher Chemical, USA) was added to the sample and sonicated for 45 min. Ice packs were used to keep the bath temperature below room temperature, with the water swapped mid-way through. Using a 5 mL plastic syringe, the MeOH extract was then pushed through a 0.22 μ m filter (Millipore) into another sample vial. An additional 2 mL (2 x 1 mL) of MeOH was added to the filter sample, and then extracted through the filter to give a combined extract \sim 10mL. This extract was then reduced to dryness using a Genevac vacuum concentrator. The dry sample was then reconstituted in 50:50 MeOH:H₂O (Optima, Fisher Chemical, USA) for analysis. The extraction efficiency of *cis*-pinonic acid was determined to be 99 \pm 15 % (mean \pm δ , 3 replicates) through spiking the standard onto a pre-baked clean filter and following the same extraction procedure. [125, 250]

6.2.4 Ultra-high performance liquid chromatography tandem mass spectrometry (UHPLC-MS²)

The extracted fractions of the filter samples were analysed using an Ultimate 3000 UHPLC (Thermo Scientific, USA) coupled to a Q Exactive Orbitrap MS (Thermo Fisher Scientific, USA) using data dependent tandem mass spectrometry (ddMS²) with heated electrospray ionization source (HESI). The UHPLC method uses a reversed-phase 5 μ m, 4.6 mm \times 100 mm, polar end capped Accucore column

(Thermo Scientific, UK) held at 40 °C. The mobile phase consisted of water (A) and methanol (B) both with 0.1% (v/v) of formic acid (98% purity, Acros Organics). Gradient elution was used, starting at 90 % (A) with a 1-minute post-injection hold, decreasing to 10 % (A) at 26 minutes, returning to the starting mobile phase conditions at 28 minutes, followed by a 2-minute hold allowing the re-equilibration of the column. The flow rate was set to 0.3 mL min⁻¹. A sample injection volume of 4 μL was used. The capillary and auxiliary gas heater temperatures were set to 320 °C, with a sheath gas flow rate of 45 (arb.) and an auxiliary gas flow rate of 20 (arb.). Spectra were acquired in the negative ionization mode with a scan range of mass-to-charge (m/z) 50 to 750. Accurate quantification of BSOA is difficult owing to a lack of authentic standards. This study employs the recently developed relative ionisation efficiency model developed in chapter 5 based on the structure of a compound. A 9-point *cis*-pinonic acid calibration ($R^2 > 0.99$) was run alongside the ambient filters and was used for the quantification of the identified markers. The quantification was achieved using the proxy standard and then corrected by dividing by the predicted RIE factors as shown in Table 5.3. This method accounts for the differences in ionisation efficiencies of the different markers.

6.2.5 Matrix Effects

Previous studies have highlighted that matrix effects associated with complex PM_{2.5} samples can suppress signal intensity of SOA markers.[125, 184, 250] The matrix effect of the ambient samples on the signal response of a range of organic acids across different RT windows was evaluated. The measured signal intensity of a series of acid standard compounds in a blank solvent matrix were compared to the signal obtained for the same concentration in the ambient aerosol extract matrix. A 10 μL mixture (50:50, MeOH: H₂O) containing 1,2,4-butane carboxylic acid, 3,3-dimethyl glutaric acid, maleic acid, *cis*-pinonic acid and sebacic acid at 10 ppm was spiked into either 100 μL of ambient filter sample extract or into 100

μL of blank 50:50 (MeOH:H₂O) solvent. The peak areas of the compounds were then determined in the spiked samples as well as the ambient samples. The matrix effect factor was then calculated by taking the compound area from the spiked ambient sample, subtracting the area of the compound in the ambient sample, and then dividing by the compound area in the spiked blank matrix. The matrix effect was only investigated at 1ppm, not over a range of concentrations, as such different matrix effects could be observed at higher or lower concentrations. If no matrix effect was present the ratio is equal to 1. Table 6.1 shows the ratios across 23 ambient samples collected throughout the 6 campaigns, which represent a mixture of high and low PM_{2.5} concentrations across different times of day. Overall, *cis*-pinonic acid showed the smallest matrix effect across the three locations, on average only a 2 % suppression was observed, although up to 42 % in Delhi. 1,2,4-butane tricarboxylic acid and Maleic acid were on average observed to have a matrix enhancement, suggesting that the matrix is facilitating the ionisation of these species. In some Guangzhou and Delhi samples over a 100 % (i.e a ratio of 2 or more) matrix enhancement was observed. This could be due to the acidity of the aerosol samples collected, enhancing ionisation efficiency, although further work is needed to understand this. The large variations across the standards and the samples highlights the uncertainty associated with MS quantification when using highly complex samples such as PM_{2.5}. Overall significant uncertainty in the matrix effects is observed, both across compounds and samples. Significant work is needed to further understand these matrix effects and our ability to account for them and potentially predict them for more accurate quantification. Future work should focus on using authentic standards for matrix effect determination and across a range of concentrations. Overall, the uncertainties from these matrix effects are less than the differences in ionisation efficiencies discussed in the previous chapters, but still significant for quantification.

Table 6.1: Measured matrix effects of 5 organic acids with their respective retention times (RT) across 23 ambient samples collected across the Delhi, Guangzhou and Beijing campaigns. A value of 1 represents no matrix effect, below 1 is a matrix suppression and above 1 a matrix enhancement. Campaign mean \pm SD and overall mean \pm SD for each sampling site and all samples are shown in bold.

| Sample ID | BTCA (RT = 1.23) | DMGA (RT = 4.43) | MA (RT = 0.75) | PA (RT = 8.0) | SA (RT = 13.14) |
|---------------------|------------------------------------|------------------------------------|-----------------------------------|-----------------------------------|-----------------------------------|
| S30 | 0.98 | 0.80 | 1.08 | 0.74 | 0.79 |
| S43 | 0.75 | 0.72 | 0.89 | 0.68 | 0.71 |
| S53 | 1.07 | 0.87 | 1.96 | 0.58 | 0.77 |
| 12 | 1.13 | 1.00 | 0.89 | 0.91 | 0.91 |
| 29 | 1.46 | 1.21 | 1.20 | 1.13 | 1.18 |
| Delhi Avg. | 1.08 \pm 0.26 | 0.92 \pm 0.19 | 1.20 \pm 0.44 | 0.81 \pm 0.22 | 0.87 \pm 0.19 |
| 9 | 1.04 | 0.88 | 0.97 | 0.83 | 0.87 |
| 129 | 0.89 | 0.79 | 0.74 | 0.90 | 0.91 |
| 132 | 0.96 | 0.88 | 0.69 | 0.88 | 0.90 |
| 165 | 1.38 | 0.94 | 1.35 | 0.84 | 0.86 |
| 185 | 2.04 | 1.04 | 1.99 | 1.15 | 0.82 |
| 237 | 1.35 | 0.90 | 0.92 | 0.69 | 0.82 |
| 258 | 1.44 | 0.95 | 1.55 | 1.68 | 0.86 |
| 267 | 1.12 | 0.87 | 0.77 | 0.73 | 0.83 |
| GZ Avg. | 1.28 \pm 0.37 | 0.91 \pm 0.07 | 1.12 \pm 0.46 | 0.96 \pm 0.32 | 0.86 \pm 0.03 |
| 12 | 1.05 | 0.98 | 1.42 | 0.95 | 0.95 |
| 49 | 1.02 | 0.94 | 1.00 | 0.87 | 0.88 |
| 71 | 0.90 | 0.95 | 1.11 | 0.86 | 0.85 |
| 76 | 1.02 | 0.98 | 1.36 | 0.94 | 0.94 |
| 133 | 1.87 | 1.04 | 1.38 | 1.41 | 0.89 |
| 155 | 1.06 | 1.00 | 0.67 | 1.32 | 0.99 |
| 162 | 1.48 | 0.97 | 1.46 | 0.88 | 0.83 |
| 181 | 1.14 | 0.97 | 0.92 | 1.01 | 0.89 |
| 278 | 1.96 | 0.99 | 1.28 | 1.54 | 0.90 |
| 318 | 1.14 | 0.97 | 1.31 | 1.03 | 0.95 |
| Beijing Avg. | 1.26 \pm 0.38 | 0.98 \pm 0.03 | 1.19 \pm 0.46 | 1.08 \pm 0.32 | 0.91 \pm 0.03 |
| Total Avg. | 1.23 \pm 0.35 | 0.94 \pm 0.10 | 1.17 \pm 0.36 | 0.98 \pm 0.28 | 0.88 \pm 0.10 |

6.2.6 Data processing and compound library

A mass spectral library containing 25 BSOA acid markers (Table 6.3) was built as discussed in Chapter 5 using the compound database function in Tracefinder 4.1 General Quan software (Thermo Fisher Scientific, USA). To build the library, compounds from previous chamber studies[190, 260, 357, 364–366] were searched for in SOA samples reacted in the York aerosol flow reactor using the Xcalibur software. [359] Peaks were then either matched to structures based on the retention times of authentic standards, or tandem mass spectrometry ion peaks. The compound was then input into the compound library in the generic form: $C_cH_hO_oN_nS_s$ (where c,h,o,n,s represent the number of carbon, hydrogen, oxygen, nitrogen and sulfur atoms respectively). The UHPLC/ESI-HR-MS data for each standard and ambient sample were analysed using Tracefinder general Quan software (Thermo Fisher Scientific). Blank subtractions were undertaken for all ambient samples, using a field blank. Tracefinder extracted compound peak areas from each sample based on the assigned library. The mass tolerance of the method was set to 3 ppm, with the RT window set to 10 s. The peak tailing factor was set to 2.0 and the detection algorithm used was Icis, with a nearest RT detection strategy. Minimum signal-to-noise (S/N) for a positive identification was set to 3.0. The suitability of the peak was also assessed for a positive identification, with the peak height at which to compare symmetry of the left and right side of the peaks set to 40 % and symmetry threshold which is the minimum percentage difference considered symmetrical set to 70 %.

6.2.7 Supplementary measurements

Gas-phase measurements of NO, NO₂ and O₃ were collected alongside the filter samples at each site. Methodologies have been outlined previously in publications for Beijing[220], Delhi [324] and Guangzhou[250]. Ion chromatography was utilised to measure inorganic ion concentrations using the filters collected across each location with methodologies discussed previously.[281] VOC measurements were

Table 6.2: Mean \pm SD values for gas phase pollutants, inorganic ions and meteorological parameters across the 6 campaigns.

| Gas phase pollutants | Beijing | | Guangzhou | | Delhi | |
|--|------------|------------|------------|------------|------------|------------|
| | Summer | Winter | Summer | Winter | Pre-mon. | Post-mon. |
| NO (ppbv) | 40.6 \pm | 4.5 \pm | 5.7 \pm | 12.1 \pm | 18.5 \pm | 123 \pm |
| | 46.5 | 10.6 | 10.4 | 22.6 | 66.2 | 185 |
| NO ₂ (ppbv) | 36.4 \pm | 21 \pm | 26.8 \pm | 28.9 \pm | 31.1 \pm | 44.7 \pm |
| | 17.2 | 12.5 | 15.1 | 20.6 | 18.7 | 24.8 |
| O ₃ (ppbv) | 54.0 \pm | 8.8 \pm | 42 \pm | 33.1 \pm | 50.3 \pm | 24.5 \pm |
| | 37.5 | 9.1 | 37.3 | 28.0 | 31.1 | 30.6 |
| Inorganic ions | | | | | | |
| SO ₄ ²⁻ ($\mu\text{g m}^{-3}$) | 13.3 \pm | 10.8 \pm | 5.6 \pm | 7.8 \pm | 16.5 \pm | 16.9 \pm |
| | 10.4 | 7.3 | 3.7 | 6.0 | 3.4 | 4.6 |
| NO ₃ ($\mu\text{g m}^{-3}$) | 17 \pm | 9.9 \pm | 3.6 \pm | 6.1 \pm | 8.3 \pm | 13.4 \pm |
| | 14.6 | 6.0 | 3.0 | 6.1 | 1.6 | 8.4 |
| NH ₄ ⁺ ($\mu\text{g m}^{-3}$) | 9.3 \pm | 3.2 \pm | NA | NA | 4.3 \pm | 5.9 \pm |
| | 9.2 | 3.0 | | | 1.4 | 4.8 |
| Met parameters | | | | | | |
| Temp ($^{\circ}\text{C}$) | 5.7 \pm | 26.6 \pm | 30.4 \pm | 18.3 \pm | 35.8 \pm | 24.7 \pm |
| | 3.9 | 5.1 | 2.86 | 4.2 | 4.5 | 4.6 |
| RH (%) | 50.3 \pm | 51.2 \pm | 77.6 \pm | 40.6 \pm | 39.4 \pm | 57.3 \pm |
| | 21.5 | 22.0 | 10.6 | 14.7 | 13.6 | 16.6 |

conducted during the Beijing[125, 375] and Delhi [309, 324] campaigns as outlined previously. Meteorological measurements were collected as outlined previously in Beijing (Chapter 2), Delhi (Chapter 4) and Guangzhou (Chapter 3). Mean concentrations and values across the 6 campaigns are given in Table 6.2.

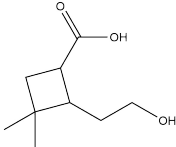
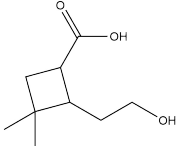
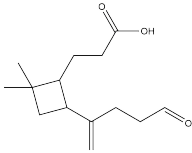
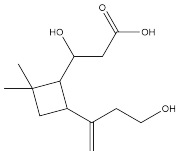
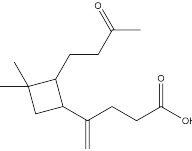
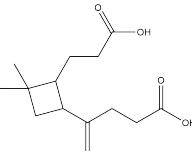
6.3 Results

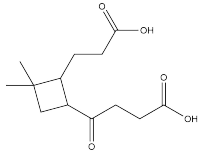
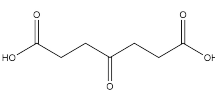
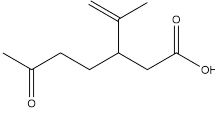
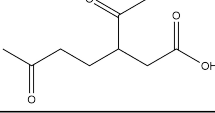
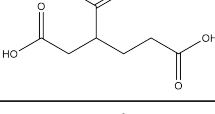
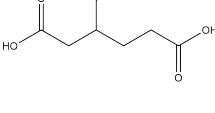
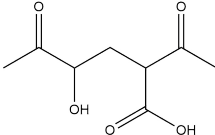
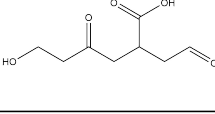
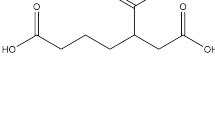
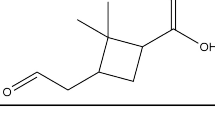
6.3.1 Aerosol Composition

In total 774 filters across the 6 campaigns were screened for organic acids using the mass spectral library. All 25 marker compounds were identified in at least one of the campaigns, however many of the organic acids were only identified in a limited number of samples. Tables Table 6.4–Table 6.8 contain the time-averaged mean concentrations of the markers and the number of observations. Only detected datapoints were included in the time-averages, with non-detected

data point omitted. Structures, molecular formulas, retention times and references are shown in Table 6.3. β -caryophyllinic acid (Bcary_253b, C₁₄H₂₂O₄) was identified in the most samples (N= 657). In contrast, Bcary_237 (C₁₄H₂₂O₃) was only identified in 3 of the 774 filters. Beijing summer and post-monsoon Delhi had similar total time averaged BSOA acid concentrations of 31.3 and 30.3 ng m⁻³ respectively. Wintertime Beijing had significantly lower time averaged BSOA acid concentrations of 5.4 ng m⁻³ than the other observations. Figure 6.1 shows the average composition of the 25 BSOA acids measured across the 6 campaigns. Limonene derived acids contributed 47.2 % of the observed acid mass across the six campaigns, ranging from 37.4 - 59.3 % and was the dominant targeted BSOA acid class in Beijing and Delhi. α -pinene derived acids contributed 34.0 % to the time averaged total BSOA acid mass across the 6 campaigns, with individual campaigns ranging from 17.7-55.6 %. β -caryophyllene derived acids contributed the least to total time averaged BSOA across the 6 campaigns, with an average contribution of 18.8 %, ranging from 7-35.6 %. Unfortunately, monoterpene concentrations were only measured during the Delhi campaigns, but showed strong seasonality as discussed in Chapter 4. Interestingly, both α -pinene and limonene were observed to have much higher concentrations during the post-monsoon campaign. The α -pinene mixing ratio averaged 0.034 ± 0.011 ppbv during the pre-monsoon campaign and 0.10 ± 0.11 ppbv during the post monsoon period. Limonene averaged 0.01 ± 0.02 ppbv and 0.42 ± 0.51 ppbv across the pre- and post-monsoon campaigns, respectively.

Table 6.3: BSOA acid markers identified in chamber samples and screened for in ambient samples.

| Tag | Name | Structure | MF | RT | RIE | Ref. |
|---------------|--|---|-------------------|-------|-------|-------|
| Bcary 171b | 2-(2-hydroxy-ethyl)-3,3-dimethyl-cyclobutane-carboxylic acid |  | $C_9H_{16}O_3$ | 9.84 | 5.88 | [366] |
| Bcary 197 | 3,3-dimethyl-2-(3-oxobutyl)-cyclobutane-carboxylic acid |  | $C_{11}H_{18}O_3$ | 12.58 | 0.83 | [366] |
| Bcary 237 | 3-[2,2-dimethyl-4-(1-methylene-4-oxo-butyl)-cyclobutyl]-propionic acid |  | $C_{14}H_{22}O_3$ | 17.44 | 0.75 | [366] |
| Bcary 241 | 3-hydroxy-3-[4-(3-hydroxy-1-methylene-propyl)-2,2-dimethylcyclobutyl]-propionic acid |  | $C_{13}H_{22}O_4$ | 9.72 | 9.73 | [366] |
| Bcary 251b | β -caryophyllonic acid |  | $C_{15}H_{24}O_5$ | 18.14 | 1.01 | [366] |
| Bcary 253b | β -caryophyllinic acid |  | $C_{14}H_{22}O_4$ | 12.97 | 15.47 | [366] |

| Tag | Name | Structure | MF | RT | RIE | Ref. |
|---------------|--|---|-------------------|-------|-------|-------|
| Bcary 255a | 4-(2-(2-carboxyethyl)-3,3-dimethylcyclobutyl)-4-oxobutanoic acid |  | $C_{13}H_{20}O_5$ | 11.95 | 10.24 | [366] |
| Lim 173a | ketonorlimonic acid |  | $C_7H_{10}O_5$ | 1.28 | 5.78 | [365] |
| Lim 183 | Limononic acid |  | $C_{10}H_{16}O_3$ | 9.47 | 0.38 | [365] |
| Lim 185a | keto Limononic acid |  | $C_9H_{14}O_4$ | 2.97 | 0.61 | [365] |
| Lim 185b | Limonic acid |  | $C_9H_{14}O_4$ | 7.96 | 4.55 | [365] |
| Lim 187a | 3-Acetylhexanedioic acid |  | $C_8H_{12}O_5$ | 1.35 | 4.72 | [365] |
| Lim 187b | 3-Hydroxy-2-butanone |  | $C_8H_{12}O_5$ | 1.85 | 1.18 | [365] |
| Lim 187c | (2-oxoethyl)-hexanoic acid |  | $C_8H_{12}O_5$ | 3.04 | 0.92 | [365] |
| Lim 203 | pentane-1,2,5-tricarboxylic acid |  | $C_8H_{12}O_5$ | 1.11 | 5.66 | [365] |
| Pin 169 | Pinalic acid |  | $C_9H_{14}O_3$ | 6.66 | 0.66 | [357] |

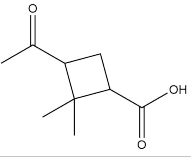
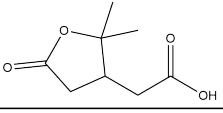
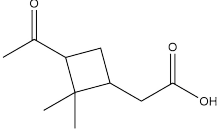
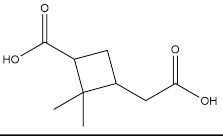
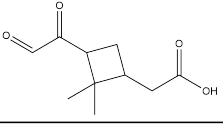
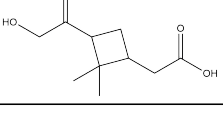
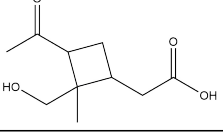
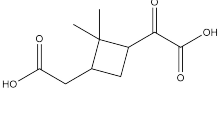
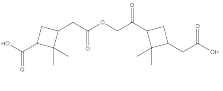
| Tag | Name | Structure | MF | RT | RIE | Ref. |
|----------|---|---|--|-------|------|-------|
| Pin 171a | Norpinonic acid |  | C ₈ H ₁₂ O ₄ | 4.89 | 1.31 | [357] |
| Pin 171b | Terpenylic acid |  | C ₈ H ₁₂ O ₄ | 3.11 | 2.51 | [357] |
| Pin 183 | <i>cis</i> -Pinonic acid |  | C ₁₀ H ₁₆ O ₃ | 8.35 | 1.00 | [357] |
| Pin 185a | Pinic acid |  | C ₉ H ₁₄ O ₄ | 6.34 | 5.93 | [357] |
| Pin 197 | Oxopinonic acid |  | C ₁₀ H ₁₄ O ₄ | 3.39 | 0.85 | [357] |
| Pin 199a | 10-hydroxy-pinonic acid |  | C ₁₀ H ₁₆ O ₄ | 4.49 | 7.26 | [357] |
| Pin 199b | 8-hydroxy-pinonic acid |  | C ₁₀ H ₁₆ O ₄ | 5.59 | 3.50 | [357] |
| Pin 213 | 2-[3-(carboxymethyl)-2,2-dimethylcyclobutyl]-2-oxoacetic acid |  | C ₁₀ H ₁₄ O ₅ | 3.39 | 5.07 | [357] |
| Pin 367 | Pinonyl-pinylnyl ester |  | C ₁₉ H ₂₈ O ₇ | 14.81 | 7.15 | [357] |

Figure 6.2 shows the corPlot (openair, R package [376]) for BSOA acid markers identified and quantified in more than 30 % of the samples (30 % still allowed for significant number of markers to be analysed, while having enough data to

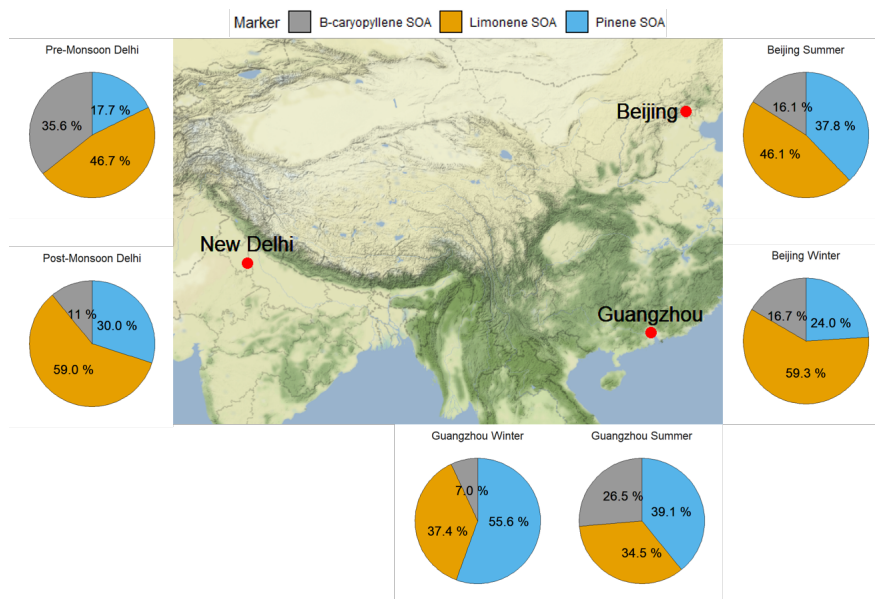


Figure 6.1: Map of filter sampling sites with pie charts highlighting the targeted BSOA acid mass composition.

undertake the analysis) analysed across the six campaigns in this study, where the numbers represent the pearson coefficient, i.e 80 equals an R of 0.8. As such, markers below the detection limit in some samples were omitted. Across the 6 campaigns, moderate ($R > 0.6$) correlations were observed between some of the α -pinene derived markers as well as to both limonene and β -caryophyllene derived markers as shown in Figure 6.2. *cis*-pinonic acid (Pinene_183, $C_{10}H_{16}O_3$) showed a moderate ($R=0.67$) correlation towards pinic acid (Pinene_185a, $C_9H_{14}O_4$), like that observed previously in Belgium ($R = 0.78$)[374], highlighting their common formation conditions. Pinic acid showed moderate correlation ($R = 0.72$) towards Terpenylic acid (pinene_171b, $C_8H_{12}O_4$), as seen previously in Belgium ($R = 0.68$).[374] Terpenylic acid showed moderate correlations towards ketonorlimonic acid (Lim_173a, $C_7H_{10}O_5$) (0.79) and Ketolimonic acid (Lim_187a, $C_8H_{12}O_5$) (0.7). Norpinonic acid (pinene_171a, $C_8H_{12}O_4$) also showed a moderate ($R = 0.63$) correlation towards ketonorlimonic acid. Moderate correlations between limonene markers identified in more than 30 % of samples were also observed across the 6 campaigns as shown in Figure 6.2. The strongest correlation was observed between Ketolimonic (Lim_185a, $C_9H_{14}O_4$) and ketonorlimonic acid (Lim_173a, $C_7H_{10}O_5$)

($R = 0.83$), moderate correlations were also observed between ketonorlimonic and Limonic acid (Lim_185b, $C_9H_{14}O_4$) ($R = 0.6$), Limonic acid and Limononic acid (Lim_183, $C_{10}H_{16}O_3$) ($R = 0.75$), Limononic acid and Limonic acid ($R = 0.75$), suggesting similar formation pathways and conditions. Moderate correlations were also observed between these limonene markers and Terpenylic acid, Norpinonic acid and β -caryophyllinic acid (B_253b, $C_{14}H_{22}O_4$).

Only three β -caryophyllene markers (255a:4-(2-(2-carboxyethyl)-3,3-dimethylcyclobutyl)-4-oxobutanoic acid, 253b: β -caryophyllinic acid and 197:3,3-dimethyl-2-(3-oxobutyl)cyclobutanecarboxylic acid) were identified in >30 % of all samples as shown in Figure 6.2. None of the β -caryophyllene markers showed moderate correlations to each other, however β -caryophyllinic acid did correlate moderately to Limononic acid ($R = 0.72$), Limonic acid (0.61) and ketonorlimonic acid ($R = 0.64$).

The BSOA acid markers identified in more than 30 % of the samples as shown in Figure 6.2 were summed and the total concentrations shown in Figure 6.3. Figure 6.3 highlights the differences in mean concentrations of the sum of these species and distributions of the measurements across each campaign. Larger variations in concentrations were observed during the Beijing summer campaign, compared to the winter campaign. Wide distributions were observed for the α -pinene and Limonene markers across the majority of the campaigns, with a narrower distribution during the Beijing winter campaign, where significantly lower concentrations were observed. Narrower distributions in comparison to the other classes of the β -caryophyllene derived BSOA acid concentrations were observed across the majority of the campaigns, but a wide distribution was observed in Guangzhou summer. Overall seasonal differences can be observed across the different marker classes. Higher BSOA acid concentrations were observed in Beijing summer in comparison to the winter campaign across the three classes. On average, higher α -pinene and Limonene marker concentrations were observed during the Delhi post-monsoon campaign compared to the pre-monsoon, but the opposite was observed for the β -caryophyllene markers.

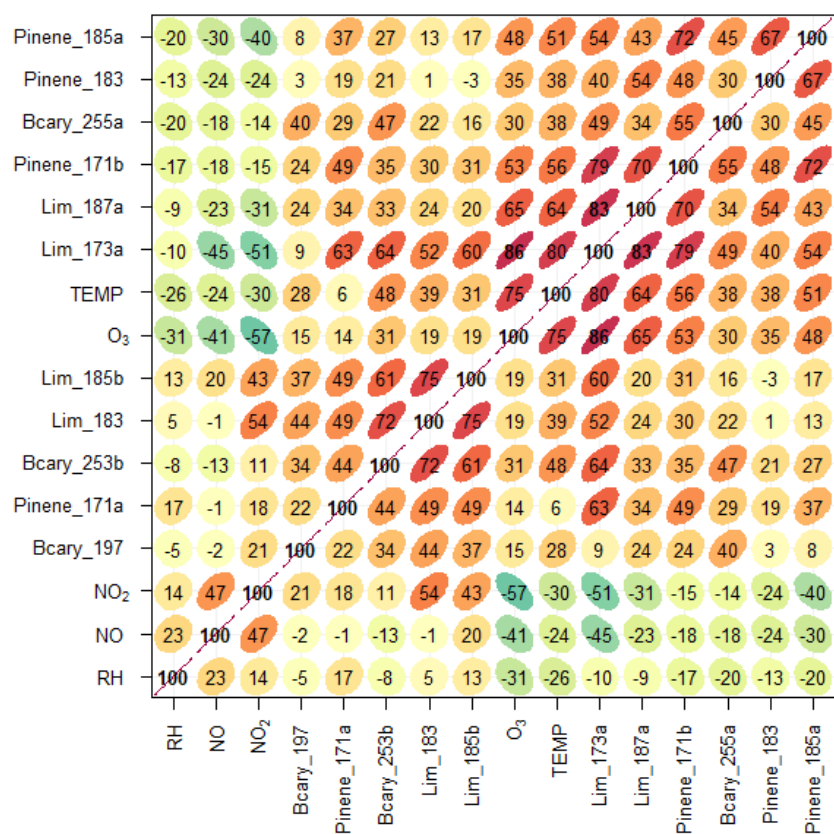


Figure 6.2: corPlot of BSOA acid markers identified in 30 % of the total samples across the 6 campaigns, alongside temperature (TEMP), ozone (O₃), NO₂, NO and relative humidity (RH).

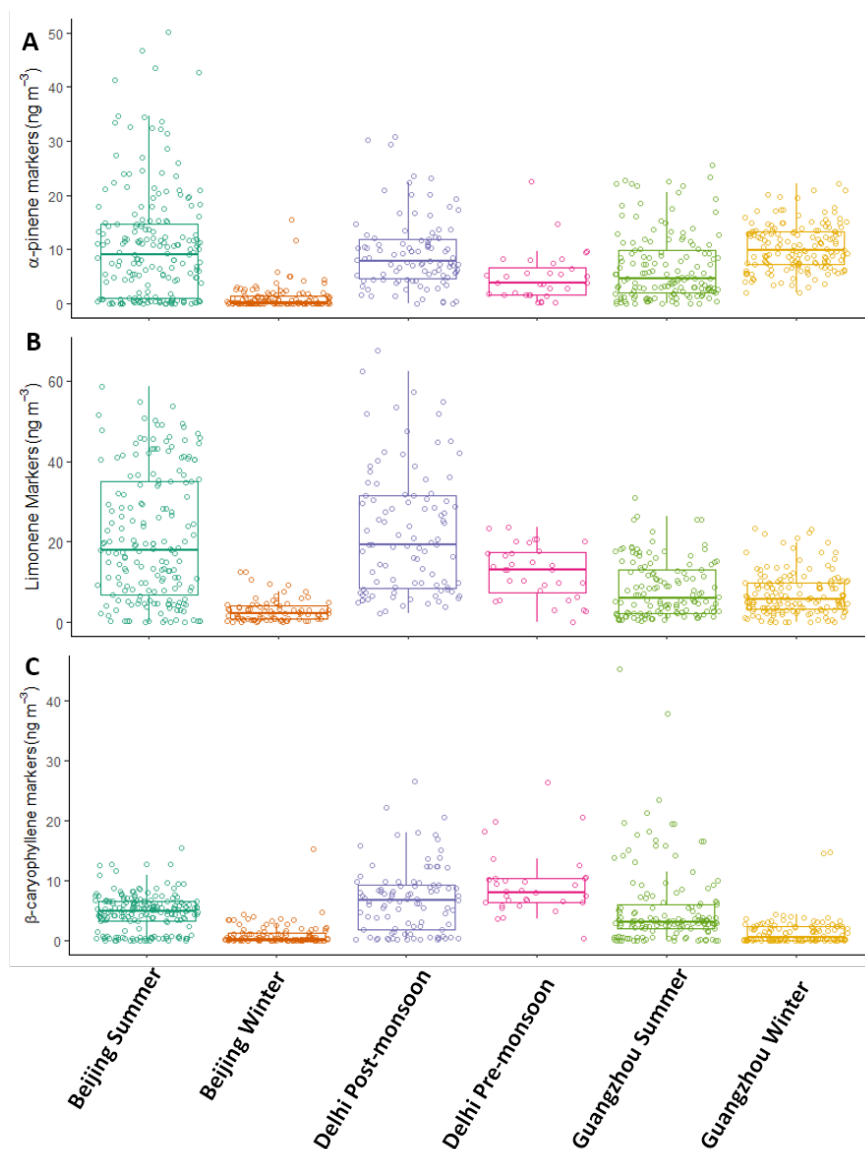


Figure 6.3: Boxplots of the sum of A- *cis*-Pinonic, *cis*-Pinic, Terpenylic and Norpinonic acids, B- Ketolimonic, ketonorlimonic, Limonic and Limononic acids and C - three β -caryophyllene markers (255a-4-(2-(2-carboxyethyl)-3,3-dimethylcyclobutyl)-4-oxobutanoic acid, 253b- β -caryophyllinic acid and 197-3,3-dimethyl-2-(3-oxobutyl)cyclobutanecarboxylic acid). The lower and upper part of the box represents the 25th and 75th percentiles, with the upper and lower lines extending no further than 1.5 * the interquartile range of the highest and lowest values within the line respectively. All observations are plotted as scattered points on top of the boxplots to highlight the distributions of concentrations within each campaign. Limonene BSOA acid marker concentrations were filtered to remove one high concentration sample (77 ng m⁻³ during the Guangzhou winter campaign).

6.3.2 α -pinene markers

Ten α -pinene derived acids were identified in at least one of the 6 campaigns in this study (Table 6.4). *cis*-pinonic acid (Pinene_183, C₁₀H₁₆O₃) and pinic acid (Pinene_185a, C₉H₁₄O₄) were the most identified markers across campaigns. *cis*-pinonic acid is one of the most studied organic acid markers and has been quantified across a variety of ambient environments including Asia, Europe and the Arctic.[271, 373, 377–382] The highest average *cis*-pinonic acid concentrations were observed in Guangzhou winter ($6.2 \pm 4.3 \text{ ng m}^{-3}$, n = 158) in comparison to the lowest which was observed in Beijing winter ($0.77 \pm 1.5 \text{ ng m}^{-3}$ n = 38). Pinic acid concentrations on average were lower than *cis*-pinonic acid and ranged from $0.14 \pm 0.16 \text{ ng m}^{-3}$ (n = 87) in Beijing winter to $1.0 \pm 0.6 \text{ ng m}^{-3}$ (n = 174) in Beijing summer. There is a lack of recent LC-MS studies quantifying *cis*-pinonic and pinic acids in the ambient atmosphere, with many recent studies using GC-MS with derivatisation as shown in Table 6.5. Across the 16 LC-MS/GC-MS measurements compiled in Table 6.5, the lowest *cis*-pinonic acid concentrations were observed in Beijing winter of this study with a time averaged concentration of $0.77 \pm 1.45 \text{ ng m}^{-3}$ (n = 38), compared to the highest observed in Guangzhou in 2012 ($30 \pm 8.1 \text{ ng m}^{-3}$) by Ren et al., 2018 using GC-MS.[383] Other LC studies did not take into account differences in ionisation efficiencies and did not investigate the effect of matrix effects on the concentrations of the acid species, while the GC methodology required the additional complexity of derivatisation. Pinic acid concentrations were generally much lower across the previous studies at the same sampling sites. The highest pinic acid concentrations were observed in a summertime Delhi campaign undertaken by Mahilang et al., 2021, with an average concentration of $8.80 \pm 3.93 \text{ ng m}^{-3}$.[380] This is in comparison to 0.28 ± 0.2 (n = 32) and 0.24 ± 0.2 (n = 64) ng m^{-3} observed in this study across pre- and post-monsoon Delhi respectively. The lowest observed pinic acid concentrations were observed in Beijing winter of this study ($0.14 \pm 0.16 \text{ ng m}^{-3}$ (n = 87)). Similar pinic acid concentrations were observed in Belgium by Gómez-González

et al., 2012 using LC-MS who used an authentic pinic acid standard.[374]

The dimer, pinonyl-pinyl ester (Pinene_367, C₁₉H₂₈O₇) had the lowest observed concentrations of the α -pinene markers, with time averaged concentrations ranging from 0.01 to 0.05 ng m⁻³. The dimer species have been shown to have high ionisation efficiencies and were predicted to have some of the highest RIE factors (Chapter 4), resulting in low concentrations. Norpinonic (Pinene_171a, C₈H₁₂O₄) and terpenylic acid (Pinene_171b, C₈H₁₂O₄) were observed in all campaigns, however norpinonic acid was only observed in three Beijing winter samples. 8-hydroxy-pinonic acid (Pinene_199b, C₁₀H₁₆O₄) was observed across all campaign (although only 1 sample in Beijing winter) with similar concentrations observed in Guangzhou winter and post-monsoon Delhi (0.41 \pm 0.31 ng m⁻³, n = 27 and 0.42 \pm 0.41 ng m⁻³, n = 78, respectively). 10-hydroxy-pinonic acid (Pinene_199a, C₁₀H₁₆O₄) was also observed across all campaigns, with the highest average concentration observed in Beijing summer (0.4 \pm 0.36, n = 40) and the lowest in Beijing winter (0.07 \pm 0.1, n = 6). Pinalic acid (Pinene_169, C₉H₁₄O₃) had some of the highest α -pinene marker concentrations, with an average concentration of 10.0 \pm 6.0 ng m⁻³ in Guangzhou winter, although was only observed in 10 of the samples. Oxopinonic acid (Pinene_197, C₁₀H₁₄O₄) and 2-[3-(carboxymethyl)-2,2-dimethylcyclobutyl]-2-oxoacetic acid (Pinene_213, C₁₀H₁₄O₅) were only observed in 18 samples each across the 6 campaigns.

Figure 6.4 shows the time series and diurnal variation of the sum of Pinonic, Pinic, Terpenylic and Norpinonic acids, those that were identified in at least 30 % of the samples across the 6 campaigns. These four markers make up a dominant proportion of the α -pinene derived concentrations across the campaigns. In the Beijing and Guangzhou observations, α -pinene derived acid concentrations were similar during the day and night, suggesting that formation occurs throughout the day or that the acids have relatively long atmospheric lifetimes. In contrast in Delhi, a distinct diurnal variation was observed, with α -pinene acid concentrations substantially lower at night compared to during the day. This is in line with the diurnals of OSi/NOSi and OS_{MT} species observed in Chapter 3 in Figure 4.11. α -

Table 6.4: Mean \pm SD for the α -pinene derived organic acid markers identified across the Beijing, Guangzhou and Delhi campaigns with the number of observations in each campaign (n =). *Pinene* is abbreviated to *P* in the marker names.

| Marker | Beijing | | Guangzhou | | Delhi | |
|--------|------------------------------|-----------------------------|------------------------------|------------------------------|-----------------------------|-----------------------------|
| | Summer | Winter | Summer | Winter | Pre-mon. | Post-mon. |
| P_169 | 6.1 \pm 6.5 (n = 7) | NA \pm NA (n = 0) | 9.32 \pm 6.78 (n = 24) | 10.06 \pm 6.06 (n = 10) | 2.41 \pm 0.15 (n = 2) | 3.55 \pm 2.77 (n = 4) |
| P_171a | 2.98 \pm 2.99 (n = 44) | 0.51 \pm 0.13 (n = 3) | 3.16 \pm 2.37 (n = 73) | 2.98 \pm 2.02 (n = 141) | 2.62 \pm 2.06 (n = 22) | 6.52 \pm 5.18 (n = 73) |
| P_171b | 7.92 \pm 4.64 (n = 79) | 1.72 \pm 1.98 (n = 37) | 5.59 \pm 4.46 (n = 65) | 6.3 \pm 3.58 (n = 13) | 5.42 \pm 2.11 (n = 10) | 4.32 \pm 2.54 (n = 70) |
| P_183 | 5.76 \pm 5.17 (n = 142) | 0.77 \pm 1.45 (n = 38) | 1.9 \pm 1.49 (n = 122) | 6.23 \pm 4.31 (n = 158) | 1.17 \pm 0.66 (n = 18) | 1.73 \pm 1.16 (n = 33) |
| P_185a | 0.98 \pm 0.64 (n = 174) | 0.14 \pm 0.16 (n = 87) | 0.41 \pm 0.34 (n = 127) | 0.5 \pm 0.27 (n = 152) | 0.28 \pm 0.2 (n = 32) | 0.24 \pm 0.2 (n = 64) |
| P_197 | NA \pm NA (n = 0) | 0.61 \pm 0.38 (n = 5) | 1.79 \pm 1.35 (n = 9) | NA \pm NA (n = 0) | NA \pm NA (n = 0) | 0.64 \pm 1.09 (n = 4) |
| P_199a | 0.4 \pm 0.36 (n = 40) | 0.07 \pm 0.09 (n = 6) | 0.16 \pm 0.07 (n = 26) | 0.17 \pm 0.13 (n = 60) | 0.1 \pm 0.06 (n = 7) | 0.22 \pm 0.08 (n = 6) |
| P_199b | 0.37 \pm 0.28 (n = 19) | 0.06 \pm NA (n = 1) | 0.07 \pm 0.09 (n = 13) | 0.1 \pm 0.06 (n = 10) | 0.41 \pm 0.31 (n = 27) | 0.42 \pm 0.41 (n = 78) |
| P_213 | 0.44 \pm 0.33 (n = 4) | 0.07 \pm 0.1 (n = 5) | 0.13 \pm 0.13 (n = 4) | 0.10 \pm 0.10 (n = 3) | 0.19 \pm NA (n = 1) | 0.47 \pm NA (n = 1) |
| P_367 | 0.01 \pm 0.05 (n = 5) | 0.02 \pm 0.03 (n = 27) | 0.01 \pm 0.01 (n = 4) | 0.01 \pm NA (n = 1) | NA \pm NA (n = 0) | 0.05 \pm 0.04 (n = 5) |

Table 6.5: Comparison of *cis*-pinonic and pinic acid concentrations between those measured in this study and previously. TS = This study

| Location | Pinonic acid | Pinic acid | Ref | Method |
|------------------------------------|--------------|-------------|-------|--------|
| Changchun, China | 1.1 ± 0.9 | 1.9 ± 2 | [384] | GC-MS |
| Mt Tai, China | 6.4 ± 4.0 | 2.3 ± 1.5 | [385] | GC-MS |
| PRD, China | 3.60 ± 3.76 | 1.25 ± 0.79 | [386] | GC-MS |
| Guangzhou Summer 2012 | 30 ± 8.1 | 3.8 ± 1.2 | [383] | GC-MS |
| Guangzhou Winter 2013 | 22 ± 1.2 | 7.1 ± 0.61 | [383] | GC-MS |
| Beijing Summer | 5.76 ± 5.17 | 0.98 ± 0.64 | [TS] | LC-MS |
| Beijing Winter | 0.77 ± 1.45 | 0.14 ± 0.16 | [TS] | LC-MS |
| Guangzhou Summer | 1.90 ± 1.49 | 0.41 ± 0.34 | [TS] | LC-MS |
| Guangzhou Winter | 6.23 ± 4.31 | 0.50 ± 0.27 | [TS] | LC-MS |
| Post monsoon Delhi 16/17 | 1.16 ± 0.61 | 1.38 ± 0.35 | [380] | GC-MS |
| Delhi Summer 16/17 | 4.18 ± 1.51 | 8.80 ± 3.93 | [380] | GC-MS |
| Delhi Pre-monsoon | 1.17 ± 0.66 | 0.28 ± 0.2 | [TS] | LC-MS |
| Delhi Post-monsoon | 1.73 ± 1.16 | 0.26 ± 0.2 | [TS] | LC-MS |
| Day Sierra Nevada Mountains, USA | 3.66 ± 0.7 | 2.2 ± 0.5 | [387] | GC-MS |
| Night Sierra Nevada Mountains, USA | 27 ± 9.1 | 6.9 ± 2.7 | [387] | GC-MS |
| Belgium | 1.79 | 0.49 | [374] | LC-MS |
| Mainz, Germany | 0.6 ± 1.01 | 1.51 ± 2.24 | [377] | LC-MS |

pinene mixing ratios peaked in the early morning or at night in Delhi (Figure 6.4), with a day-time minimum. However due to a lack of oxidants at night, limited nocturnal formation of acids is expected at this location. During the morning when photochemistry starts to occur, α -pinene undergoes oxidation with OH radicals, leading to the increased concentration of α -pinene derived acids in the particle phase. Significant variations in distributions were observed in Figure 6.3, ranging from below LOD to around 50 ng m^{-3} . Across the 6 campaigns, periods of low and high concentrations were observed. During the early part of the Beijing summer campaign, very low α -pinene derived acid concentrations were observed, in line with low NO concentrations ($< 5 \text{ ppbv}$). The early part of the Guangzhou summer campaign was influenced by typhoon Wipha, in-line with lower α -pinene acid concentrations.

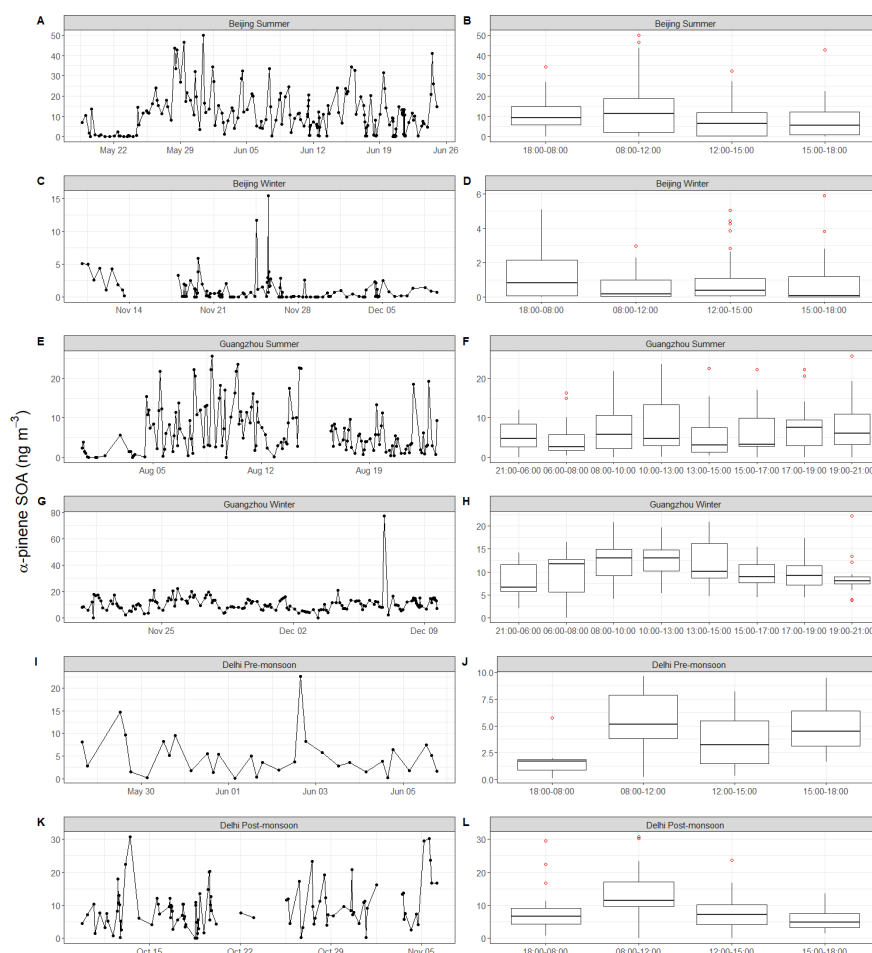


Figure 6.4: Time series and diurnal variations of the sum of the α -pinene derived BSOA acid markers: *cis*-Pinonic, Pinic, Terpenylic and Norpinonic acids across the Beijing, Guangzhou and Delhi campaigns. The lower and upper part of the box represents the 25th and 75th percentiles, with the upper and lower lines extending no further than 1.5 \times the interquartile range of the highest and lowest values within the line respectively.

6.3.3 Limonene markers

Eight limonene markers were identified across the 6 campaigns as shown in Table 6.6. Limononic acid (Lim_183, $C_{10}H_{16}O_3$) was identified in 3 campaigns, with similar time averaged concentrations in Guangzhou winter and pre-monsoon Delhi ($4.4 \pm 2.8 \text{ ng m}^{-3}$, $n = 110$ and $4.8 \pm 3.6 \text{ ng m}^{-3}$, $n = 26$,) respectively), while higher concentrations were observed in post-monsoon Delhi ($14.3 \pm 13.3 \text{ ng m}^{-3}$, $n = 71$). Limonic acid (Lim_185b, $C_9H_{14}O_4$) concentrations were observed to be an order of magnitude lower than limononic acid, with campaign average concentrations ranging $0.1 - 0.6 \text{ ng m}^{-3}$. Limonic acid has been shown previous in chamber studies to have a low yield, although limononic acid yields have not been measured to date.[388] These concentrations are roughly half of those observed previously in a Boreal Forest in Finland using LC-MS and an authentic standard ($0.6-1.7 \text{ ng m}^{-3}$).[373] Limonic acid has also previously been quantified in Belgium with average day and night concentrations of 0.62 and 1.38 ng m^{-3} respectively using LC-MS with *cis*-pinonic acid as a surrogate standard.[374] Ketolimonic acid (Lim_187a, $C_8H_{12}O_5$) was observed across both Beijing and Delhi campaigns with campaign average concentrations between 0.6 and 6.7 ng m^{-3} . Seasonal differences showed significant enhancement in Beijing during summer ($6.7 \pm 5.1 \text{ ng m}^{-3}$, $n = 138$) compared to winter ($0.6 \pm 0.6 \text{ ng m}^{-3}$, $n = 43$). Lower concentrations were observed in Corsica, 0.15 ng m^{-3} using GC-MS.[389] Ketonorlimonic acid (Lim_173a, $C_7H_{10}O_5$) was observed across the Beijing and Guangzhou campaigns, with campaign averages ranging from $1.9 - 14.1 \text{ ng m}^{-3}$. Again, significant seasonal differences in concentrations were observed between the Beijing summer ($14.1 \pm 9.5 \text{ ng m}^{-3}$, $n = 102$) and winter ($1.9 \pm 2.1 \text{ ng m}^{-3}$, $n = 45$) campaigns. Ketonorlimonic was previously quantified in Corsica with a concentration of 0.2 ng m^{-3} using pinic acid as a proxy standard using GC-MS.[389] Lim_187b ($C_8H_{12}O_5$) had the highest time-averaged concentration ($28.45 \pm 17.71 \text{ ng m}^{-3}$) of any marker quantified in this study during summertime Beijing, however it was only observed in eight filter samples, with high concentrations ($> 45 \text{ ng m}^{-3}$)

observed towards the end of the campaign. High total limonene derived acid concentrations were observed during the same period as shown in Figure 6.5 as well as high concentrations of isoprene derived OS as shown in Figure 2.9. Lim_187c ($C_8H_{12}O_5$) was also only observed in Beijing in a limited number of samples, but in high concentrations in summer. These two isomers have been shown to form from the reaction of ozone with limonic acid.[388] The aging of limonic acid to further markers could therefore explain the low concentrations of limonic acid observed across the campaigns. The high concentrations of these Lim_187 isomers during certain periods could therefore represent periods where aged air masses are influencing the sampling sites.

The time series and average diurnal variation of the sum these limonene-derived acids :ketolimonic, ketonorlimonic, limonic and limononic acids are shown in Figure 6.5. During the Beijing summer campaign, a significant depression in concentrations is observed at the start of the campaign as observed for the α -pinene markers. Significantly less identifications were made in the Beijing winter campaign, with higher concentrations towards the end of the campaign. Across both Beijing campaigns, on average, higher concentrations were observed during the day, compared to the night, as expected in line with biogenic emission profiles. However, the diurnal variations are not strong, suggesting either continuous formation of markers, or non-local sources influencing the site. During the Guangzhou summer campaign, cleaner diurnal variations can be observed, with marker concentrations on average increasing during the afternoon, with the lowest concentrations observed during the morning. During the Guangzhou winter campaign, the diurnal profile is less defined, with more outliers and variation, suggesting non-local sources could be influencing the site. Finally, strong diurnal variation were observed in Delhi, as observed for the α -pinene markers. Low marker concentrations were observed at night, before a significant increase during the morning sample.

Table 6.6: Mean \pm SD for the Limonene derived acid markers identified across the Beijing, Guangzhou and Delhi campaigns with the number of observations in each campaign (n =). *Limonene* is abbreviated to *Lim* in the marker names.

| Marker | Beijing | | Guangzhou | | Delhi | |
|----------|---------------------------------|--------------------------------|---------------------------------|---------------------------------|--------------------------------|----------------------------------|
| | Summer | Winter | Summer | Winter | Pre-mon. | Post-mon. |
| Lim_173a | 14.11 \pm 9.5 (n = 102) | 1.89 \pm 2.13 (n = 45) | 7.17 \pm 6.85 (n = 126) | 5.31 \pm 3.07 (n = 104) | 7.71 \pm 2.89 (n = 4) | 13.4 \pm 6.2 (n = 14) |
| Lim_183 | 6.37 \pm 7.6 (n = 45) | 3.22 \pm 2.29 (n = 25) | 1.2 \pm 0.92 (n = 19) | 4.39 \pm 2.84 (n = 110) | 4.79 \pm 3.58 (n = 26) | 14.34 \pm 13.27 (n = 71) |
| Lim_185a | 2.54 \pm 2.48 (n = 51) | 0.54 \pm 1.03 (n = 31) | 2.28 \pm 1.59 (n = 6) | 1.62 \pm 1.07 (n = 7) | 4.01 \pm 2.62 (n = 5) | 5.64 \pm 3.26 (n = 7) |
| Lim_185b | 0.21 \pm 0.27 (n = 58) | 0.07 \pm 0.04 (n = 20) | 0.07 \pm 0.04 (n = 15) | 0.10 \pm 0.10 (n = 83) | 0.17 \pm 0.22 (n = 27) | 0.59 \pm 0.36 (n = 64) |
| Lim_187a | 6.67 \pm 5.09 (n = 138) | 0.64 \pm 0.59 (n = 43) | NA \pm NA (n = 0) | NA \pm NA (n = 0) | 4.97 \pm 2.54 (n = 29) | 5.57 \pm 2.44 (n = 93) |
| Lim_187b | 28.45 \pm 17.71 (n = 8) | 3.47 \pm 4 (n = 32) | NA \pm NA (n = 0) | NA \pm NA (n = 0) | NA \pm NA (n = 0) | 21.54 \pm 2.94 (n = 2) |
| Lim_187c | 15.55 \pm 4.63 (n = 7) | 1.76 \pm 6.81 (n = 6) | NA \pm NA (n = 0) | Inf \pm NA (n = 0) | NA \pm NA (n = 0) | NA \pm NA (n = 0) |
| Lim_203a | 4.89 \pm 3.78 (n = 8) | 0.91 \pm 0.78 (n = 26) | 1.95 \pm 0.9 (n = 6) | 1.47 \pm 0.85 (n = 14) | 4.08 \pm 2.12 (n = 5) | 7.16 \pm 3.35 (n = 27) |

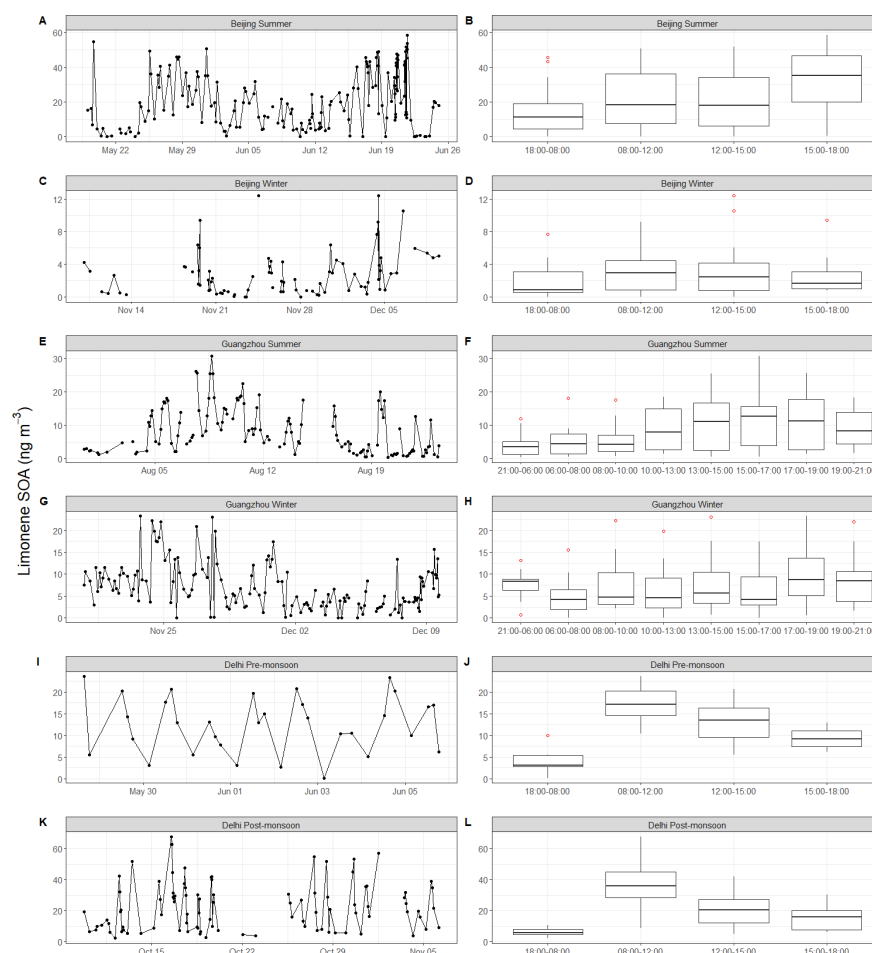


Figure 6.5: Time series and diurnal variations of the sum of the Limonene derived acid markers: Ketolimonic, Ketonorlimonic, Limonic and Limononic acids across the Beijing, Guangzhou and Delhi campaigns. The lower and upper part of the box represents the 25th and 75th percentiles, with the upper and lower lines extending no further than 1.5 * the interquartile range of the highest and lowest values within the line respectively.

6.3.4 β -caryophyllene

Seven β -caryophyllene markers were quantified across the 6 campaigns as shown in Table 6.7. Bcary_197 (3,3-dimethyl-2-(3-oxobutyl)cyclobutanecarboxylic acid, $C_{11}H_{18}O_3$) was the dominant β -caryophyllene marker observed, contributing between 37.3 % and 89.3 % of the β -caryophyllene derived acid concentration. Time averaged concentrations ranged from 1.32 ± 8.04 ng m⁻³ (n= 53) in Beijing winter, to 7.6 ± 4.83 ng m⁻³ (n = 31) in pre-monsoon Delhi. β -caryophyllinic acid (Bcary_253b, $C_{14}H_{22}O_4$) was observed across all 6 campaigns, contributing on average 5.3 ± 1 % to the total β -caryophyllene marker concentrations, with average concentrations ranging from 0.1-0.16 ng m⁻³. Vestenius et al., 2014 synthesised an authentic standard of β -caryophyllinic acid and quantified β -caryophyllinic acid throughout the year at a boreal forest site with concentrations ranging from 1.2 ng m⁻³ in winter to 10.9 ng m⁻³ in summer (Table 6.8).

Figure 6.6 shows the time series and diurnal variations of the sum of the three β -caryophyllene markers; Bcary_197 (3,3-dimethyl-2-(3-oxobutyl)cyclobutanecarboxylic acid, $C_{11}H_{18}O_3$), β -caryophyllinic acid (Bcary_253b, $C_{14}H_{22}O_4$) and Bcary_255a (4-(2-(2-carboxyethyl)-3,3-dimethylcyclobutyl)-4-oxobutanoic acid, $C_{13}H_{20}O_5$) that were identified in >30 % of samples. During the summer Beijing campaign, low concentrations were observed at the start of the campaign, as observed for the α -pinene and limonene markers. During the summer Guangzhou campaign, a significant increase in concentrations was observed at the start of the campaign, with concentrations dropping from around 40 ng m⁻³ to below 10 ng m⁻³ for the remainder of the campaign. Interestingly this is the opposite of what was observed for the α -pinene and limonene markers. This peak occurred during typhoon Wipha, suggesting the source of this peak is non-local sources. During the Delhi pre-monsoon a less defined diurnal variations as observed compared to the α -pinene and limonene markers, with similar average concentrations observed throughout the day, suggesting non-local sources, or long atmospheric lifetimes. However, like the other marker classes a strong diurnal was observed during the

Table 6.7: Mean \pm SD for the β -caryophyllene derived acid markers identified across the Beijing, Guangzhou and Delhi campaigns with the number of observations in each campaign (n =). β -caryophyllene is abbreviated to *Bcary* in the marker names.

| Marker | Beijing | | Guangzhou | | Delhi | |
|------------|---------------------------------|--------------------------------|---------------------------------|--------------------------------|--------------------------------|--------------------------------|
| | Summer | Winter | Summer | Winter | Pre-mon. | Post-mon. |
| Bcary_171b | 0.18 \pm 0.2 (n = 58) | 0.03 \pm 0.06 (n = 19) | 0.11 \pm 0.06 (n = 61) | 0.07 \pm 0.06 (n = 15) | 0.37 \pm 0.42 (n = 14) | 0.24 \pm 0.61 (n = 27) |
| Bcary_197 | 5.24 \pm 2.17 (n = 152) | 1.32 \pm 8.04 (n = 53) | 5.01 \pm 6.89 (n = 126) | 2.17 \pm 2.38 (n = 61) | 7.6 \pm 4.83 (n = 31) | 6.32 \pm 4.65 (n = 71) |
| Bcary_237 | 0.4 \pm 0.06 (n = 2) | 1.76 \pm NA (n = 1) | NA \pm NA (n = 0) | NA \pm NA (n = 0) | NA \pm NA (n = 0) | NA \pm NA (n = 0) |
| Bcary_241 | 0.08 \pm 0.06 (n = 8) | 0.02 \pm 0.01 (n = 6) | 0.01 \pm 0.01 (n = 3) | NA \pm NA (n = 0) | 0.08 \pm 0.06 (n = 14) | 0.08 \pm 0.06 (n = 21) |
| Bcary_251b | 0.37 \pm 0.33 (n = 22) | 0.28 \pm 0.78 (n = 6) | 0.16 \pm 0.06 (n = 2) | 0.27 \pm 2.95 (n = 40) | NA \pm NA (n = 0) | 0.46 \pm 0.25 (n = 10) |
| Bcary_253b | 0.31 \pm 0.23 (n = 190) | 0.1 \pm 0.14 (n = 109) | 0.21 \pm 0.14 (n = 133) | 0.12 \pm 0.09 (n = 96) | 0.46 \pm 0.24 (n = 32) | 0.38 \pm 0.55 (n = 97) |
| Bcary_255a | 0.2 \pm 0.15 (n = 89) | 0.03 \pm 0.03 (n = 5) | 0.11 \pm 0.06 (n = 101) | 0.08 \pm 0.05 (n = 66) | 0.2 \pm 0.24 (n = 30) | 0.12 \pm 0.11 (n = 45) |

Table 6.8: Comparison of β -caryophyllinic acid concentrations between those measured in this study and previously. TS = This study

| Location | β -caryophyllinic acid (ng m ⁻³) | Ref | Method |
|-------------------------------|--|-------|--------|
| Changchun, China | 1.5 ± 2.3 | [384] | GC-MS |
| Mt Tai, China | 16.3 ± 8.6 | [385] | GC-MS |
| Mt Hua, China | 2.2 ± 1.2 | [379] | GC-MS |
| Guangzhou, China | 4.04 ± 2.58 | [390] | GC-MS |
| Shanghai, China | 0.58 ± 0.75 | [391] | GC-MS |
| Beijing Summer | 0.31 ± 0.2 | [TS] | LC-MS |
| Beijing Winter | 0.1 ± 0.14 | [TS] | LC-MS |
| Guangzhou Summer | 0.21 ± 0.14 | [TS] | LC-MS |
| Guangzhou Winter | 0.12 ± 0.09 | [TS] | LC-MS |
| Kathmandu, Nepal | 18.7 ± 9.4 | [378] | GC-MS |
| Delhi Pre-monsoon | 0.46 ± 0.24 | [TS] | LC-MS |
| Delhi Post-monsoon | 0.4 ± 0.55 | [TS] | LC-MS |
| Summer Boreal forest, Finland | 10.9 ± 12.1 | [373] | LC-MS |

post-monsoon campaign, with low nocturnal concentrations compared to daytime.

6.3.5 Impact of Ozone and Temperature

6.3.5.1 Ozone

Previous chamber studies investigating organic acid formation pathways and SOA yields from α -pinene, limonene and β -caryophyllene have highlighted their ozonolysis and photochemical pathways. [41, 165, 273, 323, 364, 365, 392] Mutzel et al., 2016 investigated the SOA yields from the reaction of α -pinene and limonene with OH radicals and found larger SOA yields from limonene (10-21 %) than α -pinene (3.4-4.3 %). However higher SOA yields have been observed from the ozonolysis of α -pinene (37-125 %) and limonene (29 – 109 %) across a range of conditions.[393] Tasoglou et al.,2015 observed much higher yields associated with β -caryophyllene + OH with yields ranging from 19.3 -70.3 % under low NO_x and 30.7 – 137.8 % under high NO_x conditions. Lower SOA yields were observed for the ozonolysis of β -caryophyllene by Winterhalter et al., 2009 (6-41 %).[394] Limited ambient studies have investigated the effect of increasing ozone concentrations on organic acid formation in the real atmosphere.[385] Ozone showed strong

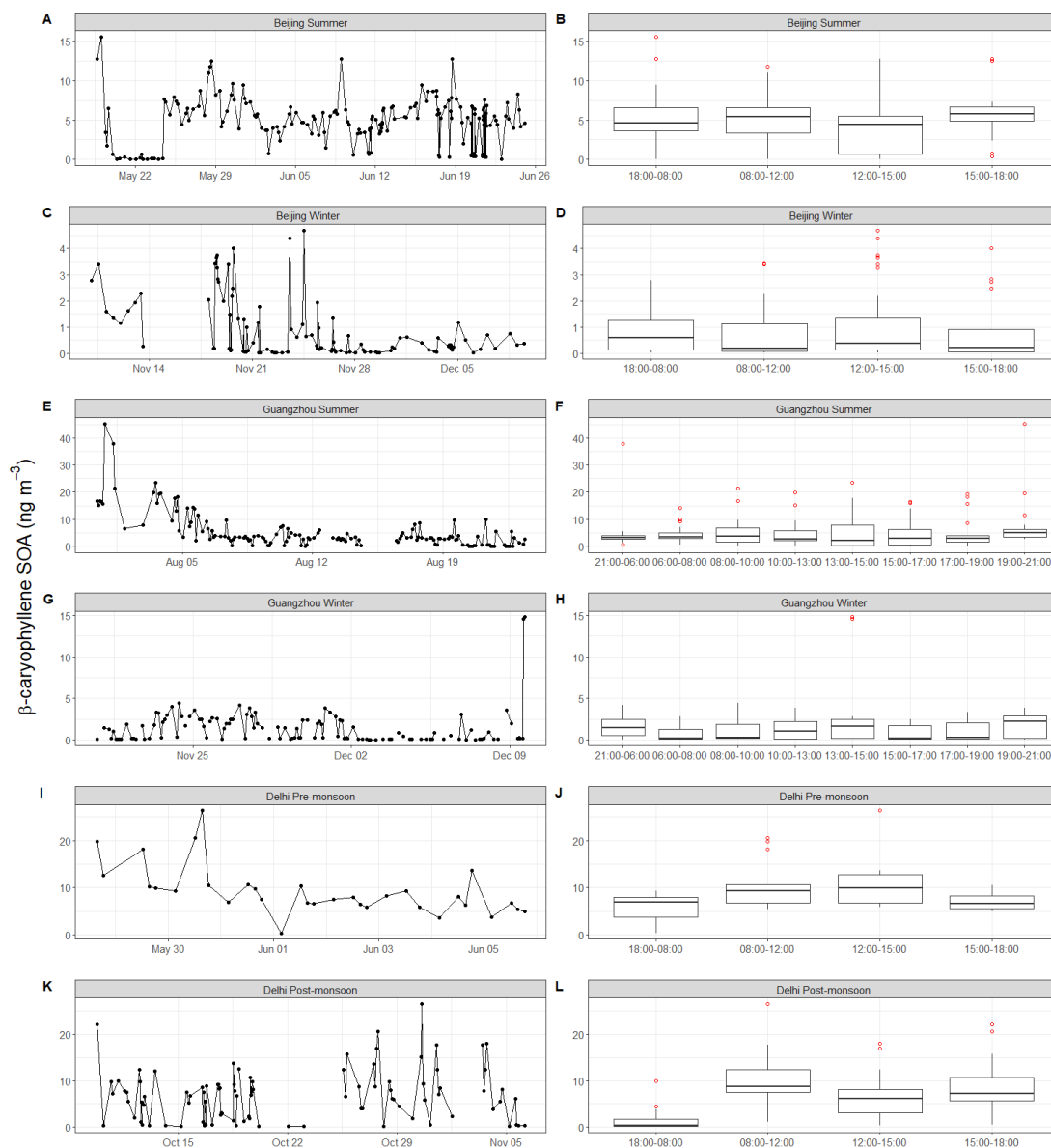


Figure 6.6: Time series and diurnal variations of the sum of the β -caryophyllene derived acid markers: Bcary_197 (3,3-dimethyl-2-(3-oxobutyl)cyclobutane-carboxylic acid, $C_{11}H_{18}O_3$), β -caryophyllinic acid (Bcary_253b, $C_{14}H_{22}O_4$) and Bcary_255a (4-(2-(2-carboxyethyl)-3,3-dimethylcyclobutyl)-4-oxobutanoic acid, $C_{13}H_{20}O_5$) across the Beijing, Guangzhou and Delhi campaigns. The lower and upper part of the box represents the 25th and 75th percentiles, with the upper and lower lines extending no further than 1.5 * the interquartile range of the highest and lowest values within the line respectively.

diurnal variations across all campaigns, with night-time minimums and midday maximums as shown in Figure 6.7. These ozone diurnal variations are expected due to ozone's photo-chemical formation pathway. Due to this pathway, it is expected that ozone concentrations would correlate with temperature as shown in Figure 6.8. Varying strengths of correlation however were observed across the campaigns, Beijing summer showed the strongest correlation ($R^2 = 0.63$), with the winter campaign having the weakest correlation ($R^2 < 0.1$). Across both Delhi campaigns no correlation was observed ($R^2 < 0.15$), suggesting the influence of non-local sources and meteorological effects. A moderate correlation ($R^2 = 0.47$) was observed during the summertime Guangzhou campaign, but a weak correlation was observed during the winter campaign ($R^2 = 0.2$).

Ozone did not directly correlate with any of the marker classes across any of the campaigns ($R^2 < 0.2$), but some marker class concentrations did increase under increasing ozone concentrations. Figure 6.9 shows the marker concentrations across all 6 campaigns correlated towards mean ozone mixing during the filter sample time.

The ozone data is presented in 20 ppb bins to aid comparison of the means and distributions. Mean marker concentrations across the three BVOCs generally increased with ozone, suggesting ozonolysis formation pathways may be important (Figure 6.9 A,B,C). Ozone can also be thought of as proxy for photochemistry, with OH radicals a key route to marker formation, meaning this correlation is unlikely to be solely based on the increased ozonolysis of BVOC precursors. At ozone concentrations above 80 ppbv, α -pinene marker concentrations decreased with increasing ozone, however the limonene and β -caryophyllene marker concentrations levelled off. This could be a result of increased losses of primary and secondary oxidation products under highly oxidising conditions. Higher temperatures are known to promote the emissions of BVOCs as discussed in the next section, which could lead to higher marker concentrations. A further complication may be the impact of ozone and temperature stresses on biogenic emissions. [395, 396] This stress on the plants could lead to a shift in the BVOC profiles.

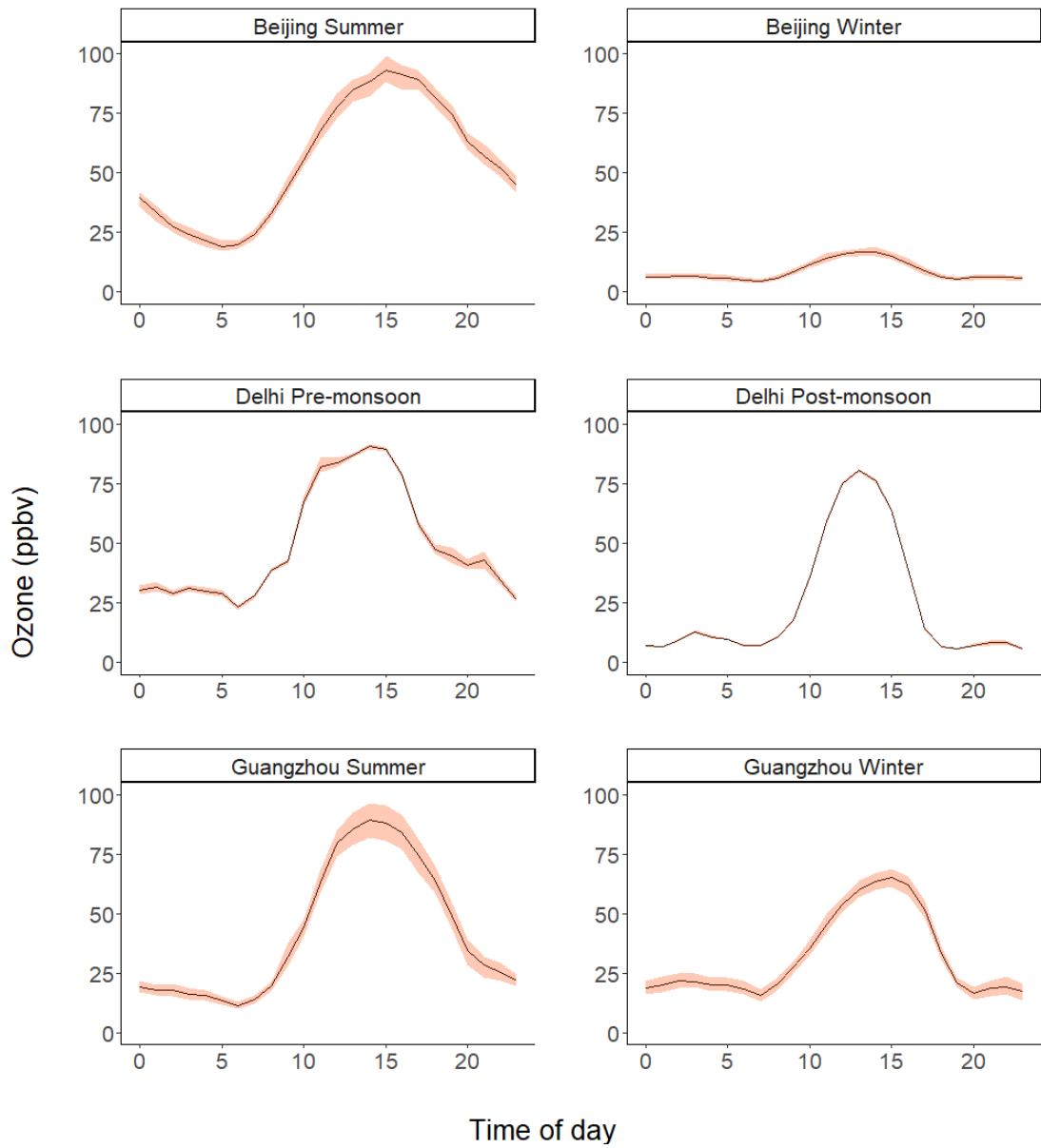


Figure 6.7: Diurnal variations of measured ozone concentrations across the Beijing, Delhi and Guangzhou campaigns.

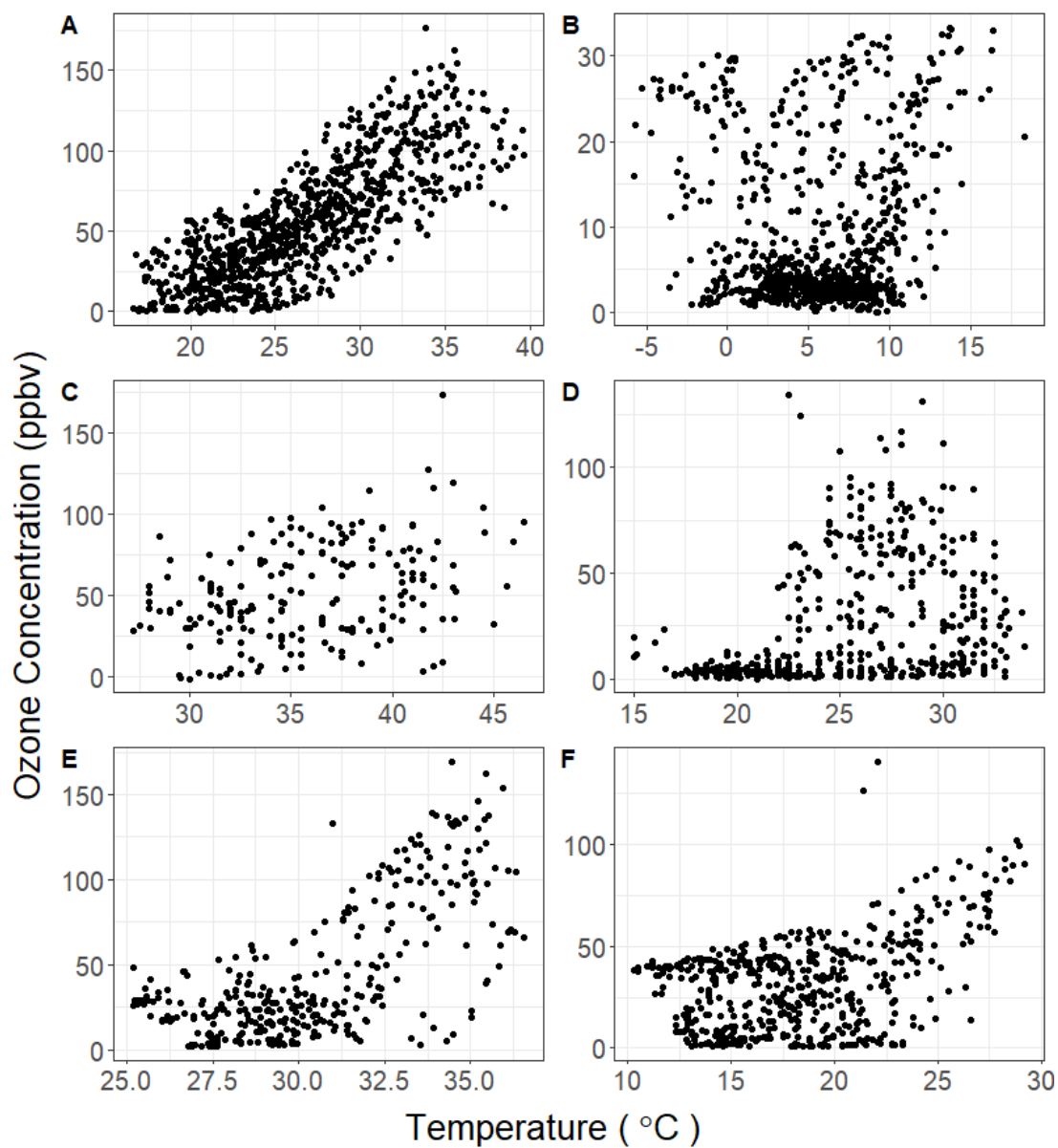


Figure 6.8: Measured ozone concentrations versus temperature for the six campaigns. Ozone concentrations and temperature were averaged to 1 hour. A- Beijing Summer, B- Beijing winter, C- Pre-monsoon Delhi, D- Post-monsoon Delhi, E - Guangzhou Summer, F- Guangzhou Winter.

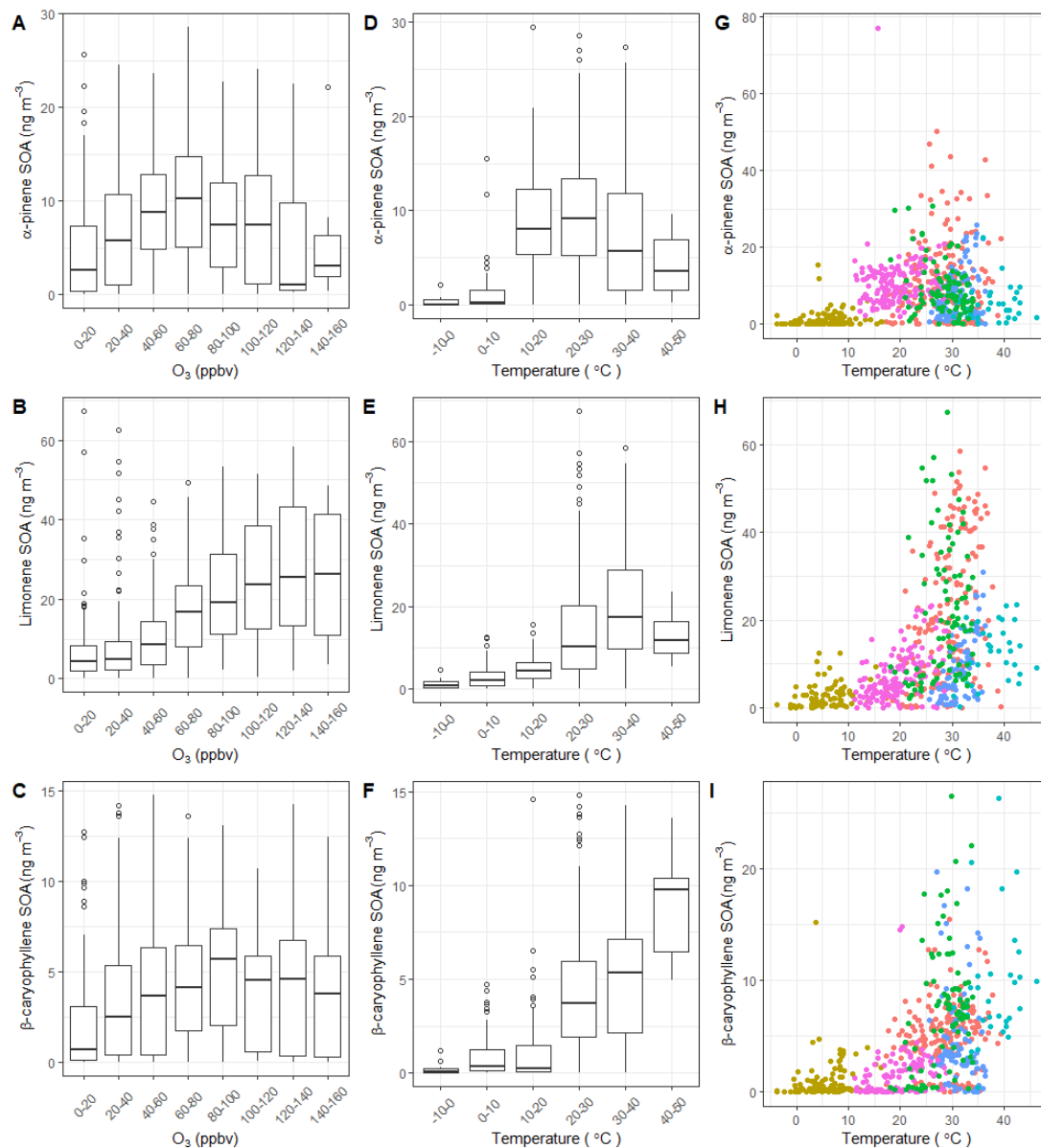


Figure 6.9: A,B,C – Correlation between total BSOA acid concentrations and binned ozone concentrations (bin size = 20 ppbv). D,E,F – Correlations between total BSOA acid concentrations and binned temperature (bin size = 10 °C). The boxplots represent the mean (horizontal middle line) with the lower and upper hinges corresponding to the 25th and 75th percentiles respectively. The upper and lower whiskers extend to the larger or smallest value no further than 1.5 * IQR from the respective hinge. G, H, I - Correlation between BSOA acid concentrations and temperature, coloured by campaign.

6.3.5.2 Temperature

Temperature has been shown to have a significant impact on α -pinene SOA yields.[372, 393, 397, 398] Simon et al., 2020 investigated the formation of α -pinene SOA across a large range of temperatures (-50 - 25 °C) and found a large decrease in highly oxidised molecule (HOM) yields with decreasing temperatures. However, the lower temperatures lead to increased nucleation rates of up to 3 orders of magnitude compensating the reduced HOM yield. Quéléver et al., 2019 also found that HOM formation decreased considerably at lower temperatures, with yields a factor of 50 lower at 0 °C than at 20 °C.[397] Kristensen et al., 2020 however found that semi-volatile organic acid intermediates and products had higher concentrations in SOA during lower temperature experiments. This was due to increased condensation as the saturation concentration decreases at lower temperature and shifts the volatility distribution.[399]

Across the 6 campaigns, temperatures ranged from -4 to 46 °C, with pre-monsoon Delhi having the highest average temperature of 38.0 ± 4.0 °C, and Beijing winter the lowest with an average of 5.6 ± 4.2 °C. As shown in Figure 6.9, higher acid marker concentrations derived from all three BVOCs were observed under higher ambient temperatures when incorporating data from all 6 campaigns, but level off at different temperatures. Figure 6.9D shows mean α -pinene marker concentrations increased up until the 20-30 °C bin, before decreasing under higher temperatures driven mainly by pre-monsoon Delhi samples (Figure 6.9G). Mean limonene marker concentrations increased significantly up until the 30 – 40 °C bin (Figure 6.9E), before concentrations dropped under the highest temperatures observed in pre-monsoon Delhi (Figure 6.9H). β -caryophyllene was observed to have an almost exponential increase in mean marker concentrations (Figure 6.9F), with the highest mean concentrations observed in the 40 – 50 °C bin. This increase in concentrations with increasing temperature is like that of isoprene observed in Guangzhou in Chapter 3, Figure 3.15. This increase in marker concentrations with temperature was also observed by Li et al., 2013 who observed *cis*-pinonic

acid and β -caryophyllinic acid concentrations increased with temperature at a forested site in China.[379] Ding et al., 2014 also observed increased monoterpene and β -caryophyllene marker concentrations with increasing temperature across 14 sites in China.[213]

The increase in concentrations with temperature could be due to several factors. Firstly, higher temperatures occur during the afternoon, with peak photo-oxidation and ozone concentrations, meaning the correlation with temperature could be an artefact. Higher temperatures are also associated with increased BVOC emissions as shown in Chapter 3 and in previous studies [400–402], especially during the summer campaigns, which could lead to increase in BSOA production. This suggests this increase is likely driven by a mixture of BVOC emissions and increased ozonolysis and/or photo-oxidation.

Temperatures above 40 °C were only observed during the day and α -pinene and limonene marker concentrations when temperatures were above 40 °C were on average lower or similar to those between 20 °C and 40 °C. The drop in concentrations above 40 °C could be due to a lack of measurements or due to plant stress leading to lower BVOC emissions. However, high temperatures could also promote the evaporation of particulate phase species back into the gas-phase.[403] In contrast, the β -caryophyllene markers showed even higher concentrations at temperatures above 40 °C, which could be due to increased emissions of β -caryophyllene under higher temperatures or increased oxidation. Previous studies have shown strong correlations between β -caryophyllene emissions and temperature.[271, 404]

6.4 Conclusion

Biogenic secondary organic acid markers from α -pinene, limonene and β -caryophyllene were quantified using a *cis*-pinonic acid response curve. Known differences in ionisation efficiencies between *cis*-pinonic acid and the markers were accounted for using relative ionisation efficiency factors estimated via a random forest model.

The markers were quantified in nearly 800 PM filters collected in Beijing, Delhi, and Guangzhou across 6 campaigns. Limonene markers contributed the most to the total organic acid concentrations, contributing on average 47.2 % compared to 34.0 % and 18.8 % for the α -pinene and β -caryophyllene markers respectively. Marker concentrations were observed to be highly impacted by temperature. The increase with temperature is likely due to increased local emissions of BVOC's and suggests that most of these markers are formed locally to the sampling sites. Overall, this study represents one of the largest molecular level investigations of BSOA acid formation in terms of filter samples and employs new quantification methods. However, significant uncertainties are still attributed to these concentrations due to a lack of authentic standards for both ionisation efficiency differences and matrix effect factors. Authentic standards are needed to improve the validity and accuracy of the predictive RIE model, which has a high uncertainty, meaning concentrations could be over or under predicted by several times. Matrix effects are less uncertain than the differences in ionisation efficiencies, but still showed significant variation in measurements across standards and samples. *cis*-pinonic acid which was used as the ionisation efficiency reference compound had limited matrix effects averaged over 23 ambient samples from the 6 campaigns. Furthermore, due to the lack of authentic standards, markers must be identified via matching markers in chamber samples to ambient samples or through tandem mass spectrometry comparisons. However, due to the complexity of the ambient samples, reliable tandem mass spectrometry measurements are hard to undertake. Future work should focus on the development of authentic standards and their relative ionisation efficiency measurements relative to readily available standards. Furthermore, the availability of a widely available tandem mass spectral library would allow for easier marker identification both in chamber and ambient samples.

Chapter 7

Summary and future work

7.1 Summary

Biogenic secondary organic aerosol (BSOA) is a key pollutant, both in rural and urban environments. BSOA formation routes have been well established in atmospheric simulation studies, but more limited studies have investigated their concentrations and formation pathways in the real atmosphere. Studies have now investigated BSOA both qualitatively and semi-quantitatively in ambient studies, but numerous complexities still surround the accurate quantification of BSOA markers. Firstly, due to the extremely complex nature of SOA, co-elution of different compounds cannot be avoided and as such, matrix effects associated with both LC and direct injections have been shown to lead to ionisation efficiency changes. Furthermore, due to the sheer number of compounds within samples, quantification via authentic standards is difficult, mainly due to their commercial availability, leading to the use of proxy standards. In this thesis BSOA markers including organosulfates (OS), nitrooxy-OS (NOS) and biogenic organic acids from a range of precursors have been quantified in ambient samples collected across three Asian megacities (Beijing, Guangzhou and Delhi). Through these studies' new methods for more accurate quantification of BSOA markers have been developed and deployed. Due to the implementation of these quantification methods comparing to previous studies is difficult as they haven't accounted for these. The ambient quantification of these species also provided insight into their atmospheric relevance, formation pathways and anthropogenic enhancements. Measurements of a range of isoprene OS and NOS species were first undertaken during a summer campaign in Beijing, China. Measurements were undertaken using UPLC-HRMS with an electrospray ionisation (ESI) source and quantified via two authentic isoprene OS standards: 2-methyl-glyceric acid (2-MG-OS) and 2-methyl-tetrol organosulfate (2-MT-OS). Additional supplementary measurements of air pollutants were taken alongside the filter collection and allowed investigation into the formation of these OS and NOS species. Initial differences in ionisation efficiencies of the two authentic standards were identified, and by using a standard

addition calibration method, differences in matrix suppression between the two markers were identified. This was an important observation, which has led to further investigations and the establishment that these complex samples suppress ion signal significantly using this type of ionisation technique. OS formation was found to be highly dependent on both photochemistry (using ozone as a proxy) and inorganic particulate sulfate for the reactive uptake of gas phase species. Extremely low afternoon NO concentrations through ozone titration allowed for the formation of high concentrations of low-NO isoprene markers. Low afternoon NO concentrations also allowed for nitrate radical chemistry to become increasingly important throughout the afternoon and into the evening. A range of NOS species were quantified with distinct formation routes proposed. Two mono-nitrated species were proposed to be formed through sequential oxidation from NO₃ then OH and showed a strong correlation to particulate sulfate. Nocturnally enhanced di and tri-nitrated markers were proposed to form from multiple NO₃ oxidation steps.

One of the main drawbacks associated with the Beijing campaign was the long filter sampling times, especially overnight, resulting in a loss of fine detail of when markers were forming. This was addressed through the collection and subsequent analysis of higher time resolution filter samples collected in Guangzhou, China. A range of OS and NOS markers from both isoprene and monoterpenes were targeted using UHPLC-HRMS and quantified using authentic and proxy standards. Building on the identified matrix effects in Beijing, further development of matrix effect factors for different standards was undertaken to correct for signal suppression, without which, concentrations would have been significantly underestimated. Strong diurnal variations of monoterpene derived OS and NOS markers were observed for the first time using offline analysis. Nocturnal enhancements in marker concentrations were observed, likely due to either precursor emission profiles or nocturnal nitrate radical chemistry. Monoterpene OS and NOS concentrations were also highly dependent on temperature. Higher temperatures at night promoted higher marker concentrations, while the opposite was observed

during the day, likely due to degradation of gas-phase precursors or particulate phase markers. Isoprene OS species were shown to be highly dependent on both particulate sulfate concentrations, for reactive uptake of gas phase intermediates, and temperature for isoprene emissions. Delhi, India represents one of the most polluted megacities in the world, and as such provides an interesting case study for SOA formation. Due to the urban nature of the sampling sites in this thesis, and the known anthropogenic sources of typically biogenic VOCs such as isoprene and monoterpenes the sources of isoprene and monoterpenes were investigated in Delhi. Both isoprene and monoterpenes positively correlated with anthropogenic combustion markers at night, but less so during the day, highlighting their mixed emission sources, with anthropogenic emissions at night, while biogenic emissions dominated during the day. Extremely high pollutant and VOC concentrations were observed in Delhi across pre- and post-monsoon campaigns, which can be explained in part by high emissions, but also due to meteorological conditions. Stagnant conditions, and a very low night-time planetary boundary layer height trapped pollutants, allowing for high concentrations to build up. The extreme levels of NO at night quenched the majority of O₃ and NO₃ nocturnal chemistry meaning degradation of VOCs at night was minimal, leading to high VOC concentrations. In the morning, rapid formation of marker compounds, likely through either ozonolysis or photo-oxidation occurred. Even though Delhi is one of the most polluted cities in the world, isoprene and monoterpene derived SOA contributed significantly to PM_{2.5} and organic aerosol and also the production of O₃. [324]

The quantification of BSOA is extremely limited due to the lack of authentic standards and is one of the main challenges the aerosol community faces going forward. Synthesis studies have highlighted differences in ionisation efficiencies for OS and biogenic organic acid markers, with the differences in the latter much more pronounced. Predictive relative ionisation efficiency (RIE) models have been shown to be able to begin to predict differences in ionisation efficiencies for a range of compounds. An in-house predictive RIE model was developed

based on measurements of readily available organic acid standards. The model showed accuracy (RMSE and R^2) in line with similar models, without the need for extremely large datasets. However, until authentic standards are readily available for comparison to these predicted factors, the true accuracy of these models for quantification is unknown. Aerosol metrics which are commonly used to infer sources and age of aerosol were shown to be highly influenced by considering the ionisation efficiency differences. Thus, highlighting the need to consider ionisation efficiencies, especially for qualitative non-targeted analysis. Due to the lack of authentic standards, limited numbers of studies have focussed on the ambient quantification of biogenic organic acid markers, as such their atmospheric concentrations are largely unknown. A library of biogenic organic acid markers was screened for and markers quantified across a filter database containing around 800 filter samples from Beijing, Delhi, and Guangzhou, comprising of one of the largest datasets to date. Differences in ionisation efficiencies were considered using predicted RIE factors. Strong seasonality between summer and winter was observed across Beijing due to its higher latitude, leading to very low concentrations during the cold winter season. Marker concentrations were observed to increase with ozone concentrations. This could be due to ozonolysis pathways but due to ozone's photo-oxidation formation this correlation could be due to ozone acting as a proxy for photochemistry or linked to higher temperatures. Temperature was also shown to be a key metric, with higher temperatures promoting higher precursor VOC concentrations, leading to higher marker concentrations.

Across the 3 locations investigated in this thesis, targeted BSOA markers have been shown to contribute significantly towards OA and $PM_{2.5}$ concentrations. In summertime Beijing isoprene OS species were shown to contribute on average 2.2 % of total oxidised organic aerosol (OOA) but up to 10.5 % on certain days. In Delhi, one of the most polluted cities in the world, total targeted OS and NOS concentrations from both isoprene and monoterpenes contributed up to 0.46 % with an average of 0.24 % of $PM_{2.5}$ during pre-monsoon and up to 0.94 % with an average of 0.31 % during the post-monsoon campaign. Similar

contributions to OOA were observed in Delhi compared to Beijing, with up to 4.2 % and 6.6 % during the pre- and post-monsoon campaigns respectively. These contributions, while relatively small on average are only for a minor portion of known, targeted BSOA markers. There are thousands of known biogenic VOC's of which only a handful have been investigated intensely enough for markers to be targeted in ambient samples as such BSOA concentrations likely make much higher contributions than observed in this study. Furthermore, with uncertainties from matrix effects and proxy standards, these contributions could be largely underpredicted or have high uncertainty. This work has also focussed on the use of negative mode ESI-MS leading to not targeting known BSOA markers such as organic nitrates which are more readily ionised in the positive mode. Overall, this study has shown the BSOA on certain days can contribute significantly to OA and PM_{2.5} mass, and is a lower limit of estimates, much larger BSOA contributions are likely occurring.

This work has also investigated the analytical challenges associated with BSOA and the known and unknown uncertainties with quantification. Due to the complex nature of these samples, matrix effects have been shown to have both an enhancement and suppression effect on different BSOA functionalities, but the effect also varies sample to sample. Isoprene OS standards: 2-MG-OS and 2-MT-OS were observed to be heavily suppressed across a selection of samples from each location with up to 94 % suppression in some samples. However, ionisation enhancement was also observed of up to 15 %, meaning a large range of uncertainties association with matrix effects have occurred. Matrix effects were also observed for authentic organic acid standards, with up to 100 % enhancement in some samples. Without authentic standards for all targeted BSOA markers, and investigation of each standard in every sample undergoing analysis, unknown uncertainties due to matrix effects will be occurring. The lack of authentic standards also means using proxy standards for quantification, leading to unknown uncertainties at this stage. The use of proxy standards for quantification likely leads to much higher uncertainties than the matrix effects from the limited work

that has been undertaken. Overall, the uncertainties associated with BSOA quantification is still a major issue and is highly variable based on standards and sample composition.

Overall, this thesis has investigated the concentrations of BSOA markers and their formation pathways in extremely polluted urban environments. The policy implications of this thesis outline the potential win-win effects of reducing anthropogenic particulate sulfate by also reducing BSOA concentrations. This thesis is also pertinent in a warming climate, where BVOC emissions in certain regions may increase leading to higher BSOA concentrations and thus have knock on effects on human and environmental health. Further, many cities are undertaking “greening” by planting trees for reasons including improving air quality. However, special attention should be made to the species of tree, limiting BVOC emissions in environments where fast oxidation and subsequent high BSOA mass will be formed.

7.2 Future work

Future work is needed to further develop our ability to accurately quantify large numbers of BSOA markers. The key area of focus should be the synthesis of authentic standards from a range of precursors. These studies should focus on sharing the synthesis process or the standards themselves with other groups. These synthesis studies should also make measurements of the observed differences in ionisation efficiencies in comparison to commonly used proxy standards. Through access to even just a limited number of authentic standards, RIE models such as developed in this work can be optimised and developed further to be more accurate. Authentic standards would also allow for matrix effects to be investigated more accurately, allowing for matrix effect factors to be further developed. Another difficulty faced during this thesis is the lack of a comprehensive tandem mass spectrometry library of species for easy comparison. Although large amounts of tandem mass spectrometry data have been accumulated over the last two

decades, is it not widely available. As such, a community open-source tandem mass spectrometry library of BSOA markers should be developed to allow for easier confirmation of BSOA markers. Finally, previous studies have relied on samples with long sampling times (12/23 hours) and generally spread out across long periods of time. As highlighted in this thesis, increases in filter sampling frequency massively increases our ability to understand formation pathways of BSOA markers in the real atmosphere. Further to this, the accumulation of large numbers of filter samples, allows for general formation pathways across several locations to be investigated. Future work should focus on the sharing of filter samples between laboratories, allowing for large databases of measurements to be built up, in turn allowing for more detailed analysis to occur.

Bibliography

- [1] Hallquist, M. et al. The formation, properties and impact of secondary organic aerosol: current and emerging issues. *Atmospheric Chemistry and Physics* 9.14 (2009), pp. 5155–5236. DOI: 10.5194/acp-9-5155-2009. URL: <http://www.atmos-chem-phys.net/9/5155/2009/>.
- [2] Xu, L. et al. Anthropogenic–Biogenic Interactions at Night: Enhanced Formation of Secondary Aerosols and Particulate Nitrogen- and Sulfur-Containing Organics from β -Pinene Oxidation. *Environmental Science & Technology* (2021), acs.est.0c07879. DOI: 10.1021/acs.est.0c07879. URL: <https://pubs.acs.org/doi/10.1021/acs.est.0c07879>.
- [3] Rosenfeld, D., Sherwood, S., Wood, R. and Donner, L. *Climate effects of aerosol-cloud interactions*. 2014. DOI: 10.1126/science.1247490. URL: www.sciencemag.org/SCIENCEVOL.
- [4] Lohmann, U. and Feichter, J. *Global indirect aerosol effects: A review*. 2005. DOI: 10.5194/acp-5-715-2005.
- [5] Satheesh, S. K. and Krishna Moorthy, K. Radiative effects of natural aerosols: A review. *Atmospheric Environment* 39.11 (2005), pp. 2089–2110. DOI: 10.1016/j.atmosenv.2004.12.029.
- [6] Dockery, D. W. et al. An Association between Air Pollution and Mortality in Six U.S. Cities. *New England Journal of Medicine* 329.24 (1993), pp. 1753–1759. DOI: 10.1056/NEJM199312093292401. URL: <http://www.nejm.org/doi/abs/10.1056/NEJM199312093292401>.

- [7] *Aerosols, their Direct and Indirect Effects — IPCC*. URL: <https://www.ipcc.ch/report/ar3/wg1/chapter-5-aerosols-their-direct-and-indirect-effects/>.
- [8] Comite, V. et al. The impact of atmospheric pollution on outdoor cultural heritage: an analytic methodology for the characterization of the carbonaceous fraction in black crusts present on stone surfaces. *Environmental Research* 201 (2021), p. 111565. DOI: 10.1016/J.ENVRES.2021.111565. URL: <https://linkinghub.elsevier.com/retrieve/pii/S0013935121008598>.
- [9] Cao, J.-j. et al. Chemical Composition of Indoor and Outdoor Atmospheric Particles at Emperor Qin's Terra-cotta Museum, Xi'an, China. *Aerosol and Air Quality Research* 11.1 (2011), pp. 70–79. DOI: 10.4209/AAQR.2010.10.0088. URL: <https://aaqr.org/articles/aaqr-10-10-0a-0088>.
- [10] Sheng, N. and Tang, U. W. Risk assessment of traffic-related air pollution in a world heritage city. *International Journal of Environmental Science and Technology* 2012 10:1 10.1 (2012), pp. 11–18. DOI: 10.1007/S13762-012-0030-1. URL: <https://link.springer.com/article/10.1007/s13762-012-0030-1>.
- [11] Anderson, L. E. et al. Lake Recovery Through Reduced Sulfate Deposition: A New Paradigm for Drinking Water Treatment. *Environmental Science and Technology* 51.3 (2017), pp. 1414–1422. DOI: 10.1021/ACS.EST.6B04889. URL: <https://pubs.acs.org/doi/full/10.1021/acs.est.6b04889>.
- [12] Skjelkvåle, B. L., Mannio, J., Wilander, A. and Andersen, T. Recovery from acidification of lakes in Finland, Norway and Sweden 1990-1999. *Hydrology and Earth System Sciences* 5.3 (2001), pp. 327–337. DOI: 10.5194/HESS-5-327-2001.
- [13] Sun, F., DAI, Y. and Yu, X. Air pollution, food production and food security: A review from the perspective of food system. *Journal of Integrative Agriculture* 16.12 (2017), pp. 2945–2962. DOI: 10.1016/S2095-3119(17)61814-8.
- [14] Hartono, D. et al. Impacts of particulate matter (PM_{2.5}) on the behavior of freshwater snail *Parafossarulus striatulus*. *Scientific Reports* 2017 7:1 7.1 (2017),

- pp. 1–8. DOI: 10.1038/s41598-017-00449-5. URL:
<https://www.nature.com/articles/s41598-017-00449-5>.
- [15] WHO. WHO | Ambient air pollution: A global assessment of exposure and burden of disease. *WHO* (2016).
- [16] Lelieveld, J. et al. The contribution of outdoor air pollution sources to premature mortality on a global scale. *Nature* 525.7569 (2015), pp. 367–371. DOI: 10.1038/nature15371. URL:
<http://www.nature.com/articles/nature15371>.
- [17] Lim, S. S. et al. A comparative risk assessment of burden of disease and injury attributable to 67 risk factors and risk factor clusters in 21 regions, 1990–2010: a systematic analysis for the Global Burden of Disease Study 2010. *The Lancet* 380.9859 (2012), pp. 2224–2260. DOI: 10.1016/S0140-6736(12)61766-8. URL:
<https://linkinghub.elsevier.com/retrieve/pii/S0140673612617668>.
- [18] Pope, C. A. et al. Lung cancer, cardiopulmonary mortality, and long-term exposure to fine particulate air pollution. *Journal of the American Medical Association* 287.9 (2002), pp. 1132–1141. DOI: 10.1001/jama.287.9.1132.
- [19] Pope, C. A. and Dockery, D. W. Health Effects of Fine Particulate Air Pollution: Lines that Connect. *Journal of the Air & Waste Management Association* 56.6 (2006), pp. 709–742. DOI: 10.1080/10473289.2006.10464485. URL: <https://www.tandfonline.com/doi/full/10.1080/10473289.2006.10464485>.
- [20] WHO. WHO | Ambient air pollution. *WHO* (2018).
- [21] Landrigan, P. J. et al. The Lancet Commission on pollution and health. *The Lancet* 391.10119 (2018), pp. 462–512. DOI: 10.1016/S0140-6736(17)32345-0. URL:
<https://linkinghub.elsevier.com/retrieve/pii/S0140673617323450>.
- [22] Kwon, H. S., Ryu, M. H. and Carlsten, C. *Ultrafine particles: unique physicochemical properties relevant to health and disease*. 2020. DOI: 10.1038/s12276-020-0405-1. URL:
<https://doi.org/10.1038/s12276-020-0405-1>.

- [23] Alemany, S. et al. Associations between air pollution and biomarkers of Alzheimer's disease in cognitively unimpaired individuals. *Environment International* 157 (2021), p. 106864. DOI: 10.1016/J.ENVINT.2021.106864.
- [24] Thiankhaw, K., Chattipakorn, N. and Chattipakorn, S. C. PM2.5 exposure in association with AD-related neuropathology and cognitive outcomes. *Environmental Pollution* 292 (2022), p. 118320. DOI: 10.1016/J.ENVPOL.2021.118320.
- [25] Calderón-Garcidueñas, L. et al. Air pollution and brain damage. *Toxicologic Pathology* 30.3 (2002), pp. 373–389. DOI: 10.1080/01926230252929954. URL: <https://journals.sagepub.com/doi/10.1080/01926230252929954>.
- [26] Park, M. et al. Differential toxicities of fine particulate matters from various sources. *Scientific Reports* 8.1 (2018), pp. 1–11. DOI: 10.1038/s41598-018-35398-0. URL: www.nature.com/scientificreports/.
- [27] Guenther, A. B. et al. The Model of Emissions of Gases and Aerosols from Nature version 2.1 (MEGAN2.1): an extended and updated framework for modeling biogenic emissions. *Geoscientific Model Development* 5.6 (2012), pp. 1471–1492. DOI: 10.5194/gmd-5-1471-2012. URL: <https://www.geosci-model-dev.net/5/1471/2012/>.
- [28] Chan, C. K. and Yao, X. Air pollution in mega cities in China. *Atmospheric Environment* 42.1 (2008), pp. 1–42. DOI: 10.1016/J.ATMOENV.2007.09.003. URL: <https://www.sciencedirect.com/science/article/pii/S1352231007007911?via%3Dihub>.
- [29] Huang, R. J. et al. High secondary aerosol contribution to particulate pollution during haze events in China. *Nature* 514.7521 (2015), pp. 218–222. DOI: 10.1038/nature13774. URL: <https://www.nature.com/articles/nature13774>.
- [30] Han, L., Zhou, W., Li, W. and Li, L. Impact of urbanization level on urban air quality: A case of fine particles (PM2.5) in Chinese cities. *Environmental Pollution* 194 (2014), pp. 163–170. DOI: 10.1016/J.ENVPOL.2014.07.022.

- [31] Gong, P. et al. Urbanisation and health in China. *Lancet (London, England)* 379.9818 (2012), p. 843. DOI: 10.1016/S0140-6736(11)61878-3. URL: [/pmc/articles/PMC3733467/%20/pmc/articles/PMC3733467/?report=abstract%20https://www.ncbi.nlm.nih.gov/pmc/articles/PMC3733467/](https://pubmed.ncbi.nlm.nih.gov/23733467/).
- [32] Cohen, B. Urban Growth in Developing Countries: A Review of Current Trends and a Caution Regarding Existing Forecasts. *World Development* 32.1 (2004), pp. 23–51. DOI: 10.1016/J.WORLDDEV.2003.04.008.
- [33] Budisulistiorini, S. H. et al. Real-Time Continuous Characterization of Secondary Organic Aerosol Derived from Isoprene Epoxydiols in Downtown Atlanta, Georgia, Using the Aerodyne Aerosol Chemical Speciation Monitor. *Environmental Science & Technology* 47.11 (2013), pp. 5686–5694. DOI: 10.1021/es400023n. URL: <http://pubs.acs.org/doi/10.1021/es400023n>.
- [34] Budisulistiorini, S. H. et al. Examining the effects of anthropogenic emissions on isoprene-derived secondary organic aerosol formation during the 2013 Southern Oxidant and Aerosol Study (SOAS) at the Look Rock, Tennessee ground site. *Atmospheric Chemistry and Physics* 15.15 (2015), pp. 8871–8888. DOI: 10.5194/acp-15-8871-2015. URL: <https://www.atmos-chem-phys.net/15/8871/2015/>.
- [35] Hettiyadura, A. P. S. et al. Organosulfates in Atlanta, Georgia: anthropogenic influences on biogenic secondary organic aerosol formation. *Atmospheric Chemistry and Physics* 19.5 (2019), pp. 3191–3206. DOI: 10.5194/acp-19-3191-2019. URL: <https://www.atmos-chem-phys.net/19/3191/2019/>.
- [36] Hettiyadura, A. P. et al. Source apportionment of organic carbon in Centreville, AL using organosulfates in organic tracer-based positive matrix factorization. *Atmospheric Environment* 186 (2018), pp. 74–88. DOI: 10.1016/J.ATMOENV.2018.05.007. URL: <https://www.sciencedirect.com/science/article/pii/S1352231018303108?via%3Dihub>.

- [37] Yee, L. D. et al. Natural and Anthropogenically Influenced Isoprene Oxidation in Southeastern United States and Central Amazon. *Environmental Science & Technology* (2020). DOI: 10.1021/acs.est.0c00805.
- [38] Xu, L. et al. Effects of anthropogenic emissions on aerosol formation from isoprene and monoterpenes in the southeastern United States. *Proceedings of the National Academy of Sciences* 112.1 (2015), pp. 37–42. DOI: 10.1073/PNAS.1417609112. URL: <https://www.pnas.org/content/112/1/37>.
- [39] Kourtchev, I. et al. Molecular Composition of Boreal Forest Aerosol from Hyytiälä, Finland, Using Ultrahigh Resolution Mass Spectrometry. *Environmental Science and Technology* 47.9 (2013), pp. 4069–4079. DOI: 10.1021/ES3051636. URL: <https://pubs.acs.org/doi/abs/10.1021/es3051636>.
- [40] Kristensen, K. et al. High-Molecular Weight Dimer Esters Are Major Products in Aerosols from α -Pinene Ozonolysis and the Boreal Forest. *Environmental Science and Technology Letters* 3.8 (2016), pp. 280–285. DOI: 10.1021/acs.estlett.6b00152. URL: <https://pubs.acs.org/sharingguidelines>.
- [41] Eijck, A. van et al. New tracer compounds for secondary organic aerosol formation from β -caryophyllene oxidation. *Atmospheric Environment* 80 (2013), pp. 122–130. DOI: 10.1016/j.atmosenv.2013.07.060.
- [42] Arashiro, M. et al. In vitro exposure to isoprene-derived secondary organic aerosol by direct deposition and its effects on COX-2 and IL-8 gene expression. *Atmospheric Chemistry and Physics* 16.22 (2016), pp. 14079–14090. DOI: 10.5194/acp-16-14079-2016.
- [43] Gaschen, A. et al. Cellular responses after exposure of lung cell cultures to secondary organic aerosol particles. *Environmental Science and Technology* 44.4 (2010), pp. 1424–1430. DOI: 10.1021/es902261m. URL: <https://pubmed.ncbi.nlm.nih.gov/20092303/>.

- [44] McDonald, J. D. et al. *Cardiopulmonary response to inhalation of biogenic secondary organic aerosol*. 2010. DOI: 10.3109/08958370903148114. URL: <https://pubmed.ncbi.nlm.nih.gov/20148748/>.
- [45] Harrison, R. M., Jones, A. M. and Lawrence, R. G. Major component composition of PM10 and PM2.5 from roadside and urban background sites. *Atmospheric Environment* 38.27 (2004), pp. 4531–4538. DOI: 10.1016/j.atmosenv.2004.05.022.
- [46] Zhang, Q. et al. Ubiquity and dominance of oxygenated species in organic aerosols in anthropogenically-influenced Northern Hemisphere midlatitudes. *Geophysical Research Letters* 34.13 (2007). DOI: 10.1029/2007GL029979. URL: <https://agupubs.onlinelibrary.wiley.com/doi/full/10.1029/2007GL029979>
<https://agupubs.onlinelibrary.wiley.com/doi/abs/10.1029/2007GL029979>
<https://agupubs.onlinelibrary.wiley.com/doi/10.1029/2007GL029979>.
- [47] Jimenez, J. L. et al. Evolution of organic aerosols in the atmosphere. *Science* 326.5959 (2009), pp. 1525–1529. DOI: 10.1126/science.1180353. URL: www.sciencemag.org/cgi/content/full/326/5959/1522/DC1.
- [48] Nozière, B. et al. *The Molecular Identification of Organic Compounds in the Atmosphere: State of the Art and Challenges*. 2015. DOI: 10.1021/cr5003485.
- [49] Kanakidou, M. et al. *Organic aerosol and global climate modelling: A review*. 2005. DOI: 10.5194/acp-5-1053-2005.
- [50] Goldstein, A. H. and Galbally, I. E. *Known and unexplored organic constituents in the earth's atmosphere*. 2007. DOI: 10.1021/es072476p.
- [51] Kelly, J. M., Doherty, R. M., O'Connor, F. M. and Mann, G. W. The impact of biogenic, anthropogenic, and biomass burning volatile organic compound emissions on regional and seasonal variations in secondary organic aerosol. *Atmospheric Chemistry and Physics* 18.10 (2018), pp. 7393–7422. DOI: 10.5194/ACP-18-7393-2018.

- [52] Heald, C. L. et al. Exploring the vertical profile of atmospheric organic aerosol: Comparing 17 aircraft field campaigns with a global model. *Atmospheric Chemistry and Physics* 11.24 (2011), pp. 12676–12696. DOI: 10.5194/ACP-11-12673-2011.
- [53] Tsigaridis, K. et al. The AeroCom evaluation and intercomparison of organic aerosol in global models. *Atmospheric Chemistry and Physics* 14.19 (2014), pp. 10845–10895. DOI: 10.5194/ACP-14-10845-2014.
- [54] Hodzic, A. et al. Rethinking the global secondary organic aerosol (SOA) budget: Stronger production, faster removal, shorter lifetime. *Atmospheric Chemistry and Physics* 16.12 (2016), pp. 7917–7941. DOI: 10.5194/ACP-16-7917-2016.
- [55] Shrivastava, M. et al. Global transformation and fate of SOA: Implications of low-volatility SOA and gas-phase fragmentation reactions. *Journal of Geophysical Research: Atmospheres* 120.9 (2015), pp. 4169–4195. DOI: 10.1002/2014JD022563. URL: <https://agupubs.onlinelibrary.wiley.com/doi/full/10.1002/2014JD022563> <https://agupubs.onlinelibrary.wiley.com/doi/abs/10.1002/2014JD022563> <https://agupubs.onlinelibrary.wiley.com/doi/10.1002/2014JD022563>.
- [56] Heald, C. L., Ridley, D. A., Kreidenweis, S. M. and Drury, E. E. Satellite observations cap the atmospheric organic aerosol budget. *Geophysical Research Letters* 37.24 (2010). DOI: 10.1029/2010GL045095. URL: <https://agupubs.onlinelibrary.wiley.com/doi/full/10.1029/2010GL045095> <https://agupubs.onlinelibrary.wiley.com/doi/abs/10.1029/2010GL045095> <https://agupubs.onlinelibrary.wiley.com/doi/10.1029/2010GL045095>.
- [57] Spracklen, D. V. et al. Aerosol mass spectrometer constraint on the global secondary organic aerosol budget. *Atmospheric Chemistry and Physics* 11.23 (2011), pp. 12109–12136. DOI: 10.5194/ACP-11-12109-2011.
- [58] Glasius, M. and Goldstein, A. H. *Recent Discoveries and Future Challenges in Atmospheric Organic Chemistry*. 2016. DOI: 10.1021/acs.est.5b05105. URL: <https://pubs.acs.org/sharingguidelines>.

- [59] Knudsen, J. T. and Gershenzon, J. The Chemical Diversity of Floral Scent. *Biology of Floral Scent* (2020), pp. 57–78. DOI: 10.1201/9780429455612-5. URL: <https://www.taylorfrancis.com/chapters/edit/10.1201/9780429455612-5/chemical-diversity-floral-scent-jette-knudsen-jonathan-gershenzon>.
- [60] Cofer, T. M., Seidl-Adams, I. and Tumlinson, J. H. From Acetoin to (Z)-3-Hexen-1-ol: The Diversity of Volatile Organic Compounds that Induce Plant Responses. *Journal of Agricultural and Food Chemistry* (2018). DOI: 10.1021/ACS.JAFC.8B03010. URL: <https://pubs.acs.org/doi/abs/10.1021/acs.jafc.8b03010>.
- [61] Pichersky, E. and Raguso, R. A. Why do plants produce so many terpenoid compounds? *New Phytologist* 220.3 (2018), pp. 692–702. DOI: 10.1111/NPH.14178.
- [62] Raguso, R. A. Start making scents: the challenge of integrating chemistry into pollination ecology. *Entomologia Experimentalis et Applicata* 128.1 (2008), pp. 196–207. DOI: 10.1111/J.1570-7458.2008.00683.X. URL: <https://onlinelibrary.wiley.com/doi/full/10.1111/j.1570-7458.2008.00683.x>
<https://onlinelibrary.wiley.com/doi/abs/10.1111/j.1570-7458.2008.00683.x>
<https://onlinelibrary.wiley.com/doi/10.1111/j.1570-7458.2008.00683.x>.
- [63] TCJ, T. and M, E. Tritrophic Interactions Mediated by Herbivore-Induced Plant Volatiles: Mechanisms, Ecological Relevance, and Application Potential. *Annual review of entomology* 63 (2018), pp. 433–452. DOI: 10.1146/ANNUREV-ENTO-020117-043507. URL: <https://pubmed.ncbi.nlm.nih.gov/29324043/>.
- [64] J, T. and K, S. Multifunctionality of herbivory-induced plant volatiles in chemical communication in tritrophic interactions. *Current opinion in insect science* 32 (2019), pp. 110–117. DOI: 10.1016/J.COIS.2019.01.003. URL: <https://pubmed.ncbi.nlm.nih.gov/31113622/>.

- [65] Z, A. and MS, C. Indirect plant defense against insect herbivores: a review. *Insect science* 25.1 (2018), pp. 2–23. DOI: 10.1111/1744-7917.12436. URL: <https://pubmed.ncbi.nlm.nih.gov/28035791/>.
- [66] Moraes, C. M. D., Mescher, M. C. and Tumlinson, J. H. Caterpillar-induced nocturnal plant volatiles repel conspecific females. *Nature* 2001 410:6828 410.6828 (2001), pp. 577–580. DOI: 10.1038/35069058. URL: <https://www.nature.com/articles/35069058>.
- [67] Piesik, D., Wenda-Piesik, A., Weaver, D. K. and Morrill, W. L. Influence of Fusarium Crown Rot Disease on Semiochemical Production by Wheat Plants. *Journal of Phytopathology* 155.7-8 (2007), pp. 488–496. DOI: 10.1111/J.1439-0434.2007.01266.X. URL: <https://onlinelibrary.wiley.com/doi/full/10.1111/j.1439-0434.2007.01266.x> <https://onlinelibrary.wiley.com/doi/abs/10.1111/j.1439-0434.2007.01266.x> <https://onlinelibrary.wiley.com/doi/10.1111/j.1439-0434.2007.01266.x>.
- [68] Hatanaka, A., Kajiwara, T. and Sekiya, J. Biosynthetic pathway for C6-aldehydes formation from linolenic acid in green leaves. *Chemistry and Physics of Lipids* 44.2-4 (1987), pp. 341–361. DOI: 10.1016/0009-3084(87)90057-0.
- [69] Dudareva, N., Negre, F., Nagegowda, D. A. and Orlova, I. Plant Volatiles: Recent Advances and Future Perspectives. <https://doi.org/10.1080/07352680600899973> 25.5 (2007), pp. 417–440. DOI: 10.1080/07352680600899973. URL: <https://www.tandfonline.com/doi/abs/10.1080/07352680600899973>.
- [70] F, L., C, B., F, B. and I, N. On the induction of volatile organic compound emissions by plants as consequence of wounding or fluctuations of light and temperature. *Plant, cell & environment* 29.9 (2006), pp. 1820–1828. DOI: 10.1111/J.1365-3040.2006.01561.X. URL: <https://pubmed.ncbi.nlm.nih.gov/16913871/>.

- [71] Turlings, T. C. and Tumlinson, J. H. Systemic release of chemical signals by herbivore-injured corn. *Proceedings of the National Academy of Sciences of the United States of America* 89.17 (1992), p. 8399. DOI: 10.1073/PNAS.89.17.8399. URL: [/pmc/articles/PMC49926/?report=abstract%20https://www.ncbi.nlm.nih.gov/pmc/articles/PMC49926/](https://www.ncbi.nlm.nih.gov/pmc/articles/PMC49926/).
- [72] KOST, C. and HEIL, M. Herbivore-induced plant volatiles induce an indirect defence in neighbouring plants. *Journal of Ecology* 94.3 (2006), pp. 619–628. DOI: 10.1111/J.1365-2745.2006.01120.X. URL: <https://besjournals.onlinelibrary.wiley.com/doi/full/10.1111/j.1365-2745.2006.01120.x%20https://besjournals.onlinelibrary.wiley.com/doi/abs/10.1111/j.1365-2745.2006.01120.x%20https://besjournals.onlinelibrary.wiley.com/doi/10.1111/j.1365-2745.2006.01120.x>.
- [73] Yamauchi, Y., Kunishima, M., Mizutani, M. and Sugimoto, Y. Reactive short-chain leaf volatiles act as powerful inducers of abiotic stress-related gene expression. *Scientific Reports* 2015 5:1 5.1 (2015), pp. 1–8. DOI: 10.1038/srep08030. URL: <https://www.nature.com/articles/srep08030>.
- [74] Lun, X. et al. Reviews of emission of biogenic volatile organic compounds (BVOCs) in Asia. *Journal of Environmental Sciences (China)* 95 (2020), pp. 266–277. DOI: 10.1016/j.jes.2020.04.043.
- [75] Otu-Larbi, F. et al. Modelling the effect of the 2018 summer heatwave and drought on isoprene emissions in a UK woodland. *Global Change Biology* 26.4 (2020), pp. 2320–2335. DOI: 10.1111/gcb.14963.
- [76] Sharkey, T. D., Wiberley, A. E. and Donohue, A. R. Isoprene Emission from Plants: Why and How. *Annals of Botany* 101.1 (2008), p. 5. DOI: 10.1093/AOB/MCM240. URL: [/pmc/articles/PMC2701830/?report=abstract%20https://www.ncbi.nlm.nih.gov/pmc/articles/PMC2701830/](https://www.ncbi.nlm.nih.gov/pmc/articles/PMC2701830/).
- [77] IPCC. *Climate Change 2013: The Physical Science Basis. Contribution of Working Group I to the Fifth Assessment Report of the Intergovernmental Panel on Climate Change*. Cambridge University Press, 2013, pp. 1–30.

- [78] Hantson, S. et al. Global isoprene and monoterpene emissions under changing climate, vegetation, CO₂ and land use. *Atmospheric Environment* 155 (2017), pp. 35–45. DOI: 10.1016/J.ATMOSENV.2017.02.010.
- [79] Schurgers, G., Arneth, A. and Hickler, T. Effect of climate-driven changes in species composition on regional emission capacities of biogenic compounds. *Journal of Geophysical Research: Atmospheres* 116.D22 (2011), p. 22304. DOI: 10.1029/2011JD016278. URL: <https://agupubs.onlinelibrary.wiley.com/doi/full/10.1029/2011JD016278>
<https://agupubs.onlinelibrary.wiley.com/doi/abs/10.1029/2011JD016278>
<https://agupubs.onlinelibrary.wiley.com/doi/10.1029/2011JD016278>.
- [80] Winkler, K., Fuchs, R., Rounsevell, M. and Herold, M. Global land use changes are four times greater than previously estimated. *Nature Communications* 2021 12:1 12.1 (2021), pp. 1–10. DOI: 10.1038/s41467-021-22702-2. URL: <https://www.nature.com/articles/s41467-021-22702-2>.
- [81] ROSENKRANZ, M., PUGH, T. A. M., SCHNITZLER, J.-P. and ARNETH, A. Effect of land-use change and management on biogenic volatile organic compound emissions – selecting climate-smart cultivars. *Plant, Cell & Environment* 38.9 (2015), pp. 1896–1912. DOI: 10.1111/PCE.12453. URL: <https://onlinelibrary.wiley.com/doi/full/10.1111/pce.12453>
<https://onlinelibrary.wiley.com/doi/abs/10.1111/pce.12453>
<https://onlinelibrary.wiley.com/doi/10.1111/pce.12453>.
- [82] Chen, W. H. et al. Regional to Global Biogenic Isoprene Emission Responses to Changes in Vegetation From 2000 to 2015. *Journal of Geophysical Research: Atmospheres* 123.7 (2018), pp. 3757–3771. DOI: 10.1002/2017JD027934. URL: <http://landcover..>
- [83] Hewitt, C. N. et al. Nitrogen management is essential to prevent tropical oil palm plantations from causing ground-level ozone pollution. *Proceedings of the National Academy of Sciences* 106.44 (2009), pp. 18447–18451. DOI: 10.1073/PNAS.0907541106. URL: <https://www.pnas.org/content/106/44/18447>
<https://www.pnas.org/content/106/44/18447.abstract>.

- [84] Pankow, J. F. An absorption model of the gas/aerosol partitioning involved in the formation of secondary organic aerosol. *Atmospheric Environment* 28.2 (1994), pp. 189–193. DOI: 10.1016/1352-2310(94)90094-9. URL: <https://linkinghub.elsevier.com/retrieve/pii/1352231094900949>.
- [85] Donahue, N. M., Robinson, A. L., Stanier, C. O. and Pandis, S. N. Coupled partitioning, dilution, and chemical aging of semivolatile organics. *Environmental Science and Technology* 40.8 (2006), pp. 2635–2643. DOI: 10.1021/es052297c. URL: <https://pubs.acs.org/doi/abs/10.1021/es052297c>.
- [86] Kroll, J. H. and Seinfeld, J. H. *Chemistry of secondary organic aerosol: Formation and evolution of low-volatility organics in the atmosphere*. 2008. DOI: 10.1016/j.atmosenv.2008.01.003.
- [87] Odum, J. R. et al. Gas/Particle Partitioning and Secondary Organic Aerosol Yields. *Environmental Science & Technology* 30.8 (1996), pp. 2580–2585. DOI: 10.1021/es950943+. URL: <https://doi.org/10.1021/es950943+>.
- [88] Donahue, N. M., Epstein, S. A., Pandis, S. N. and Robinson, A. L. A two-dimensional volatility basis set: 1. organic-aerosol mixing thermodynamics. *Atmospheric Chemistry and Physics* 11.7 (2011), pp. 3303–3318. DOI: 10.5194/acp-11-3303-2011.
- [89] Donahue, N. M., Kroll, J. H., Pandis, S. N. and Robinson, A. L. A two-dimensional volatility basis set-Part 2: Diagnostics of organic-aerosol evolution. *Atmospheric Chemistry and Physics* 12.2 (2012), pp. 615–634. DOI: 10.5194/acp-12-615-2012.
- [90] Donahue, N. M. et al. How do organic vapors contribute to new-particle formation? *Faraday Discussions* 165.0 (2013), pp. 91–104. DOI: 10.1039/c3fd00046j. URL: <https://pubs.rsc.org/en/content/articlehtml/2013/fd/c3fd00046j%20>
<https://pubs.rsc.org/en/content/articlelanding/2013/fd/c3fd00046j>.
- [91] Huang, W. et al. Chemical Characterization of Highly Functionalized Organonitrates Contributing to Night-Time Organic Aerosol Mass Loadings and

- Particle Growth. *Environmental Science and Technology* 53.3 (2019), pp. 1165–1174. DOI: 10.1021/acs.est.8b05826. URL: <https://pubs.acs.org/doi/abs/10.1021/acs.est.8b05826>.
- [92] Ehn, M. et al. Gas phase formation of extremely oxidized pinene reaction products in chamber and ambient air. *Atmospheric Chemistry and Physics* 12.11 (2012), pp. 5113–5127. DOI: 10.5194/acp-12-5113-2012.
- [93] Lee, S. H. et al. *New Particle Formation in the Atmosphere: From Molecular Clusters to Global Climate*. 2019. DOI: 10.1029/2018JD029356. URL: <https://agupubs.onlinelibrary.wiley.com/doi/full/10.1029/2018JD029356><https://agupubs.onlinelibrary.wiley.com/doi/abs/10.1029/2018JD029356><https://agupubs.onlinelibrary.wiley.com/doi/10.1029/2018JD029356>.
- [94] Sipila, M. et al. The role of sulfuric acid in atmospheric nucleation. *Science* 327.5970 (2010), pp. 1243–1246. DOI: 10.1126/science.1180315. URL: <http://science.sciencemag.org/>.
- [95] Zhang, R. et al. *Nucleation and growth of nanoparticles in the atmosphere*. 2012. DOI: 10.1021/cr2001756. URL: <https://pubs.acs.org/doi/abs/10.1021/cr2001756>.
- [96] Atkinson, R. Gas-phase tropospheric chemistry of volatile organic compounds: 1. Alkanes and alkenes. *Journal of Physical and Chemical Reference Data* 26.2 (1997), pp. 215–290. DOI: 10.1063/1.556012. URL: <https://aip.scitation.org/doi/abs/10.1063/1.556012>.
- [97] Atkinson, R. and Arey, J. Gas-phase tropospheric chemistry of biogenic volatile organic compounds: A review. *Atmospheric Environment* 37.SUPPL. 2 (2003), pp. 197–219. DOI: 10.1016/S1352-2310(03)00391-1.
- [98] Lu, K. D. et al. Observation and modelling of OH and HO₂ concentrations in the Pearl River Delta 2006: A missing OH source in a VOC rich atmosphere. *Atmospheric Chemistry and Physics* 12.3 (2012), pp. 1541–1569. DOI: 10.5194/acp-12-1541-2012.

- [99] Wolfe, G. M. et al. Mapping hydroxyl variability throughout the global remote troposphere via synthesis of airborne and satellite formaldehyde observations. *Proceedings of the National Academy of Sciences of the United States of America* 166.23 (2019), pp. 11171–11180. DOI: 10.1073/pnas.1821661116. URL: www.pnas.org/cgi/doi/10.1073/pnas.1908931116www.pnas.org.
- [100] Heard, D. E. et al. High levels of the hydroxyl radical in the winter urban troposphere. *Geophysical Research Letters* 31.18 (2004), p. 18112. DOI: 10.1029/2004GL020544. URL: <https://agupubs.onlinelibrary.wiley.com/doi/full/10.1029/2004GL020544><https://agupubs.onlinelibrary.wiley.com/doi/abs/10.1029/2004GL020544><https://agupubs.onlinelibrary.wiley.com/doi/10.1029/2004GL020544>.
- [101] Stone, D., Whalley, L. K. and Heard, D. E. Tropospheric OH and HO₂ radicals: Field measurements and model comparisons. *Chemical Society Reviews* 41.19 (2012), pp. 6348–6404. DOI: 10.1039/c2cs35140d. URL: www.rsc.org/csr.
- [102] Atkinson, R. et al. Evaluated kinetic and photochemical data for atmospheric chemistry: Volume II - Gas phase reactions of organic species. *Atmospheric Chemistry and Physics* 6.11 (2006), pp. 3625–4055. DOI: 10.5194/acp-6-3625-2006.
- [103] Newland, M. J. et al. Low-NO atmospheric oxidation pathways in a polluted megacity. *Atmospheric Chemistry and Physics* 21.3 (2021), pp. 1613–1625. DOI: 10.5194/acp-21-1613-2021.
- [104] Hamilton, J. F. et al. Key Role of NO₃ Radicals in the Production of Isoprene Nitrates and Nitrooxyorganosulfates in Beijing. *Environmental Science and Technology* 55.2 (2021), pp. 842–853. DOI: 10.1021/acs.est.0c05689. URL: <https://pubs.acs.org/doi/abs/10.1021/acs.est.0c05689>.
- [105] Hakola, H. et al. In situ measurements of volatile organic compounds in a boreal forest. *Atmospheric Chemistry and Physics* 12.23 (2012), pp. 11665–11678. DOI: 10.5194/acp-12-11665-2012.

- [106] Wennberg, P. O. et al. Gas-Phase Reactions of Isoprene and Its Major Oxidation Products. *Chemical Reviews* 118.7 (2018), pp. 3337–3390. DOI: 10.1021/acs.chemrev.7b00439. URL: <http://pubs.acs.org/doi/10.1021/acs.chemrev.7b00439>.
- [107] Novelli, A. et al. Experimental and theoretical study on the impact of a nitrate group on the chemistry of alkoxy radicals. *Physical Chemistry Chemical Physics* 23.9 (2021), pp. 5474–5495. DOI: 10.1039/D0CP05555G. URL: <https://pubs.rsc.org/en/content/articlehtml/2021/cp/d0cp05555g%20>
<https://pubs.rsc.org/en/content/articlelanding/2021/cp/d0cp05555g>.
- [108] Vereecken, L. Computational study of the stability of α -nitroxy-substituted alkyl radicals. *Chemical Physics Letters* 466.4-6 (2008), pp. 127–130. DOI: 10.1016/J.CPLETT.2008.10.042.
- [109] Isoprene NO₃ Oxidation Products from the RO₂ + HO₂ Pathway. *The Journal of Physical Chemistry A* 119.40 (2015), pp. 10158–10171. DOI: 10.1021/acs.jpca.5b06355. URL: <http://pubs.acs.org/doi/10.1021/acs.jpca.5b06355>.
- [110] Kuwata, K. T., Hermes, M. R., Carlson, M. J. and Zogg, C. K. Computational studies of the isomerization and hydration reactions of acetaldehyde oxide and methyl vinyl carbonyl oxide. *Journal of Physical Chemistry A* 114.34 (2010), pp. 9192–9204. DOI: 10.1021/JP105358V/SUPPL{_}FILE/JP105358V{_}SI{_}001.PDF. URL: <https://pubs.acs.org/doi/full/10.1021/jp105358v>.
- [111] Ehn, M. et al. A large source of low-volatility secondary organic aerosol. *Nature* 506.7489 (2014), pp. 476–479. DOI: 10.1038/nature13032. URL: <https://www.nature.com/articles/nature13032>.
- [112] Crounse, J. D. et al. Autoxidation of organic compounds in the atmosphere. *Journal of Physical Chemistry Letters* 4.20 (2013), pp. 3513–3520. DOI: 10.1021/jz4019207. URL: <https://pubs.acs.org/doi/abs/10.1021/jz4019207>.

- [113] Iyer, S. et al. Molecular mechanism for rapid autoxidation in α -pinene ozonolysis. *Nature Communications* 2021 12:1 12.1 (2021), pp. 1–6. DOI: 10.1038/s41467-021-21172-w. URL: <https://www.nature.com/articles/s41467-021-21172-w>.
- [114] Bianchi, F. et al. *Highly Oxygenated Organic Molecules (HOM) from Gas-Phase Autoxidation Involving Peroxy Radicals: A Key Contributor to Atmospheric Aerosol*. 2019. DOI: 10.1021/acs.chemrev.8b00395. URL: <https://pubs.acs.org/sharingguidelines>.
- [115] Pye, H. O. et al. Anthropogenic enhancements to production of highly oxygenated molecules from autoxidation. *Proceedings of the National Academy of Sciences of the United States of America* 116.14 (2019), pp. 6641–6646. DOI: 10.1073/pnas.1810774116. URL: <https://www.pnas.org/content/116/14/6641>
<https://www.pnas.org/content/116/14/6641.abstract>.
- [116] Heald, C. L. et al. Predicted change in global secondary organic aerosol concentrations in response to future climate, emissions, and land use change. *Journal of Geophysical Research Atmospheres* 113.5 (2008). DOI: 10.1029/2007JD009092.
- [117] Pandis, S. N., Paulson, S. E., Seinfeld, J. H. and Flagan, R. C. Aerosol formation in the photooxidation of isoprene and β -pinene. *Atmospheric Environment. Part A. General Topics* 25.5-6 (1991), pp. 997–1008. DOI: 10.1016/0960-1686(91)90141-S. URL: <https://linkinghub.elsevier.com/retrieve/pii/096016869190141S>.
- [118] Claeys, M. Formation of Secondary Organic Aerosols Through Photooxidation of Isoprene. *Science* 303.5661 (2004), pp. 1173–1176. DOI: 10.1126/science.1092805. URL: <http://www.sciencemag.org/cgi/doi/10.1126/science.1092805>.
- [119] Carlton, A. G., Wiedinmyer, C. and Kroll, J. H. A review of Secondary Organic Aerosol (SOA) formation from isoprene. *Atmospheric Chemistry and Physics* 9.14 (2009), pp. 4987–5005. DOI: 10.5194/acp-9-4987-2009. URL: <http://www.atmos-chem-phys.net/9/4987/2009/>.

- [120] Kroll, J. H. et al. Secondary organic aerosol formation from isoprene photooxidation. *Environmental Science and Technology* 40.6 (2006), pp. 1869–1877. DOI: 10.1021/es0524301. URL: <https://pubs.acs.org/doi/abs/10.1021/es0524301>.
- [121] Paulot, F. et al. Unexpected Epoxide Formation in the Gas-Phase Photooxidation of Isoprene. *Science* 325.5941 (2009), pp. 730–733. DOI: 10.1126/science.1172910. URL: <http://www.sciencemag.org/cgi/doi/10.1126/science.1172910>.
- [122] Kourtchev, I. et al. Observation of 2-methyltetrols and related photo-oxidation products of isoprene in boreal forest aerosols from Hyytiälä, Finland. *Atmospheric Chemistry and Physics* 5.10 (2005), pp. 2761–2770. DOI: 10.5194/ACP-5-2761-2005.
- [123] Chen, Q. et al. Submicron particle mass concentrations and sources in the Amazonian wet season (AMAZE-08). *Atmospheric Chemistry and Physics* 15.7 (2015), pp. 3687–3701. DOI: 10.5194/acp-15-3687-2015. URL: <https://www.atmos-chem-phys.net/15/3687/2015/>.
- [124] Glasius, M. et al. Organosulfates in aerosols downwind of an urban region in central Amazon. *Environmental Science: Processes & Impacts* 20.11 (2018), pp. 1546–1558. DOI: 10.1039/C8EM00413G. URL: <http://xlink.rsc.org/?DOI=C8EM00413G>.
- [125] Bryant, D. J. et al. Strong anthropogenic control of secondary organic aerosol formation from isoprene in Beijing. *Atmospheric Chemistry and Physics* 20.12 (2020), pp. 7531–7552. DOI: 10.5194/acp-20-7531-2020. URL: <https://www.atmos-chem-phys.net/20/7531/2020/>.
- [126] Wang, Y. et al. The secondary formation of organosulfates under interactions between biogenic emissions and anthropogenic pollutants in summer in Beijing. *Atmospheric Chemistry and Physics* 18.14 (2018), pp. 10693–10713. DOI: 10.5194/acp-18-10693-2018. URL: <https://www.atmos-chem-phys.net/18/10693/2018/>.

- [127] Surratt, J. D. et al. Reactive intermediates revealed in secondary organic aerosol formation from isoprene. *Proceedings of the National Academy of Sciences* 107.15 (2010), pp. 6640–6645. DOI: 10.1073/pnas.0911114107. URL: <http://www.pnas.org/cgi/doi/10.1073/pnas.0911114107>.
- [128] Lin, Y. H. et al. Isoprene epoxydiols as precursors to secondary organic aerosol formation: Acid-catalyzed reactive uptake studies with authentic compounds. *Environmental Science and Technology* 46.1 (2012), pp. 250–258. DOI: 10.1021/es202554c.
- [129] Lin, Y. H. et al. Light-absorbing oligomer formation in secondary organic aerosol from reactive uptake of isoprene epoxydiols. *Environmental Science and Technology* 48.20 (2014), pp. 12012–12021. DOI: 10.1021/es503142b. URL: <https://pubs.acs.org/doi/abs/10.1021/es503142b>.
- [130] Lin, Y. H. et al. Epoxide as a precursor to secondary organic aerosol formation from isoprene photooxidation in the presence of nitrogen oxides. *Proceedings of the National Academy of Sciences of the United States of America* 110.17 (2013), pp. 6718–6723. DOI: 10.1073/pnas.1221150110.
- [131] Orlando, J. J., Tyndall, G. S. and Paulson, S. E. Mechanism of the OH-initiated oxidation of methacrolein. *Geophysical Research Letters* 26.14 (1999), pp. 2191–2194. DOI: 10.1029/1999GL900453. URL: <https://agupubs.onlinelibrary.wiley.com/doi/full/10.1029/1999GL900453>
<https://agupubs.onlinelibrary.wiley.com/doi/abs/10.1029/1999GL900453>
<https://agupubs.onlinelibrary.wiley.com/doi/10.1029/1999GL900453>.
- [132] Chan, M. N. et al. Characterization and quantification of isoprene-derived epoxydiols in ambient aerosol in the southeastern united states. *Environmental Science and Technology* 44.12 (2010), pp. 4590–4596. DOI: 10.1021/es100596b. URL: <https://pubs.acs.org/doi/abs/10.1021/es100596b>.
- [133] Nguyen, T. B. et al. Mechanism of the hydroxyl radical oxidation of methacryloyl peroxyxynitrate (MPAN) and its pathway toward secondary organic aerosol formation in the atmosphere. *Physical Chemistry Chemical Physics* 17.27 (2015), pp. 17914–17926. DOI: 10.1039/c5cp02001h.

- [134] Surratt, J. D. et al. Organosulfate Formation in Biogenic Secondary Organic Aerosol. *The Journal of Physical Chemistry A* 112.36 (2008), pp. 8345–8378. DOI: 10.1021/jp802310p. URL: <https://pubs.acs.org/doi/10.1021/jp802310p>.
- [135] Gómez-González, Y. et al. Characterization of organosulfates from the photooxidation of isoprene and unsaturated fatty acids in ambient aerosol using liquid chromatography - electrospray ionization mass spectrometry. *Journal of Mass Spectrometry* 43.3 (2008), pp. 371–382. DOI: 10.1002/jms.1329. URL: <http://doi.wiley.com/10.1002/jms.1329>.
- [136] Rudziński, K. J., Gmachowski, L. and Kuznietsova, I. Reactions of isoprene and sulphony radical-anions - A possible source of atmospheric organosulphites and organosulphates. *Atmospheric Chemistry and Physics* 9.6 (2009), pp. 2129–2140. DOI: 10.5194/acp-9-2129-2009.
- [137] Chen, Y. et al. Heterogeneous Hydroxyl Radical Oxidation of Isoprene Epoxydiol-Derived Methyltetrol Sulfates: Plausible Formation Mechanisms of Previously Unexplained Organosulfates in Ambient Fine Aerosols. *Environmental Science & Technology Letters* 0.1a (2020). DOI: 10.1021/acs.estlett.0c00276.
- [138] Riva, M. et al. Effect of Organic Coatings, Humidity and Aerosol Acidity on Multiphase Chemistry of Isoprene Epoxydiols. *Environmental Science and Technology* 50.11 (2016), pp. 5580–5588. DOI: 10.1021/acs.est.5b06050.
- [139] Smith, M. L., Bertram, A. K. and Martin, S. T. Deliquescence, efflorescence, and phase miscibility of mixed particles of ammonium sulfate and isoprene-derived secondary organic material. *Atmospheric Chemistry and Physics* 12.20 (2012), pp. 9613–9628. DOI: 10.5194/acp-12-9613-2012.
- [140] You, Y. et al. Images reveal that atmospheric particles can undergo liquid-liquid phase separations. *Proceedings of the National Academy of Sciences of the United States of America* 109.33 (2012), pp. 13188–13193. DOI: 10.1073/pnas.1206414109. URL: <https://www.pnas.org/content/109/33/13188%20https://www.pnas.org/content/109/33/13188.abstract>.

- [141] Zhou, S. et al. Multiphase reactivity of polycyclic aromatic hydrocarbons is driven by phase separation and diffusion limitations. *Proceedings of the National Academy of Sciences of the United States of America* 116.24 (2019), pp. 11658–11663. DOI: 10.1073/pnas.1902517116. URL: <https://www.pnas.org/content/116/24/11658><https://www.pnas.org/content/116/24/11658.abstract>.
- [142] Shrestha, M. et al. On Surface Order and Disorder of α -Pinene-Derived Secondary Organic Material. *The Journal of Physical Chemistry A* 119.19 (2015), pp. 4609–4617. DOI: 10.1021/jp510780e. URL: <http://pubs.acs.org/doi/10.1021/jp510780e>.
- [143] Riva, M. et al. Increasing Isoprene Epoxydiol-to-Inorganic Sulfate Aerosol Ratio Results in Extensive Conversion of Inorganic Sulfate to Organosulfur Forms: Implications for Aerosol Physicochemical Properties. *Environmental Science & Technology* (2019), acs.est.9b01019. DOI: 10.1021/acs.est.9b01019. URL: <http://pubs.acs.org/doi/10.1021/acs.est.9b01019>.
- [144] Zhang, Y. et al. Effect of the Aerosol-Phase State on Secondary Organic Aerosol Formation from the Reactive Uptake of Isoprene-Derived Epoxydiols (IEPOX). *Environmental Science and Technology Letters* 5.3 (2018), pp. 167–174. DOI: 10.1021/acs.estlett.8b00044. URL: <https://pubs.acs.org/sharingguidelines>.
- [145] Drozd, G. T., Woo, J. L. and McNeill, V. F. Self-limited uptake of α -pinene oxide to acidic aerosol: The effects of liquid-liquid phase separation and implications for the formation of secondary organic aerosol and organosulfates from epoxides. *Atmospheric Chemistry and Physics* 13.16 (2013), pp. 8255–8263. DOI: 10.5194/acp-13-8255-2013.
- [146] Olson, N. E. et al. Reactive Uptake of Isoprene Epoxydiols Increases the Viscosity of the Core of Phase-Separated Aerosol Particles. *ACS Earth and Space Chemistry* 3.8 (2019), pp. 1402–1414. DOI: 10.1021/acsearthspacechem.9b00138. URL: <https://pubs.acs.org/sharingguidelines>.

- [147] Zhang, Y. et al. Joint Impacts of Acidity and Viscosity on the Formation of Secondary Organic Aerosol from Isoprene Epoxydiols (IEPOX) in Phase Separated Particles. *ACS Earth and Space Chemistry* 3.12 (2019), pp. 2646–2658. DOI: 10.1021/acsearthspacechem.9b00209.
- [148] Schmedding, R. et al. A-Pinene-Derived organic coatings on acidic sulfate aerosol impacts secondary organic aerosol formation from isoprene in a box model. *Atmospheric Environment* 213 (2019), pp. 456–462. DOI: 10.1016/j.atmosenv.2019.06.005.
- [149] Nestorowicz, K. et al. Chemical composition of isoprene SOA under acidic and non-acidic conditions: effect of relative humidity. *Atmospheric Chemistry and Physics* 18.24 (2018), pp. 18101–18121. DOI: 10.5194/acp-18-18101-2018. URL: <https://www.atmos-chem-phys.net/18/18101/2018/>.
- [150] Doughty, D. et al. Nocturnal isoprene declines in a semi-urban environment. *Journal of Atmospheric Chemistry* 72.3-4 (2015), pp. 215–234. DOI: 10.1007/s10874-012-9247-0. URL: <https://link.springer.com/article/10.1007/s10874-012-9247-0>.
- [151] Kashyap, P., Kumar, A., Kumar, R. P. and Kumar, K. Biogenic and anthropogenic isoprene emissions in the subtropical urban atmosphere of Delhi. *Atmospheric Pollution Research* 10.5 (2019), pp. 1691–1698. DOI: 10.1016/j.apr.2019.07.004.
- [152] Ng, N. L. et al. Secondary organic aerosol (SOA) formation from reaction of isoprene with nitrate radicals (NO₃). *Atmospheric Chemistry and Physics* 8.14 (2008), pp. 4117–4140. DOI: 10.5194/acp-8-4117-2008.
- [153] Hoyle, C. R. et al. *A review of the anthropogenic influence on biogenic secondary organic aerosol*. 2011. DOI: 10.5194/acp-11-321-2011.
- [154] Zhang, H. et al. Monoterpenes are the largest source of summertime organic aerosol in the southeastern United States. *Proceedings of the National Academy of Sciences of the United States of America* 115.9 (2018), pp. 2038–2043. DOI: 10.1073/pnas.1717513115. URL: www.pnas.org/cgi/doi/10.1073/pnas.1717513115.

- [155] Edwards, P. M. et al. Transition from high- to low-NO_x control of night-time oxidation in the southeastern US. *Nature Geoscience* 10.7 (2017), pp. 490–495. DOI: 10.1038/ngeo2976. URL: www.nature.com/naturegeoscience.
- [156] Eddingsaas, N. C., VanderVelde, D. G. and Wennberg, P. O. Kinetics and Products of the Acid-Catalyzed Ring-Opening of Atmospherically Relevant Butyl Epoxy Alcohols. *Journal of Physical Chemistry A* 114.31 (2010), pp. 8106–8113. DOI: 10.1021/JP103907C. URL: <https://pubs.acs.org/doi/full/10.1021/jp103907c>.
- [157] Weber, R. J., Guo, H., Russell, A. G. and Nenes, A. High aerosol acidity despite declining atmospheric sulfate concentrations over the past 15 years. *Nature Geoscience* 9.4 (2016), pp. 282–285. DOI: 10.1038/ngeo2665. URL: <http://nadp.sws.uiuc.edu/amon>.
- [158] Rengarajan, R., Sudheer, A. K. and Sarin, M. M. Aerosol acidity and secondary organic aerosol formation during wintertime over urban environment in western India. *Atmospheric Environment* 45.11 (2011), pp. 1940–1945. DOI: 10.1016/j.atmosenv.2011.01.026.
- [159] Pye, H. O. et al. *The acidity of atmospheric particles and clouds*. 2020. DOI: 10.5194/acp-20-4809-2020.
- [160] Zhang, B. et al. Significant contrasts in aerosol acidity between China and the United States. *Atmospheric Chemistry and Physics* 21.10 (2021), pp. 8341–8356. DOI: 10.5194/acp-21-8341-2021.
- [161] Sarrafzadeh, M. et al. Impact of NO_x and OH on secondary organic aerosol formation from β -pinene photooxidation. *Atmospheric Chemistry and Physics* 16.17 (2016), pp. 11237–11248. DOI: 10.5194/acp-16-11237-2016. URL: <https://www.atmos-chem-phys.net/16/11237/2016/>.
- [162] Wildt, J. et al. Suppression of new particle formation from monoterpene oxidation by NO_x. *Atmospheric Chemistry and Physics* 14.6 (2014), pp. 2789–2804. DOI: 10.5194/acp-14-2789-2014.

- [163] Zhao, D. et al. Effects of NO_x and SO₂ on the secondary organic aerosol formation from photooxidation of α -pinene and limonene. *Atmospheric Chemistry and Physics* 18.3 (2018), pp. 1611–1628. DOI: 10.5194/acp-18-1611-2018.
- [164] Ng, N. L. et al. Effect of NO_x level on secondary organic aerosol (SOA) formation from the photooxidation of terpenes. *Atmospheric Chemistry and Physics* 7.19 (2007), pp. 5159–5174. DOI: 10.5194/acp-7-5159-2007.
- [165] Tasoglou, A. and Pandis, S. N. Formation and chemical aging of secondary organic aerosol during the β -caryophyllene oxidation. *Atmospheric Chemistry and Physics* 15.11 (2015), pp. 6035–6046. DOI: 10.5194/acp-15-6035-2015.
- [166] Jayne, J. T. et al. *Development of an aerosol mass spectrometer for size and composition analysis of submicron particles*. 2000. DOI: 10.1080/027868200410840. URL: <https://www.tandfonline.com/action/journalInformation?journalCode=uast20>.
- [167] Ng, N. L. et al. Changes in organic aerosol composition with aging inferred from aerosol mass spectra. *Atmospheric Chemistry and Physics* 11.13 (2011), pp. 6465–6474. DOI: 10.5194/acp-11-6465-2011.
- [168] Kroll, J. H. et al. Chamber studies of secondary organic aerosol growth by reactive uptake of simple carbonyl compounds. *Journal of Geophysical Research Atmospheres* 110.23 (2005), pp. 1–10. DOI: 10.1029/2005JD006004.
- [169] Cubison, M. J. et al. Effects of aging on organic aerosol from open biomass burning smoke in aircraft and laboratory studies. *Atmospheric Chemistry and Physics* 11.23 (2011), pp. 12049–12064. DOI: 10.5194/acp-11-12049-2011.
- [170] Grieshop, A. P., Logue, J. M., Donahue, N. M. and Robinson, A. L. Laboratory investigation of photochemical oxidation of organic aerosol from wood fires 1: Measurement and simulation of organic aerosol evolution. *Atmospheric Chemistry and Physics* 9.4 (2009), pp. 1263–1277. DOI: 10.5194/acp-9-1263-2009.

- [171] Aiken, A. C. et al. O/C and OM/OC ratios of primary, secondary, and ambient organic aerosols with high-resolution time-of-flight aerosol mass spectrometry. *Environmental Science and Technology* 42.12 (2008), pp. 4478–4485. DOI: 10.1021/es703009q.
- [172] Huang, W. et al. Seasonal characteristics of organic aerosol chemical composition and volatility in Stuttgart, Germany. *Atmospheric Chemistry and Physics* 19.18 (2019), pp. 11687–11700. DOI: 10.5194/ACP-19-11687-2019.
- [173] Surratt, J. D. et al. Evidence for Organosulfates in Secondary Organic Aerosol. *Environmental Science & Technology* 41.2 (2007), pp. 517–527. DOI: 10.1021/es062081q. URL: <https://pubs.acs.org/doi/10.1021/es062081q>.
- [174] Gallimore, P. J. and Kalberer, M. Characterizing an Extractive Electrospray Ionization (EESI) Source for the Online Mass Spectrometry Analysis of Organic Aerosols. *Environmental Science and Technology* 47.13 (2013), pp. 7324–7331. DOI: 10.1021/ES305199H. URL: <https://pubs.acs.org/doi/full/10.1021/es305199h>.
- [175] Eliuk, S. and Makarov, A. *Evolution of Orbitrap Mass Spectrometry Instrumentation*. 2015. DOI: 10.1146/annurev-anchem-071114-040325. URL: www.annualreviews.org.
- [176] Zubarev, R. A. and Makarov, A. Orbitrap mass spectrometry. *Analytical Chemistry* 85.11 (2013), pp. 5288–5296. DOI: 10.1021/ac4001223. URL: <https://pubs.acs.org/sharingguidelines>.
- [177] Kourtchev, I. et al. Effects of anthropogenic emissions on the molecular composition of urban organic aerosols: An ultrahigh resolution mass spectrometry study. *Atmospheric Environment* 89 (2014), pp. 525–532. DOI: 10.1016/j.atmosenv.2014.02.051.
- [178] Kourtchev, I. et al. Molecular composition of biogenic secondary organic aerosols using ultrahigh-resolution mass spectrometry: comparing laboratory and field studies. *Atmospheric Chemistry and Physics* 14.4 (2014), pp. 2155–2167. DOI: 10.5194/acp-14-2155-2014. URL: <https://acp.copernicus.org/articles/14/2155/2014/>.

- [179] Kourtchev, I. et al. Molecular composition of fresh and aged secondary organic aerosol from a mixture of biogenic volatile compounds: a high-resolution mass spectrometry study. *Atmospheric Chemistry and Physics* 15.10 (2015), pp. 5683–5695. DOI: 10.5194/acp-15-5683-2015. URL: <https://acp.copernicus.org/articles/15/5683/2015/>.
- [180] Kourtchev, I. et al. Molecular composition of organic aerosols in central Amazonia: An ultra-high-resolution mass spectrometry study. *Atmospheric Chemistry and Physics* 16.18 (2016), pp. 11899–11913. DOI: 10.5194/acp-16-11899-2016.
- [181] Nizkorodov, S. A., Laskin, J. and Laskin, A. Molecular chemistry of organic aerosols through the application of high resolution mass spectrometry. *Physical Chemistry Chemical Physics* 13.9 (2011), pp. 3612–3629. DOI: 10.1039/c0cp02032j.
- [182] Tong, H. et al. Molecular composition of organic aerosols at urban background and road tunnel sites using ultra-high resolution mass spectrometry. *Faraday Discussions* 189.0 (2016), pp. 51–68. DOI: 10.1039/c5fd00206k. URL: <https://pubs.rsc.org/en/content/articlehtml/2016/fd/c5fd00206k> <https://pubs.rsc.org/en/content/articlelanding/2016/fd/c5fd00206k>.
- [183] Wozniak, A. S. et al. Technical Note: Molecular characterization of aerosol-derived water soluble organic carbon using ultrahigh resolution electrospray ionization Fourier transform ion cyclotron resonance mass spectrometry. *Atmospheric Chemistry and Physics* 8.17 (2008), pp. 5099–5111. DOI: 10.5194/ACP-8-5099-2008.
- [184] Wang, Y. et al. Organosulfates in atmospheric aerosols in shanghai, china: Seasonal and interannual variability, origin, and formation mechanisms. *Atmospheric Chemistry and Physics* 21.4 (2021), pp. 2959–2980. DOI: 10.5194/acp-21-2959-2021.
- [185] Brüggemann, M. et al. Quantification of known and unknown terpenoid organosulfates in PM10 using untargeted LC–HRMS/MS: contrasting summertime rural Germany and the North China Plain. *Environmental*

- Chemistry* 16.5 (2019), p. 333. DOI: 10.1071/EN19089. URL:
<http://www.publish.csiro.au/?paper=EN19089>.
- [186] Brüggemann, M. et al. *Organosulfates in Ambient Aerosol: State of Knowledge and Future Research Directions on Formation, Abundance, Fate, and Importance*. 2020. DOI: 10.1021/acs.est.9b06751. URL:
<https://dx.doi.org/10.1021/acs.est.9b06751>.
- [187] Cui, T. et al. Development of a hydrophilic interaction liquid chromatography (HILIC) method for the chemical characterization of water-soluble isoprene epoxydiol (IEPOX)-derived secondary organic aerosol. *Environmental Science: Processes & Impacts* 20.11 (2018), pp. 1524–1536. DOI: 10.1039/C8EM00308D. URL: <http://xlink.rsc.org/?DOI=C8EM00308D>.
- [188] Tisler, S., Pattison, D. I. and Christensen, J. H. Correction of Matrix Effects for Reliable Non-target Screening LC–ESI–MS Analysis of Wastewater. *Analytical Chemistry* 93.24 (2021), pp. 8432–8441. DOI: 10.1021/acs.analchem.1c00357. URL: <https://doi.org/10.1021/acs.analchem.1c00357>.
- [189] Kundu, S. et al. Evidence and quantitation of aromatic organosulfates in ambient aerosols in Lahore, Pakistan. *Atmospheric Chemistry and Physics* 13.9 (2013), pp. 4865–4875. DOI: 10.5194/acp-13-4865-2013.
- [190] Kenseth, C. M. et al. Synthesis of Carboxylic Acid and Dimer Ester Surrogates to Constrain the Abundance and Distribution of Molecular Products in α -Pinene and β -Pinene Secondary Organic Aerosol. *Environmental Science & Technology* (2020). DOI: 10.1021/acs.est.0c01566.
- [191] Rattanavaraha, W. et al. Assessing the impact of anthropogenic pollution on isoprene-derived secondary organic aerosol formation in PM_{2.5} collected from the Birmingham, Alabama, ground site during the 2013 Southern Oxidant and Aerosol Study. *Atmospheric Chemistry and Physics* 16.8 (2016), pp. 4897–4914. DOI: 10.5194/acp-16-4897-2016. URL:
<https://www.atmos-chem-phys.net/16/4897/2016/>.

- [192] Wang, Y. et al. Synthesis of Four Monoterpene-Derived Organosulfates and Their Quantification in Atmospheric Aerosol Samples. *Environmental Science & Technology* 51.12 (2017), pp. 6791–6801. DOI: 10.1021/acs.est.7b01179. URL: <https://pubs.acs.org/doi/10.1021/acs.est.7b01179>.
- [193] Huang, R.-J. et al. Organosulfates in atmospheric aerosol: synthesis and quantitative analysis of PM_{2.5} from Xi'an, northwestern China. *Atmospheric Measurement Techniques* 11.6 (2018), pp. 3447–3456. DOI: 10.5194/amt-11-3447-2018. URL: <https://www.atmos-meas-tech.net/11/3447/2018/>.
- [194] Wang, Y., Tong, R. and Yu, J. Z. Chemical Synthesis of Multifunctional Air Pollutants: Terpene-Derived Nitrooxy Organosulfates. *Environmental Science & Technology* (2021), acs.est.1c00348. DOI: 10.1021/acs.est.1c00348. URL: <https://pubs.acs.org/doi/10.1021/acs.est.1c00348>.
- [195] Wang, Y. et al. Monoterpene and Sesquiterpene α -Hydroxy Organosulfates: Synthesis, MS/MS Characteristics, and Ambient Presence. *Environmental Science and Technology* 53.21 (2019), pp. 12278–12290. DOI: 10.1021/acs.est.9b04703. URL: <https://pubs.acs.org/sharingguidelines>.
- [196] Liigand, J., Laaniste, A. and Kruve, A. pH Effects on Electrospray Ionization Efficiency. *Journal of the American Society for Mass Spectrometry* 28.3 (2017), pp. 461–469. DOI: 10.1007/s13361-016-1563-1.
- [197] Liigand, J. et al. Quantification for non-targeted LC/MS screening without standard substances. *Scientific Reports* 10.1 (2020), pp. 1–10. DOI: 10.1038/s41598-020-62573-z. URL: <https://www.nature.com/articles/s41598-020-62573-z>.
- [198] Kruve, A. Strategies for drawing quantitative conclusions from non-targeted liquid chromatography high-resolution mass spectrometry analysis. *Analytical Chemistry* (2020), acs.analchem.9b03481. DOI: 10.1021/acs.analchem.9b03481. URL: <https://pubs.acs.org/doi/abs/10.1021/acs.analchem.9b03481>.

- [199] Hu, J., Wang, Y., Ying, Q. and Zhang, H. Spatial and temporal variability of PM_{2.5} and PM₁₀ over the North China Plain and the Yangtze River Delta, China. *Atmospheric Environment* 95 (2014), pp. 598–609. DOI: 10.1016/J.ATMOSENV.2014.07.019. URL: <https://www.sciencedirect.com/science/article/pii/S1352231014005408?via%3Dihub>.
- [200] Pope, C. A. Review: Epidemiological Basis for Particulate Air Pollution Health Standards. *Aerosol Science and Technology* 32.1 (2000), pp. 4–14. DOI: 10.1080/027868200303885. URL: <http://www.tandfonline.com/doi/abs/10.1080/027868200303885>.
- [201] Jerrett, M. et al. Long-Term Ozone Exposure and Mortality. *New England Journal of Medicine* 360.11 (2009), pp. 1085–1095. DOI: 10.1056/NEJMoa0803894. URL: <http://www.nejm.org/doi/abs/10.1056/NEJMoa0803894>.
- [202] Beelen, R. et al. Effects of long-term exposure to air pollution on natural-cause mortality: an analysis of 22 European cohorts within the multicentre ESCAPE project. *The Lancet* 383.9919 (2014), pp. 785–795. DOI: 10.1016/S0140-6736(13)62158-3. URL: <https://www.sciencedirect.com/science/article/pii/S0140673613621583?via%3Dihub>.
- [203] Laurent, O. et al. Sources and contents of air pollution affecting term low birth weight in Los Angeles County, California, 2001–2008. *Environmental Research* 134 (2014), pp. 488–495. DOI: 10.1016/J.ENVRES.2014.05.003. URL: <https://www.sciencedirect.com/science/article/pii/S0013935114001546?via%3Dihub>.
- [204] Ostro, B. et al. Associations of Mortality with Long-Term Exposures to Fine and Ultrafine Particles, Species and Sources: Results from the California Teachers Study Cohort. *Environmental Health Perspectives* 123.6 (2015), pp. 549–556. DOI: 10.1289/ehp.1408565. URL: <https://ehp.niehs.nih.gov/doi/10.1289/ehp.1408565>.

- [205] Hu, J. et al. Premature Mortality Attributable to Particulate Matter in China: Source Contributions and Responses to Reductions. *Environmental Science & Technology* 51.17 (2017), pp. 9950–9959. DOI: 10.1021/acs.est.7b03193. URL: <http://pubs.acs.org/doi/10.1021/acs.est.7b03193>.
- [206] Hu, W. et al. Chemical composition, sources, and aging process of submicron aerosols in Beijing: Contrast between summer and winter. *Journal of Geophysical Research: Atmospheres* 121.4 (2016), pp. 1955–1977. DOI: 10.1002/2015JD024020. URL: <http://doi.wiley.com/10.1002/2015JD024020>.
- [207] Zhang, Y. et al. Seasonal characterization of components and size distributions for submicron aerosols in Beijing. *Science China Earth Sciences* 56.5 (2013), pp. 890–900. DOI: 10.1007/s11430-012-4515-z. URL: <http://link.springer.com/10.1007/s11430-012-4515-z>.
- [208] Zhang, Q. et al. Understanding atmospheric organic aerosols via factor analysis of aerosol mass spectrometry: a review. *Analytical and Bioanalytical Chemistry* 401.10 (2011), pp. 3045–3067. DOI: 10.1007/s00216-011-5355-y. URL: <http://link.springer.com/10.1007/s00216-011-5355-y>.
- [209] Sun, Y. et al. Source apportionment of organic aerosol from 2-year highly time-resolved measurements by an aerosol chemical speciation monitor in Beijing, China. *Atmospheric Chemistry and Physics* 18.12 (2018), pp. 8469–8489. DOI: 10.5194/acp-18-8469-2018. URL: <https://www.atmos-chem-phys.net/18/8469/2018/>.
- [210] Zhang, Y. et al. High Contribution of Nonfossil Sources to Submicrometer Organic Aerosols in Beijing, China. *Environmental Science & Technology* 51.14 (2017), pp. 7842–7852. DOI: 10.1021/acs.est.7b01517. URL: <http://pubs.acs.org/doi/10.1021/acs.est.7b01517>.
- [211] Hu, J. et al. Modeling biogenic and anthropogenic secondary organic aerosol in China. *Atmospheric Chemistry and Physics* 17.1 (2017), pp. 77–92. DOI: 10.5194/acp-17-77-2017. URL: <https://www.atmos-chem-phys.net/17/77/2017/>.

- [212] Kleindienst, T. E. et al. Estimates of the contributions of biogenic and anthropogenic hydrocarbons to secondary organic aerosol at a southeastern US location. *Atmospheric Environment* 41.37 (2007), pp. 8288–8300. DOI: 10.1016/J.ATMOSENV.2007.06.045. URL: <https://www.sciencedirect.com/science/article/pii/S135223100700581X?via%3Dihub>.
- [213] Ding, X. et al. Spatial distributions of secondary organic aerosols from isoprene, monoterpenes, β -caryophyllene, and aromatics over China during summer. *Journal of Geophysical Research: Atmospheres* 119.20 (2014), pp. 11, 877–11, 891. DOI: 10.1002/2014JD021748. URL: <http://doi.wiley.com/10.1002/2014JD021748>.
- [214] Wang, Q. et al. Impact of Secondary Organic Aerosol Tracers on Tracer-Based Source Apportionment of Organic Carbon and PM _{2.5} : A Case Study in the Pearl River Delta, China. *ACS Earth and Space Chemistry* 1.9 (2017), pp. 562–571. DOI: 10.1021/acsearthspacechem.7b00088. URL: <http://pubs.acs.org/doi/10.1021/acsearthspacechem.7b00088>.
- [215] Robinson, N. H. et al. Evidence for a significant proportion of Secondary Organic Aerosol from isoprene above a maritime tropical forest. *Atmospheric Chemistry and Physics* 11.3 (2011), pp. 1039–1050. DOI: 10.5194/acp-11-1039-2011. URL: <http://www.atmos-chem-phys.net/11/1039/2011/>.
- [216] Hu, W. W. et al. Characterization of a real-time tracer for isoprene epoxydiols-derived secondary organic aerosol (IEPOX-SOA) from aerosol mass spectrometer measurements. *Atmospheric Chemistry and Physics* 15.20 (2015), pp. 11807–11833. DOI: 10.5194/acp-15-11807-2015. URL: <https://www.atmos-chem-phys.net/15/11807/2015/>.
- [217] Zhang, Y. et al. Limited formation of isoprene epoxydiols-derived secondary organic aerosol under NO_x-rich environments in Eastern China. *Geophysical Research Letters* 44.4 (2017), pp. 2035–2043. DOI: 10.1002/2016GL072368. URL: <http://doi.wiley.com/10.1002/2016GL072368>.

- [218] He, Q.-F. et al. Secondary Organic Aerosol Formation From Isoprene Epoxides in the Pearl River Delta, South China: IEPOX- and HMML-Derived Tracers. *Journal of Geophysical Research: Atmospheres* 123.13 (2018), pp. 6999–7012. DOI: 10.1029/2017JD028242. URL: <http://doi.wiley.com/10.1029/2017JD028242>.
- [219] Wang, X. K. et al. Molecular characterization of atmospheric particulate organosulfates in three megacities at the middle and lower reaches of the Yangtze River. *Atmospheric Chemistry and Physics* 16.4 (2016), pp. 2285–2298. DOI: 10.5194/acp-16-2285-2016. URL: <https://www.atmos-chem-phys.net/16/2285/2016/>.
- [220] Shi, Z. et al. Introduction to the special issue “In-depth study of air pollution sources and processes within Beijing and its surrounding region (APHH-Beijing)”. *Atmospheric Chemistry and Physics* 19.11 (2019), pp. 7519–7546. DOI: 10.5194/acp-19-7519-2019. URL: <https://www.atmos-chem-phys.net/19/7519/2019/>.
- [221] Hamilton, J. F., Lewis, A. C., Carey, T. J. and Wenger, J. C. Characterization of Polar Compounds and Oligomers in Secondary Organic Aerosol Using Liquid Chromatography Coupled to Mass Spectrometry. *Analytical Chemistry* 80.2 (2008), pp. 474–480. DOI: 10.1021/ac701852t. URL: <https://pubs.acs.org/doi/10.1021/ac701852t>.
- [222] Fu, P., Kawamura, K., Kanaya, Y. and Wang, Z. Contributions of biogenic volatile organic compounds to the formation of secondary organic aerosols over Mt. Tai, Central East China. *Atmospheric Environment* 44.38 (2010), pp. 4817–4826. DOI: 10.1016/j.atmosenv.2010.08.040. URL: <https://linkinghub.elsevier.com/retrieve/pii/S1352231010007259>.
- [223] Lee, B. H. et al. An Iodide-Adduct High-Resolution Time-of-Flight Chemical-Ionization Mass Spectrometer: Application to Atmospheric Inorganic and Organic Compounds. *Environmental Science & Technology* 48.11 (2014), pp. 6309–6317. DOI: 10.1021/es500362a. URL: <http://pubs.acs.org/doi/10.1021/es500362a>.

- [224] Priestley, M. et al. Observations of Isocyanate, Amide, Nitrate, and Nitro Compounds From an Anthropogenic Biomass Burning Event Using a ToF-CIMS. *Journal of Geophysical Research: Atmospheres* (2018). DOI: 10.1002/2017JD027316. URL: <http://doi.wiley.com/10.1002/2017JD027316>.
- [225] Lopez-Hilfiker, F. D. et al. A novel method for online analysis of gas and particle composition: description and evaluation of a Filter Inlet for Gases and AEROSols (FIGAERO). *Atmospheric Measurement Techniques* 7.4 (2014), pp. 983–1001. DOI: 10.5194/amt-7-983-2014. URL: <https://www.atmos-meas-tech.net/7/983/2014/>.
- [226] Bannan, T. J. et al. A method for extracting calibrated volatility information from the FIGAERO-HR-ToF-CIMS and its experimental application. *Atmospheric Measurement Techniques* 12.3 (2019), pp. 1429–1439. DOI: 10.5194/amt-12-1429-2019. URL: <https://www.atmos-meas-tech.net/12/1429/2019/>.
- [227] Zhou, W. et al. Production of N₂O₅ and ClNO₂ in summer in urban Beijing, China. *Atmospheric Chemistry and Physics* 18.16 (2018), pp. 11581–11597. DOI: 10.5194/acp-18-11581-2018. URL: <https://www.atmos-chem-phys.net/18/11581/2018/>.
- [228] Bannan, T. J. et al. The first UK measurements of nitryl chloride using a chemical ionization mass spectrometer in central London in the summer of 2012, and an investigation of the role of Cl atom oxidation. *Journal of Geophysical Research: Atmospheres* 120.11 (2015), pp. 5638–5657. DOI: 10.1002/2014JD022629. URL: <http://doi.wiley.com/10.1002/2014JD022629>.
- [229] Hopkins, J. R., Jones, C. E. and Lewis, A. C. A dual channel gas chromatograph for atmospheric analysis of volatile organic compounds including oxygenated and monoterpene compounds. *Journal of Environmental Monitoring* 13.8 (2011), p. 2268. DOI: 10.1039/c1em10050e. URL: <http://xlink.rsc.org/?DOI=c1em10050e>.

- [230] Whalley, L. K. et al. The chemistry of OH and HO₂ radicals in the boundary layer over the tropical Atlantic Ocean. *Atmospheric Chemistry and Physics* 10.4 (2010), pp. 1555–1576. DOI: 10.5194/acp-10-1555-2010.
- [231] Le Breton, M. et al. The first airborne comparison of N₂O₅ measurements over the UK using a CIMS and BBCEAS during the RONOCO campaign. *Analytical Methods* 6.24 (2014), pp. 9731–9743. DOI: 10.1039/c4ay02273d. URL: <https://pubs.rsc.org/en/content/articlehtml/2014/ay/c4ay02273d%20>
<https://pubs.rsc.org/en/content/articlelanding/2014/ay/c4ay02273d>.
- [232] Lu, K. D. et al. Nighttime observation and chemistry of HO_x in the Pearl River Delta and Beijing in summer 2006. *Atmospheric Chemistry and Physics* 14.10 (2014), pp. 4979–4999. DOI: 10.5194/acp-14-4979-2014.
- [233] Wang, Y. et al. The ion chemistry and the source of PM_{2.5} aerosol in Beijing. *Atmospheric Environment* 39.21 (2005), pp. 3771–3784. DOI: 10.1016/j.atmosenv.2005.03.013.
- [234] Nguyen, T. B. et al. High-resolution mass spectrometry analysis of secondary organic aerosol generated by ozonolysis of isoprene. *Atmospheric Environment* 44.8 (2010), pp. 1032–1042. DOI: 10.1016/J.ATMOSENV.2009.12.019. URL: <https://www.sciencedirect.com/science/article/pii/S135223100901053X?via%3Dihub>.
- [235] Riva, M., Budisulistiorini, S. H., Zhang, Z. and Gold, A. Chemical characterization of secondary organic aerosol constituents from isoprene ozonolysis in the presence of acidic aerosol. *Atmospheric Environment* 130 (2016), pp. 5–13. DOI: 10.1016/J.ATMOSENV.2015.06.027. URL: <https://www.sciencedirect.com/science/article/pii/S1352231015301680?via%3Dihub>.
- [236] Li, J. et al. Characterization of isoprene-derived secondary organic aerosols at a rural site in North China Plain with implications for anthropogenic pollution effects. *Scientific Reports* 8.1 (2018), p. 535. DOI: 10.1038/s41598-017-18983-7. URL: <http://www.nature.com/articles/s41598-017-18983-7>.

- [237] Jacobs, M. I., Burke, W. J. and Elrod, M. J. Kinetics of the reactions of isoprene-derived hydroxynitrates: Gas phase epoxide formation and solution phase hydrolysis. *Atmospheric Chemistry and Physics* 14.17 (2014), pp. 8933–8946. DOI: 10.5194/acp-14-8933-2014.
- [238] Krechmer, J. E. et al. Ion mobility spectrometry–mass spectrometry (IMS–MS) for on- and offline analysis of atmospheric gas and aerosol species. *Atmospheric Measurement Techniques* 9.7 (2016), pp. 3245–3262. DOI: 10.5194/amt-9-3245-2016. URL: <https://www.atmos-meas-tech.net/9/3245/2016/>.
- [239] Surratt, J. D. et al. Chemical composition of secondary organic aerosol formed from the photooxidation of isoprene. *Journal of Physical Chemistry A* 110.31 (2006), pp. 9665–9690. DOI: 10.1021/jp061734m.
- [240] Nguyen, Q. T. et al. Understanding the anthropogenic influence on formation of biogenic secondary organic aerosols in Denmark via analysis of organosulfates and related oxidation products. *Atmospheric Chemistry and Physics* 14.17 (2014), pp. 8961–8981. DOI: 10.5194/acp-14-8961-2014. URL: <https://www.atmos-chem-phys.net/14/8961/2014/>.
- [241] Low-volatility compounds contribute significantly to isoprene secondary organic aerosol (SOA) under high-NOX conditions. *Atmospheric Chemistry and Physics* 19.11 (2019), pp. 7255–7278. DOI: 10.5194/acp-19-7255-2019. URL: <https://www.atmos-chem-phys.net/19/7255/2019/>.
- [242] Spolnik, G. et al. Improved UHPLC-MS/MS Methods for Analysis of Isoprene-Derived Organosulfates. *Analytical Chemistry* 90.5 (2018), pp. 3416–3423. DOI: 10.1021/acs.analchem.7b05060. URL: <http://pubs.acs.org/doi/10.1021/acs.analchem.7b05060>.
- [243] Jenkin, M. E., Young, J. C. and Rickard, A. R. The MCM v3.3.1 degradation scheme for isoprene. *Atmospheric Chemistry and Physics* 15.20 (2015), pp. 11433–11459. DOI: 10.5194/acp-15-11433-2015. URL: <https://www.atmos-chem-phys.net/15/11433/2015/>.

- [244] Kwan, A. J. et al. Peroxy radical chemistry and OH radical production during the NO₃-initiated oxidation of isoprene. *Atmospheric Chemistry and Physics* 12.16 (2012), pp. 7499–7515. DOI: 10.5194/acp-12-7499-2012. URL: <https://www.atmos-chem-phys.net/12/7499/2012/>.
- [245] Lee, B. H. et al. Highly functionalized organic nitrates in the southeast United States: Contribution to secondary organic aerosol and reactive nitrogen budgets. *Proceedings of the National Academy of Sciences of the United States of America* 113.6 (2016), pp. 1516–21. DOI: 10.1073/pnas.1508108113. URL: <http://www.ncbi.nlm.nih.gov/pubmed/26811465>
<http://www.pubmedcentral.nih.gov/articlerender.fcgi?artid=PMC4760802>.
- [246] Cole-Filipiak, N. C., O'Connor, A. E. and Elrod, M. J. Kinetics of the Hydrolysis of Atmospherically Relevant Isoprene-Derived Hydroxy Epoxides. *Environmental Science & Technology* 44.17 (2010), pp. 6718–6723. DOI: 10.1021/es1019228. URL: <https://pubs.acs.org/doi/10.1021/es1019228>.
- [247] Darer, A. I., Cole-Filipiak, N. C., O'Connor, A. E. and Elrod, M. J. Formation and stability of atmospherically relevant isoprene-derived organosulfates and organonitrates. *Environmental Science and Technology* 45.5 (2011), pp. 1895–1902. DOI: 10.1021/es103797z.
- [248] Zaveri, R. A., Shilling, J. E., Fast, J. D. and Springston, S. R. Efficient Nighttime Biogenic SOA Formation in a Polluted Residual Layer. *Journal of Geophysical Research: Atmospheres* (2020). DOI: 10.1029/2019JD031583. URL: <https://onlinelibrary.wiley.com/doi/abs/10.1029/2019JD031583>.
- [249] Chamber-based insights into the factors controlling IEPOX SOA yield, composition, and volatility. *Atmospheric Chemistry and Physics Discussions* (2019), pp. 1–20. DOI: 10.5194/acp-2019-271. URL: <https://www.atmos-chem-phys-discuss.net/acp-2019-271/>.
- [250] Bryant, D. J. et al. Importance of Oxidants and Temperature in the Formation of Biogenic Organosulfates and Nitrooxy Organosulfates. *ACS Earth and Space Chemistry* (2021), acsearthspacechem.1c00204. DOI: 10.1021/ACSEARTHSPACECHEM.1C00204. URL: <https://pubs.acs.org/doi/full/10.1021/acsearthspacechem.1c00204>.

- [251] Wang, X. et al. Chemical Characteristics of Organic Aerosols in Shanghai: A Study by Ultrahigh-Performance Liquid Chromatography Coupled With Orbitrap Mass Spectrometry. *Journal of Geophysical Research: Atmospheres* 122.21 (2017), pp. 703–11. DOI: 10.1002/2017JD026930.
- [252] Iinuma, Y., Böge, O., Kahnt, A. and Herrmann, H. Laboratory chamber studies on the formation of organosulfates from reactive uptake of monoterpene oxides. *Physical Chemistry Chemical Physics* 11.36 (2009), pp. 7985–7997. DOI: 10.1039/b904025k.
- [253] Kristensen, K. and Glasius, M. Organosulfates and oxidation products from biogenic hydrocarbons in fine aerosols from a forest in North West Europe during spring. *Atmospheric Environment* 45.27 (2011), pp. 4546–4556. DOI: 10.1016/j.atmosenv.2011.05.063. URL: <https://linkinghub.elsevier.com/retrieve/pii/S1352231011005802>.
- [254] Froyd, K. D. et al. Contribution of isoprene-derived organosulfates to free tropospheric aerosol mass. *Proceedings of the National Academy of Sciences of the United States of America* 107.50 (2010), pp. 21360–21365. DOI: 10.1073/pnas.1012561107. URL: <http://www.espo.nasa.gov/missions.php>.
- [255] Huang, R.-J. et al. High secondary aerosol contribution to particulate pollution during haze events in China. *Nature* 514.7521 (2014), pp. 218–222. DOI: 10.1038/nature13774. URL: <http://www.nature.com/articles/nature13774>.
- [256] Sheesley, R. J. et al. Year-round radiocarbon-based source apportionment of carbonaceous aerosols at two background sites in South Asia. *Journal of Geophysical Research Atmospheres* 117.10 (2012). DOI: 10.1029/2011JD017161.
- [257] Kirillova, E. N. et al. Water-soluble organic carbon aerosols during a full New Delhi winter: Isotope-based source apportionment and optical properties. *Journal of Geophysical Research: Atmospheres* 119.6 (2014), pp. 3476–3485. DOI: 10.1002/2013JD020041. URL: <http://doi.wiley.com/10.1002/2013JD020041>.

- [258] Kirillova, E. N. et al. ^{13}C - and ^{14}C - based study of sources and atmospheric processing of water-soluble organic carbon (WSOC) in South Asian aerosols. *Journal of Geophysical Research: Atmospheres* 118.2 (2013), pp. 614–626. DOI: 10.1002/jgrd.50130. URL: <http://doi.wiley.com/10.1002/jgrd.50130>.
- [259] Iinuma, Y. et al. Evidence for the existence of organosulfates from β -pinene ozonolysis in ambient secondary organic aerosol. *Environmental Science and Technology* 41.19 (2007), pp. 6678–6683. DOI: 10.1021/es070938t. URL: <https://pubs.acs.org/sharingguidelines>.
- [260] Chan, M. N. et al. Influence of aerosol acidity on the chemical composition of secondary organic aerosol from β -caryophyllene. *Atmospheric Chemistry and Physics* 11.4 (2011), pp. 1735–1751. DOI: 10.5194/acp-11-1735-2011.
- [261] Shalamzari, M. S. et al. Characterization of polar organosulfates in secondary organic aerosol from the unsaturated aldehydes 2-E-pentenal, 2-E-hexenal, and 3-Z-hexenal. *Atmospheric Chemistry and Physics* 16.11 (2016), pp. 7135–7148. DOI: 10.5194/acp-16-7135-2016.
- [262] Nozière, B., Ekström, S., Alsberg, T. and Holmström, S. Radical-initiated formation of organosulfates and surfactants in atmospheric aerosols. *Geophysical Research Letters* 37.5 (2010), n/a–n/a. DOI: 10.1029/2009GL041683. URL: <http://doi.wiley.com/10.1029/2009GL041683>.
- [263] Schindelka, J., Iinuma, Y., Hoffmann, D. and Herrmann, H. Sulfate radical-initiated formation of isoprene-derived organosulfates in atmospheric aerosols. *Faraday Discussions* 165.0 (2013), pp. 237–259. DOI: 10.1039/c3fd00042g. URL: <https://pubs.rsc.org/en/content/articlehtml/2013/fd/c3fd00042g> <https://pubs.rsc.org/en/content/articlelanding/2013/fd/c3fd00042g>.
- [264] Hu, K. S., Darer, A. I. and Elrod, M. J. Thermodynamics and kinetics of the hydrolysis of atmospherically relevant organonitrates and organosulfates. *Atmospheric Chemistry and Physics* 11.16 (2011), pp. 8307–8320. DOI: 10.5194/acp-11-8307-2011.

- [265] Passananti, M. et al. Organosulfate Formation through the Heterogeneous Reaction of Sulfur Dioxide with Unsaturated Fatty Acids and Long-Chain Alkenes. *Angewandte Chemie - International Edition* 55.35 (2016), pp. 10336–10339. DOI: 10.1002/anie.201605266. URL: <https://onlinelibrary.wiley.com/doi/full/10.1002/anie.201605266> %20<https://onlinelibrary.wiley.com/doi/abs/10.1002/anie.201605266> %20<https://onlinelibrary.wiley.com/doi/10.1002/anie.201605266>.
- [266] Kristensen, K. et al. Denuder/filter sampling of organic acids and organosulfates at urban and boreal forest sites: Gas/particle distribution and possible sampling artifacts. *Atmospheric Environment* 130 (2016), pp. 36–53. DOI: 10.1016/j.atmosenv.2015.10.046.
- [267] Brüggemann, M. et al. Overestimation of Monoterpene Organosulfate Abundance in Aerosol Particles by Sampling in the Presence of SO₂. *Environmental Science and Technology Letters* 8 (2020), pp. 206–211. DOI: 10.1021/acs.estlett.0c00814. URL: <https://dx.doi.org/10.1021/acs.estlett.0c00814>.
- [268] Wang, K. et al. UHPLC-Orbitrap mass spectrometric characterization of organic aerosol from a central European city (Mainz, Germany) and a Chinese megacity (Beijing). *Atmospheric Environment* 189 (2018), pp. 22–29. DOI: 10.1016/j.atmosenv.2018.06.036. URL: <https://doi.org/10.1016/j.atmosenv.2018.06.036>.
- [269] Le Breton, M. et al. Online gas- and particle-phase measurements of organosulfates, organosulfonates and nitrooxy organosulfates in Beijing utilizing a FIGAERO ToF-CIMS. *Atmospheric Chemistry and Physics* 18.14 (2018), pp. 10355–10371. DOI: 10.5194/acp-18-10355-2018. URL: <https://www.atmos-chem-phys.net/18/10355/2018/>.
- [270] He, Q. F. et al. Organosulfates from pinene and isoprene over the pearl river delta, South China: Seasonal variation and implication in formation mechanisms. *Environmental Science and Technology* (2014). DOI: 10.1021/es501299v.

- [271] Hansen, A. M. et al. Organosulfates and organic acids in Arctic aerosols: Speciation, annual variation and concentration levels. *Atmospheric Chemistry and Physics* 14.15 (2014), pp. 7807–7823. DOI: 10.5194/acp-14-7807-2014.
- [272] Kahnt, A. et al. One-year study of nitro-organic compounds and their relation to wood burning in PM10 aerosol from a rural site in Belgium. *Atmospheric Environment* 81 (2013), pp. 561–568. DOI: 10.1016/j.atmosenv.2013.09.041.
- [273] Eddingsaas, N. C. et al. α -pinene photooxidation under controlled chemical conditions-Part 2: SOA yield and composition in low-and high-NO_x environments. *Atmospheric Chemistry and Physics* 12.16 (2012), pp. 7413–7427. DOI: 10.5194/acp-12-7413-2012.
- [274] Ng, N. L. et al. Nitrate radicals and biogenic volatile organic compounds: oxidation, mechanisms, and organic aerosol. *Atmospheric Chemistry and Physics* 17.3 (2017), pp. 2103–2162. DOI: 10.5194/acp-17-2103-2017. URL: <https://www.atmos-chem-phys.net/17/2103/2017/>.
- [275] Liebmann, J. et al. Alkyl nitrates in the boreal forest: formation via the NO³⁻, OH⁻ and O₃-induced oxidation of biogenic volatile organic compounds and ambient lifetimes. *Atmospheric Chemistry and Physics* 19.15 (2019), pp. 10391–10403. DOI: 10.5194/acp-19-10391-2019.
- [276] Gao, K. and Zhu, T. Analytical methods for organosulfate detection in aerosol particles: Current status and future perspectives. *Science of The Total Environment* 784 (2021), p. 147244. DOI: 10.1016/j.scitotenv.2021.147244. URL: <https://linkinghub.elsevier.com/retrieve/pii/S0048969721023159>.
- [277] Javed, M., Bashir, M. and Zaineb, S. Analysis of daily and seasonal variation of fine particulate matter (PM_{2.5}) for five cities of China. *Environment, Development and Sustainability* (2021), pp. 1–29. DOI: 10.1007/s10668-020-01159-1. URL: <https://doi.org/10.1007/s10668-020-01159-1>.

- [278] Zou, Y. et al. One-year characterization and reactivity of isoprene and its impact on surface ozone formation at a suburban site in Guangzhou, China. *Atmosphere* 10.4 (2019). DOI: 10.3390/ATMOS10040201.
- [279] Chan, M. N. et al. Influence of aerosol acidity on the chemical composition of Secondary Organic Aerosol from β -caryophyllene. *Atmospheric Chemistry and Physics Discussions* 10.11 (2010), pp. 29249–29289. DOI: 10.5194/acpd-10-29249-2010. URL: <http://www.atmos-chem-phys-discuss.net/10/29249/2010/>.
- [280] Trufelli, H., Palma, P., Famiglini, G. and Cappiello, A. *An overview of matrix effects in liquid chromatography-mass spectrometry*. 2011. DOI: 10.1002/mas.20298.
- [281] Xu, J. et al. An interlaboratory comparison of aerosol inorganic ion measurements by ion chromatography: Implications for aerosol pH estimate. *Atmospheric Measurement Techniques* 13.11 (2020), pp. 6325–6341. DOI: 10.5194/AMT-13-6325-2020.
- [282] Sheehan, P. E. and Bowman, F. M. Estimated effects of temperature on secondary organic aerosol concentrations. *Environmental Science and Technology* 35.11 (2001), pp. 2129–2135. DOI: 10.1021/es001547g. URL: <https://pubs.acs.org/sharingguidelines>.
- [283] Zheng, J., Zheng, Z., Yu, Y. and Zhong, L. Temporal, spatial characteristics and uncertainty of biogenic VOC emissions in the Pearl River Delta region, China. *Atmospheric Environment* 44.16 (2010), pp. 1960–1969. DOI: 10.1016/j.atmosenv.2010.03.001.
- [284] Hatch, L. E. et al. Highly Speciated Measurements of Terpenoids Emitted from Laboratory and Mixed-Conifer Forest Prescribed Fires. *Environmental Science & Technology* 53.16 (2019), pp. 9418–9428. DOI: 10.1021/ACS.EST.9B02612. URL: <https://pubs.acs.org/doi/abs/10.1021/acs.est.9b02612>.
- [285] Ciccioni, P. et al. DETERMINATION OF VOLATILE ORGANIC COMPOUNDS (VOC) EMITTED FROM BIOMASS BURNING OF MEDITERRANEAN VEGETATION SPECIES BY GC-MS.

- <http://dx.doi.org/10.1081/AL-100103604> 34.6 (2006), pp. 937–955. DOI: 10.1081/AL-100103604. URL: <https://www.tandfonline.com/doi/abs/10.1081/AL-100103604>.
- [286] Gilman, J. B. et al. Biomass burning emissions and potential air quality impacts of volatile organic compounds and other trace gases from fuels common in the US. *Atmospheric Chemistry and Physics* 15.24 (2015), pp. 13915–13938. DOI: 10.5194/ACP-15-13915-2015.
- [287] Hatch, L. E. et al. Identification and quantification of gaseous organic compounds emitted from biomass burning using two-dimensional gas chromatography-time-of-flight mass spectrometry. *Atmospheric Chemistry and Physics* 15.4 (2015), pp. 1865–1899. DOI: 10.5194/ACP-15-1865-2015.
- [288] Stewart, G. J. et al. Emissions of intermediate-volatility and semi-volatile organic compounds from domestic fuels used in Delhi, India. *Atmospheric Chemistry and Physics* 21.4 (2021), pp. 2407–2426. DOI: 10.5194/ACP-21-2407-2021.
- [289] Klein, F. et al. Indoor terpene emissions from cooking with herbs and pepper and their secondary organic aerosol production potential. *Scientific Reports* 2016 6:1 6.1 (2016), pp. 1–7. DOI: 10.1038/srep36623. URL: <https://www.nature.com/articles/srep36623>.
- [290] Ye, C. et al. Chemical characterization of oxygenated organic compounds in the gas phase and particle phase using iodide CIMS with FIGAERO in urban air. *Atmospheric Chemistry and Physics* 21.11 (2021), pp. 8455–8478. DOI: 10.5194/acp-21-8455-2021. URL: <https://acp.copernicus.org/articles/21/8455/2021/>.
- [291] Suarez-Bertoa, R. et al. Atmospheric fate of a series of carbonyl nitrates: Photolysis frequencies and OH-oxidation rate constants. *Environmental Science and Technology* 46.22 (2012), pp. 12502–12509. DOI: 10.1021/es302613x. URL: <https://pubs.acs.org/doi/abs/10.1021/es302613x>.
- [292] Jones, C. E., Hopkins, J. R. and Lewis, A. C. In situ measurements of isoprene and monoterpenes within a south-east Asian tropical rainforest. *Atmospheric*

- Chemistry and Physics* 11.14 (2011), pp. 6971–6984. DOI: 10.5194/acp-11-6971-2011.
- [293] Bryant, D. J. et al. Strong anthropogenic control of secondary organic aerosol formation from isoprene in Beijing. *In press* (2019).
- [294] Worton, D. R. et al. Observational insights into aerosol formation from isoprene. *Environmental Science and Technology* 47.20 (2013), pp. 11403–11413. DOI: 10.1021/es4011064. URL: <https://pubs.acs.org/sharingguidelines>.
- [295] Lee, J. D. et al. Ozone photochemistry and elevated isoprene during the UK heatwave of August 2003. *Atmospheric Environment* 40.39 (2006), pp. 7598–7613. DOI: 10.1016/j.atmosenv.2006.06.057.
- [296] Nations, U., Economic, D. of, Affairs, S. and Division, P. *World Urbanization Prospects The 2018 Revision*. Tech. rep. 2018.
- [297] Balakrishnan, K. et al. The impact of air pollution on deaths, disease burden, and life expectancy across the states of India: the Global Burden of Disease Study 2017. *The Lancet Planetary Health* 3.1 (2019), e26–e39. DOI: 10.1016/S2542-5196(18)30261-4.
- [298] Bhandari, S. et al. Sources and atmospheric dynamics of organic aerosol in New Delhi, India: insights from receptor modeling. *Atmospheric Chemistry and Physics* 20.2 (2020), pp. 735–752. DOI: 10.5194/acp-20-735-2020. URL: <https://www.atmos-chem-phys.net/20/735/2020/>.
- [299] Chowdhury, Z. et al. Source apportionment and characterization of ambient fine particles in Delhi. *Symposium on Air Quality Measurement Methods and Technology 2004*. 2004, pp. 13–24.
- [300] Hama, S. M. et al. Four-year assessment of ambient particulate matter and trace gases in the Delhi-NCR region of India. *Sustainable Cities and Society* 54 (2020). DOI: 10.1016/j.scs.2019.102003.
- [301] Kanawade, V. P. et al. What caused severe air pollution episode of November 2016 in New Delhi? *Atmospheric Environment* 222 (2020). DOI: 10.1016/j.atmosenv.2019.117125.

- [302] Miyazaki, Y. et al. Dicarboxylic acids and water-soluble organic carbon in aerosols in New Delhi, India, in winter: Characteristics and formation processes. *Journal of Geophysical Research Atmospheres* 114.19 (2009). DOI: 10.1029/2009JD011790.
- [303] Nagar, P. K. et al. Characterization of PM_{2.5} in Delhi: role and impact of secondary aerosol, burning of biomass, and municipal solid waste and crustal matter. *Environmental Science and Pollution Research* 24.32 (2017), pp. 25179–25189. DOI: 10.1007/s11356-017-0171-3.
- [304] Elzein, A. et al. A comparison of PM_{2.5}-bound polycyclic aromatic hydrocarbons in summer Beijing (China) and Delhi (India). *Atmospheric Chemistry and Physics* 20.22 (2020), pp. 14303–14319. DOI: 10.5194/ACP-20-14303-2020.
- [305] Singh, D. P., Gadi, R. and Mandal, T. K. Characterization of Gaseous and Particulate Polycyclic Aromatic Hydrocarbons in Ambient Air of Delhi, India. *Polycyclic Aromatic Compounds* 32.4 (2012), pp. 556–579. DOI: 10.1080/10406638.2012.683230.
- [306] Singh, B. P., Kumar, K. and Jain, V. K. Source identification and health risk assessment associated with particulate- and gaseous-phase PAHs at residential sites in Delhi, India. *Air Quality, Atmosphere and Health* (2021). DOI: 10.1007/S11869-021-01035-5.
- [307] Yadav, A. K. et al. Fine Particulate Matter Bound Polycyclic Aromatic Hydrocarbons and Carbonaceous Species in Delhi's Atmosphere: Seasonal Variation, Sources, and Health Risk Assessment. *Aerosol Science and Engineering* 2021 5:2 5.2 (2021), pp. 193–213. DOI: 10.1007/S41810-021-00094-6. URL: <https://link.springer.com/article/10.1007/s41810-021-00094-6>.
- [308] Sharma, S. K. and Mandal, T. K. Chemical composition of fine mode particulate matter (PM_{2.5}) in an urban area of Delhi, India and its source apportionment. *Urban Climate* 21 (2017), pp. 106–122. DOI: 10.1016/j.uclim.2017.05.009.

- [309] Stewart, G. J. et al. Sources of non-methane hydrocarbons in surface air in Delhi, India. *Faraday Discussions* 226.0 (2021), pp. 409–431. DOI: 10.1039/D0FD00087F. URL: <https://pubs.rsc.org/en/content/articlehtml/2021/fd/d0fd00087f%20> <https://pubs.rsc.org/en/content/articlelanding/2021/fd/d0fd00087f>.
- [310] Bhandari, S. et al. Sources and atmospheric dynamics of organic aerosol in New Delhi, India: Insights from receptor modeling. *Atmospheric Chemistry and Physics* 20.2 (2020), pp. 735–752. DOI: 10.5194/acp-20-735-2020.
- [311] Sawlani, R. et al. The severe Delhi SMOG of 2016: A case of delayed crop residue burning, coincident firecracker emissions, and atypical meteorology. *Atmospheric Pollution Research* 10.3 (2019), pp. 868–879. DOI: 10.1016/j.apr.2018.12.015.
- [312] Schnell, J. L. et al. Exploring the relationship between surface PM _{2.5} and meteorology in Northern India. *Atmospheric Chemistry and Physics* 18.14 (2018), pp. 10157–10175. DOI: 10.5194/acp-18-10157-2018. URL: <https://www.atmos-chem-phys.net/18/10157/2018/>.
- [313] Sinha, V., Kumar, V. and Sarkar, C. Chemical composition of pre-monsoon air in the Indo-Gangetic Plain measured using a new air quality facility and PTR-MS: High surface ozone and strong influence of biomass burning. *Atmospheric Chemistry and Physics* 14.12 (2014), pp. 5921–5941. DOI: 10.5194/acp-14-5921-2014.
- [314] Gani, S. et al. Submicron aerosol composition in the world’s most polluted megacity: the Delhi Aerosol Supersite study. *Atmospheric Chemistry and Physics* 19.10 (2019), pp. 6843–6859. DOI: 10.5194/acp-19-6843-2019. URL: <https://www.atmos-chem-phys.net/19/6843/2019/>.
- [315] None, S., R, G., SK, S. and TK, M. Seasonal variation, source apportionment and source attributed health risk of fine carbonaceous aerosols over National Capital Region, India. *Chemosphere* 237 (2019). DOI: 10.1016/J.CHEMOSPHERE.2019.124500. URL: <https://pubmed.ncbi.nlm.nih.gov/31549639/>.

- [316] Reyes-Villegas, E. et al. PM1 composition and source apportionment at two sites in Delhi, India, across multiple seasons. *Atmospheric Chemistry and Physics* 21.15 (2021), pp. 11655–11667. DOI: 10.5194/ACP-21-11655-2021.
- [317] Du, Z. et al. A yearlong study of water-soluble organic carbon in Beijing I: Sources and its primary vs. secondary nature. *Atmospheric Environment* 92 (2014), pp. 514–521. DOI: 10.1016/j.atmosenv.2014.04.060.
- [318] Kirillova, E. N., Sheesley, R. J., Andersson, A. and Gustafsson, Ö. Natural abundance ^{13}C and ^{14}C analysis of water-soluble organic carbon in atmospheric aerosols. *Analytical Chemistry* 82.19 (2010), pp. 7973–7978. DOI: 10.1021/ac1014436.
- [319] Szidat, S. et al. Source apportionment of aerosols by ^{14}C measurements in different carbonaceous particle fractions. *Radiocarbon*. Vol. 46. 1. University of Arizona, 2004, pp. 475–484. DOI: 10.1017/S0033822200039783.
- [320] Wozniak, A. S., Bauer, J. E. and Dickhut, R. M. Characteristics of water-soluble organic carbon associated with aerosol particles in the eastern United States. *Atmospheric Environment* 46 (2012), pp. 181–188. DOI: 10.1016/j.atmosenv.2011.10.001.
- [321] Elser, M. et al. New insights into PM_{2.5} chemical composition and sources in two major cities in China during extreme haze events using aerosol mass spectrometry. *Atmospheric Chemistry and Physics* 16.5 (2016), pp. 3207–3225. DOI: 10.5194/ACP-16-3207-2016.
- [322] Lanz, V. A. et al. Characterization of aerosol chemical composition with aerosol mass spectrometry in Central Europe: An overview. *Atmospheric Chemistry and Physics* 10.21 (2010), pp. 10453–10471. DOI: 10.5194/ACP-10-10453-2010.
- [323] Hoffmann, T. et al. Formation of organic aerosols from the oxidation of biogenic hydrocarbons. *Journal of Atmospheric Chemistry* 26.2 (1997), pp. 189–222. DOI: 10.1023/A:1005734301837. URL: <https://link.springer.com/article/10.1023/A:1005734301837>.

- [324] Nelson, B. et al. In situ Ozone Production is highly sensitive to Volatile Organic Compounds in the Indian Megacity of Delhi. *Atmospheric Chemistry and Physics Discussions* (2021), pp. 1–36. DOI: 10.5194/ACP-2021-278.
- [325] Cash, J. M. et al. Seasonal analysis of submicron aerosol in Old Delhi using high-resolution aerosol mass spectrometry: chemical characterisation, source apportionment and new marker identification. *Atmospheric Chemistry and Physics* 21.13 (2021), pp. 10133–10158. DOI: 10.5194/ACP-21-10133-2021. URL: <https://acp.copernicus.org/articles/21/10133/2021/>.
- [326] *Import Surface Meteorological Data from NOAA Integrated Surface Database (ISD) • worldmet*. URL: <https://davidcarslaw.github.io/worldmet/index.html>.
- [327] Sommariva, R. et al. AtChem (version 1), an open-source box model for the Master Chemical Mechanism. *Geoscientific Model Development* 13.1 (2020), pp. 169–183. DOI: 10.5194/GMD-13-169-2020.
- [328] Acton, W. J. F. et al. Surface-atmosphere fluxes of volatile organic compounds in Beijing. *Atmospheric Chemistry and Physics* 20.23 (2020), pp. 15101–15125. DOI: 10.5194/ACP-20-15101-2020.
- [329] Coggon, M. M. et al. Significant anthropogenic monoterpene emissions from fragrances and other consumer products in New York City. *AGUFM 2018* (2018), A32E–08. URL: <https://ui.adsabs.harvard.edu/abs/2018AGUFM.A32E..08C/abstract>.
- [330] BC, M. et al. Volatile chemical products emerging as largest petrochemical source of urban organic emissions. *Science (New York, N.Y.)* 359.6377 (2018), pp. 760–764. DOI: 10.1126/SCIENCE.AAQ0524. URL: <https://pubmed.ncbi.nlm.nih.gov/29449485/>.
- [331] Galloway, M. M. et al. Glyoxal uptake on ammonium sulphate seed aerosol: Reaction products and reversibility of uptake under dark and irradiated conditions. *Atmospheric Chemistry and Physics* 9.10 (2009), pp. 3331–3345. DOI: 10.5194/acp-9-3331-2009.

- [332] Liao, J. et al. Airborne measurements of organosulfates over the continental U.S. *Journal of Geophysical Research* 120.7 (2015), pp. 2990–3005. DOI: 10.1002/2014JD022378. URL: <https://agupubs.onlinelibrary.wiley.com/doi/full/10.1002/2014JD022378>
<https://agupubs.onlinelibrary.wiley.com/doi/abs/10.1002/2014JD022378>
<https://agupubs.onlinelibrary.wiley.com/doi/10.1002/2014JD022378>.
- [333] Gaston, C. J. et al. Reactive Uptake of an Isoprene-Derived Epoxydiol to Submicron Aerosol Particles. *Environmental Science & Technology* 48.19 (2014), pp. 11178–11186. DOI: 10.1021/es5034266. URL: <http://pubs.acs.org/doi/10.1021/es5034266>.
- [334] Wu, C. et al. Photolytically Induced Changes in Composition and Volatility of Biogenic Secondary Organic Aerosol from Nitrate Radical Oxidation during Night-to-day Transition. *Atmospheric Chemistry and Physics Discussions* (2021), pp. 1–29. DOI: 10.5194/ACP-2021-347.
- [335] Kumar, P., Kumar, S. and Yadav, S. Seasonal variations in size distribution, water-soluble ions, and carbon content of size-segregated aerosols over New Delhi. *Environmental Science and Pollution Research* 25.6 (2018), pp. 6061–6078. DOI: 10.1007/S11356-017-0954-6.
- [336] Ding, J. et al. Aerosol pH and its driving factors in Beijing. *Atmospheric Chemistry and Physics* 19.12 (2019), pp. 7939–7954. DOI: 10.5194/ACP-19-7939-2019.
- [337] Wang, Y. et al. Synthesis and Hydrolysis of Atmospherically Relevant Monoterpene-Derived Organic Nitrates. *Environmental Science & Technology* (2021), acs.est.1c05310. DOI: 10.1021/ACS.EST.1C05310. URL: <https://pubs.acs.org/doi/abs/10.1021/acs.est.1c05310>.
- [338] Daellenbach, K. R. et al. Impact of anthropogenic and biogenic sources on the seasonal variation in the molecular composition of urban organic aerosols: a field and laboratory study using ultra-high-resolution mass spectrometry. *Atmospheric Chemistry and Physics* 19.9 (2019), pp. 5973–5991. DOI:

- 10.5194/acp-19-5973-2019. URL:
<https://acp.copernicus.org/articles/19/5973/2019/>.
- [339] Liigand, P., Liigand, J., Kaupmees, K. and Kruve, A. 30 Years of research on ESI/MS response: Trends, contradictions and applications. *Analytica Chimica Acta* 1152 (2021), p. 238117. DOI: 10.1016/J.ACA.2020.11.049.
- [340] Steimer, S. S. et al. Differences in the composition of organic aerosols between winter and summer in Beijing: A study by direct-infusion ultrahigh-resolution mass spectrometry. *Atmospheric Chemistry and Physics* 20.21 (2020), pp. 13303–13318. DOI: 10.5194/ACP-20-13303-2020.
- [341] C, G. et al. Direct target and non-target analysis of urban aerosol sample extracts using atmospheric pressure photoionisation high-resolution mass spectrometry. *Chemosphere* 224 (2019), pp. 786–795. DOI: 10.1016/J.CHEMOSPHERE.2019.02.151. URL: <https://pubmed.ncbi.nlm.nih.gov/30851530/>.
- [342] Cai, J. et al. Molecular composition and photochemical evolution of water-soluble organic carbon (WSOC) extracted from field biomass burning aerosols using high-resolution mass spectrometry. *Atmospheric Chemistry and Physics* 20.10 (2020), pp. 6115–6128. DOI: 10.5194/ACP-20-6115-2020.
- [343] Rincón, A. G., Calvo, A. I., Dietzel, M. and Kalberer, M. Seasonal differences of urban organic aerosol composition – an ultra-high resolution mass spectrometry study. *Environmental Chemistry* 9.3 (2012), p. 298. DOI: 10.1071/EN12016. URL: <http://www.publish.csiro.au/?paper=EN12016>.
- [344] Steimer, S. S. et al. Seasonal Differences in the Composition of Organic Aerosols in Beijing: a Study by Direct Infusion Ultrahigh Resolution Mass Spectrometry (). DOI: 10.5194/acp-2019-1009. URL: <https://doi.org/10.5194/acp-2019-1009>.
- [345] Pereira, K. L. et al. An Automated Methodology for Non-targeted Compositional Analysis of Small Molecules in High Complexity Environmental Matrices Using Coupled Ultra Performance Liquid Chromatography Orbitrap Mass Spectrometry. *Environmental Science & Technology* (2021),

- acs.est.0c08208. DOI: 10.1021/acs.est.0c08208. URL:
<https://pubs.acs.org/doi/10.1021/acs.est.0c08208>.
- [346] O'Brien, R. E. et al. Molecular characterization of S- and N-containing organic constituents in ambient aerosols by negative ion mode high-resolution Nanospray Desorption Electrospray Ionization Mass Spectrometry: CalNex 2010 field study. *Journal of Geophysical Research: Atmospheres* 119.22 (2014), pp. 706–12. DOI: 10.1002/2014JD021955. URL:
<http://doi.wiley.com/10.1002/2014JD021955>.
- [347] Bé, A. G. et al. Cloud Activation Potentials for Atmospheric α -Pinene and β -Caryophyllene Ozonolysis Products. *ACS Central Science* 3.7 (2017), pp. 715–725. DOI: 10.1021/ACSCENTSCI.7B00112. URL:
<https://pubs.acs.org/doi/full/10.1021/acscentsci.7b00112>.
- [348] Parshintsev, J. et al. Solid-phase extraction of organic compounds in atmospheric aerosol particles collected with the particle-into-liquid sampler and analysis by liquid chromatography–mass spectrometry. *Talanta* 80.3 (2010), pp. 1170–1176. DOI: 10.1016/J.TALANTA.2009.09.004.
- [349] Oss, M., Krueve, A., Herodes, K. and Leito, I. Electrospray ionization efficiency scale of organic compound. *Analytical Chemistry* 82.7 (2010), pp. 2865–2872. DOI: 10.1021/ac902856t. URL: <https://pubs.acs.org/sharingguidelines>.
- [350] Krueve, A., Kaupmees, K., Liigand, J. and Leito, I. Negative electrospray ionization via deprotonation: Predicting the ionization efficiency. *Analytical Chemistry* 86.10 (2014), pp. 4822–4830. DOI: 10.1021/ac404066v.
- [351] Mayhew, A. W., Topping, D. O. and Hamilton, J. F. New Approach Combining Molecular Fingerprints and Machine Learning to Estimate Relative Ionization Efficiency in Electrospray Ionization. *ACS Omega* (2020). DOI: 10.1021/acsomega.0c00732. URL:
<https://dx.doi.org/10.1021/acsomega.0c00732>.
- [352] Alfaro, C. M. et al. Investigations of Analyte-Specific Response Saturation and Dynamic Range Limitations in Atmospheric Pressure Ionization Mass Spectrometry. *Analytical Chemistry* 86.21 (2014), pp. 10639–10645. DOI:

10.1021/AC502984A. URL:

<https://pubs.acs.org/doi/abs/10.1021/ac502984a>.

- [353] Henriksen, T., Juhler, R. K., Svensmark, B. and Cech, N. B. The relative influences of acidity and polarity on responsiveness of small organic molecules to analysis with negative ion electrospray ionization mass spectrometry (ESI-MS). *Journal of the American Society for Mass Spectrometry* 16.4 (2005), pp. 446–455. DOI: 10.1016/J.JASMS.2004.11.021. URL: <https://pubs.acs.org/doi/abs/10.1016/j.jasms.2004.11.021>.
- [354] Ehrmann, B. M., Henriksen, T. and Cech, N. B. Relative importance of basicity in the gas phase and in solution for determining selectivity in electrospray ionization mass spectrometry. *Journal of the American Society for Mass Spectrometry* 19.5 (2011), pp. 719–728. DOI: 10.1016/J.JASMS.2008.01.003. URL: <https://pubs.acs.org/doi/abs/10.1016/j.jasms.2008.01.003>.
- [355] Gioumouxouzis, C. I., Kouskoura, M. G. and Markopoulou, C. K. Negative electrospray ionization mode in mass spectrometry: A new perspective via modeling. *Journal of Chromatography B* 998-999 (2015), pp. 97–105. DOI: 10.1016/J.JCHROMB.2015.06.009.
- [356] Mandra, V. J., Kouskoura, M. G. and Markopoulou, C. K. Using the partial least squares method to model the electrospray ionization response produced by small pharmaceutical molecules in positive mode. *Rapid Communications in Mass Spectrometry* 29.18 (2015), pp. 1661–1675. DOI: 10.1002/RCM.7263. URL: <https://analyticalsciencejournals.onlinelibrary.wiley.com/doi/full/10.1002/rcm.7263>
<https://analyticalsciencejournals.onlinelibrary.wiley.com/doi/abs/10.1002/rcm.7263>.
- [357] Zhang, X. et al. Formation and evolution of molecular products in α -pinene secondary organic aerosol. *Proceedings of the National Academy of Sciences of the United States of America* 112.46 (2015), pp. 14168–14173. DOI:

10.1073/pnas.1517742112. URL:
www.pnas.org/cgi/doi/10.1073/pnas.1517742112.

- [358] Dong, J. et al. ChemDes: An integrated web-based platform for molecular descriptor and fingerprint computation. *Journal of Cheminformatics* 7.1 (2015), p. 60. DOI: 10.1186/s13321-015-0109-z. URL: <https://jcheminf.biomedcentral.com/articles/10.1186/s13321-015-0109-z>.
- [359] Pereira, K. L. et al. A new aerosol flow reactor to study secondary organic aerosol. *Atmospheric Measurement Techniques* 12.8 (2019), pp. 4519–4541. DOI: 10.5194/amt-12-4519-2019.
- [360] Finessi, E. et al. Improving the Quantification of Secondary Organic Aerosol Using a Microflow Reactor Coupled to HPLC-MS and NMR to Manufacture Ad Hoc Calibration Standards. *Analytical Chemistry* 86.22 (2014), pp. 11238–11245. DOI: 10.1021/AC5028512. URL: <https://pubs.acs.org/doi/abs/10.1021/ac5028512>.
- [361] Kuhn, M. Building Predictive Models in R Using the caret Package. *Journal of Statistical Software, Articles* 28.5 (2008), pp. 1–26. DOI: 10.18637/jss.v028/i05.
- [362] Krueve, A. and Kaupmees, K. Predicting ESI/MS Signal Change for Anions in Different Solvents. *Analytical Chemistry* 89.9 (2017), pp. 5079–5086. DOI: 10.1021/acs.analchem.7b00595.
- [363] Wang, T. et al. Standard substances free quantification makes LC/ESI/MS non-targeted screening of pesticides in cereals comparable between labs. *Food Chemistry* 318 (2020), p. 126460. DOI: 10.1016/J.FOODCHEM.2020.126460. URL: <https://www.sciencedirect.com/science/article/pii/S0308814620303228?via%3Dihub>.
- [364] Hammes, J. et al. Carboxylic acids from limonene oxidation by ozone and hydroxyl radicals: Insights into mechanisms derived using a FIGAERO-CIMS. *Atmospheric Chemistry and Physics* 19.20 (2019), pp. 13037–13052. DOI: 10.5194/acp-19-13037-2019.

- [365] Witkowski, B. and Gierczak, T. Characterization of the limonene oxidation products with liquid chromatography coupled to the tandem mass spectrometry. *Atmospheric Environment* 154 (2017), pp. 297–307. DOI: 10.1016/j.atmosenv.2017.02.005.
- [366] Alfara, M. R. et al. The effect of photochemical ageing and initial precursor concentration on the composition and hygroscopic properties of β -caryophyllene secondary organic aerosol. *Atmospheric Chemistry and Physics* 12.14 (2012), pp. 6417–6436. DOI: 10.5194/acp-12-6417-2012. URL: <https://www.atmos-chem-phys.net/12/6417/2012/>.
- [367] Kundu, S. et al. High molecular weight SOA formation during limonene ozonolysis: Insights from ultrahigh-resolution FT-ICR mass spectrometry characterization. *Atmospheric Chemistry and Physics* 12.12 (2012), pp. 5523–5536. DOI: 10.5194/ACP-12-5523-2012.
- [368] Putman, A. L. et al. Ultrahigh-resolution FT-ICR mass spectrometry characterization of α -pinene ozonolysis SOA. *Atmospheric Environment* 46 (2012), pp. 164–172. DOI: 10.1016/J.ATMOSENV.2011.10.003.
- [369] Moise, T., Flores, J. M. and Rudich, Y. Optical Properties of Secondary Organic Aerosols and Their Changes by Chemical Processes. *Chemical Reviews* 115.10 (2015), pp. 4400–4439. DOI: 10.1021/CR5005259. URL: <https://pubs.acs.org/doi/full/10.1021/cr5005259>.
- [370] Guenther, A. et al. Estimates of global terrestrial isoprene emissions using MEGAN (Model of Emissions of Gases and Aerosols from Nature). *Atmospheric Chemistry and Physics* 6.11 (2006), pp. 3181–3210. DOI: 10.5194/acp-6-3181-2006. URL: <http://www.atmos-chem-phys.net/6/3181/2006/>.
- [371] Mutzel, A. et al. Monoterpene SOA - Contribution of first-generation oxidation products to formation and chemical composition. *Atmospheric Environment* 130 (2016), pp. 136–144. DOI: 10.1016/j.atmosenv.2015.10.080.

- [372] Simon, M. et al. Molecular understanding of new-particle formation from α -pinene between -50 and +25 °C. *Atmospheric Chemistry and Physics* 20.15 (2020), pp. 9183–9207. DOI: 10.5194/acp-20-9183-2020.
- [373] Vestenius, M. et al. Acidic reaction products of monoterpenes and sesquiterpenes in atmospheric fine particles in a boreal forest. *Atmospheric Chemistry and Physics* 14.15 (2014), pp. 7883–7893. DOI: 10.5194/ACP-14-7883-2014.
- [374] Gómez-González, Y. et al. Chemical characterisation of atmospheric aerosols during a 2007 summer field campaign at Brasschaat, Belgium: Sources and source processes of biogenic secondary organic aerosol. *Atmospheric Chemistry and Physics* 12.1 (2012), pp. 125–138. DOI: 10.5194/ACP-12-125-2012.
- [375] Whalley, L. K. et al. Evaluating the sensitivity of radical chemistry and ozone formation to ambient VOCs and NO_x in Beijing. *Atmospheric Chemistry and Physics* 21.3 (2021), pp. 2125–2147. DOI: 10.5194/ACP-21-2125-2021.
- [376] Carslaw, D. C. and Ropkins, K. Openair - An R package for air quality data analysis. *Environmental Modelling and Software* 27-28 (2012), pp. 52–61. DOI: 10.1016/j.envsoft.2011.09.008.
- [377] Zhang, Y. Y. et al. Seasonal cycle and temperature dependence of pinene oxidation products, dicarboxylic acids and nitrophenols in fine and coarse air particulate matter. *Atmospheric Chemistry and Physics* 10.16 (2010), pp. 7859–7873. DOI: 10.5194/ACP-10-7859-2010.
- [378] Islam, M. R. et al. Ambient air quality in the Kathmandu Valley, Nepal, during the pre-monsoon: Concentrations and sources of particulate matter and trace gases. *Atmospheric Chemistry and Physics* 20.5 (2020), pp. 2927–2951. DOI: 10.5194/ACP-20-2927-2020.
- [379] Li, J. J. et al. Observation of biogenic secondary organic aerosols in the atmosphere of a mountain site in central China: Temperature and relative humidity effects. *Atmospheric Chemistry and Physics* 13.22 (2013), pp. 11535–11549. DOI: 10.5194/ACP-13-11535-2013.

- [380] Mahilang, M. et al. Biogenic secondary organic aerosol formation in an urban area of eastern central India: Seasonal variation, size distribution and source characterization. *Environmental Research* 195 (2021), p. 110802. DOI: 10.1016/J.ENVRES.2021.110802.
- [381] Li, W. et al. Molecular characterization of biomass burning tracer compounds in fine particles in Nanjing, China. *Atmospheric Environment* 240 (2020), p. 117837. DOI: 10.1016/J.ATMOSENV.2020.117837.
- [382] Drooge, B. L. van et al. Organic molecular tracers in atmospheric PM₁ at urban intensive traffic and background sites in two high-insolation European cities. *Atmospheric Environment* 188 (2018), pp. 71–81. DOI: 10.1016/J.ATMOSENV.2018.06.024.
- [383] Ren, Y. et al. Seasonal variation and size distribution of biogenic secondary organic aerosols at urban and continental background sites of China. *Journal of Environmental Sciences* 71 (2018), pp. 32–44. DOI: 10.1016/J.JES.2017.11.016.
- [384] Wu, X. et al. Molecular composition and source apportionment of fine organic aerosols in Northeast China. *Atmospheric Environment* 239 (2020), p. 117722. DOI: 10.1016/J.ATMOSENV.2020.117722.
- [385] Yi, Y. et al. Molecular characteristics and formation mechanisms of biogenic secondary organic aerosols in the summer atmosphere at Mt. Tai on the North China plain. *Aerosol and Air Quality Research* 19.12 (2019), pp. 2671–2682. DOI: 10.4209/aaqr.2019.10.0515.
- [386] Ding, X., Wang, X.-M. and Zheng, M. The influence of temperature and aerosol acidity on biogenic secondary organic aerosol tracers: Observations at a rural site in the central Pearl River Delta region, South China. *Atmospheric Environment* 45.6 (2011), pp. 1303–1311. DOI: 10.1016/j.atmosenv.2010.11.057. URL: <https://linkinghub.elsevier.com/retrieve/pii/S1352231010010289>.
- [387] Cahill, T. M. et al. Secondary organic aerosols formed from oxidation of biogenic volatile organic compounds in the Sierra Nevada Mountains of California. *Journal of Geophysical Research: Atmospheres* 111.D16 (2006),

- p. 16312. DOI: 10.1029/2006JD007178. URL:
<https://onlinelibrary.wiley.com/doi/full/10.1029/2006JD007178%20>
<https://onlinelibrary.wiley.com/doi/abs/10.1029/2006JD007178%20>
<https://agupubs.onlinelibrary.wiley.com/doi/10.1029/2006JD007178>.
- [388] Jaoui, M. et al. Analysis of secondary organic aerosol compounds from the photooxidation of d-limonene in the presence of NO_x and their detection in ambient PM_{2.5}. *Environmental Science and Technology* 40.12 (2006), pp. 3819–3828. DOI: 10.1021/es052566z. URL:
<https://pubs.acs.org/doi/full/10.1021/es052566z>.
- [389] Rossignol, S. et al. Organic aerosol molecular composition and gas–particle partitioning coefficients at a Mediterranean site (Corsica). *Journal of Environmental Sciences* 40 (2016), pp. 92–104. DOI:
 10.1016/J.JES.2015.11.017.
- [390] Yuan, Q. et al. Seasonal cycles of secondary organic aerosol tracers in rural Guangzhou, Southern China: The importance of atmospheric oxidants. *Environmental pollution (Barking, Essex : 1987)* 240 (2018), pp. 884–893. DOI:
 10.1016/J.ENVPOL.2018.05.009. URL:
<https://pubmed.ncbi.nlm.nih.gov/29793196/>.
- [391] Zhu, W. et al. Characteristics and contributions of biogenic secondary organic aerosol tracers to PM_{2.5} in Shanghai, China. *Atmospheric Pollution Research* 9.2 (2018), pp. 179–188. DOI: 10.1016/J.APR.2017.09.001.
- [392] Zhao, D. F. et al. Secondary organic aerosol formation from hydroxyl radical oxidation and ozonolysis of monoterpenes. *Atmospheric Chemistry and Physics* 15.2 (2015), pp. 991–1012. DOI: 10.5194/ACP-15-991-2015.
- [393] Saathoff, H. et al. Temperature dependence of yields of secondary organic aerosols from the ozonolysis of α -pinene and limonene. *Atmospheric Chemistry and Physics* 9.5 (2009), pp. 1551–1577. DOI: 10.5194/ACP-9-1551-2009.
- [394] Winterhalter, R. et al. The gas-phase ozonolysis of β -caryophyllene (C₁₅H₂₄). Part I: an experimental study. *Physical Chemistry Chemical Physics* 11.21 (2009), pp. 4152–4172. DOI: 10.1039/B817824K. URL:

<https://pubs.rsc.org/en/content/articlehtml/2009/cp/b817824k>
<https://pubs.rsc.org/en/content/articlelanding/2009/cp/b817824k>.

- [395] Loreto, F., Pinelli, P., Manes, F. and Kollist, H. Impact of ozone on monoterpene emissions and evidence for an isoprene-like antioxidant action of monoterpenes emitted by *Quercus ilex* leaves. *Tree physiology* 24.4 (2004), pp. 361–367. DOI: 10.1093/TREEPHYS/24.4.361. URL: <https://pubmed.ncbi.nlm.nih.gov/14757575/>.
- [396] Peñuelas, J., Llusà, J. and Gimeno, B. S. Effects of ozone concentrations on biogenic volatile organic compounds emission in the Mediterranean region. *Environmental Pollution* 105.1 (1999), pp. 17–23. DOI: 10.1016/S0269-7491(98)00214-0.
- [397] Quelever, L. L. et al. Effect of temperature on the formation of highly oxygenated organic molecules (HOMs) from alpha-pinene ozonolysis. *Atmospheric Chemistry and Physics* 19.11 (2019), pp. 7609–7625. DOI: 10.5194/ACP-19-7609-2019.
- [398] Jensen, L. N. et al. Temperature and volatile organic compound concentrations as controlling factors for chemical composition of α -pinene-derived secondary organic aerosol. *Atmospheric Chemistry and Physics* 21.15 (2021), pp. 11545–11562. DOI: 10.5194/ACP-21-11545-2021.
- [399] Kristensen, K. et al. The Aarhus Chamber Campaign on Highly Oxygenated Organic Molecules and Aerosols (ACCHA): Particle formation, organic acids, and dimer esters from α -pinene ozonolysis at different temperatures. *Atmospheric Chemistry and Physics* 20.21 (2020), pp. 12549–12567. DOI: 10.5194/ACP-20-12549-2020.
- [400] Maja, M. M. et al. The effect of warming and enhanced ultraviolet radiation on gender-specific emissions of volatile organic compounds from European aspen. *The Science of the total environment* 547 (2016), pp. 39–47. DOI: 10.1016/J.SCITOTENV.2015.12.114. URL: <https://pubmed.ncbi.nlm.nih.gov/26780130/>.

- [401] Yatagai, M., Ohira, M., Ohira, T. and Nagai, S. Seasonal variations of terpene emission from trees and influence of temperature, light and contact stimulation on terpene emission. *Chemosphere* 30.6 (1995), pp. 1137–1149. DOI: 10.1016/0045-6535(95)00006-T.
- [402] Ibrahim, M. A. et al. Elevation of night-time temperature increases terpenoid emissions from *Betula pendula* and *Populus tremula*. *Journal of Experimental Botany* 61.6 (2010), p. 1583. DOI: 10.1093/JXB/ERQ034. URL: [/pmc/articles/PMC2852659/%20/pmc/articles/PMC2852659/?report=abstract%20https://www.ncbi.nlm.nih.gov/pmc/articles/PMC2852659/](https://pmc/articles/PMC2852659/%20/pmc/articles/PMC2852659/?report=abstract%20https://www.ncbi.nlm.nih.gov/pmc/articles/PMC2852659/).
- [403] Warren, B., Austin, R. L. and Cocker, D. R. Temperature dependence of secondary organic aerosol. *Atmospheric Environment* 43.22-23 (2009), pp. 3548–3555. DOI: 10.1016/J.ATMOENV.2009.04.011.
- [404] Hellén, H. et al. Sesquiterpenes and oxygenated sesquiterpenes dominate the VOC (C5-C20) emissions of downy birches. *Atmospheric Chemistry and Physics* 21.10 (2021), pp. 8045–8066. DOI: 10.5194/ACP-21-8045-2021.